JOINT EUROPEAN TORUS

JET–P(94)40

Many Authors

JET Papers presented to 18th Symposium on Fusion Technology (SOFT-18)

(Karlsruhe, Germany, 22–26 August 1994)

JET Papers presented to 18th Symposium on Fusion Technology (SOFT-18)

(Karlsruhe, Germany, 22–26 August 1994)

Many Authors

JET-Joint Undertaking, Culham Science Centre, OX14 3DB, Abingdon, UK

Preprint of Papers to be published in the Proceedings of
18th Symposium on Fusion Technology (SOFT-18)
(Karlsruhe, Germany, 22–26 August 1994)

"This document contains JET information in a form not yet suitable for publication. The report has been prepared primarily for discussion and information within the JET Project and the Associations. It must not be quoted in publications or in Abstract Journals. External distribution requires approval from the Publications Officer, JET Joint Undertaking, Abingdon, Oxon, OX14 3EA, UK".

"Enquiries about Copyright and reproduction should be addressed to the Publications Officer, EFDA, Culham Science Centre, Abingdon, Oxon, OX14 3DB, UK."

The contents of this preprint and all other JET EFDA Preprints and Conference Papers are available to view online free at www.iop.org/Jet. This site has full search facilities and e-mail alert options. The diagrams contained within the PDFs on this site are hyperlinked from the year 1996 onwards.

JET Papers presented to
18th Symposium on Fusion Technology (SOFT-18)
(Karlsruhe, Germany, 22-26 August 1994)

Thermal Considerations and Cooling System for the JET Divertor Coils

N Dolgetta, E Bertolini, P Butcher, M Cooke, J R Last, V Marchese, P Miele, G Sannazzaro, A Tesini.

JET Joint Undertaking, Abingdon, Oxon, OX14 3EA, UK.

Abstract —**The recently installed and now operational JET divertor coils, have copper conductor and epoxy glass-kapton insulation, but are situated inside the JET vacuum vessel, which can be operated up to 350°C. Despite being insulated, in normal conditions, by the high vacuum, the coils are radiation heated by the surrounding enviroment, and also ohmically by current pulses during operation. The coils are cooled by insulating organic fluid and the copper conductor operating temperature ranges from 10°C to 65°C. The main concern is to maintain the epoxy at a safe temperature and to limit the thermally developed interturn shear stress. The cooling system is designed to limit the maximum differential temperature to 20°C, and it can operate in open and closed loop modes.**

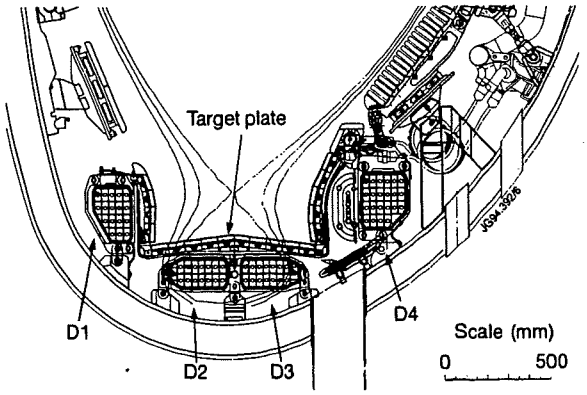

Fig.1. Divertor coils, target plate and cryopump installed in the vacuum vessel

I. Introduction

The divertor coils and cooling system were installed in 1993 and JET restarted operation in February 1994. Since the restart the thermal performance of the coils has been monitored in order to interpret the measured heat power load to the coils, and the temperatures measured on the Inconel casing. The aim is to estimate if any part of the epoxy-glass may be subjected to temperatures which might undermine its properties as insulating or structural material. Direct measurements of the epoxy temperature are not available. The present Mk1 divertor target plate is supported on the divertor coils, and its alignment ultimately relies on the mechanical stability of the epoxy. Calculations were also made to evaluate faults such as loss of vacuum or failure of the coil cooling system.
The coil cooling system proceeded in parallel to the coil. Measurements on the cooling system enabled the thermal power load to be determined.

II. Coil features and enviroment

The divertor coils, are enclosed in thin Inconel casings (thickness 1.2 mm), which were also their impregnation-curing mould. They are anchored to the vessel by 32 clamps, allowing for radial expansion due to forces and temperature variations. Pads welded on the casing top surface of coils D2 and D3 support the target plate structure. The target plate is generally water cooled at about 70.°C, but operation with uncooled target plate proceeded for several months, and this may still be required for conditioning baking of the vessel. The coils are provided with radiation heat shields over about 75% of their surface (11 layers of polished stainless steel with a nominal 0.1mm spacing and 2.mm from the casing); the remaining 25% being unscreened, in particular the sections at the clamps, pads and coil terminations.
The shields considerably lessen the heat power load, which would otherwise require 50% of the available cooling power. However at the clamps and D2,D3 pads, combined heat radiation and conduction may produce a concentration of heat flux; for this reason the coil assembly includes copper plates, at the top and bottom of the coil, spreading the heat and protecting the ground insulation. Of most concern, from the thermal point of view is, the epoxy that, for structural purposes, fills the gap between casing and

electrical insulation or copper plates, which is not protected by this feature.

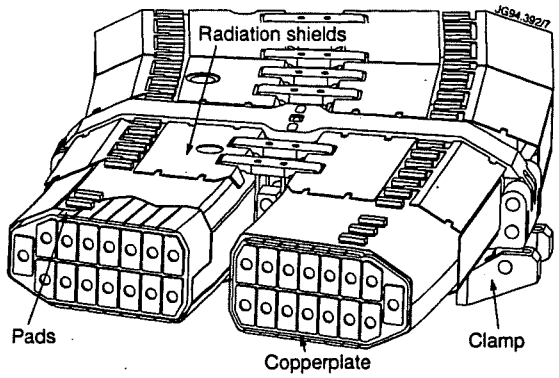

Fig. 2. Divertor coils D2, D3 section

III. THERMAL ASSESSMENT

A. Thermal power load and temperature measurements

Temperature of the casings is monitored, at four points per coil, at two positions (Octant 3 and 6), and at the top and bottom. The thermocouples welded on the casing are 20.mm from the clamps and indicate the temperature at the unshielded part of the casing.

The cooling system is used for the thermal power load measurements since, in steady state conditions, the power is given by:

$$Q = \dot{m}C\Delta T$$

$\dot{m}$ *Coolant mass flow,* C *Coolant thermal capacity,* ΔT *differential temperature.*

To assess the power scaling and the main heat transfer mechanism to the coils, measurements were performed with the vacuum vessel at several temperatures, in steady state conditions, between 150°C and 250°C (with no target plate cooling). To confirm the above result the cooling system was stopped for 1 hr. leaving stationary coolant in the coil (vessel at 250°C). A temperature increase of 10°C of coil and coolant was observed at the restart of the cooling flow, consistent with the measured thermal power and coil mass. A loss of vacuum in vessel would increase the thermal power load to the coils. Tests were performed, to assess the effect of a vacuum loss up to 1 bar of air in vessel, considering that in the past JET experience, in the worst event, pressure rose up to 400.mbar. Gases H_2, and N_2 were injected in flowing and stationary conditions, up to 10 mbar pressure, with the vessel at 150°C and, 250°C respectively. The effects on the coolant differential temperature, due to the increased heat power, are shown in Fig.3 for coil D4. In this case 10.mbar N_2 was maintained in vessel for four hours (from 0 to 4 hrs) to reach stationary conditions, then reistablishing the normal high vacuum. The differential temperature appears to double, while the undershoot at 10.hr is due to fluctuation in the coolant inlet temperature. Tests were repeated with the cooled target plate (vessel at 250°C), although, thermal power loading, failure of the cooling system, and vacuum loss pose less serious damage.

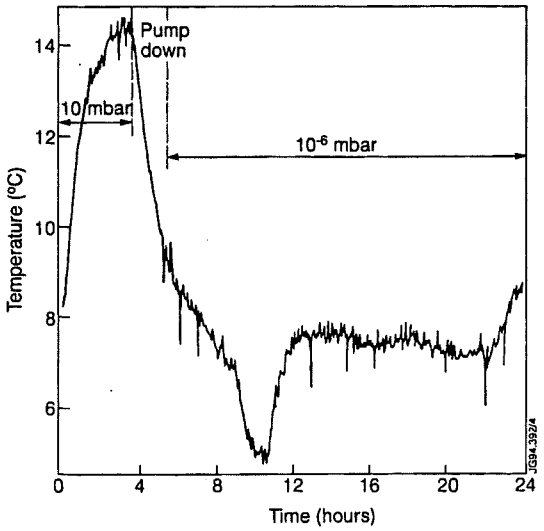

Fig.3. D4 Coolant differential temperature during 10.mbar N_2 *injection in vessel*

B. Interpretation and modelling

A model representative of the casing shielding non uniformity has been developed; parameters have been determined so as to obtain consistency between the measured power and temperatures. The measured thermal power load dependence with the vessel temperature scales as the radiation law. Casing surfaces screened by the heat shields contribute marginally, about 10% of the heat power load to the coil. Their equivalent emissivity is about 0.01, a factor of about 1/20 compared to the unshielded casing surfaces. The underlying epoxy is in all cases less than 5°C higher than the coil copper. The radiative power is essentially transmitted through the unshielded casing parts, where the underlying epoxy is about 30°C higher than the coil copper. Measurements and model predictions, in high vacuum, are in agreement if the emissivity assumed is 0.3, compared to the nominal value

for polished Inconel of 0.15. This is conceivable considering the blackening effect on the surface due to glow discharge conditioning and plasma operation. Molecular conduction is the main means of heat transfer across the interspace between casing and epoxy, estimated at about 20W/°Cm², compared to radiation ≃5W/°Cm². This interspace, which is pumped down to ≃0.1 – 1.mbar, was formed during resin polymerisation. The clamp conductive contribution appears negligible, possibly due to a low pressure on the contact between casing-clamp, and in the pins linking the clamp to the vessel. The contact pressure, depending on coil and target plate weight, but also on the deflection profile of vessel could not be defined beforehand. The epoxy layer underlying coils D2,D3 pads is the most critically affected by the vessel temperature, because of the observed, larger than expected, heat conduction from the target plate graphite tiles to the supporting Inconel structure. Also the graphite tiles bulk temperature may increase to hundreds of degrees higher than the vessel temperature with repeated pulsed plasma operation. With an uncooled target plate, operation proceeded with maximum vessel temperature up to 250°C, and the pads underlying epoxy is estimated to have reached ≃180°C. The effect on the epoxy disappears with a cooled target plate. Baking and operation with the target plate uncooled have now been restricted to a maximum vessel temperature of 200°C, while, with target cooled, this temperature will be allowed to rise to 320°C.

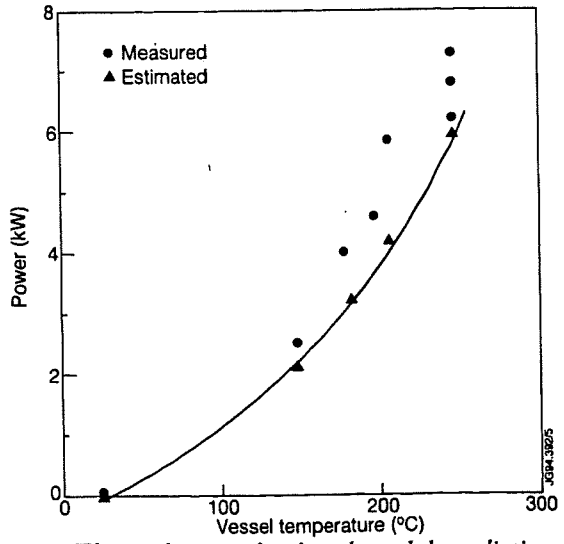

Fig.4. Thermal power load and model prediction for D4

In case of a considerable water leak to the vessel, or vacuum loss, heat transfer to the coil, would increase by molecular gas conduction at first and then by convection. Decay in the effectiveness of the radiation shields, spaced 0.1mm apart, is an important effect, with the radiative power to the coils increasing also at pressure as low as ≃0.1mbar during glow discharge conditioning. Test results of in vessel gas up to 10.mbar pressure, were in agreement with predictions, considering natural convection and shields loss of effectiveness. Procedures, in some cases requiring to lower the vessel temperature at 20°C/hr, were laid down to safe guard the coils, in case of failure of target or coil cooling.

IV. Cooling System

A. Design parameter

The cooling system is designed for the following requirements.

- Limit the thermally developed shear stress in the interturn insulation
- High cooling rate
- High electrical resistance coolant
- Limit the pressure of the cooling circuit and flow velocity

Shear stress is developed in the interturn insulation due to the thermal gradient between turns and the coil spurs. This has been estimated to be of the order of 0.5 MPa/°C, resulting in 10.MPa for a temperature difference of 20°C, between adjacent turns. This is to be compared with a shear stress at breaking of 45.MPa, for specimen at 20°C, and of 22.MPa at 80.°C. During cycled operation, the maximum differential temperature of the coil parallel cooling channels (2 for D1,D2, D3, and 3 for D4) is limited to 20°C by limiting the coil measured differential temperature to 15°C, and so maintaining the shear stress to < 10 MPa. The largest I^2t allowed is $21.10^9 A^2s$, corresponding to a flat top of 40.kA for 8.s, and a temperature increase of 47°C; in this most demanding case the estimated cooling time is 60.min..

The coolant choice was CFC113, as for the JET TF coils, an organic insulating fluid, which would prevent the coils from developing interturn faults in case of an internal leak through a brazed joint. Besides this remote possibility, CFC cooling provides an insulation resistance to earth > 1MΩ, a factor more than

100 times higher than water, resulting in sensitive detection of any change in the coil insulation to earth. On the other hand CFC has only 30% of the heat capacity of the equivalent water volume, requires special handling procedures, and in the event of a leakage the cooling system may have to be stopped, unless secondary containment is provided. Pressure in the circuit is limited to 18.Bars, compared to a bursting test pressure of fitting and hoses of 250.Bars; flow velocity is limited to 3 m/s, to avoid erosion .

Table 1 Divertor coil cooling system capacity, ΔT=15°C

	Coil	D1	D2	D3	D4
Main flow	Flow rate (m^3/hr)	3.96	4.32	5.04	7.92
	Pressure (bars)	6.0	7.4	10.8	13.1
	Cooling (KW)	22	24	28	43
Emergency flow	Flow rate (m^3/hr)	1.47	1.42	1.24	1.90
	Pressure (bars)	1.0	1.0	1.0	1.0
	Cooling (KW)	8	8	7.5	10.5

JG94.392/1

B. Cooling system layout and operation

The main cooling system, individual to each divertor coil, is connected in parallel to the TF coils system, providing a resevoir of cold fluid at 5.Bars, and avoiding the need for new heat exchangers. The main cooling system schematic and components is shown in Fig.5.

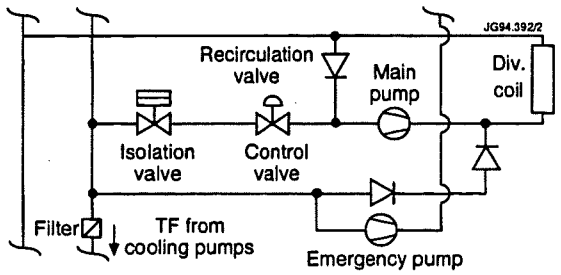

Fig.5. Cooling circuit diagram for one divertor coil (repeated for each coil).

During operation in closed loop, the control valve is closed before the start of the power pulse, setting the cooling to full recirculation; following the pulse the valve is automatically operated to control the differential temperature to 15°C. The design ensures that the fluid leaving the coil reaches the recirculation path in less than 10.s. In case the differential temperature of 20°C is exceeded, during open loop operation or failure of the control, the isolation valve closes forcing the flow to full recirculation.

An "Emergency cooling system" is also installed, in parallel and with common pump for the four coils, operating only in open loop mode, capable of extracting the thermal power load to the coil and limited operation.

Early operational experience, in open loop mode, showed a cooling time of the coils longer than expected. Due to the large heat load, the outlet coolant temperature of the heat exchanger, in common to TF and Divertor coils, would increase, after a pulse, to 30°C, limiting the cooling rate of the Divertor coils. A new dedicated heat exchanger, cooling the fluid from the TF system to the Divertor coils is being considered. Full commissioning in closed loop mode is now to preceed.

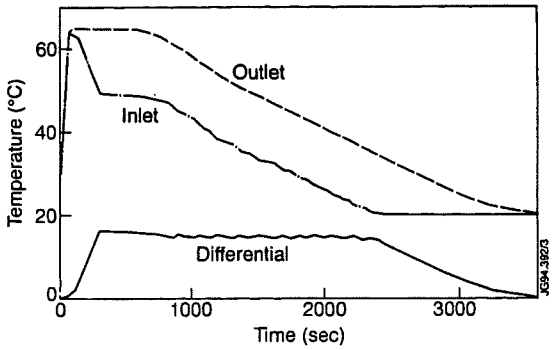

Fig.6 D4 Cooling evolution for high I^2t pulse

V. Conclusion

The divertor coils performance and vessel temperature, have gradually been increased after having established safe thermal conditions for their operation.

Present restrictions will be reviewed and possibly relaxed with the Mk2 divertor configuration as the critical pads on D2, D3 coils will not be in contact with the target plate.

References

[1] J.R. Last et al, "The JET divertor magnetic configuration and coil design.", Proceeding of the 16th Symposium on Fusion Technology, London 1990.

[2] N. Dolgetta et al, "JET Divertor Coils Manufacture, Assembly and Testing.", Proceeding of the 13th International Conference on Magnet Technology, Victoria, British Columbia, 1993.

[3] M. Cooke et al, "Organic Cooling Fluids for the JET Toroidal and Divertor Field Coils", presented at the 15th Symposium of Fusion Engineering, Hyannis, Massachusetts 1993.

Operational Safety of the JET In-Vessel Divertor Cryopump System

S Papastergiou, P Ageladarakis, W Obert, E Thompson.

JET Joint Undertaking, Abingdon, Oxon, OX14 3EA, UK.

ABSTRACT

A large condensation cryopump forms an integral part of the pumped divertor recently installed inside the JET torus. A detailed heat transfer model which incorporates radiative, conductive and convective heat transfer has been developed to predict the time-dependent behaviour of the high emissivity liquid nitrogen (LN) cooled chevron structure and also the low emissivity LN cooled back plate of the cryopump. In addition, the behaviour of surrounding components for a wide range of adverse scenarios has also been investigated. The model has been validated through a series of experiments.

These studies have enabled tokamak operation criteria to be defined which will ensure that the cryopump will not be over-stressed during normal operation and/or abnormal scenarios.

The studies of the behaviour of water cooled components in the vicinity of the cryopump which are at risk of freezing due to the proximity of the LN cooled structure of the cryopump have resulted in establishing criteria for the water flow and vacuum vessel temperature under all of the envisaged adverse scenarios.

1. INTRODUCTION

The tokamak environment is particularly hostile to a cryopump and high thermal stresses may occur during adverse scenarios like loss of vacuum, water, cryogens, etc. Figure 1 gives a cross-section of the JET Divertor Cryopump and its associated components, namely the water cooled baffles and target shields together with one of the divertor coils with its own thermal shields (1, 2).

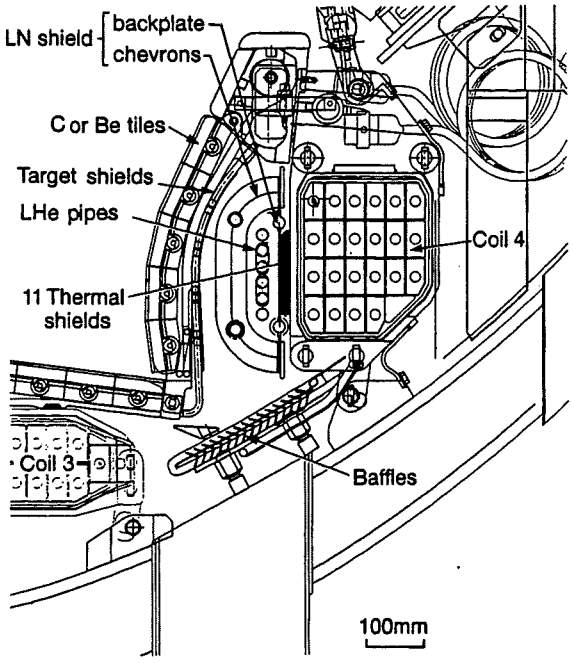

Figure 1. Cross-section of the JET Divertor Cryopump and surrounding components.

2. OPERATIONAL RISKS

a) The temperature differences (ΔT) between the black chevrons and the low emissivity backplate of the cryopump should not exceed 150°C. Linear stress analysis predicts yielding with a ΔT of approximately 40°C. However, expansion gaps and bellows in the system allow this larger value of 150°C.

b) Loss of water flow in the baffles may result in freezing or boiling of the water and stress the pipework.

c) Similarly, stop of water flow in the target shields may result in freezing of the water there.

3. MATHEMATICAL MODEL

When water is not running in the system, the general equations governing the behaviour of the system are:

$$\Sigma W_j = m_j C_{pj} dT_j/dt \qquad (1)$$

$$\Sigma W_j = \sum_{i=1}^{j} \left\{ \phi_{ij} C_{ij} A_j \left(T_j^4 - T_i^4 \right) + h_m A_j \left(T_j - T_i \right) + \right.$$

$$\left. + \left(K_m A_j / \ell_{ji} \right) \left(T_j - T_i \right) \right\} \qquad (2)$$

$$C_{ij} = \varepsilon_i \varepsilon_j \sigma$$

where:

$j = 1,2,3 \ldots$ different masses/equations under investigation.

T_j = temperature of mass j

m_j = mass j
C_{pj} = specific heat of mass j
t = time
A_j = area of mass j
φ_{ij} = view factor between the masses ij
ε_j = emissivity of mass j
σ = Stefan-Bolzman constant
h_m = convection coefficient
K_m = conduction coefficient
ℓ_{ji} = conduction distance between masses i, j.

The SI system of units is used throughout the model.

The above set of equations (1) is solved in a step by step approach. The solution is given by the following equation.

$$T_{tj} = T_{t-1,j} + \Sigma W_j \, \Delta t/(m_j C_{pj}) \qquad (3)$$

where

T_{tj}, $T_{t-1,j}$ = the temperatures of mass j at time steps t and t-1 respectively.

Δt = Integration time step. This is small to avoid numerical instabilities but long enough for the water to go through the system.

If there is a fluid (water, gas) running through a mass, then the set of equations (1) takes the form

$$m_j C_{pj} \frac{dT_j}{dt} \pm \Sigma W_j = \dot{M} C_p' dT' = KA dT'' \qquad (4)$$

where

$\dot{M}$ = fluid flow rate
C_p' = specific heat of fluid
KA = characteristic of the heat exchanger
dT_j, dT', dT'' = temperature differences in component, fluid and heat exchanger respectively.

Equations (3) are also solved in a step by step approach assuming that in a small time step Δt, the temperature of the component is constant. Under these conditions the solution is given by the following equations.

$$\dot{M} C_p(T'_{t+1} - T'_{in}) = KA(T_t - (T'_{t+1} + T'_{in})/2) \qquad (5)$$

$$m_j C_{pj}(T_t - T_{t+1}) \pm \Delta t \Sigma W_j = \dot{M} C_p(T_{t'+1} - T'_{in})\Delta t \qquad (6)$$

where

T'_{in} = fluid input temperature.

Equation (2) indicates that all three forms of heat transfer are taken into account. Radiation dominates only when there is good vacuum ($< 10^{-3}$mbar) Conduction is considered when there is physical contact or, in case of an air leak, when the Grashof number is less than 10^7. Convection starts when this number is higher and for the geometry involved this corresponds to approximately 2mbar. Typical conduction and convection parameters are: 0.026W/(mK) for gas nitrogen at 20°C and 5.5W/(m^2K) with 1bar air leak between chevrons (at 77K) and target shields (at 520K). In the analysis several assumptions have been made:

- The thermal mass and temperature of the graphite and inconel in the target modules are constant and unaffected by freeze-up scenarios. This is because the thermal mass of the graphite (0.9MJ/°C, 1200kg) and of inconel (1.28MJ/°C, 1300kg) are large compared to the thermal mass of the cryopump (26MJ, 330kg) for the full temperature excursion of 77K to 280K. In addition, the thermal mass of the hot air in case of air leaks again is small and does not affect significantly the inconel and graphite temperatures.
- Following water introduction into cooled components inside the machine, the temperatures of graphite and inconel are different. Graphite is always at higher temperatures (165°C when the vacuum vessel is at 250°C) than the water cooled inconel which is at ~20°C. In the event of an air leak in the machine, these temperatures tend to equalise but again during the phenomena under investigation, we assume that these temperatures do not alter. This was because it can be shown that the time constants of these events are different. It takes longer for the temperatures of graphite and inconel to equalise than for instance the onset of freezing.

It should be noted that in applying these models to simulate the abnormal operating scenarios of the cryopump, we experienced difficulties in some of the input parameters. These are:

- Empirical convection coefficients at low pressures. (It was assumed that the Nusselt number is proportional to the square root of pressure.)
- Characteristics of the heat exchangers. These, for instance, depend on many parameters some of them ill defined (ie, brazing joints).
- The dynamic flow and temperature of the gas inside the tokamak during air leaks.

4. EXPERIMENTAL MODEL VALIDATION

A series of experiments was undertaken to validate the model. Figure 2 gives comparisons between theory and experiment of cooling the baffles with ambient gas nitrogen from a vessel temperature of 220°C. The agreement is good.

Figure 3 shows also good comparison between theory and experiment in warm-up of a cryopump quadrant in a test tank.

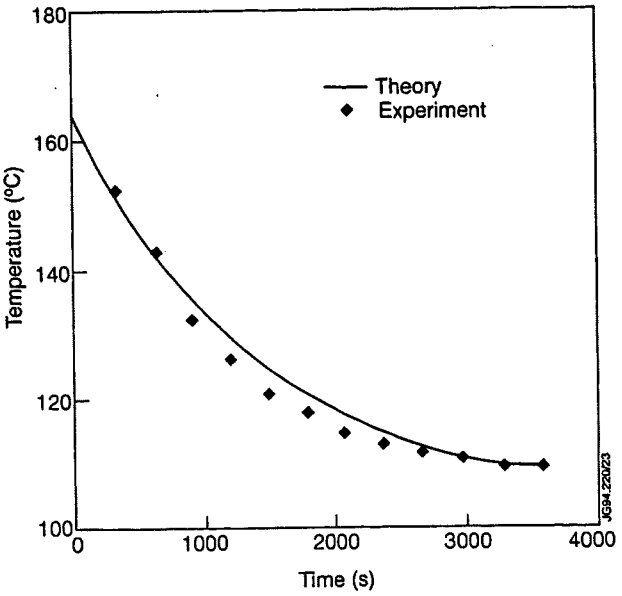

Figure 2. Exit temperatures of gas nitrogen during cooldown of baffles from 220°C.

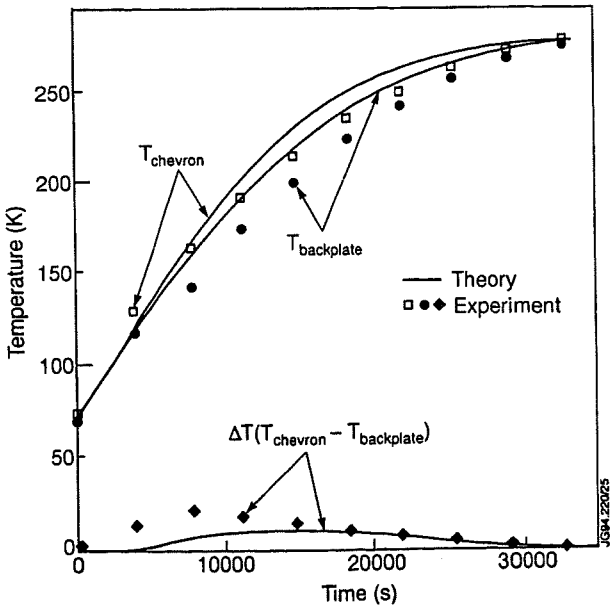

Figure 3. Cryopump warm-up in a vacuum test tank with good vacuum.

5. RESULTS

Figure 4 gives the predicted temperature evolution of the baffles, chevrons and backplate during warm-up of the cryopump with bad vacuum vessel at 250°C, stop of LN flow and loss of water flow. The temperature difference between backplate and chevrons of less than 150°C is allowable.

The model shows that at vessel temperatures above 100°C, no freezing of water in the baffles is possible if there is loss of flow.

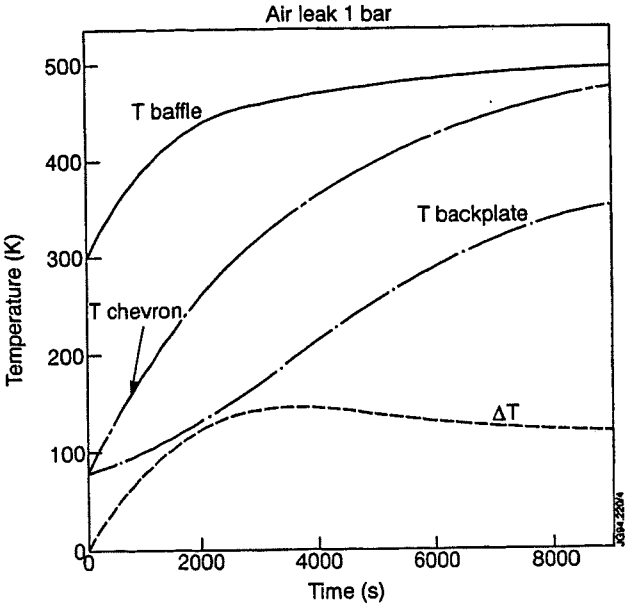

Figure 4. Temperature evolution in the cryopump with bad vacuum, vessel hot (250°C), loss of water flow and stop of LN flow.

Figure 5 attempts to analyse the risk of freezing of target shields, as a function of vessel temperature in the event of stoppage of the water flow. It is assumed that the water enters the system at 300 K (27 °C). The effect of the high temperature Carbon (C) or Beryllium (Be) tiles is demonstrated. The low emissivity Be results in higher probability of freezing since it protects less than C the target shields even with loss of vacuum when convection (not radiation) dominates the heat transfer. In addition Figure 5 shows the effect of different heat transfer assumptions, with regard to the gas dynamic mechamisms of the air leak, on the model predictions. It is shown that the freeze-up risk of the target shields is high even at elevated vessel temperatures. For instance with a vessel temperature of 250 °C (523 K), and inlet water temperature of 18 °C the model predicts freeze-up of the shields under any assumption.

With good vacuum however no risk of freezing the target shield exists provided the vessel temperature is above 400 K.

As far as boiling of water inside the system (with abnormal operation, loss of water flow and vessel hot) is concerned, it was shown that the time constants of such an event are much longer than the time constants of re-instating flow or draining. Thus pressurisation of the pipework due to water boiling is not possible.

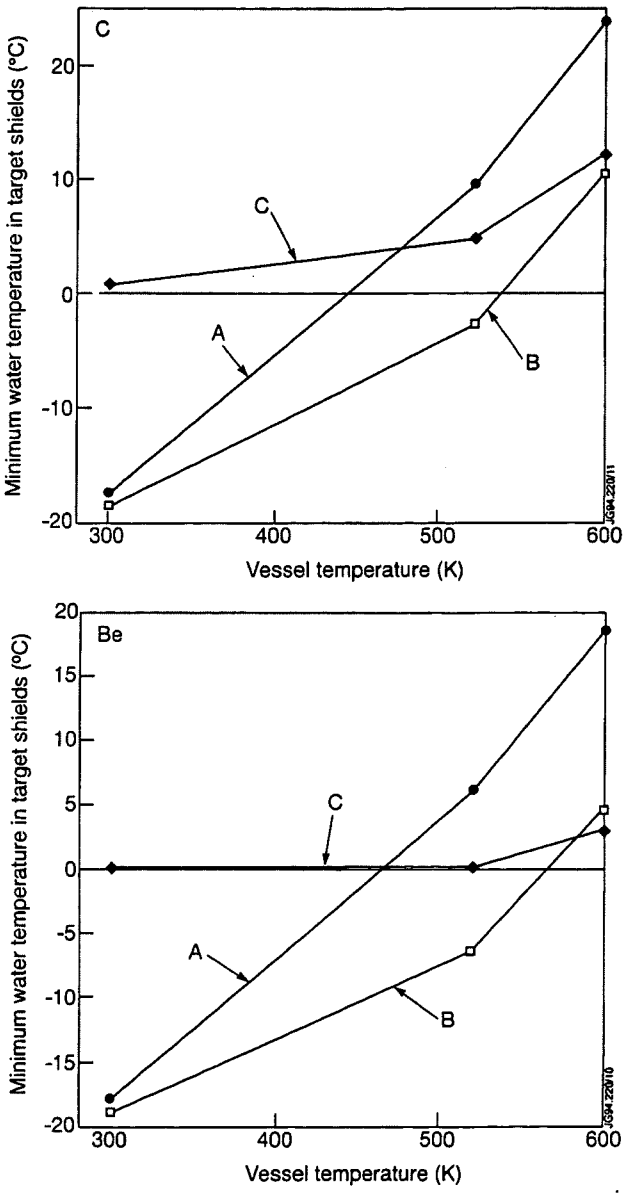

Figure 5. Minimum target shield temperatures as a function of vessel temperature and different assumptions in the heat transfer modes.

A: Optimistic assumptions (hot air at the rear of the target shields), 1 bar air leak.
B: Realistic, 1 bar air leak.
C: 15 mbar air leak.

6. CONCLUSIONS

The analysis resulted in guidelines to protect the cryopump and the associated in-vessel components against abnormal scenarios. These are:

- No cooldown of the cryopump without water inside the internal components of the vacuum vessel, while the vessel temperature is above 100°C.
- No freeze-up risk of baffles with vessel temperature above 100°C.
- No freeze-up risk of the target shields with good vacuum and vessel temperature higher than 400 K.
- The risk of freezing the target shields with loss of vacuum is appreciable even at high vessel temperatures. Thus an effective gas flushing system* is triggered to remove water from pipework in such an event.
- No risks occur due to boiling of the cooling water.

REFERENCES

1. W. Obert, S. Papastergiou, JET Pumped Divertor Cryopump, proceedings Symposium of Fusion Technology, London, UK (1990) 488-492.
2. S. Papastergiou, W. Obert and E. Thompson, Material Selection, Qualification and Manufacturing of the In-vessel Divertor Cryopump for JET, proceedings of Inter. Cryogenic Mater. Conf., Albuquerque, USA (1993) to appear.

ACKNOWLEDGMENT

The experimental data of cooling the baffles with nitrogen, used in Figure 2, were provided by M Cooke and P Butcher of the JET Machine Services Group.

* In designing such gas flushing system, care has to be taken to account for possible parallel loops in the pipework. These may result in residual stagnant water, being present in pipes with high hydraulic resistance, despite the gas flushing. Such water pockets are at risk of freezing.

Visualisation of Thermal Contact with a Commercial CCD Video System

H D Falter, D Ciric, F D Long.

JET Joint Undertaking, Abingdon, Oxon, OX14 3EA, UK.

Summary

The integrity of the thermal contact between armour material and actively cooled heat sink can be visualised by cooling the component below the freezing point of water. If the component is cold enough the surface will quickly be covered by frost from the humidity in the air. Running water through the cooling channels will heat the component and the surface will defrost. Regions with reduced thermal contact can be identified by a delayed defrosting. Comparisons with tests done with a infrared thermal imaging system and with power test in the JET Neutral Beam Test Bed prove that the test gives viable results.

1 INTRODUCTION

Actively cooled dump plates in Fusion devices are made of composite materials with beryllium or Carbon Fibre Composites (CFC) as armour materials and copper alloys or molybdenum alloys as heat sinks. The heat flux can be as high as 15 - 20 MW/m^2 and requires a perfect joint between heat sink and armour. Testing of these joints is normally performed by heating the armour tile in vacuum with an electron - or ion beam. Power densities of several MW/m^2 are required for a good assessment of the braze joints[1,2]. Ultrasonic examinations and X-ray applications have been used with some success to monitor the integrity of the braze [1].

The easiest way to produce thermal gradients is probably to flow water through the cooling channel of a preheated or precooled test section. Faults in the thermal contact between heat sink and armour will show up as a distortion of the temperature distribution on the surface. All that is required is a sufficiently fast and accurate measurement of the surface temperature distribution.

As every driver knows from the heated rear windscreen of this car, defrosting starts above the heating wire and then the defrosted zone spreads away from the wire. The transition between frosted and defrosted zone is sharp, well defined, and clearly visible. Using this observation we can visualise the heat transfer from the heat sink to the armour by monitoring the defrosting sequence. We demonstrate in this paper, that the frequency and resolution of commercial domestic TV equipment is sufficient to visualise significant faults in thermal contact between armour and heat sink of divertor test sections.

2 EXPERIMENTAL SET-UP.

To start with the test section is cooled down in a conventional chest freezer to approximately -15 to -20 °C. When the cold test section is exposed to air the surface gradually covers with frost. This frost coverage will be denser if the humidity in the air is increased (hot water near by). The frosted, cold component is then heated up by flowing tap water through the water channels. The defrosting is filmed with a commercial CCD camera from a distance of approximately 1 metre. The process is recorded with

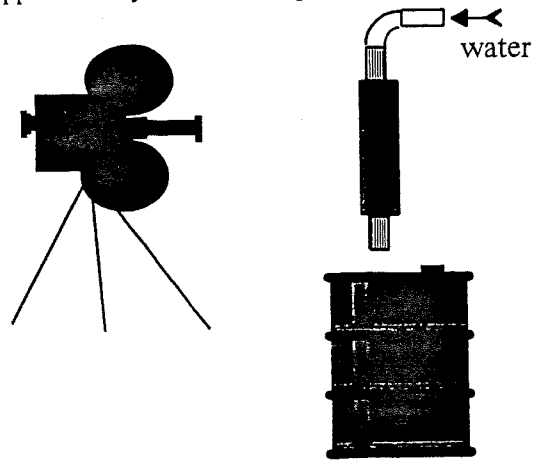

Fig. 1: The cooled and frosted test section is heated up with tap water and the defrosting is monitored.

a S VHS [4] video recorder. With a mirror behind the test section, all 4 sides of the test section can be monitored simultaneously.

The examination of the test section is carried out using a slow motion replay in which the spreading of the defrosting is observed. Areas with reduced thermal contact will show a delayed defrosting.

3 RESULTS

3.1 CFC divertor test sections

We have applied the frosting test to a number of different test sections, mainly Carbon Fibre Composites (CFC) blocks brazed onto a cooling pipe through the centre of the CFC tile.

A typical defrosting sequence is shown in Fig. 2 for a test section with 17 CFC tiles of 27 x 19 x 6 mm^3 brazed to a TZM pipe of 12.7 mm external diameter. Water flow direction during the defrosting is from right to left.

The top picture of the defrosting sequence shows that the two end tile defrost first. The second and third picture from the top show frost on exactly those tiles which had an increased surface temperature during beam exposure (tiles 3 and 11) as shown by the surface temperature profile above the defrosting sequence. This temperature distribution was measured with an IR imaging system after exposure to an energetic particle beam. The vertical grid lines in the profile correspond approximately to the gaps between the tiles. The exposed surface during beam testing was the forward facing surface in Fig. 2. We also note that the defrosting of one tile is not uniform in the sense that the surface of one side can defrost before or after the neighbouring surface of the same tile.

In the case of Fig. 2 the test section was cooled to -200 °C and the tiles have to be warmed up by approximately 200 °C before defrosting occurs. This warm-up time is long compared with the time the water needs to flow through the test section and we can detect all faults in one frame - the frame in the middle of the defrosting sequence in Fig. 2.

If we use a conventional freezer to cool the component, the temperature is much higher (-15°C) and the heat-up time is much shorter, so that the water velocity can not be neglected. This is demonstrated in Fig. 3: Again water flows from right to left and defrosting is expected to proceed from right to

Fig. 2: Defrosting sequence of a CFC monoblock test section with the surface temperature distribution during beam exposure (top) and the defrosting sequence below.

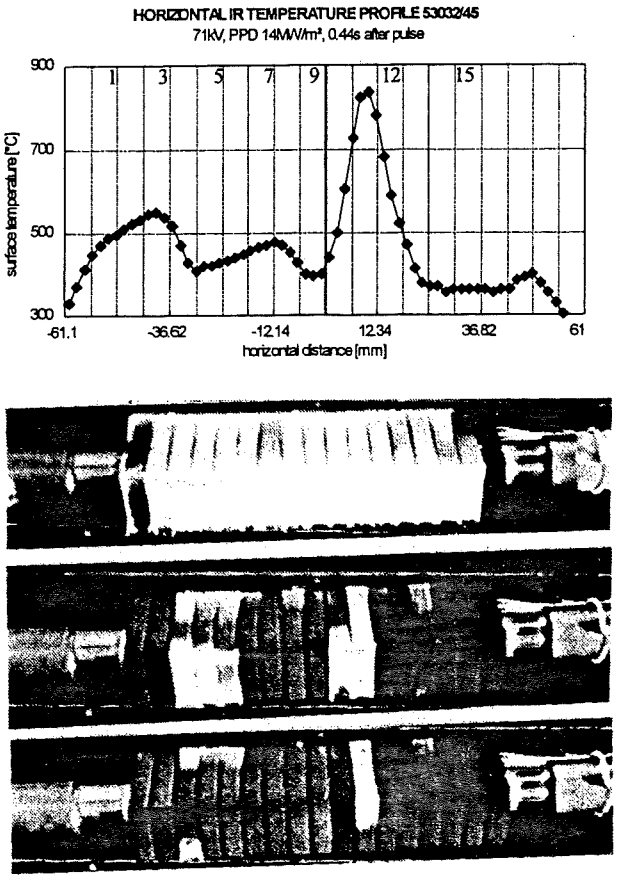

left. The first picture of the defrosting sequence indicates (just) that the second tile from the right defrosts before the first tile from right and hence that the first tile from the right has a bad thermal contact. The second picture of the defrosting sequence (some hundred milliseconds later) shows the first three tiles at the right fully defrosted. Of the next three tiles the one in the middle (tile 6) is clearly delayed with respect to its neighbours (tiles 5 & 7) and we conclude that tile 6 also has a reduced thermal contact.

Finally on the last picture of the defrosting sequence we see that tiles 3 and 4 are clearly delayed.

Fig. 5: Defrosting of an accelerator grid with some blocked water channels

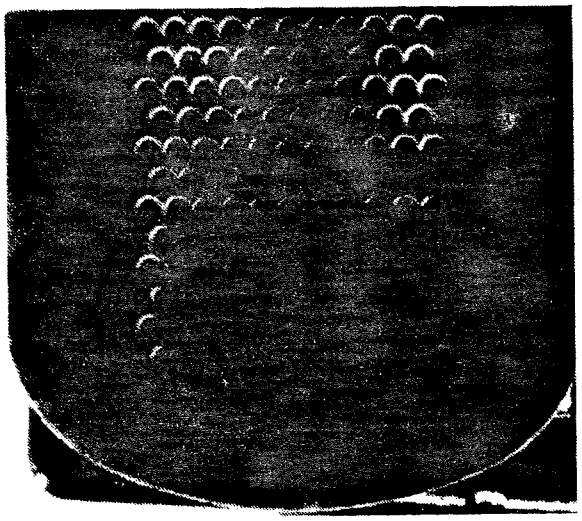

The test is carried out as with the divertor test sections: The grid is cooled down in a freezer, frosted over and heated to room temperature with tap water flowing through the grids.

The result of the defrosting test is shown in Fig. 5. The first five channels from left to right are blocked by the internal frozen water in the channel,

Fig. 6: Warm-up sequence of Fig. 5 recorded with a thermal imaging system.

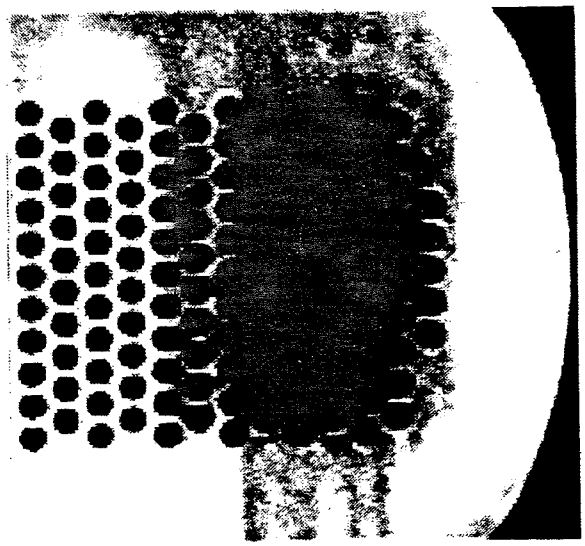

the next cooling channel (channel 6) is free, channel 7 is blocked, and all the channels right from channel 7 are free. The same defrosting sequence was also monitored with an infrared imaging system and the result is shown in Fig. 6. The grey scale in Fig. 6 matches that of Fig. 5 with black for warm (unfrosted) and white for cold (frosted). Again we can identify blocked channels but the resolution from defrosting appears to be better. In fact using the complete defrosting sequence the detailed structure of the cooling channels can be visualised. Fig. 7 shows a frame in which the water is supplied from the left. We can see the water manifold at the left and the individual channels leading into the grid area. We can also see the individual channels exiting from the grid at the right.

Fig. 7: Defrosting frame of a n accelerator grid showing the left water manifold and the cooling channels.

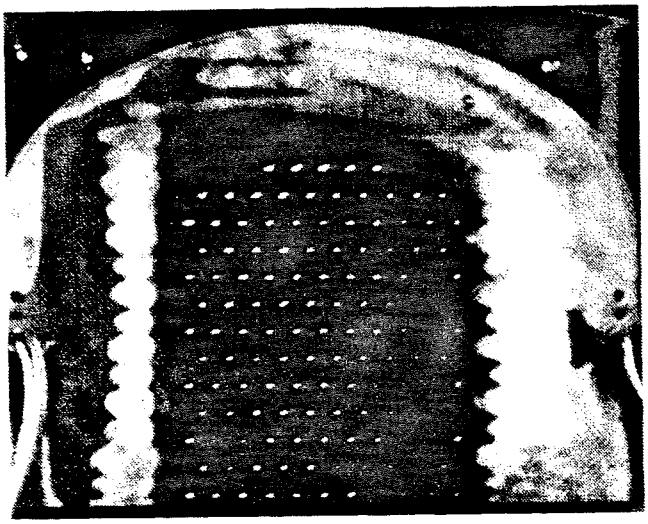

1 A Cardella et al , Fusion Technology 1992, pp 211- 215 Proceedings of the 17th SOFT, Rome, Italy, 14-18 Sept. 1992.

2 M Araki et al, Fusion Technology 1992, pp 166 - 170, Proceedings of the 17th SOFT, Rome, Italy, 14-18 Sept. 1992G.

3 P Adorno et al, Fusion Technology 1992, pp 339 - 343, Proceedings of the 17th SOFT, Rome, Italy, 14-18 Sept. 1992.

4 Panasonic video cassette recorder AG - 7355, COHU 4710 CCIR series monochrome solid state CCD camera.

Temperature profile (top) and the light emission after exposure (bottom) confirm that the thermal contact of tiles 3 and 4 is strongly reduced, that of tiles 6 and 10 is slightly reduced compared to the good tiles.

In all tests we observed that end tiles defrost considerably faster. This is clearly seen in Fig. 2. A consequence of that is, that a fault on the end tiles is somewhat harder to identify.

We can also see in Fig. 3 that the defrosting starts from the point which is closest to the cooling pipe. The first (top) picture of the defrosting sequence shows clearly that the side surface defrosts faster than the top surface. The reason is the reduced distance between surface and cooling pipe which is 6.8 mm for the top surface and 3.2 mm for the side surface. Both observations clearly prove, that the time of defrosting is defined by temperature rather than surface conditions.

Fig. 3: Defrosting sequence of a CFC test section pre-cooled to - 15 °C with the temperature profile after exposure at the top, the defrosting sequence in the middle and the light emission after beam exposure at the bottom.

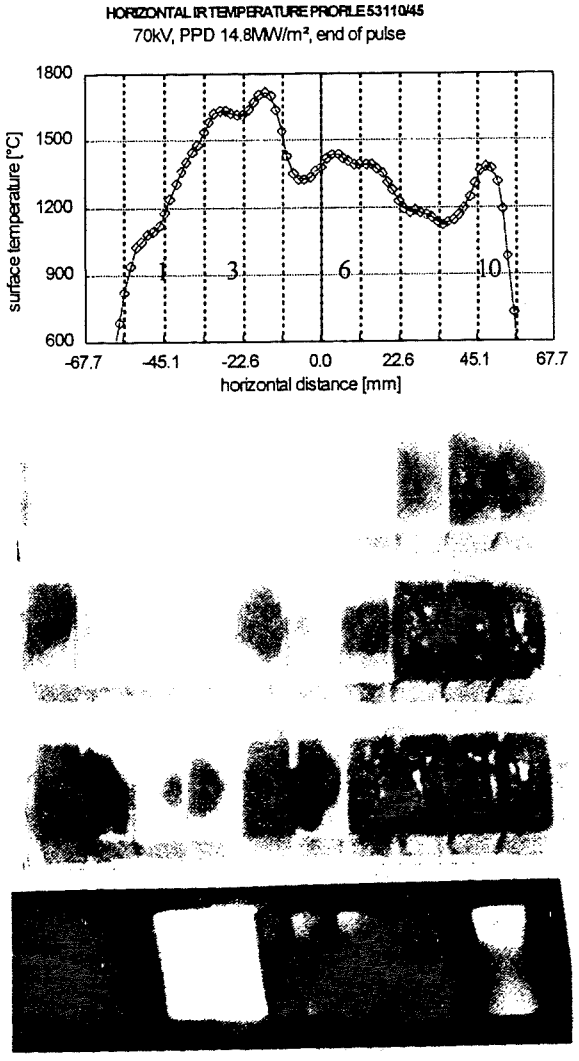

3.2 Accelerator grids

The accelerator grids of the JET beam injection sources are actively cooled. Small cooling channels are embedded into the copper as shown in Fig. 4. The grids are made by electro-deposition with the cooling channels filled with a conducting wax onto the copper base plate. Then copper is built up by electrodeposition over the top of the base plate and the cooling channels. After the electrodeposition the wax is removed. The wax does not give a good contrast on X-ray pictures and it is difficult to check if the wax has been removed quantitatively. To check if the defrosting method could be applied, we deliberately left some water in the cooling channels of the grid prior to cooling the grids. This water will cause some blockage of cooling channels which should be identified by the defrosting test.

Fig. 4: Schematic of the actively cooled JET injector grids showing the cooling channels between the grid holes.

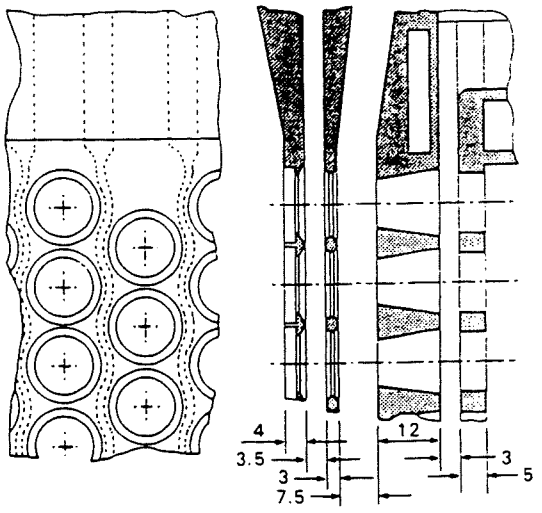

Grid No.	1	2	3	4	
Voltage	80	73	-2	0	kV
Cooling Channel Depth	1.8	1.4	2.4	2.4	mm
Cooling Channel Width	1.4	1.4	2.4	2.4	mm

Light Emission from Graphite Surfaces during Beam Bombardment, Observation and Consequences for use of Graphite in Divertors

D Ciric, H D Falter, P Massmann, K N Mellon.

JET Joint Undertaking, Abingdon, Oxon, OX14 3EA, UK.

A substantial amount of visible and infrared light is emitted from the target surface during the bombardment of graphite and carbon fibre composite targets by high power particle beams. The emission is caused by the presence of a micron size carbon particles loosely bound to the target surface which reach the radiation equilibrium with the incoming beam within milliseconds. The carbon particle coverage can be reduced by extensive high power beam (≥15 MW/m²) bombardment and can be correlated with methane release from carbon targets. These observations have important consequences for the use of such materials for plasma facing components in, e.g., divertors.

1. INTRODUCTION

During the design phase of the JET MkII divertor [1] tests of a large number of graphite samples from many different manufacturers have been carried out at JET Neutral Beam Test Bed. These tests show that a substantial amount of visible and infrared light is emitted from the tile surface during the bombardment of the tile by hydrogen and helium beams with power densities ranging between 5 and 30 MW/m². The effect was observed on both actively cooled and inertial tiles made of various Carbon Fibre Composite (CFC) materials.

A quantitative explanation for the observation made under all experimental conditions has been developed by assuming the presence of small particles (micron size) which are loosely bound to the target surface. These rapidly achieve radiation equilibrium with the incident power density. Consequently, particles heat up to high temperatures where sublimation rates are not negligible.

2. EXPERIMENT

CFC tiles are placed at the beam centre line of the JET Neutral Beam Test Bed at a distance of 7 metres from the beam source (Figure 1). Tiles are exposed to particle beams with peak power densities ranging between 5 and 30 MW/m², with a pulse duration between 0.5 and 10 seconds. Beam power density distribution along two lines perpendicular to the beam axis is measured by an array of inertial copper blocks (inertial calorimeter).

The CFC target surface temperature distribution is measured by an AGEMA Thermovision 900 SW infrared imaging system. Infrared (IR) images are recorded at a rate of 15 Hz. One-dimensional line images are recorded at faster rates - up to 2.55 kHz. The IR imaging system has a temperature range 0 - 2000°C and the accuracy of 1%. Several thermocouples are used to monitor the CFC target bulk temperature. The emissivity of the target is determined from the comparison between IR and thermocouple signals when the target is heated up to a thermal equilibrium at several hundred °C.

Every beam pulse is recorded using two CCD video cameras. The methane release from the target during the beam pulse is monitored by measuring the corresponding gas flow rate with a residual gas analyser.

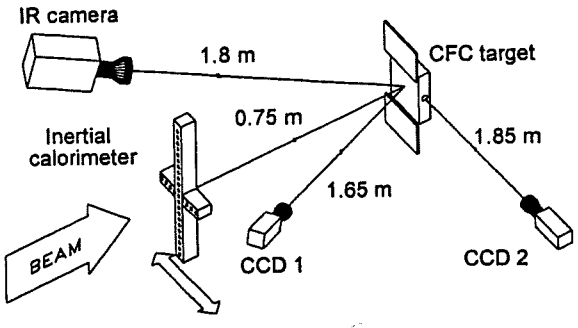

Figure 1: Layout of the experiment.

2. OBSERVATIONS

Intensive infrared light emission distorts the signal recorded by the thermal imaging system used to asses thermal properties of the CFC material. This is illustrated on Figures 2 and 3. Figure 2 shows two images of the Mitsubishi MFC-1 tile exposed to a 17 MW/m² hydrogen beam for 0.5 s. Only the second image, recorded after the beam pulse, reflects the true surface temperature of the CFC target. This is clearly visible from temperature distributions (Figure 3) derived from IR images shown in Figure 2. The temperature distribution in Figure 3.a shows "hot spots" attributed to the high temperature carbon particles. It should be noted that the target was machined by grinding and ultrasonically cleaned before the experiment. Images similar to those shown in Figure 2 were also recorded by video cameras.

A rapid step change in the surface temperature is observed when the beam is switched on or off. Figure 4 shows the fast time trace (0.39 ms resolution) of the Dunlop DMS-704 CFC target exposed to 30 MW/m² modulated hydrogen beam. The time constant of this step change in surface temperature is in the millisecond region. The "noise" present in the infrared signal during the beam on periods corresponds to the fluctuations in the power density caused by the variation of the beam current. This target was also machined by grinding but was not cleaned ultrasonically before the test.

Particle sizes in the range 1-10 μm can be inferred from the measured radiation characteristics in agreement with that observed for the size of particles which can be mechanically removed from the surface.

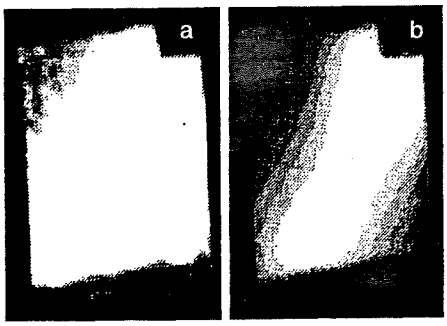

Figure 2: IR images of the Mitsubishi MFC-1 target exposed to 17 MW/m² Hydrogen beam for 0.5 s: a) end of pulse, b) 0.1 s after the end of pulse.

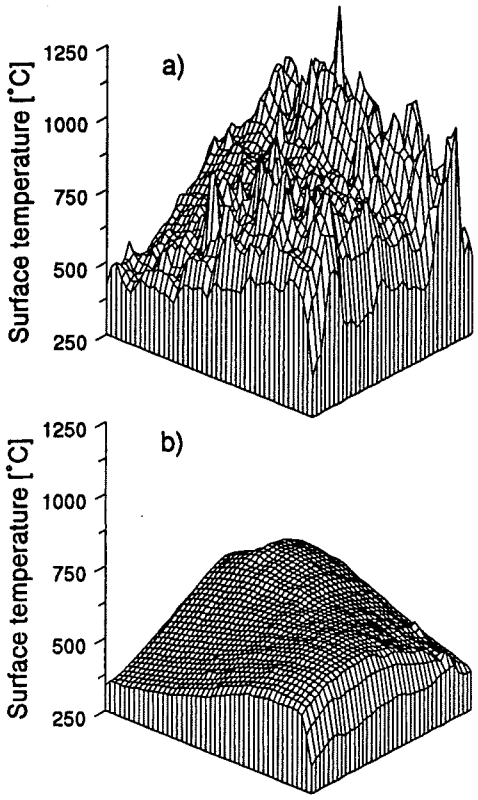

Figure 3: Temperature distributions of the MFC-1 target derived from IR images shown in Figure 2.

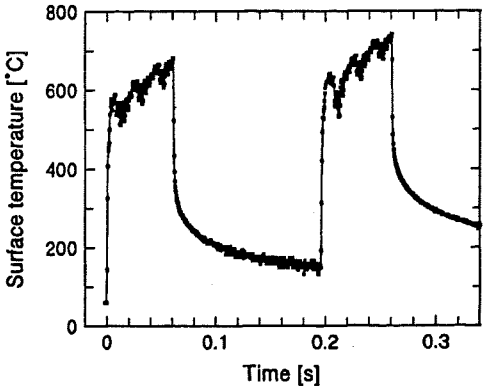

Figure 4. Surface temperature trace of the Dunlop DMS-704 target exposed to 30 MW/m² modulated Hydrogen beam.

Similar effects were observed for practically all CFC materials tested (more than 15 samples made by 5 different manufacturers). In some cases only isolated high temperature "islands" were observed, while for some materials the entire surface of the tile

was radiating at very high temperature during the beam pulse. The intensity of the radiation was much higher for targets which were not ultrasonically cleaned prior to the test. It was also observed that the amplitude of the temperature step increases with the beam power density.

3. MODEL

We assume that the radiation power density $W(T_M)$ measured by the IR imaging system is a linear combination of two signals: one representing the true surface temperature of the material - $W(T_B)$, and one representing the temperature of the carbon particles loosely bound to the CFC target - $W(T_P)$. The weighting function is the carbon particle coverage θ (≤ 1):

$$W(T_M) = \theta\, W(T_P) + (1-\theta)\, W(T_B). \quad (1)$$

The radiation power density $W(T)$ is determined by the instrumental function of the IR imaging system which is:

$$W(T) = \frac{R}{\exp(B/T) - F}, \quad (2)$$

where R, B and F are calibration constants.

The temperature of the carbon particles (T_P) is determined from the radiation equilibrium condition:

$$p = f \sigma T_P^4, \quad (3)$$

where p is the beam power density, σ is the Stefan-Boltzman constant and f is the form factor determined by the ratio of the radiating and absorbing area of the particle. Form factor f (the only free parameter in the model) is determined by the shape and the orientation of the particle with respect to the incoming heat flux. For the particle of spherical shape the value of f is $4\pi r^2/\pi r^2 = 4$. For particles of irregular shapes one could expect values of $f \sim 10$. Figure 5 illustrates the influence of the form factor f on the particle temperature. The heat conduction from the high temperature particle to the target material is neglected in the model, but can be introduced by an increase in the value of f.

The surface temperature of the bulk material will initially follow the $t^{1/2}$ law:

$$T_B(t) - T_{B0} = p A \sqrt{t}, \quad (4)$$

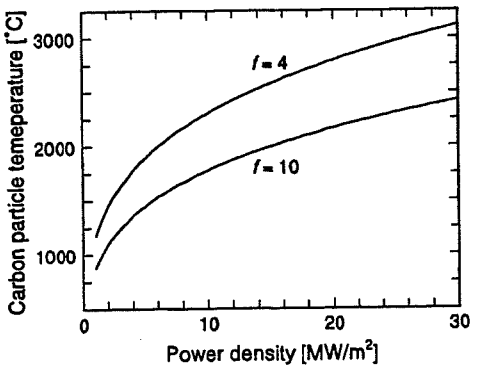

Figure 5. Carbon particle temperature determined from the radiation equilibrium condition.

where T_{B0} is the bulk surface temperature prior to the beam pulse, p is the beam power density, t is time and A is the parameter determined by thermal properties of the material.

The surface coverage θ and parameter A can be determined by the least square fit of the equation (1) to the IR camera signal - $W(T_M(t))$. Since thermal properties of CFC materials are temperature dependent, the parameter A also varies with temperature. To avoid this uncertainty, the fitting procedure should be restricted to a fixed temperature range (e.g. 300 - 1000°C), in which case the value of A remains constant. The typical result of the fitting procedure is shown in Figure 6.

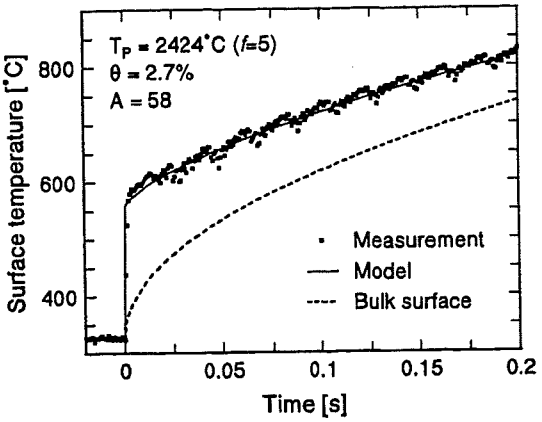

Figure 6. Initial surface temperature rise of the Dunlop DMS-704 target exposed to 15 MW/m² hydrogen beam.

4. RESULTS AND DISCUSSION

The amplitude of the step change in the surface temperature is the measure of the carbon particle

coverage. This temperature step was observed on all investigated targets. The surface particle coverage of up to 10% was deduced by applying the above described model with $f = 5$. It should be noted that the particle coverage is dependent on the value of the form factor f. Nevertheless, by applying one fixed value of f, the relative change of the particle coverage during the test can be determined with reasonable accuracy.

It was established that the amplitude of the step, and hence the surface coverage, can be reduced by extended exposures of the target to high power (≥15 MW/m²) particle beams. In some experiments the methane release from the target during its exposure to the beam was measured. We found that the methane production can be correlated with the particle coverage (Figure 7).

For some of the tested samples the step change in the surface temperature was not observed in the initial stages of the experiment. For those targets the measured surface temperature follows the $t^{1/2}$ law (left diagram in Figure 8). However, after extended exposures to high power particle beams the reappearance of the temperature step corresponding to low particle coverage was found. Figure 8 shows time traces of the surface temperatures at the beginning and at the end of one such test. The Dunlop DMS-704 sample, which was machined by milling and ultrasonically cleaned before the test, was exposed to a sequence of 2 s long hydrogen beam pulses at 15 MW/m². The result of the test was that the surface coverage was gradually increased during the course of the experiment to a saturation value of 0.8%.

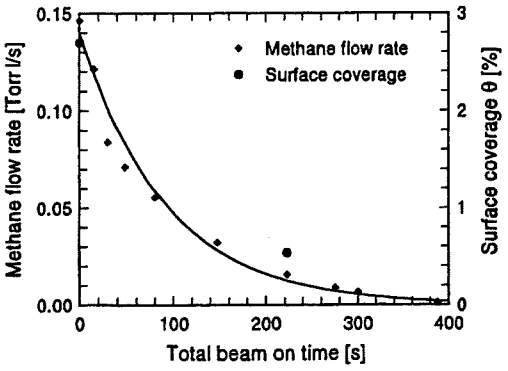

Figure 7. Methane release and carbon particle coverage during the endurance test of the Dunlop DMS-704 using 15 MW/m² hydrogen beam. The target was not cleaned ultrasonically prior to the test.

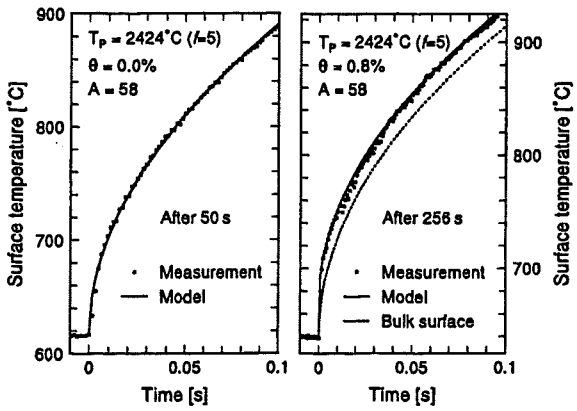

Figure 8. Temperature traces recorded during the endurance test of the Dunlop DMS-704 using 15 MW/m² hydrogen beam. The target was cleaned ultrasonically prior to the test.

Our findings can be summarised as follows:

- *The presence of high temperature carbon particles loosely bound to the CFC material surface should be taken into account when interpreting IR thermometry data.*
- *The initial coverage of the surface by these particles can be shown to be ≤10% and reduces to ≤1% by extended exposure to the high power beam.*
- *Initially particle-free tiles develop a low coverage (≤1%) after long exposures to high power beams.*

These observations have important consequences for the use of CFC materials as plasma facing components. They suggest that, in terms of impurity production, the surface condition of the material could be at least as important as its bulk thermal properties. Although we have shown that the surfaces can be cleaned (conditioned) by extended exposure to high heat fluxes, this would translate into many tens or even hundreds of plasma discharges. Further work is required to assess the in situ wall cleaning or conditioning in terms of the removal of micron sized particles.

REFERENCE

1. H. Altmann *et al.*, "Design of the JET MkII Divertor with Large Carbon Reinforced Carbon CFC Tiles", These proceedings

Beam Profiles Measurement using a Unidirectional CFC-Target and Infrared Imaging

D Ciric, H D Falter, J G A Fanthome,
P Massmann, K N Mellon.

JET Joint Undertaking, Abingdon, Oxon, OX14 3EA, UK.

We present a new high resolution beam diagnostic system for particle beams at MW power levels. The technique combines unidirectional properties of the Mitsubishi MFC-1 material with infrared imaging, and is used to measure the two-dimensional beam power density distribution. The application of the technique is demonstrated in characterisation of energetic neutral particle beams extracted from the JET high current tetrode ion source.

1. INTRODUCTION

Accurate measurements of the properties of energetic particle beams is important for beam handling and injection into tokamaks. Beam alignment, divergence, and power density distribution are critical parameters which affect overall injection efficiency. Incorrectly aligned or focused beams can cause serious damage to beamline components.

Common techniques used for high power beam diagnostics are inertial and water calorimetry [1], where power density is determined from the thermal response of copper blocks or cooling fluids. Both techniques provide one-dimensional beam profiles.

We developed a new high resolution diagnostic to measure the properties of energetic particle beams. Two-dimensional beam profiles are determined from the thermal response of highly anisotropic Carbon Fibre Composite (CFC) target exposed to energetic particle beams.

2. MEASUREMENT TECHNIQUE

The 40 mm thick 150×200 mm² CFC target (Mitsubishi MFC-1) is placed at the beam centre line of the JET Neutral Beam Test Bed at a distance of 7 metres from the beam source (Figure 1). The target is exposed to particle beams with peak power densities ranging between 5 and 30 MW/m², with a pulse length $\leq$ 0.5 s. Power density distribution along two lines perpendicular to the beam axis can be measured by an array of inertial copper blocks (cross calorimeter). The surface temperature of the

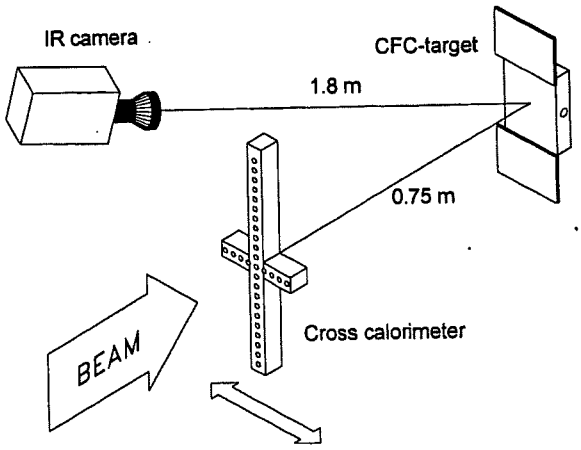

Figure 1. Experimental layout.

target is measured by an AGEMA Thermovision 900 SW infrared imaging system. Infrared (IR) images are recorded at a rate of 15 Hz. The IR imaging system has a temperature range 0-2000°C and the accuracy of 1%. Several thermocouples are used to monitor the CFC target bulk temperature. The emissivity of ε=0.8 is determined from the comparison between IR and thermocouple signals when the target was heated up to a thermal equilibrium at several hundred °C.

Figure 2 shows two IR images of the CFC target recorded 0.15 seconds after the target was exposed for 0.3 seconds to a 25 MW/m² Helium beam. The first image clearly shows two separate beams originating from two grid halves of the JET high current tetrode PINI. The second image was obtained for the same ion source parameters, except that the beam was steered so that the upper half of

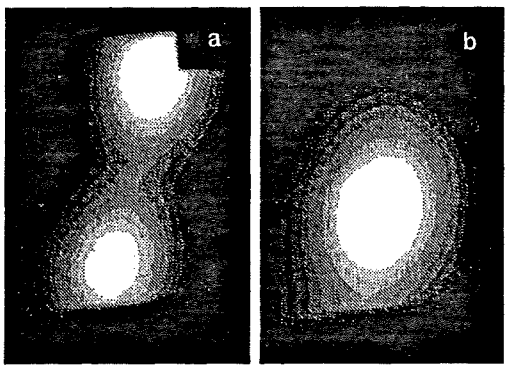

Figure 2. Infrared images of the CFC target exposed to a 25 MW/m² Helium beam for 0.3 s.

the beam is centred on the target. The footprint of the beam is clearly visible long after the pulse. This is illustrated in Figure 3, where the horizontal profile through the beam centre (Figure 2.b) is plotted versus the elapsed time after the pulse. The temperature is corrected for the initial target temperature.

The fact that the target surface temperature distribution reflects the beam power density distribution long after the beam pulse is the consequence of the unidirectional thermal properties of the Mitsubishi MFC-1 target. This material has high thermal conductivity in the direction of the beam (k_z) and low lateral thermal conductivity ($k_{x,y}$)

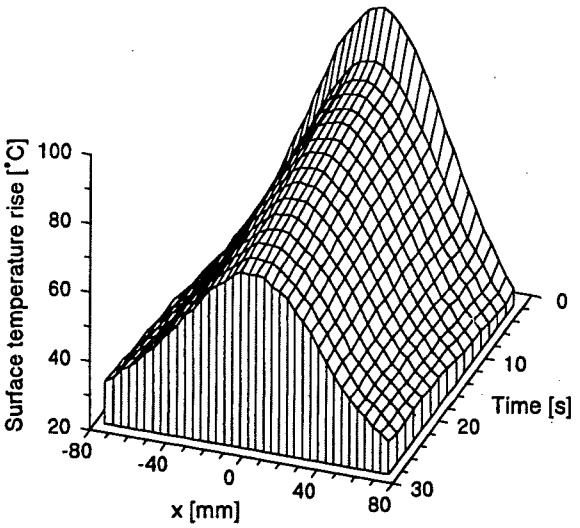

Figure 3. Horizontal temperature profile through the centre of the beam during the target cooldown.

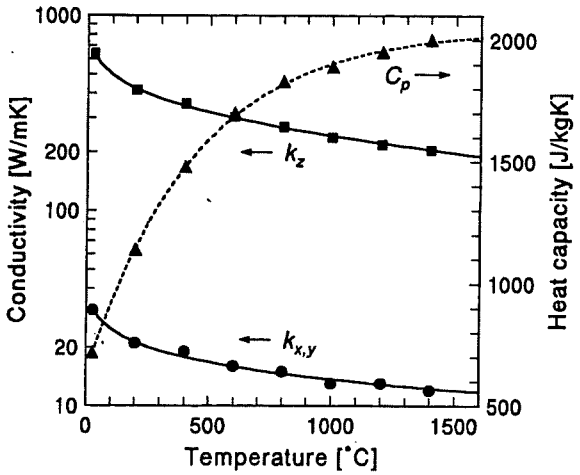

Figure 4. Thermal properties of the MFC-1 target.

[2]. The ratio $k_z/k_{x,y} \approx 20$ remains practically constant over the wide temperature range (Figure 4). For that reason the thermal equilibrium in the beam direction is reached within seconds while the lateral thermal equilibrium is reached after ~10 minutes.

3. POWER DENSITY EVALUATION

The particle beam power density distribution can be obtained by normalising the surface temperature to the power density determined by the inertial calorimeter. However, as thermal properties of the Mitsubishi MFC-1 material are known, it is possible to determine the power density directly from the temperature distribution.

The relation between the beam power density and the target temperature is

$$p = \frac{T - T_0}{F\tau}, \qquad (1)$$

where p is the power density, τ is the pulse length, and T and T_0 are the equilibrium target temperatures before and after the pulse. If the material properties do not vary with temperature, F is a constant determined by the size , density and heat capacity of the inertial block. Factor F defines the increase in equilibrium temperature per unit energy density on the target. Since thermal properties of the MFC-1 material are strongly dependent on temperature, one should run a finite element code to determine the factor F which is, in this case, temperature dependent - $F=F(T_0)$. It is sufficient to run the code

in a one-dimensional approximation due to the highly anisotropic thermal conductivity of the material. To check this assumption, the measured surface temperature for power densities of 9.8 and 4.4 MW/m² and the beam pulse length of 5 s is compared to the results of TOPAZ2D [3] finite element simulation in Figure 5. The numbers in brackets are the actual power densities used in the simulation.

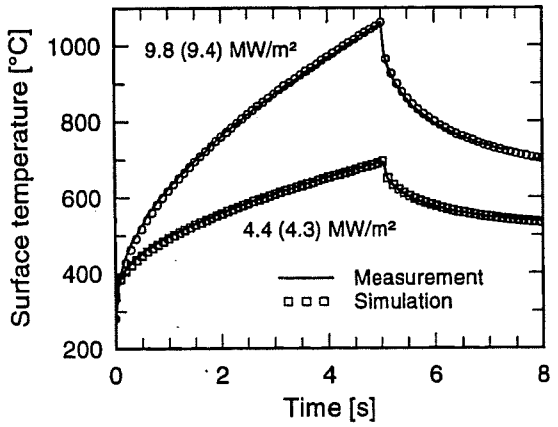

Figure 5. Surface temperature of the MFC-1 target exposed to high power hydrogen beam for 5 s.

The time required to reach thermal equilibrium is dependent on the energy deposited on the target. To avoid long cooldown times, the maximum energy density should be below 10 MJ/m². The finite element simulation was used to determine function $F(T_0)$. The initial target temperature was varied between 25 and 250°C for the heat flux range 1-50 MW/m². The energy flux was maintained at 3 MJ/m² by varying the heat flux pulse length between 0.06 and 3 s. Calculated values of $F(T_0)$ decrease from 16 to 10 °Cm²/MJ for the considered temperature range and 40 mm thick MFC-1 target. From the measurements (and simulation) we found that the target is in thermal equilibrium (in the beam direction) after ~4s.

Power density at point (x,y) on the surface is determined by:

$$p(x,y) = \frac{T(x,y) - T_0(x,y)}{F(T_0)\tau}. \qquad (2)$$

T and T_0 are surface temperatures before and 4s after the beam pulse.

A computer code was developed to calculate power density distribution from two IR images. The code reads binary image files and transforms them into a rectangular $p(x, y)$-grid. The code requires 4 reference points on the IR image defining a rectangle in the (x,y)-space. Surface temperature at point (x,y) is determined by overlaying the rectangular mesh on an IR image and by calculating the temperature in the grid nodes from the temperature in the four neighbouring pixels. The code produces power density contour plots or colour zone plots and runs under MS-Windows. The code also provides tools for interactive analysis of the beam power density distribution (normalisation, averaging, curve fitting, profiles, etc.).

RESULTS AND DISCUSSION

The technique described above was used to analyse the properties of particle beams from the JET high current tetrode PINI 11A. As an illustration the power density contours for a 51 kV, 17.5 A Helium beam are shown in Figure 6. This power density distribution is obtained from the IR image shown in Figure 2b. The peak power density is above 25 MW/m² and the beam divergence is 0.38°.

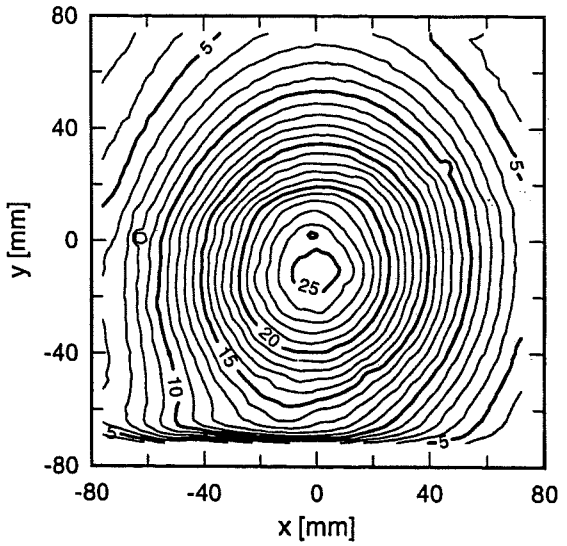

Figure 6. Power density contours of the 51 kV, 17.5 A Helium beam.

The one-dimensional beam power density profiles measured by conventional inertial and IR calorimetry agree very well (Figure 7). The error bar in Figure 7 represents 5% standard deviation which, in this particular case, corresponds to 1.3°C. From Figure 7 we can conclude that the noise level in the IR calorimetry is considerably lower, and that the resolution of this method is much higher - for 1.8 m distance between the target and the IR camera the resolution is ~2×2 mm².

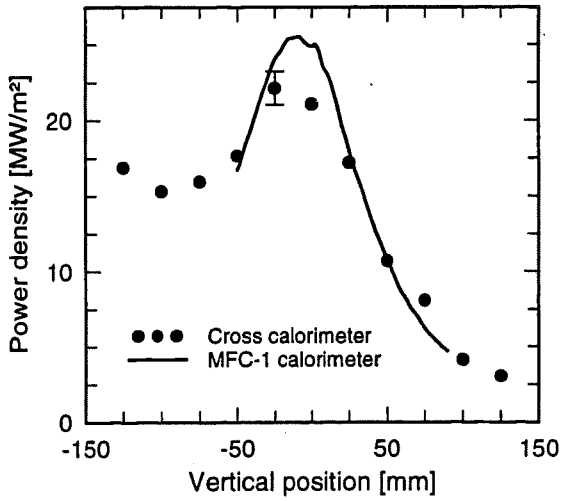

Figure 7. Comparison between conventional and infrared calorimetry.

Although the lateral heat diffusion is significantly lower then the longitudinal one, it is not negligible (Figure 2). To account for this effect the power density distribution is determined by normalising the temperature distribution recorded immediately after the pulse to the equilibrium one.

The IR calorimetry using the anisotropic CFC target is far superior compared to the conventional calorimetry methods. This is clearly demonstrated by power density distribution shown in Figure 8. The power density contours shown in Figure 8 correspond to the IR image given in Figure 2a. The horizontal profile along the y=0 line shows perfectly aligned beam with peak power density of ~14 MW/m², while the actual beam has two separate components with peak power density of 25 MW/m².

The resolution of the IR calorimetry is considerably higher, the accuracy is comparable, and the information much more detailed then in the conventional calorimetry. Since the CFC target can withstand temperatures in excess of 1500°C, the IR calorimetry can be used for very high power beams (>200 MW/m²). One limitation of the method is relatively short pulse length. To avoid overheating of the target, the maximum energy density should be below 10 MJ/m². The method does not require very fast IR imaging systems as the time between two recorded images is a few seconds.

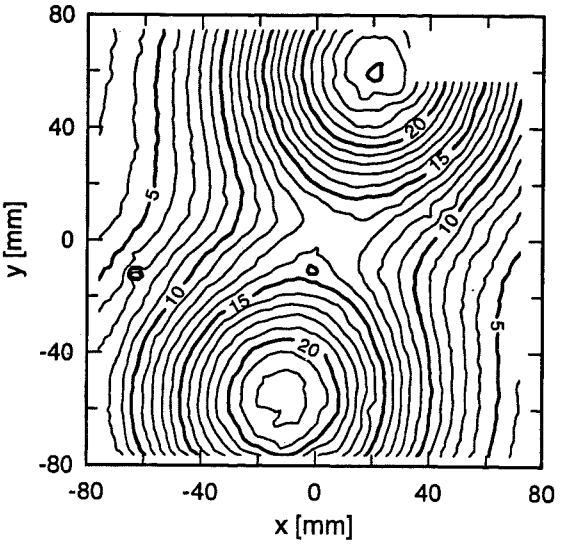

Figure 8. Power density distribution for a 51 kV, 17.5 A Helium beam (infrared image in Figure 2a).

A new 20 mm thick 400×200 mm² calorimeter made of Mitsubishi MFC-1A material is presently being constructed and will be used for the characterisation of the JET neutral injector ion sources as a routine diagnostic.

ACKNOWLEDGEMENT

We would like to thank the Mitsubishi Kasei Corporation for providing us with the MFC-1 and MFC-1A targets.

REFERENCES

1. P. Massmann *et al.*, Proceedings of the VII International Conference on High-Power Particle Beams, Karslruhe, Germany, 1988, p. 1449.
2. M. Araki, private communication.
3. A. B Shapiro, UCID-20824, Lawrence Livermore National Laboratory, 1986.

Progress on the Inactive Commissioning and Upgrade of the JET Cryogenic Distillation System

P Boucquey, C Morf[1], F Delvart, J Mart.

JET Joint Undertaking, Abingdon, Oxon, OX14 3EA, UK.
[1] Sulzer Chemtech Winterthur, Switzerland.

The JET Active Gas Handling System (AGHS) is now fully installed and most subsystems have been or are being commissioned. In particular, the Cryogenic Distillation System (CD), dedicated to the separation of hydrogen isotopes has been successfully tested with H/D mixtures.

Eight commissioning runs totalling 4237 h of operation were carried out from February 1991 to December 1993. Minor deficiencies revealed during the tests have been corrected and since then the plant has operated very reliably. Protium of very high purity (>99.9996%) and fairly pure deuterium (>99.998%) were produced on a continuous mode.

The CD system fully meets its specifications for H/D separation. Commissioning with tritium will then take place mid 1995 to demonstrate that the CD system is capable of detritiating protium down to a very low level of HT (less than 5ppb).

1. INTRODUCTION AND STATUS OF THE AGHS

The tritium phase of the JET Joint European Torus is presently planned to be conducted in 1996. In preparation for this phase, JET has built a fusion fuel processing facility[1, 2]: the Active Gas Handling System (AGHS). This system is designed to collect exhaust gases from the torus and its associated systems, remove impurities (mainly tritiated water and tritiated methane) and separate the hydrogen isotopes into pure species which will be recycled to the torus. The AGHS is capable of processing a daily throughput of 5 moles of tritium mixed with 15 moles of deuterium and 150 moles of protium. Fig 1 presents the overall AGHS flow diagram.

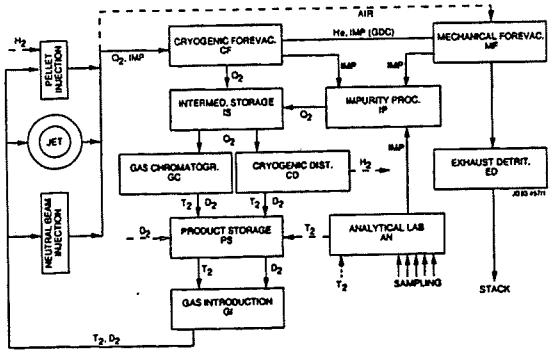

Fig 1: Overall AGHS flow diagram

All the subsystems except the Gas Introduction System have been commissioned successfully with hydrogen, deuterium and other test gases[3].

The commissioning of the interconnecting lines between subsystems and the operation of several subsystems as a whole (ie: CD, IS, PS, AN) is now well under way.

Tests of the safety related devices and commissioning of the hardwired safety interlocks are currently in progress.

Tritium commissioning of the AGHS is due to start by the end of 1994.

2. AIM AND DUTIES OF THE CRYOGENIC DISTILLATION SYSTEM AT JET

The Cryogenic distillation system (CDS) is designed to process in parallel:

- a high protium/low tritium stream coming from the Multi Pellet Injector
- a DT mixture recovered from the torus and its auxiliaries

The tritium concentration in the feed gases is expected to range from 1 to 27 atom percent.

The products specifications require the deuterium and tritium streams to be enriched to 99%. The protium product must contain less than 5ppb of tritium to be released to atmosphere with a negligible impact on the environment (10Ci/y).

3. PROCESS DESCRIPTION

The CDS (Fig 2) comprises three interconnected packed columns working at cryogenic temperature (18 to 26K) and two room temperature equilibrators. The columns are housed in an 11m high stainless steel vessel working as a secondary containment kept under vacuum (p<10-6mbar) by sputter and getter pumps. This vessel is thermally insulated and actively cooled by a circulation of 18K helium through copper coils surrounding the thermal shields. Fig 3 shows a view of the process components when the process cold box and the shielding are removed.

The columns are filled with a stainless steel packing which promotes the isotopic separation due to the difference in volatilities of the six isotopic species of hydrogen: H2, HD, HT, D2, DT, T2. The overall efficiency of the cascade is around 260 theoritical plates. The equilibrators are filled with a special catalyst to convert the mixed species into elemental protium, deuterium and tritium.

The driving force needed to circulate the gas throughout the cascade is given by four static transfer pumps.

The cascade is operated in recycle mode as long as the tritium concentration monitored by the on-line tritium ionisation chambers is out of specification, otherwise the production mode operates: pure protium, deuterium and tritium are drawn off from the top of column 1 and 3 and the bottom of column 3, respectively.

The refrigeration power needed to cool down the thermal shields, the column walls and the condensers is supplied by a Sulzer TCF20 helium refrigerator capable of delivering 528W at 16.9K. The temperature is controlled with an accuracy of 0.05K.

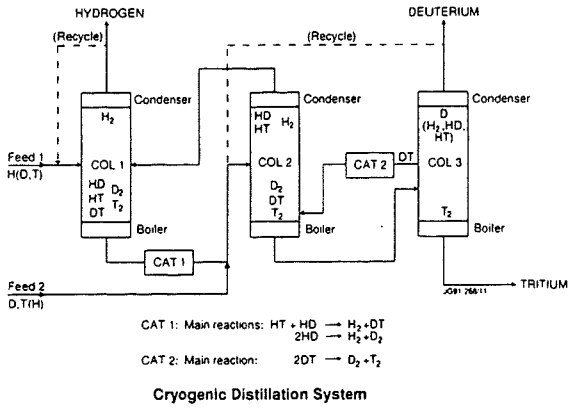

Fig 2: Flow diagram of the CD system

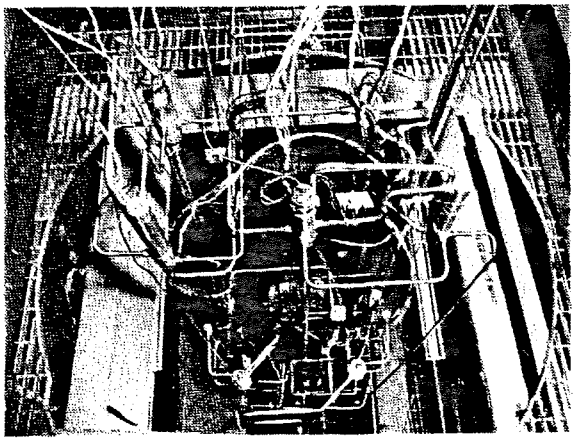

Fig 3: View of the process components with the secondary containment removed

4. SAFETY ASPECTS

A probabilistic and deterministic safety analysis has shown that probabilities of failures and their corresponding tritium emissions to the atmosphere were well below the safety guidelines. The plant has been designed to be safe and simple to operate.

The pressure in the columns is kept slightly above atmospheric pressure to avoid oxygen ingress. The primary process containment is built in compliance with high construction standards (ASME VIII) and was severely tested during the manufacturing, the erection and the commissioning. The overall leak rate in less than 1E-8mbar/l/s.

The process lines are double contained within stainless steel vessels capable of recovering up to 300% of the nominal gas load in case of emergency. Each vessel can withstand a pressure of 5bara.

Special care had also be taken during the design phase to minimise the tritium inventory into the system and finally, special components were developed to increase the reliability of the process to minimise the maintenance: ie static syphon pumps are used to drive the gas through the cascade instead of mechanical pumps which are prone to failure.

5. CONTROL OF THE COOLDOWN SEQUENCE

A dedicated automatic sequence controls the cooldown of the process. The coolant is first sent towards the columns' condensers, the column cooldown lines and the shielding of the cold box. When outlet helium temperature reaches 25K, the flow rates through the helium condensers are reduced

and the condenser controllers start to control around 10W the power delivered to the condensers. The reboilers heaters and their associated level controllers are switched on as soon as liquefaction takes place into the columns. Syphon pumps are switched on to establish internal recycling flows through the cascade. Pressure in the columns is also controlled around 1.2bara by adjusting the condensing power of columns 1 and 2. The cooldown lines are shut as soon as the hydrodynamic conditions in the system are stabilised to enable the column to work at near-adiabatic conditions. At this stage, the coolant is sent merely into the process condensers and the cold box shielding, the distillation cascade is in total reflux.

The cooldown sequence is achieved within 40 hours as indicated in the chart below (Fig 4). A cooling power of 200W is needed to run the process at its nominal design values (160W for the shielding, 40W for the gas liquefaction).

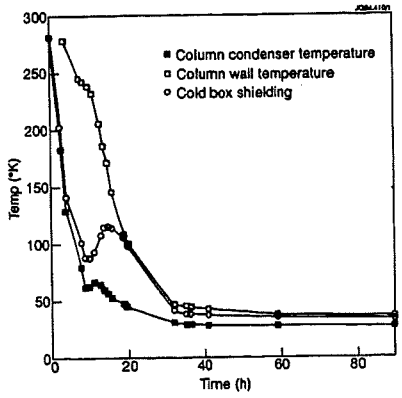

Fig 4: Cooldown curve

6. STUDY OF STEADY STATE AND DEUTERIUM TRANSPORT

Several 100-hour runs were carried out with protium and mixtures to study steady state conditions. The plant was running very steadily in all the operating configurations (Fig 5). Artificial disturbances created on flow rates and reboiler levels were settled down smoothly by the control loops. Nevertheless, we noticed a tendency to oscillations, probably due to the siphon pumps, when the columns are operated at high pressure drop (>8mbar).

The plant was operated in the recycle mode for 35 hours and gas samples were taken from the top of column 1 and the bottom of column 3. Protium purity removed at the top of column 1 was found to be better than 99.9985% whereas 99.977% deuterium was drawn off from the bottom of column 3 showing that deuterium transport occurred as expected through the distillation cascade.

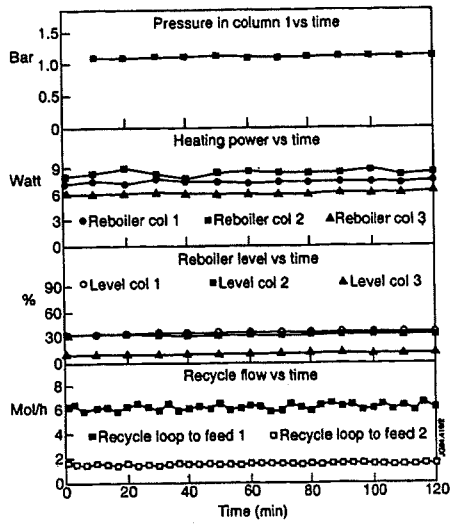

Fig 5: Steady state trends in normal operation

7. RESULTS OF ISOTOPE SEPARATION RUNS

Performance tests were carried out with a wide spectrum of hydrogen mixtures: [%H2,%D2]= [90,10], [80,20], [50,50], [25,75]. The distillation cascade was run on a continuous basis in the normal operation mode. Gas samples were taken at 8h interval from the product lines and analysed by high resolution mass spectrometry at CEA Bruyères Le Châtel, France.

Protium of very high purity (>99.9996 atom percent) and fairly pure deuterium (>99.998 atom percent) were produced in the system over long period of time (100h).

REFERENCES

[1] J L Hemmerich et al, "Key components of the JET Active Gas Handling System-Experimental programme and test results" Fusion Engineering and design 11 (1989), 93-100

[2] R Haange et al, "General overview of the Active Gas Handling Systems at JET", Fusion Technology, 14 (1989), 469-475

[3] J L Hemmerich et al, "Installation and Inactive Commissioning of the JET Active Gas Handling System", 15th SOFT (1993)

Transient Adiabatic/Isothermal Calorimetry Tests on JET Uranium Beds for Tritium Storage

L Serio, J L Hemmerich, R Lässer, P Milverton.

JET Joint Undertaking, Abingdon, Oxon, OX14 3EA, UK.
[1] CERN, 1211 Geneva 23, Switzerland.

ABSTRACT

Absorption of tritium on metal hydride beds is the safest and most compact method for storage of large inventories. Direct inventory assay in such storage beds is only possible by calorimetry. Ohmic heating tests were performed on JET uranium beds to evaluate their calorimetric characteristics in the power range from 0.5 to 10 watts (corresponding to tritium inventories of 1.5 to 30 grams T_2). It was found that the best reproducibility (±1% or ±0.1 watt, whichever is greater) can be achieved by cooling the U-beds with the test power (simulating tritium inventory) turned on and measuring the temperature rise rate at a fixed time (3 hours) after stopping the coolant gas flow. Data taken during this transient from adiabatic (start) to isothermal (temperature equilibrium) conditions are least affected by ambient temperature fluctuations and the quality of the insulating vacuum.

1. INTRODUCTION

A JET-design uranium bed (U-bed)[1] contains uranium powder in a horizontal primary container with a heat transfer structure for heating and cooling (figs 1 and 2).

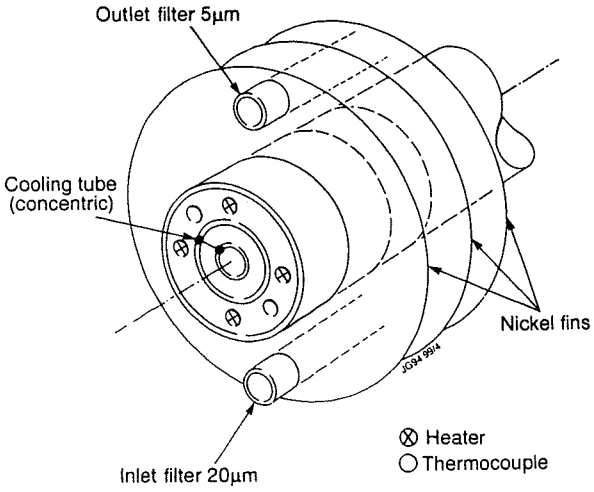

Fig 1: Sketch of the heat transfer structure of the JET U-beds

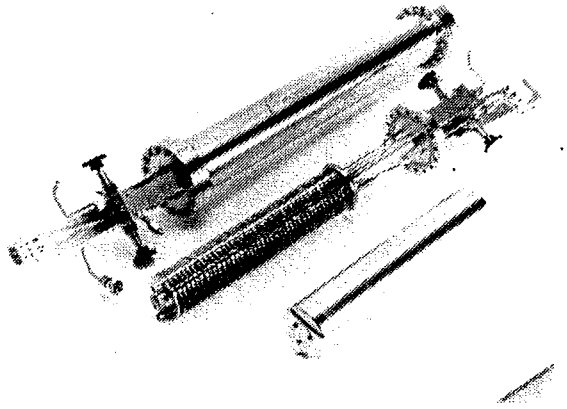

Fig 2: Photograph of the first and secondary containments of the JET U-beds

The U-bed consists of a central tube containing electrical heaters, vacuum furnace brazed in copper sleeves, and a concentric tube gas-cooling device. On its outside, it carries nickel fins transferring the heat flow from the core to the powder.

The primary containment is installed in a secondary containment and four of those assemblies are contained in an evacuated vessel. This tertiary containment offers the advantage of good thermal insulation by vacuum and permits implementation of calorimetry[2]. The accurate measurement of thermal energy released by the tritium in the storage bed is the easiest method to measure tritium inventories on

uranium hydride beds through the β energy released to the powder and the surrounding structure. The tritium decay heat is 0.324±0.001W/g[3]. This method requires only determination of the temperature rise of the U-bed, provided that the heat capacity of the complete structure and any heat flow through the containment walls is well defined. The central heat transfer structure of the U-beds provides near isothermal conditions throughout the primary containment, while the evacuated secondary and tertiary containment lead to predominantly radiative heat loss with some conduction through the support structure. Thus the temperature rise is related to the heating power, or tritium inventory, by the following energy balance equation:

$$C_p \, d\theta/dt = q - \alpha \, (\theta - \theta_0) - \beta \, (\theta^4 - \theta_0^4) \qquad [1]$$

where θ is the temperature of the U-bed, C_p its heat capacity, q the total amount of heat generated by the tritium decay inside the U-bed, α and β are the heat conduction and heat radiation coefficients and θ_0 is the environment temperature in which the U-bed is located (all the coefficients are strictly positive).

Equation [1] has two special solutions:

a) at the start of the measurement, where $\theta = \theta_0$, the rate of temperature rise together with C_p yields q directly (adiabatic);

b) at equilibrium, where $d\theta/dt = 0$, the heat coefficients α and β could be defined by runs at two different input powers (isothermal).

From our tests we found, however, that the best reproducibility of results was obtained during a transient condition, ie the temperature derivative measured at 3 hours after the start of each test run.

2. ANALYTICAL SOLUTION OF THE POWER BALANCE EQUATION

The energy balance equation [1] can be analytically solved in order to give the temperature evolution in time.

$$\int_0^t d\tau = \int_0^\theta f(T) \, dT \qquad [2]$$

$$f(T) = \frac{1}{\frac{q}{C_p} - \frac{\alpha}{C_p}(T - T_o) - \frac{\beta}{C_p}(T^4 - T_o^4)} \qquad [3]$$

$$F(\Theta) = \int_0^\theta f(T) \, dt \qquad [4]$$

From the Theorem Torricelli-Barrow, F(θ) can be derived in any interval starting from zero, in which f(T) is continuous. The integral in the above specified interval is a combination of two logarithms and the sum of a logarithm and the inverse function of the tangent. The full analytical solution can be found in reference [4].

3. EXPERIMENTAL SET-UP

During the calorimetry tests the secondary and tertiary containment were evacuated to better than 10^{-7}mbar to insulate the U-beds from the environment and to define the heat conduction path along the central tube, while the primary containment was filled with 100mbar helium for better heat transfer from the heaters to the structure. With tritium in the uranium powder this might not be necessary because the heating will be more homogeneously distributed through the uranium tritide powder. Later tests with tritium will be required to establish the correct measuring conditions.

The calorimetry system consisted of a thermocouple ice point reference (ISOTECH ZEREF 136), two pairs of already installed thermocouples for each of the eight U-beds, two thermocouples to measure the outside temperature of the housing and the flange of each tertiary containment unit, a DC power supply (30V, 2A) to ohmically simulate the presence of tritium in the U-beds by applying a defined power to the internal heaters, and a data acquisition system to record all the temperature and power data every 2.5 minutes.

The data acquisition system consisted of: 1 Personal Computer (486 with LabWindows software), IEEE interface card, Keithley 182 nanovoltmeter, Keithley 7001 Scanner with Keithley 7011 40 channel matrix card.

For a complete heat-up curve including asymptotic temperature measurements, the power was applied for seven days using the first day to determine the base line starting temperature by means of nitrogen gas cooling.

For temperature derivative measurements the heating and cooling time were reduced to 5 hours and 19 hours, respectively.

4. TEST RESULTS

Fig 3 shows typical results of the temperature evolution versus time for one U-bed operated at different power levels.

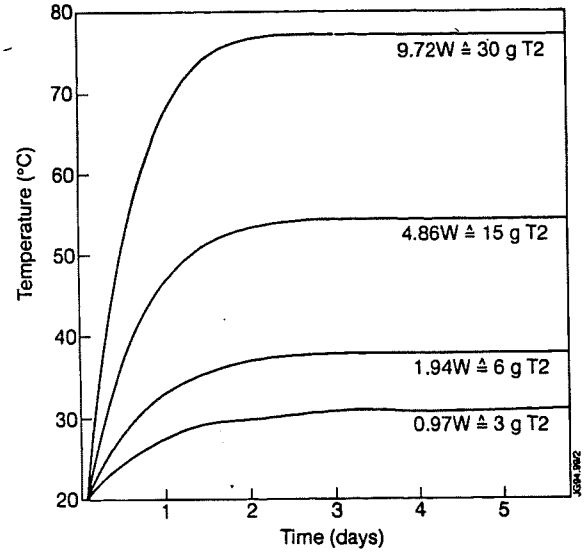

Fig 3: Temperature evolution versus time with cooling gas flow off (obtained by electrically simulating the decay heat of tritium)

The temperature (θ) response of the U-beds was measured as a function of electrical power (q) ranging from 0.5W ($\cong$ 1.5g T_2) to 10W ($\cong$ 31g T_2) and the data were fitted to calculate the three unknown parameters of the power balance equation: the heat loss coefficients for conduction (α) and radiation (β) were derived from the equilibrium temperature reached by the U-beds, and their heat capacity (C_p) was calculated from the temperature derivative at 3 hours after start of heating. The result for one U-bed is shown in fig 4.

The coefficients found were used in the analytical solution of the power balance equation and the results compared with experimental data (fig 3) from an additional test run. The decrease of the temperature (dot-dashed curve) after reaching a maximum is due to

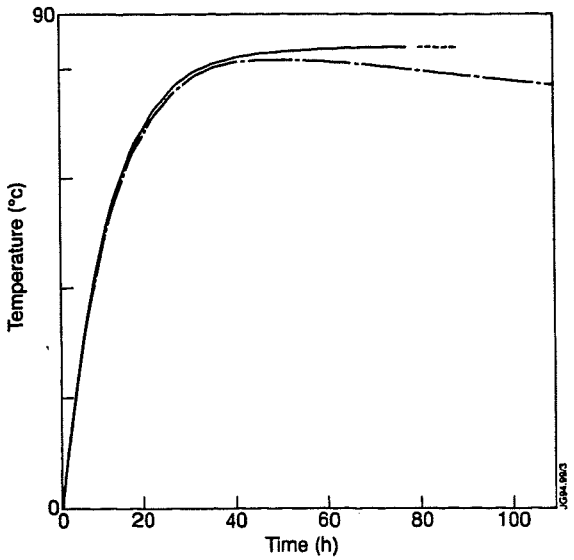

Fig 4: Comparison of analytical solution (solid line), raw data (dot-dashed line) obtained without continuously pumping the secondary and tertiary containments, and raw data (dashed line) obtained with continuously pumping the two containments. The electrical power applied was 9.2W.

increased conductive heat losses because the secondary and tertiary containments were not pumped continuously. This run also shows the sensitivity of equilibrium performance on the quality of the insulating vacuum: the "droop" of the experimental curve is caused by a gradual pressure rise from 1 x 10^{-7} to 3 x 10^{-5}mbar, increasing the thermal conductance losses, whereas the initial temperature rise is not affected.

A comparison between the applied heating power and the measured temperature derivative showed a power dependence of the heat capacity (fig 5). This is due to the fact that the mechanical structure contributes to the heat capacity (containment walls, support structure, etc). Through the radiative part of the heat transfer mechanism, this contribution leads to a temperature dependence of the time constants involved, which makes the effective heat capacity a function of heating power.

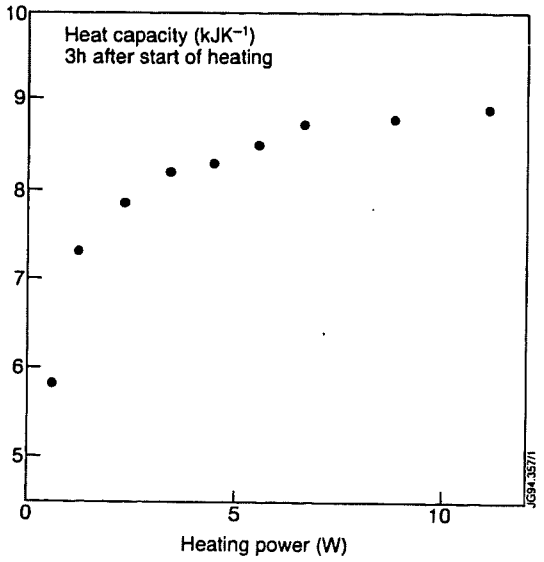

Fig 5: Variation of effective heat capacity with heating power

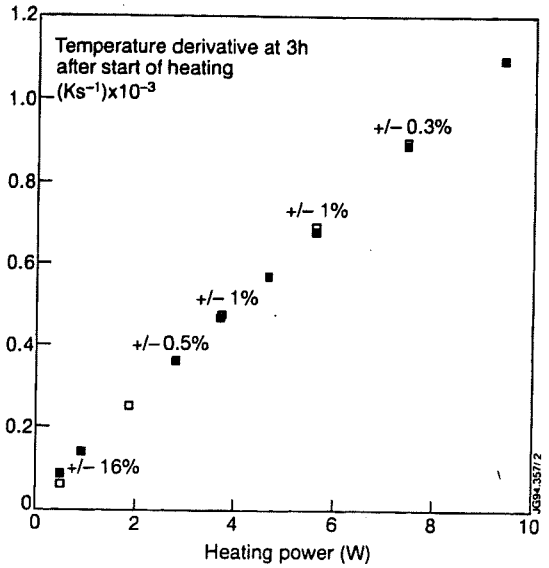

Fig 6: Calibration data of one of the eight JET U-beds for tritium storage

5. CONCLUSIONS

With the analytical solution of the energy balance equation it would have been possible to calculate, measuring the temperature, the tritium inventory in the U-beds at any time. Unfortunately the U-bed geometry and the heat conductive and radiative paths can not be described by the simple theoretical model given above. The model is only valid for a single heat capacity with isothermal surface, a single conduction path and radiative heat transfer to another isothermal sink at temperature θ_0. Without the homogeneous boundary conditions only the use of a finite elements analysis together with the temperature profiles in the U-bed and the surrounding structures would give accurate results.

An easier and reasonably accurate method is to use an empirical calibration curve to obtain the heating power as a function of the temperature derivative at a specific time after the start of heating.

This solution was finally adopted, ie electrical heating and gas cooling were applied for 12 hours, then the gas cooling was stopped and the temperature derivative measured 3 hours later. The calibration data of one of the eight U-beds thus obtained are shown in fig 6. The temperature derivative is plotted against the heating power.

The reproducibility of the results of this empirical method was found, after several runs using various powers between 0.5W (≈1.5g of T_2) and 10W (≈31g of T_2), to be better than +/- 1% or 0.1W, whichever is greater; the deviations are primarily due to ambient temperature fluctuations.

This performance is satisfactory for JET requirements. Future U-bed designs, however, should address the specific requirements of calorimetry, implementation of isothermal boundary conditions and a purely conductive (temperature and power independent) heat loss path.

6. ACKNOWLEDGEMENTS

The authors would like to thank Prof M D'Aprile, University of Calabria, Italy, for fruitful discussions concerning the analytical solution of the power balance equation and A C Bell for continuous support.

REFERENCES

[1] J L Hemmerich et al, "Key Components of the JET Active Gas Handling System - Experimental Programme and Test Results", Fusion Engineering and Design 11 (1989) 93-100

[2] J L Hemmerich, L Serio and P Milverton, "High Resolution Tritium Calorimetry Based on Inertial Temperature Control", Rev Sci Instr 65(5), 1994, 1616-1620

[3] P C Souers, "Hydrogen Properties for Fusion Energy", University of California Press (1986)

[4] L Serio, "Adiabatic Calorimetry Tests on JET Uranium Beds for Tritium Storage", JET Internal Report - JET IR(94)01

Modification of the JET Vacuum Vessel Support and Restraint System

G Sannazzaro, G Celentano, A Miller, T Raimondi,
S G Saunders, J Tait, J van Veen, M Wykes[1].

JET Joint Undertaking, Abingdon, Oxon, OX14 3EA, UK.
[1] ITER EDA, Naka, Japan.

1.0 SUMMARY

Since 1983, after the first plasma vertical instability, the support and restraint system has been continuously modified and upgraded to cope with the new design and operational requirement. Fig. 1 shows how the vessel supports and restraints have changed over the life of JET. With the divertor phase, new loads are applied to the vacuum vessel supports and restraints leading to a revision of the complete system.

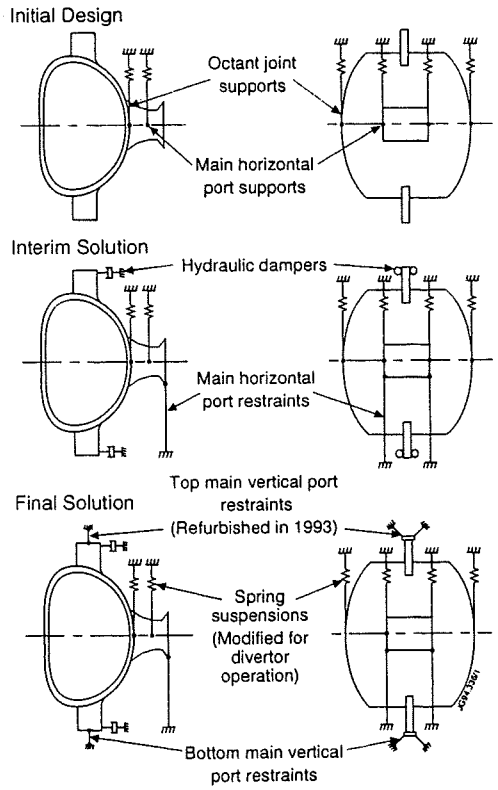

Fig. 1 JET vacuum vessel supports and restraint system from initial design to present day

The elastic suspensions at the equatorial plane have been modified to cope with the increase in vessel weight. The vessel restraints have been modified and tested to cope with the new electromagnetic load in equilibrium and plasma instability.
This paper briefly describes the overall philosophy of the vessel support system, the modification and the tests that have been done. Some experimental results are also reported on the behaviour of the supports and restraints.

2.0 THE VERTICAL LOADS ON THE VACUUM VESSEL

With the installation of the divertor coils and components inside the vacuum vessel, the total deadweight of the vessel has increased considerably from 145 tonnes (estimated) to 240 tonnes (measured).

The electromagnetic forces have also changed considerably. Before the installation of the divertor coils, the magnetic loads were mainly dynamic forces applied in a timescale of tenth of milliseconds in a plasma disruption or vertical instability. With the divertor coils inside the vessel, magnetic forces are exerted on the vessel during the whole length of the pulse. The maximum vertical static load on the vessel in a plasma equilibrium configuration is 5.1 MN. The maximum vertical disruption force on the vessel is estimated to be about 8-8.5 MN.

3.0 THE VESSEL SUPPORT AND RESTRAINT SYSTEM

The overall support system of the vacuum vessel is shown in fig. 2. It is composed of the elastic supports at the equatorial plane and the vertical restraints attached to the main vertical and horizontal ports.

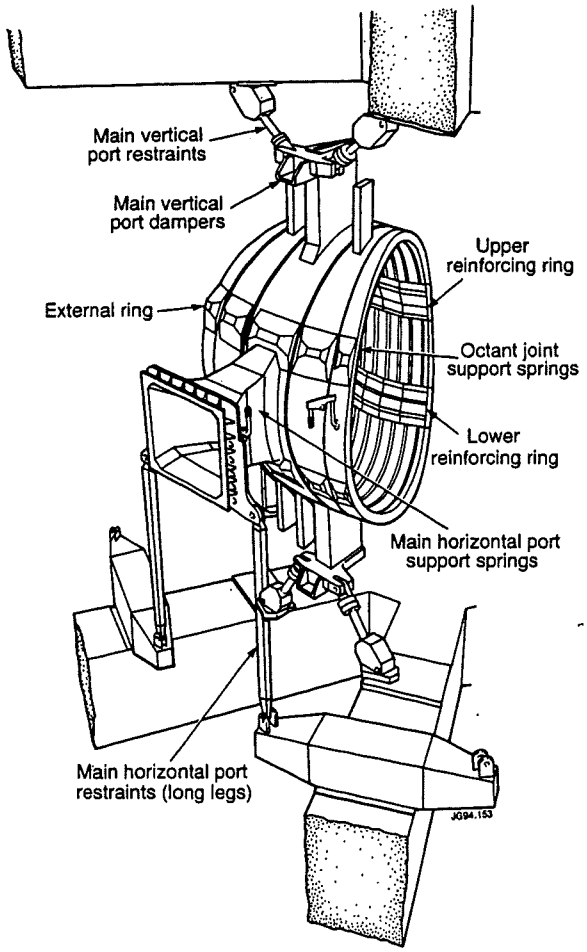

Fig 2 JET vacuum vessel supports and restraints

3.1 THE VESSEL ELASTIC SUPPORTS

The vacuum vessel dead weight is supported by 16 elastic suspensions at the octant joints (OJ) and 16 elastic suspensions at the vessel main horizontal ports.

They are connected to the vessel at the equatorial plane in order to allow free and symmetric thermal expansion.

When the vessel is at room temperature, the vessel weight (240 tonnes) is completely taken by the elastic suspensions. (66% by OJ and 34% by MHP).

During the 1992-93 shutdown the elastic suspensions have been modified to cope with the increase in vessel weight. One of the major concern was the strength of the insulation bushes that avoid electrical shortage of the vessel with the mechanical structure. The substitution of them would have required a much longer shutdown. Some spare bushes, identical to those installed on the machines, have been mechanically tested without failure to 192 KN (0J suspensions) and 120 KN (MHP suspensions. These values are much larger than the maximum expected loads.

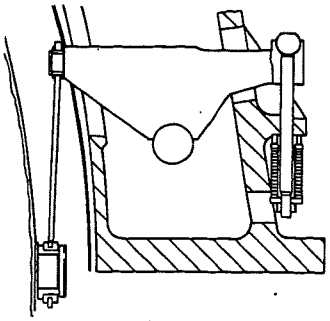

a) Octant Joint suspension

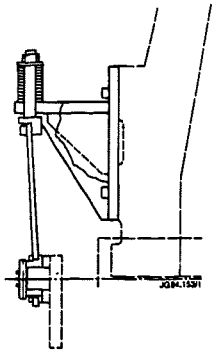

b) MHP suspension

Fig.3 Vacuum vessel elastic supports

During the vessel warm-up to the final temperature, part of the vessel weight (about 60 KN per octant) is transferred to the restraints at the bottom main vertical ports (MVP). That is obtained locking the bottom MVP brakes before the top ones.

In a plasma instability, the mechanical vertical oscillations of the vessel, generate an increase in the maximum compressive force on each octant joint suspensions up to 50 KN giving a maximum total load of 130 KN per OJ suspension.

3.2 THE VESSEL RESTRAINTS

The vessel restraints have the task of taking the vertical magnetic loads on the divertor coils and vacuum vessel during operation.

The restraints at the main horizontal ports (see fig. 2) hold the port in position in order to prevent any vertical load being transferred from/to all the equipment connected to the port. The proportion of the vertical magnetic force that they take in plasma operation is small (about 9%). Most of the load is taken by the main vertical port (MVP) restraints.

Each upper and lower MVP has two brakes assemblies (total 32) which mechanically connect each MVP to the horizontal transformer limbs as shown in figs. 2 and 4.

Each brake assembly is composed by a drum supported by springs and centered to a housing (1mm clearance on the radius). The support legs that links the drum to the vessel MVP flange is connected to the drum via a spheric bearing with an eccentricity of 20mm respect to the drum centre. During the vessel warm-up, the brake drum are free to rotate on roller bearings as the vessel expands vertically and displaces the leg into the brake housing.

The locking of the brakes is actuated by a device that is basically composed by a finger pressing against the drum with a forces of about 10 KN. The friction between the finger and the drum force the drum to rotate around the contact line and move toward the housing. As the two grit blasted surfaces of drum and housing get in contact, no further internal movement can take place and the subsequent vessel thermal expansion creates a compressive preload on the MVP. The lower MVP restraints are locked before the top ones in order to generate a total preload of about 2 MN and 1.5 MN on the lower and upper MVPs.

This thermal preload guarantees that the locking system is active during operation and reduces the vessel oscillations because all the clearances in the brake assemblies are already recovered when the vertical magnetic forces arise.

The MVP restraints have been designed to work mainly in compression. The thermal preload and the gaps in the brake assemblies guarantee that, even in very severe vertical instabilities, very small tensile forces are applied.

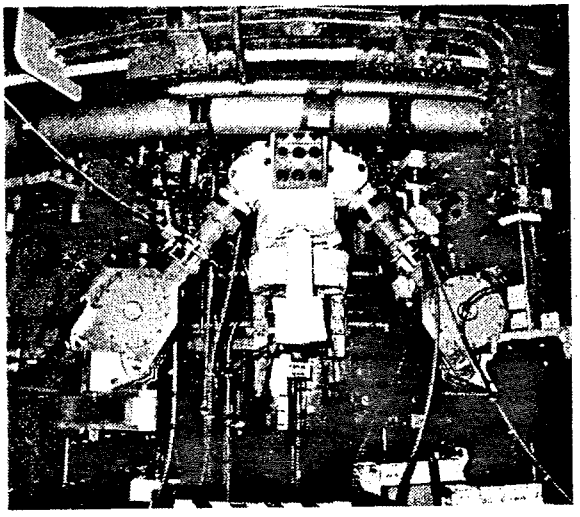

Fig.4 Vacuum vessel MVP restraints

The MVP restraints were installed in 1987 and had been used until 1992. During this operational period they showed a tendency to slip.

In the 1992-93 shutdown the contact surfaces of the drum and the housing have been remachined and grit blasted to increase the frictional force. A new frictional material has been used for the locking device.

The new refurbished brakes with the locking device have been tested statically (slowly increasing load up to 1.2 MN) and dynamically (vibration load at 15 Hz superimposed to different levels of preload).

4.0 OPERATIONAL EXPERIENCES

The MVP restraints are instrumented with strain gauges that are used to compute the applied vertical force. The readings from the strain gauges are monitored during every warm-up and cool-down phase to check the leg preload. Displacement transducers are also installed. They show whether the MVPs are moving freely.

The vessel temperature has been cycled several times from room to operational temperature. The brakes did not show any anomalous behaviour and the measured thermal preload obtained locking them before reaching the final temperature is in very good agreement with that predicted.

At the time of publishing this paper the performed number of JET pulses after the divertor installation is about 2800 (from JET PULSE No. 27968 to 30780). The maximum vertical force F_V on the MVP restraints is 1.8 MN for pulse 29429 (see fig. 5). This force is computed adding all the signals from the strain gauges. The maximum force on a single octant in the same pulse is 360 KN which is more than 1/8 of the vertical force F_V. This indicates that the reaction forces are not uniformly distributed.

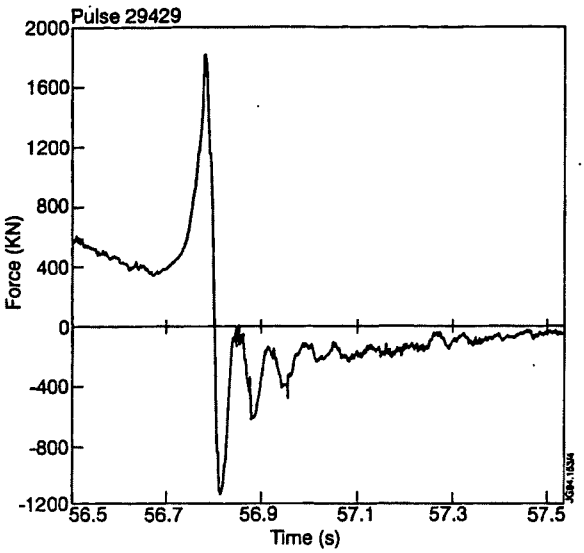

Fig. 5 Vertical force on MVP restraints in JET Pulse No: 29429

5.0 CONCLUSIONS

The MVP restraints and elastic supports have been successfully laboratory tested under static and dynamic conditions.

During operation the control system that locks and unlocks the MVP restraints has been commissioned successfully. The locking operation is done remotely as required for the tritium operation.

The vertical reaction forces due to the magnetic load in a vertical plasma instability are not uniformly distributed on the 8 octants. That could be due to dynamic mechanical effects and/or non symmetric distribution of the applied load.

6.0 REFERENCES

[1] P. Noll et al. - "Electromagnetic forces during JET divertor operation - Proceeding of the 23nd International EMF Workshop UTNL-R-0302 - TOKAI, JAPAN - Sept 1993.

The Applications of Waste Management Systems in Support of the JET Divertor Shutdown

D Collins, G Atkins, S J Booth, A D Haigh, C May, G Newbert.

JET Joint Undertaking, Abingdon, Oxon, OX14 3EA, UK.

ABSTRACT

A large number of facilities, resources and procedures were necessary for supporting efficient in-vessel work, particularly in handling activated waste and materials potentially contaminated with tritium and beryllium. These procedures were operated in practice during a demanding two year shutdown. This paper details the developments and the lessons learned.

Personnel entered the vessel via the Torus Access Cabin (TAC) which has been extended to incorporate an enlarged workshop and demountable platform. A waste sorting area has been added for the efficient sentencing of waste without holding up TAC operations. Waste quarantine procedures were operated successfully resulting in a radioactive waste volume reduction of a factor of 3. Further reductions, by a factor of 6, have been achieved by compaction. The equivalent of $20m^3$ of compacted radioactive waste and $300m^3$ of uncompacted beryllium waste was dispatched from the TAC during the shutdown.

The JET vacuum vessel forms the boundary of the beryllium and radiation controlled areas. A variety of contamination control techniques have been developed including isolators and tents manufactured in a PVC workshop. 356 isolators and 18 tents were made, 3 of which were compatible with pressurised suit use. Over $5700m^2$ of PVC and PU were used and numerous practical manufacturing techniques were developed.

The vessel decontamination was carried out in full pressurised suits. Over 5200 suited entries using 350 suits were made, and a stock of over 300 full and half face respirators was available. The decontamination facility, for suits and respiratory protection, operated successfully and criterion for pressurised suit re-issue and final disposal were developed.

INTRODUCTION

During any JET shutdown the number of personnel working inside the vacuum vessel is limited by the physical constraints of such a confined space. At any one time the number of in-vessel members is restricted to between two and eight. However, this number is small when compared with the much larger work force required to support them and to ensure that work is carried out safely and efficiently.

TORUS ACCESS CABIN

The Torus Access Cabin (TAC) enables personnel to enter and exit the JET vessel in a controlled manner and, along with decontamination and workshop facilities, includes the boundary of the radiation and beryllium contamination controlled areas [1].

Experience from past shutdowns has shown that its original configuration (figure 1) was too cramped and restrictive for the work due to be undertaken during the 'divertor' shutdown.

As a result, a suite of extension modules were manufactured which integrated the existing TAC facilities with additional features to increase the number of tasks which could be carried out in the controlled area -operations box- and streamline the waste disposal and material transfer routes .

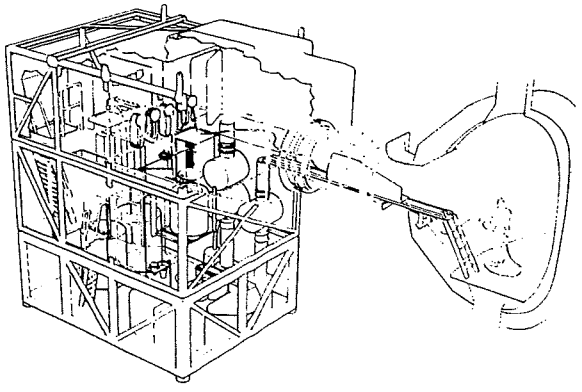

Figure 1 Original TAC configuration

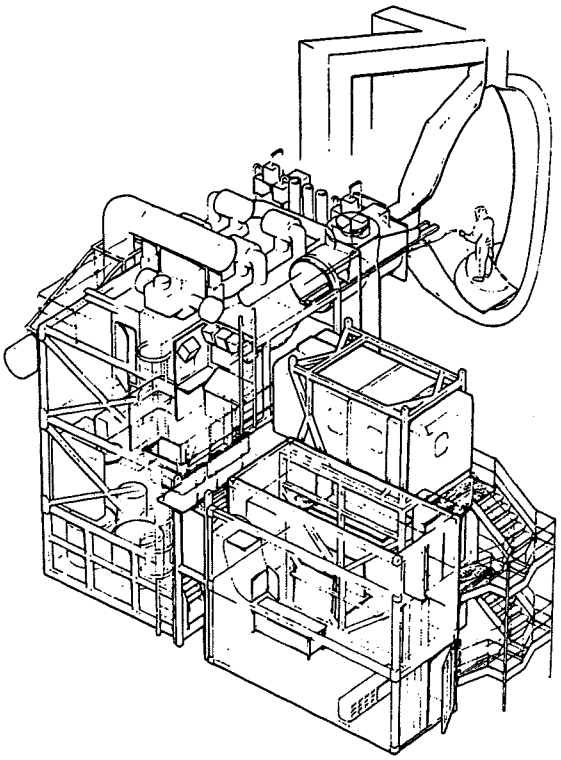

Figure 2 TAC in its new configuration

A modular design was chosen for the extension to give maximum flexibility for the 'divertor' shutdown and for other shorter interventions (figure 2). The extension system comprises two unitary stacks joined to the TAC, by means of a mid-level 'gallery'. The first stack of units houses the 'Alnor system' in the lower, entry control, module. Above is the mid-level change cabin and, at top-level is the 'operations box extension'. This virtually doubled the controlled area workshop space.

The second stack is created from ISO type containers. The lower 'Waste Management' container is joined to the gallery via a chute through which all the used full suits and soft
waste is transferred out of the TAC.

Above is the 'component' container for the bulk transfer, to and from the TAC, of drummed in-vessel components. Docking and undocking of this ISO container is by means of a special double PVC membrane which avoids the need for Health Physics clearance. This membrane is attached and operated in such a way as to present a clean, closed face on both the controlled area openings, TAC gallery and ISO container, to the Torus Hall environment.

Toward the end of the 'divertor' shutdown, a platform was installed to allow posting of large components into the controlled area. The platform was based on a half height ISO container and attached to the operations box extension via a tented airlock.

TAC OPERATION

The 'divertor' shutdown was divided into phases, each dependant on the intended work and the degree of in-vessel contamination. During phase 1 (vessel strip-out) high contamination levels required the TAC to be used for the control of pressurised suit operations. In the second phase (divertor coil build) contamination levels had dropped considerably and personnel were able to work in a decreasing and progressively less irksome level of respiratory protection. Full pressurised suits were re-introduced, briefly, in order to conduct a vessel cleaning exercise using the CO_2 blasting technique, prior to the third and final (rebuild) phase .

Full and continuous operation of the TAC was crucial to complete the shutdown on time. Waste Management Group personnel manned the TAC throughout the 22 month 'divertor' shutdown, including prolonged operation periods where 3 shift teams were in attendance, 24 hours per day, 7 days per week.

Each shift team comprised a shift technician supervising a controller, whose function is to ensure the safety of in vessel workers, a clean and a dirty side dresser to control the spread of contamination and a support operative to assist in the handling and sentencing of waste . In total 15 men were deployed on TAC support.

Each member of the team was pre-qualified to perform at least 2 of the above tasks. This enabled individual shift members to take breaks but allowed in-vessel work to continue without interruption.

SUIT AND RPE CLEANING FACILITY

During the 'divertor' shutdown over 5200 hours of in-vessel full suited operations were carried out. JET has a stock of approximately 350 full suits (figure 3) and throughout this shutdown each was recycled up to 7 times. The recycling of full pressurised suits and all other JET respiratory protection equipment (RPE) takes place in a dedicated cleaning facility (figure 4). The facility is fitted out with 2 cleaning / process lines and a drying area where smears are taken of each suit, both internally and externally, for beryllium and tritium contamination. They are then transferred to the inspection area were the suits are checked and refurbished with repairs being made, using RF welding equipment, to any small tears etc. All the internal communications equipment is tested

and air filters changed before each is returned to storage, ready for re-issue.

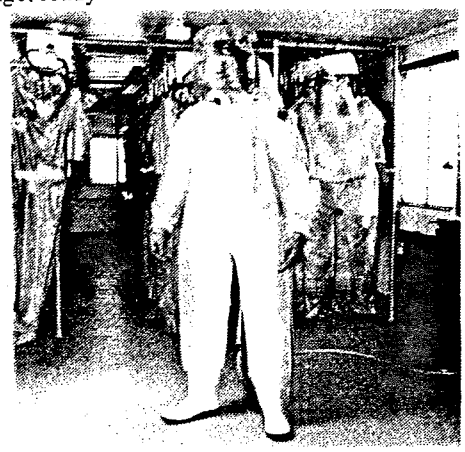

Figure 3 JET full pressurised suit

This facility was operated for an extended period, during the 'divertor' shutdown, utilising a workforce of 6 people working 10 hours per day, 6 days per week. This enabled approximately 20 suits per day to be re-cycled.

Figure 4 Suit cleaning / process line

In addition to the full pressurised suits, JET has the following stocks:

120 half suits
175 full face masks
100 half face masks
50 ventilated helmets

Throughout the 'divertor' shutdown the full range of available RPE was used in the various facilities on the JET site, all being cleaned and processed in this facility.

ISOLATORS AND TENTS FOR CONTAMINATION CONTROL

The JET vacuum vessel forms the boundary of a beryllium and radiological controlled area. In order to control the potential spread of contamination, a variety of techniques have been developed. To support this requirement, a PVC workshop was established to manufacture tents and isolators to the exact requirements of JET engineers (figure 5).

Figure 5 PVC workshop

Throughout the shutdown Waste Management Group have continued to developed new techniques and have been required to produce a diverse variety of items, from very large tents, (figure 6) compatible with full pressurised suit operation, to very small, delicate isolator for camcorders etc. .

A total of 18 large to medium tents along with over 350 isolators were produced during the 'divertor' shutdown and, even though many tents and isolators were cleaned and re-used, the staff in the PVC workshop used over 5700m2 of PU and PVC.

A new technique adopted for the production of tents and isolators was to include as many potential ports flaps and feedthroughs as possible because these were the most frequent reason for modifications to these fabrications. These ports were left sealed and if needed the inner membrane would be cut away.

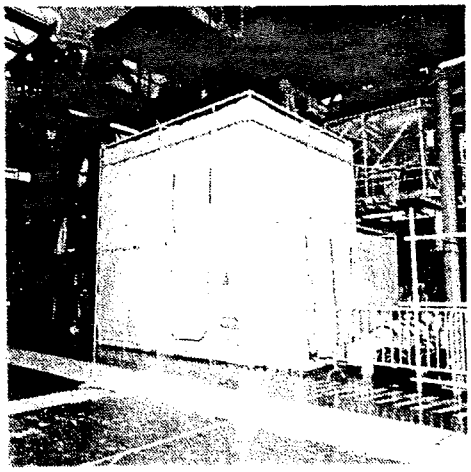

Figure 6 Large PVC tent

WASTE MANAGEMENT

Long before the 'divertor' shutdown began it was foreseen that, in order to cope with the volume of waste and redundant in-vessel components, a dedicated Waste Handling Facility (WHF) was required. Such a facility was constructed[2] in time for the start of the divertor shutdown and used to great effect (figure 7).
The main function of this facility is to reduce, by re-packaging, the volume of the waste and components it receives and to prepare samples and consignments of waste for off-site disposal to the Drigg repository.

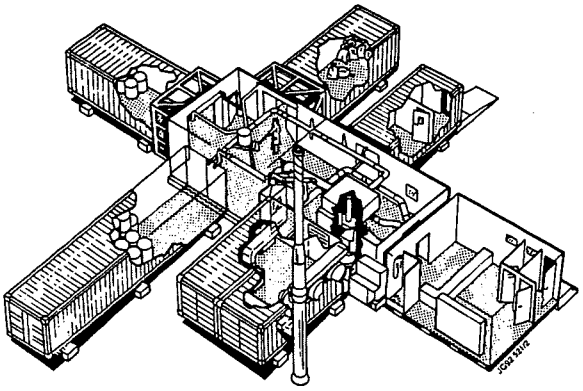

Figure 7 Waste Handling Facility

The WHF facility is constructed from modular steel enclosures that were built and tested at individual manufacturers then erected and integrated on the JET site.
The following are features of the facility:

ISO container docking system
In-drum compactor
Waste sorting and sampling station
High integrity sampling glovebox
High specification ventilation system
Specialised internal handling devices

WASTE MANAGEMENT PROCEDURES

The practical aspects of radioactive waste collection, storage, sorting and preparation for despatch are supported by an administration system based on a computerised data base. The data allows individual packages of waste to be grouped, sampled, packed and despatched in a controlled and traceable manner.
Volume reduction is an important feature of waste disposal at JET. This is achieved using the WHF 'In-drum' compactor which, for soft radioactive waste, has reduced 370m^3 (3700 x 100 litre bags) down to a volume of 57m^3, a reduction factor of more than 6.

A further reduction of in the volume of radioactive waste, removed from the TAC, was achieved by operating a quarantine procedure in which waste was set aside from an accurately defined area and for a given period of time. The area was then surveyed to demonstrate the absence of radioactive contamination. On receipt of satisfactory results the waste was categorised appropriately. In this way, 4.7m^3 of radioactive waste was despatched from the TAC during the shutdown. Had the quarantine procedure not been implemented this figure would have been 17.5m^3 a volume reduction factor of 3.

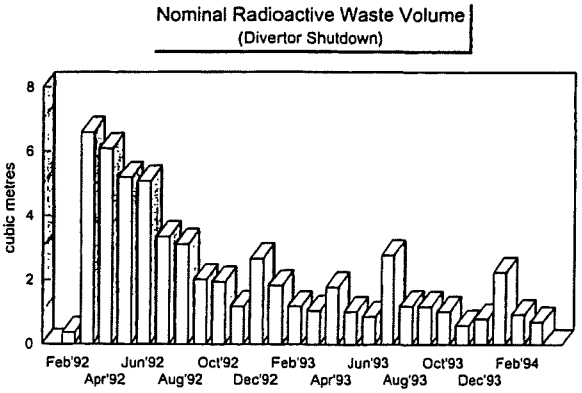

A technique for low level tritium assay has been developed in a joint collaboration between the Polytechnic of Milan and at JET. In the UK, demonstration of a radioactive concentration lower than 0.4 Bq/g enables waste disposal options other than consignment to radioactive waste repositories.

SUMMARY

During the long 'divertor' shutdown practicality of the waste management systems and procedures, for the handling of tritium and beryllium contamination and activated components, have been demonstrated. This has been much more than an academic exercise and proves that the technology is available and, that continued development of these systems, will benefit the project and the fusion community in general.

REFERENCES

1 S J Booth et al, "Beryllium related Maintenance on JET" 16th SOFT, London (1990)

2 D Collins et al,"Design and construction of a facility for the handling and packaging of radwastes from JET operations" WM93 , Tucson USA (1993)

Comparison between Actively Cooled Divertor Dump Plates with Beryllium and CFC Armour

H D Falter, D Ciric, E B Deksnis, P Massmann, K Mellon, A Peacock, M Akiba[1], M Araki[1], K Sato[1], S Suzuki[1], A Cardella[2].

JET Joint Undertaking, Abingdon, Oxon, OX14 3EA, UK.
[1] Naka Fusion Research Establishment, JAERI, 801-1 Naka-machi, Naka-gun, Ibaraki-ken, 311-01, Japan.
[2] ITER EDA, Max-Planck Institute für Plasma Physik, Boltzmannstrasse 2, D 8046 Garching, Germany.

Summary

Actively cooled test sections with beryllium and graphite armour all withstand power densities between 15 and 20 MW/m². Beryllium as structural material fails mechanically at low power densities. Monoblocks appear to be the most rigid design but frequently large variations in surface temperature are observed. All other test sections show a uniform surface temperature distribution.

1 INTRODUCTION

The design of divertor and first wall target plates is vital for the performance of a tokamak experiment. In preparation of an actively cooled divertor for JET we have tested cooled target plates with beryllium and Carbon Fibre Composite (CFC) armour. The tests have been performed in collaboration with NET and JAERI. The tests were to establish power density limits and to assess the reliability of the manufacturing process. Individual tests are partially covered in specialised papers [1 & 2]. The test rig and test procedures are identical to those used for previous tests [3].

2 TEST SECTIONS

2.1 Composite beryllium test sections

Beryllium tiles with a thickness of 1.5, 2, and 3 mm are brazed to a hypervapotron heat sink made from CuCrZr.

2.2 Directly cooled beryllium Vapotron.

This test section was supplied by ITER and consists of a 46 mm od cylinder. A spiral groove, 4 mm deep with a 3 mm pitch, is cut into the 9 mm thick wall (Fig. 2).

2.3 Carbon composite test sections.

Four different designs have been tested:

1 Monoblock design (CFC cubes brazed onto a central TZM cooling pipe as per NET divertor design [4].

2 Saddle type design: A saddle shaped CFC armour and a copper backing block of identical shape are brazed to each other and to a central cooling pipe (JAERI design [5]).

3 Flat tiles: Flat 7 mm thick CFC tiles are brazed to a copper heat sink (JAERI design).

4 Multitube: 200 x 150 x 40 mm CFC tile with 6 cooling channels made from OFHC copper (JET mark II actively cooled divertor).

The test sections are shown in Fig. 3.

Fig. 1: Test section with beryllium tiles brazed to a CuCrZr vapotron heat sink.

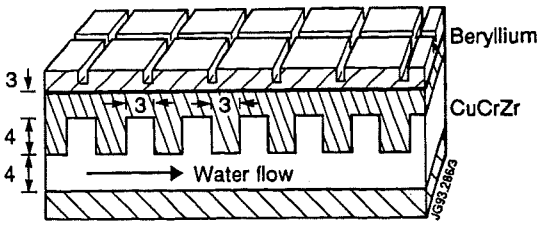

Fig. 2: Directly cooled beryllium test section

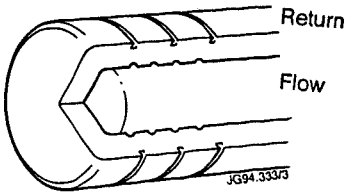

Fig. 3: Test sections with CFC armour.

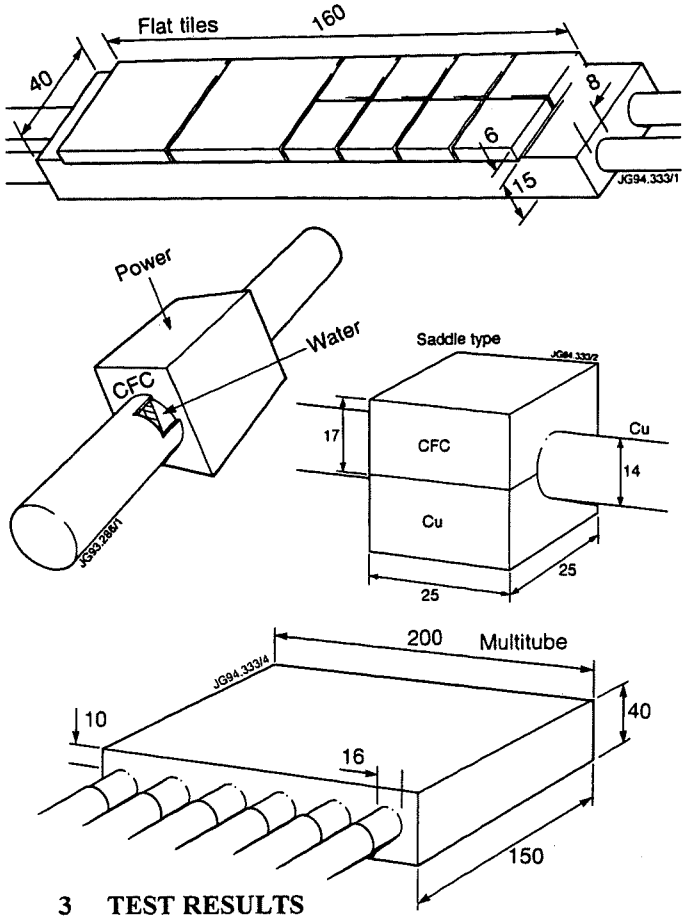

3 TEST RESULTS

A comparison of the most important test results with the various test sections is compiled in Table 1.

3.1 Brazed beryllium armour tiles

The destructive limit of these tiles is between 16 and 19 MW/m^2 for tiles of 1.5 to 3 mm thickness. The uniformity of the braze is generally good. Five out of eight test sections, made by induction brazing, have been tested so far and were without fault in the exposed area. Dump plates with 2 mm thick tiles show a surface temperature of approximately 800°C at a power density of 16 MW/m^2. An endurance test on two test sections with 1000 cycles at power densities between 11 and 15 MW/m^2 has been completed successfully. Details of the test results are reported in [2 and 3].

3.2 Directly cooled beryllium test section

So far we have tested one target plate where the beryllium is used as structural material. The test section failed after 34 pulses at a power density of 5.1 MW/m^2. The fault was a water leak in the exposed area. Fatigue cracks are visible on the tile surface. Approximately 1.5 mgr of beryllium was found in the water used for cooling and flushing the test section. (Water was only running from 5 seconds before a pulse to 5 s after the pulse).

3.3 Flat CFC tiles brazed to a copper heat sink.

The peak power density was limited to 19 MW/m^2 by critical heat flux in the cooling water channel. The surface temperature distribution was very uniform (Fig. 4). The temperature at the edges of two tiles is approximately 5% higher. This small non uniformity did not spread during the test. However, as we were close to critical heat flux, we did not apply a significant number of long pulses at high power density. The peak surface temperature is 570^0 for 10 MW/m^2 (excluding the hot spots).

Fig. 4: Surface temperature profiles

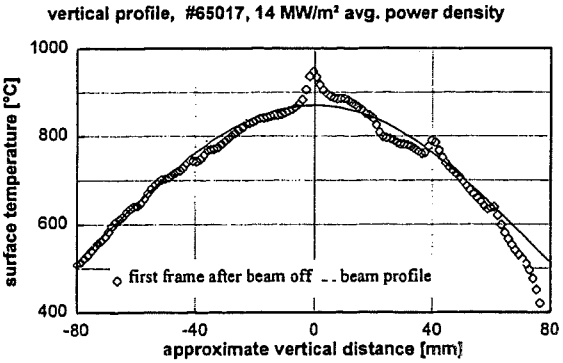

3.4 Saddle type test section.

This design had been very successful in previous tests sustaining up to 25 MW/m^2 at long pulses and 1000 cycles at 20 MW/m^2 [5]. The test section tested at JET had a small non uniformity in the surface temperature at the left edge of several tiles, in which lack of braze in the bonding interface was found after the test. Long pulses (15s) at 20 MW/m^2 lead to a rapid growth of the non uniform area of the hottest tile and more than 50% of the surface of this tile became detached within 8 pulses. The peak surface temperature at 10 MW/m^2 is 670 °C - again excluding the non uniform areas. The surface temperature distribution at the beginning and at the end of the long destructive pulses is shown in Fig. 5.

3.5 CFC monoblock test section

A full module of the NET divertor design with six individual monoblock test sections from 3 different manufacturers was tested.

Fig. 5: Surface temperature of the saddle type test section before and during destruction.

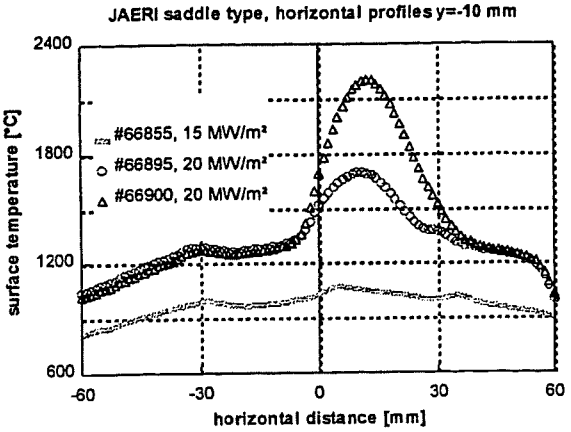

The surface temperature distribution after a 18 MW/m² pulse is shown in Fig. 6. The best test section shows a non uniformity of 10% in temperature over 26% of the surface, the worst has a non uniformity in excess of 50% in temperature over 63% of the surface. The peak power density was limited by the surface temperature of the hottest areas. During a total of 365 pulses we observed an increase in surface temperature of approximately 10% at constant power density on all the test sections, but non of the test sections deteriorated catastrophically.

While the module was exposed to power, the conductivity of the cooling water deteriorated significantly due to Molybdenum being dissolved. From the flow rate and the increase in water conductivity we estimate that 10 mg/s of Molybdenum is being dissolved during beam on.

Neighbouring tiles which get significantly different surface temperatures during exposure, also show a different temperature rise (Fig. 7). The initial temperature rise is defined by $\frac{dT}{dt} = \frac{2}{\sqrt{\pi}} \frac{\Phi}{\sqrt{c_p \rho k}} \sqrt{t}$ where Φ is the power density, c_p the specific heat, ρ the density, and k the thermal conductivity. As the tiles which get hotter also show a faster initial temperature rise we have to conclude that the tiles have reduced thermal properties rather than a faulty braze contact. A similar observation is made with respect to the increase in tile temperature during the test. The rise in surface temperature with exposure time is accompanied by an increase in the inertial temperature rise at the

Fig. 6: Temperature contours on the NET divertor module, taken after a 18 MW/m² pulse

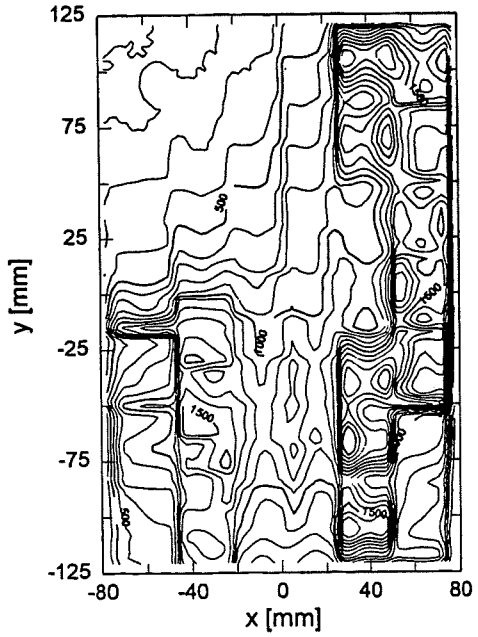

beginning of the pulse (Fig. 8) The initial temperature step in Fig. 8 is due to not fully contacted graphite on the surface and is dealt with in paper [6] in more detail.

3.6 CFC Multitube test section

The surface temperature distribution is quite uniform with two small areas with an excessive temperature of less than 10% (Fig. 9) The peak surface temperature is higher than for the other CFC designs due to an increased distance between surface and cooling channel. Two tiles have been tested so far

Fig. 7: Initial temperature rise of neighbouring tiles during one pulse

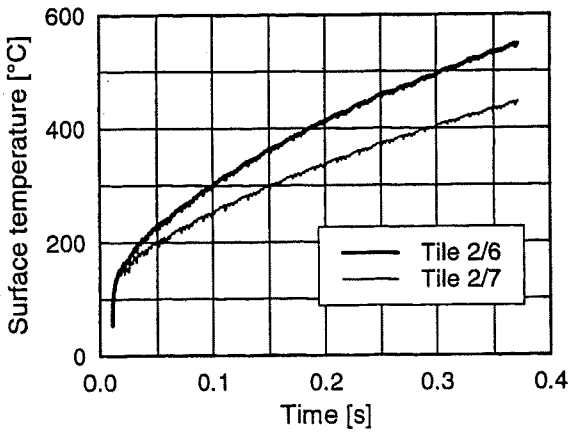

TABLE 1:	AREA		PEAK SURFACE		AREA WITH EXC.		destructive	PULSES
	TOTAL	TESTED	TEMP [10MW/m²]		TEMPERATURE		LIMIT	total
	mm²	mm²	max	min	>10%	>50%	MW/m²	
JAERI FLAT TILE	6560	6560	570	500	0%	0%	>19	211
JAERI SADDLE TYPE	2500	2500	670	580			20.5	54
NET DIVERTOR PROTOTYPE	64512	32000					>18.5	365
max			1800	1000	72.00%	63.00%		365
min			880	720	14.00%	0.00%		365
avg			1275	817	40.17%	13.33%		365
JET CFC MULTITUBE	30000	30000	1000	900	0	0	>15	21
2MM BE TILES	24300	11000	400	400			17	1000
BE VAPOTRON	13800	8800					5	34

Fig. 8: Initial temperature rise early and late in the test.

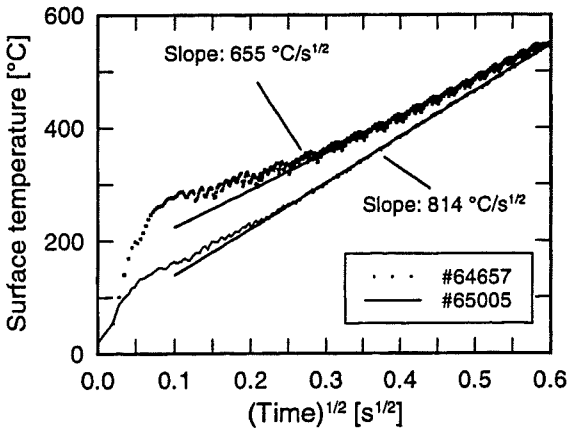

Fig. 9: Surface temperature distribution on the CFC multitube 0.6 s after a 3s pulse with 15 MW/m²

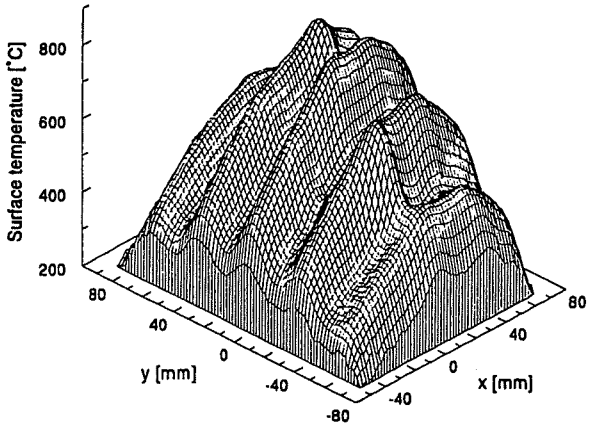

without an attempt to determine the endurance of this design. The uniformity and performance of both tiles is similar to each other.

4 COMPARISON.

All test sections - with the exception of the directly cooled beryllium - withstand comparable power densities of 15 - 20 MW/m². The monoblock design appears to be the least vulnerable method in the sense that no catastrophic failures have been observed, but the large variation in surface temperature limits the peak power density which can be applied in a divertor . The lowest surface temperature is observed with the high conductivity unidirectional CFC tiles which also shows good uniformity. The drawback of this design is that a reduced thermal contact appears to spread faster than in the case of the monoblock design, although these designs have the possibility of in-situ repair.

The beryllium composite dump plates show good uniformity. The drawback of this design is that the armour plate has to be either thin (2 mm) or the power density is limited by the surface temperature. The failure with beryllium tiles is catastrophic: Local melting with droplet formation, or complete detachment of the respective tile.

References

1 A. Cardella et al, " Design manufacturing and thermo-mechanical testing of a relevant size monoblock divertor prototype, this conference

2 C Ibbot et al, "Further development in the brazing of beryllium to CuCrZr", this conference (poster

3 H D Falter, "Testing of plasma facing materials for divertors in the JET Neutral Beam Test Bed, SPIE Vol. 1997 High Heat Flux Engineering II (1993), 170-181

4 A. Cardella et al., Design Manufacturing and Testing of the Monoblock Divertor, 17th Symposium on Fusion Technology, Rome (Italy), Sept. 14-18, 1992

5 S Suzuki et al, "High Heat Flux experiments of Saddle Type Divertor Module", Proc. of 6th Int. . Conf.. on Fusion Materials, Stresa, Italy 27/9 - 1/10, 1993, to be published in J. of Nucl. Mater.)

6 D Ciric et al, "Light emission from graphite surfaces during beam bombardment, observation and consequences for use of graphite in divertors", this conference (poster A 250)

A Combined Divertor and Bulk Plasma Density Control System

M Gadeberg, P Andrew, T Budd, T Hartrampf,
J How, H S Jensen, A Peacock.

JET Joint Undertaking, Abingdon, Oxon, OX14 3EA, UK.

A density control system capable of controlling gas introduction into JET in divertor experiments and using a variety of feedback signals is described. Combined feedback control using the bulk plasma density and ion saturation current from a Langmuir probe is demonstrated. Planned system upgrades are presented.

1. INTRODUCTION

A new torus gas introduction and control system has been implemented at JET. The system has been designed to control the plasma density in feedback mode using 10 gas introduction modules positioned around the vessel. Apart from using the bulk plasma density for feedback the system may also control some of the gas modules for feedback on other signals.

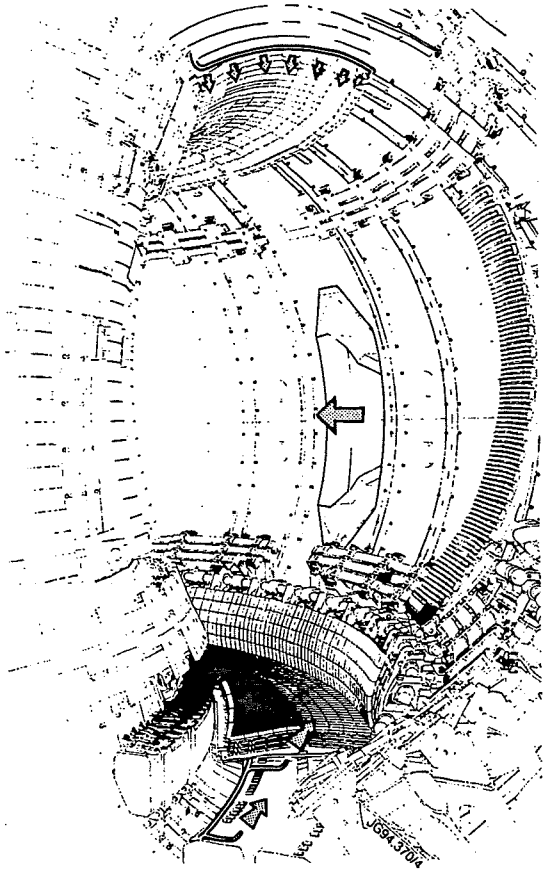

Fig 1. Layout of gas introduction inside torus. Four radial lines at top of torus, one of which is extended to LHCD launcher in midplane, two modules feeding through main horizontal port and four toroidal lines in divertor

2. EXPERIMENTAL SET-UP

A total of 10 gas introduction modules (GIMs) are installed on JET, two of them feeding in the torus midplane, four distributed around the top of the vessel and four modules distributed around the divertor area at the bottom of the torus (fig 1).

Modules in the bottom have distribution lines with pipework sized to ensure even distribution in toroidal direction in the new divertor. The modules at the top of the machine have radially extended

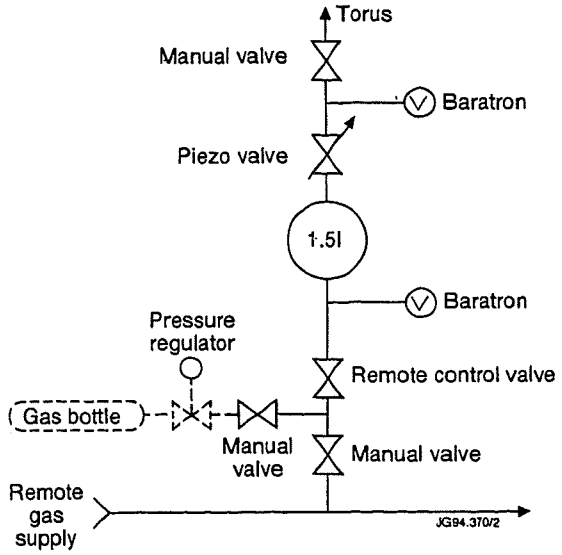

Fig 2. Schematic of a single gas introduction module

distribution lines. The distribution line for one of the top modules is extended to the torus midplane next to the LHCD antenna. The midplane modules are feeding the torus through a main horizontal port.

Each of the GIMs has a 1.5 l reservoir located close to the torus (fig 2). Between plasma pulses this reservoir is filled either from a remote gas supply system or from a local gas bottle. The local bottle option is normally used when operation with a special gas in a single module is required.

The four top modules share one remote supply line as do the four modules in the divertor area. Each of the remaining two modules in the midplane has its own remote supply line. The filling pressure for the remote supply lines can be remotely adjusted. During a plasma pulse the reservoirs are isolated from the supply systems (remote and local) and gas is fed to the torus through an analogue piezo valve. The pressure drop in the reservoir is used to calculate the gas flow after the pulse. A flow rate of 100 mbl/s from each GIM is achieved when operating with 500 - 600 mb deuterium. The gas flow response time at this flow rate is 150 - 200 ms. The maximum operating pressure is 1200 mb.

The piezo valves are controlled by two CAMAC based microprocessors, one for the top and midplane modules and one for the divertor modules. The two microprocessors run identical software to control the opening of the piezo valves.

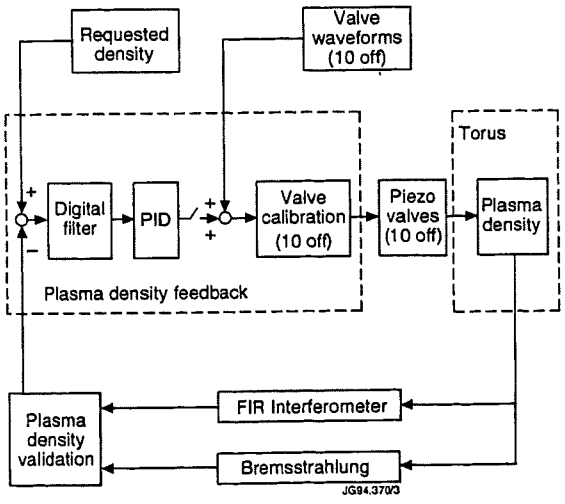

Fig 3. Schematic of feedback control system

For convenience each piezo valve may be controlled using three time windows and a waveform which specifies the percentage opening of the piezo valve. The three time windows specify the duration of a gas puff with fully open valve, the period when the waveform will be applied and time when feedback control of the valve should take place, respectively. During feedback control, the pre-set valve opening waveform is used for feed forward control. Many combinations of puff, pre-programmed and feedback time windows may be applied. A schematic of the control system is shown in fig 3.

The main signal used for feedback control of the gas system is the electron line density measured by the FIR interferometer. A weighted average of pre-selected interferometer channels is used to represent the bulk plasma density. In cases when the interferometer signal becomes invalid during a pulse, say due to a fringe jump, the system changes to use a horizontal and/or a vertical Bremsstrahlung signal. The density is derived from the Bremsstrahlung signal by taking the square root of the raw data and applying a calibration constant. The calibration constant is recalculated on every plasma pulse where the interferometer and Bremsstrahlung signals are available.

Other signals may also be used for feedback control of the gas modules. These include divertor tile temperature, divertor electron density as measured by microwave interferometry, a number of spectroscopic signals and FIR interferometry with a different channel selection and weighting to the bulk plasma measurement.

Each of the microprocessors may use only one of the above signals for feedback control. If the bulk plasma density is being used the corresponding gas modules are said to be in the primary loop and gas modules controlled by any other signal are in the secondary loop.

The primary loop is an essential part of normal plasma operation, whereas the secondary loop is of an experimental nature to try to control such parameters as divertor density, divertor tile temperature, LHCD coupling etc.

Feedback Control

The feedback control uses a transfer function of the following form

$$K_c\left(1+\frac{1}{s*T_I}\right)\left(\frac{1+s*T_D}{1+s*\frac{T_D}{\alpha}}\right)$$

Here K_c is the gain factor, T_I and T_D are integral and derivative time constants, respectively, and α is a limit for high frequency derivative roll-off, s is the Laplace transform variable. The particular transfer function was derived from earlier experiments on JET and was used in operation prior to the installation of the pumped divertor. The time constants and α are adjustable from pulse to pulse and for the primary loop a pre-programmed waveform is used for the gain. The error signal is digitally smoothed before the transfer function is applied. The output from the transfer function is then added to the pre-programmed waveform for each gas module which operates in feedback mode. The value which is in terms of 0 - 100 % opening of the piezo valve is finally translated into a voltage for the piezo valve. The calibration of valve opening vs. piezo driving voltage is highly non-linear and varies from valve to valve; the loop however remains stable under these conditions.

The secondary loop uses a similar scheme as outlined above for the primary loop, but with the following modifications. The gain used in the secondary loop is a constant, adjustable from pulse to pulse. The operation of the secondary loop is inhibited if the bulk plasma density exceeds a pre-set limit. This limit is independent of primary loop feedback operation. This is to avoid that the secondary loop would overfuel the main plasma. The error signals are updated on a 5 ms time scale; however, the feedback signal is only updated on a 100 ms time scale in order to match the general response time of the system and avoid instabilities. Dead times within the system are substantially lower than the time constants in the feedback loop and are thus of no concern.

3. OPERATIONAL EXPERIENCE

The primary density feedback loop has been operated since the restart of JET operations in early 1994. An example of the performance of main density control is show in fig 4.

The system currently suffers from the interferometer density measurements not being ideal. The interferometer channels which are currently being processed in real time all include the divertor plasma. This situation, however, is likely to change in the near future when the lateral interferometer channels have been commissioned.

Experiments have also been done, where the four divertor gas modules have been controlled in parallel in feedback mode by the secondary loop using the ion saturation current from a divertor Langmuir probe for feedback, fig 5. In these experiments the primary loop controlling the bulk plasma density was running from 0.8 to 12 s and the secondary loop from 14.5 to 24 s. It can be observed that due to high out-gassing the primary loop is only feeding the plasma during the first few seconds of the discharge, the plasma density exceeding the requested waveform. The feed forward waveform for the main gas valve requested 20 % opening of the piezo valve. At 12 s the pre-programmed gas waveform is applied to the divertor GIMs followed at 14.5 s by application of

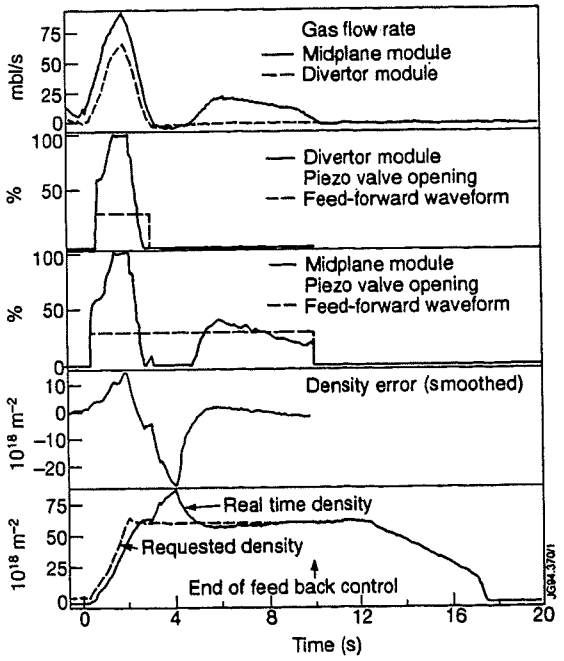

Fig 4. Gas system data for pulse 30786. Midplane module timing: puff 80 ms @ -0.4 s and feedback 0.5 - 10 s. Divertor module timing: feedback 0.8 - 3.0 s. Feed forward waveform at 30 % opening for both modules.

the feedback term. The feedback term has been operationally limited to adjust the pre-programmed waveform by maximum ± 20 % valve opening, and due to the large error signal this limit is in effect until 20.2 s at which time the feedback system is starting to control properly and maintaining the requested waveform.

The purpose of the experiments which formed the basis for the results in fig 5 was to control the detachment of the divertor plasma from the divertor tiles. The result of these experiments will be reported elsewhere.

4. SYSTEM UPGRADE

The present implementation of the density control system is very tight in memory space and imposes restrictions in the operational use of the system. In order to get rid of these constraints work is in progress to move the implementation from being CAMAC based to residing in VME.

The new VME implementation will allows us to select any combination of gas modules to be controlled by the primary and secondary feedback loops.

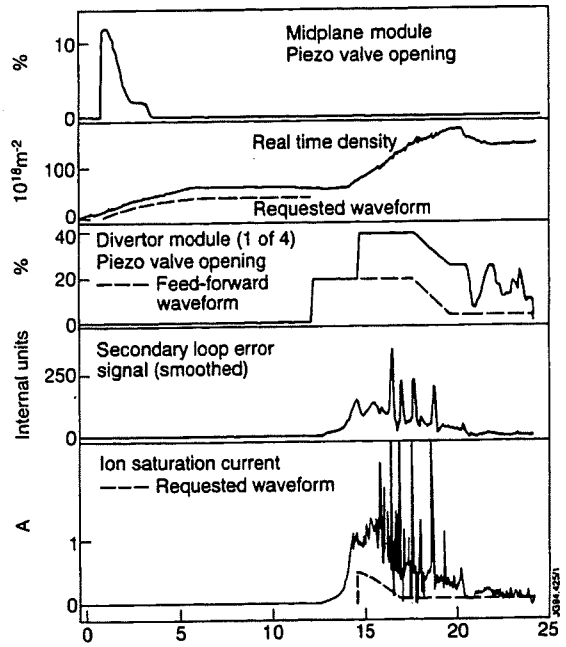

Fig 5. Operation of primary and secondary loop for pulse 31204. Midplane module timing: puff 60 ms @ -0.5 s and feedback 0.8 - 12 s. Divertor module timing: feedback 14.5 - 24 s.

When the new centrifuge pellet injector becomes available, this will also be interfaced with the density feedback system. The centrifuge pellet injector will be capable of injecting deuterium pellets of cubic length 2 and 3 mm at a variable rate up to 40 pellets/s corresponding to a fuelling rate of 1000 mbl/s for up to 60 s. The centrifuge control system is designed to accept an analogue fuelling rate and launch pellets accordingly. The density feedback system will be modified to include a further feedback loop to cater for the centrifuge injection. It will be possible select either the bulk plasma density or any of the secondary loop signals for feedback control of the centrifuge pellet injection. The new transfer function is expected to have different characteristics due to the different fuelling physics.

5. CONCLUSIONS

The density control system is working as one of the key elements in JET operations. The successful operation of the secondary loop for control of the divertor gas modules has been demonstrated.

An upgraded version of the control system which will eventually include pellet fuelling is under development

First Operational Experience with the new Plasma Position and Current Control System of JET

M Garribba, M L Browne, D J Campbell, Z Hudson, R Litunovsky, V Marchese, F Milani, J Mills, P Noll, S Puppin, F Sartori, L Scibile, A Tanga, I Young.

JET Joint Undertaking, Abingdon, Oxon, OX14 3EA, UK.

1. Abstract

The Pumped Divertor phase of JET involves the use of plasma configurations with complex control requirements. Therefore a new Plasma Position and Current Control system (PPCC) has been developed. It consists of two separate subsystems: Vertical Stabilisation (VS) and plasma Shape and Current Control (SC). SC performs a real time calculation of the plasma boundary using the Xloc algorithm [1]. It uses a full multivariable decoupling control algorithm which is applied to a combination of plasma wall-gaps and currents directly controlled [2]. SC and VS were brought into operation during the past months. The paper describes the operation of the system and reports on the performances achieved during the 1994 campaign.

2. Hardware Construction

Both SC and VS are VME digital systems using two floating point Digital Signal Processors (DSP) TMS320C40 running at 40MHz.

The Poloidal Field (PF) circuit currents and other few measurements are digitised by SC. The plasma-wall gaps and the X-point position are measured in real time using the Xloc algorithm [1] running on 91 magnetic signals sent through a fast optical link running at 16Mbyte/s (Figure 1).

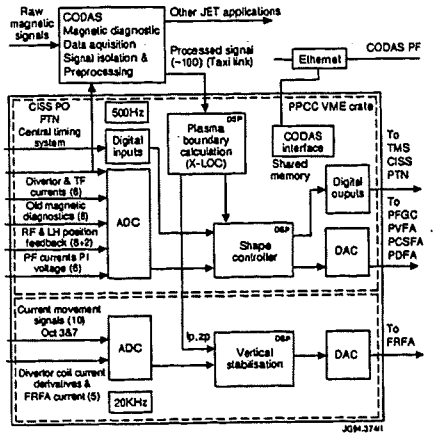

Figure 1. Hardware block diagram

VS is based on the measurement of the plasma current moment derivative. This is achieved by summing thirty-two magnetic signals in a passive summation stage and grouped to provide ten inputs to the ADC. Signals from opposite toroidal locations in the machine are used to minimise the influence of plasma n = 1 modes on the measurement. In addition the divertor coil current derivatives are digitised because they are included in the measurement path and their contribution has to be subtracted to obtain the plasma vertical current moment alone. The analogue to digital conversion is carried out on standard ADCs on the VME bus. This produces a delay in the order of 20μs from when the signals are digitised to the moment they are available for processing in the DSPs. VS is implemented on two DSPs with a 20kHz sampling time.

Both systems are interfaced with the Control and Data Acquisition System (CODAS) of JET through an Ethernet link running on a dedicated Motorola 68040 processor. This processor is used only for off line activities.

3. Plasma Shape and Current Control

The block diagram of the SC system is shown in Figure 2. It decouples nine loops simultaneously either in current control, or controlling the plasma shape through a plasma-wall gap control. The control algorithm and the model of the PF circuit and the plasma used to derive it are described in [2]. It is worth noting that the control matrix varies during the pulse and is recalculated in real time according to preprogrammed changes in the control mode or due to circuits currents that reach saturation in the attempt of fulfilling a gap request.

In case of current saturation the controller abandons the control of the gap which is more closely related to that current and resumes the gap control only when the demand waveform asks it to go back in the linear regime. The SC drives eight thyristor bridges and one flywheel generator used for the plasma current control [3].

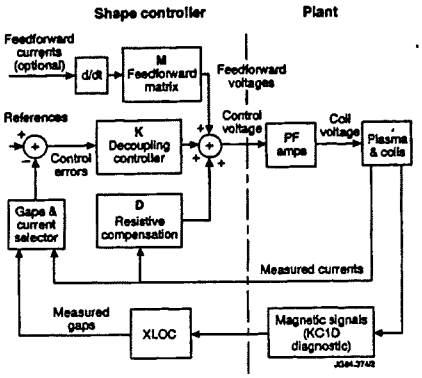

Figure 2. SC block diagram

Figure 3 shows the plasma boundary as reconstructed by the shape controller during pulse 30693 at the times 14.5s and 17.5s. This is a 2MA X-point plasma with an Ohmic phase (14.5s βp = 0.16) and an H-mode phase (17.5s βp = 0.65). The figure clearly shows that the location of the control points is not affected by the change in βp.

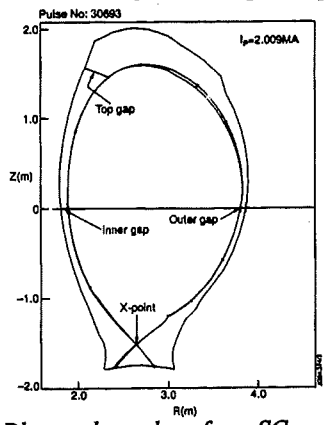

Figure 3. Plasma boundary from SC

Figure 4 shows a typical pulse during the Gap control phase.

At 14.5 seconds into the discharge the Gap control is switched on and the desired X-point configuration is formed. A step of 4cm is applied to the X-point vertical position to verify the effectiveness of the decoupling action. The plasma centroid vertical

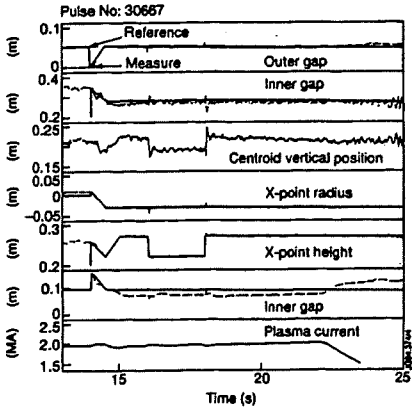

Figure 4. Typical Gap control discharge

position (not controlled) is shown together with the response to the step of the Top Gap which is the most closely coupled quantity with the X-point height.

Figure 5 shows a pulse with the X-point sweeping activated. The sweeping is performed applying to the X-point radius a 4Hz triangular demand waveform.

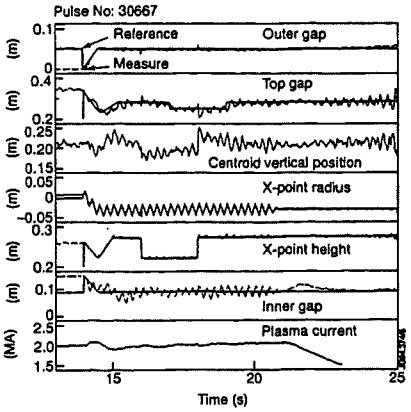

Figure 5. Sweeping of X-point in Gap Control

During the sweeping steps were applied both in the Top Gap and in the X-point Height demands to check that no degradation of the time responses or the decoupling take place.

The Inner Gap is coupled to the sweeping and shows a deviation from its reference by ±1cm. This is due to the choice of the time response of 100ms on this gap, selected in order to avoid huge voltage swings on the power supplies.

An integral term was added on the Inner Gap control to correct the static error of 2cm visible in Figure 4.
The transition phase from current control to gap control at 14.5s during the pulse is visible in both Figures 4 and 5. It should be noted that, in order to avoid voltage saturation, the demand waveforms are matched to the measured gaps at the transition time and then are linearly interpolated to reach their pre-programmed value.
It is important to point out that the gap control cannot be applied throughout the pulse. The plasma boundary reconstruction codes do not give reliable results for plasma currents below 100kA and therefore cannot be used during breakdown. However the plasma radial position control is very critical during the breakdown phase which is carried out using the flux extrapolation method historically used at JET [3].
SC carries out internal checks which demand a premature pulse termination in case of faults. Watchdogs are applied on the control errors. If the control error exceeds consistently a threshold for too much time the pulse is terminated. Checks on data consistency from the ADCs and maximum delays of transmission on the optical links are applied.
SC is interfaced to the Plasma Protection System (PTN) of JET to which it sends a termination message whenever it decides to initiate a controlled shutdown. From PTN it can receive two requests. A *Slow* and a *Fast* termination can be requested depending on the level of the fault detected.
Termination scenarios are implemented using waveforms which are relative to the termination time and are rescaled with the actual values of the gaps or the currents which are controlled.

4. ICRH Coupling Resistance Feedback

Included in the decoupling scheme is the control of the plasma ICRH antenna coupling resistance. This control mode is preferred to the Outer Gap control when radio frequency heating is applied.
The Outer Gap control is replaced by the translation of the ICRH coupling resistance error into a gap error by means of an appropriate gain and can therefore compensate for changes in the RF coupling at critical times like during an L to H mode transition.

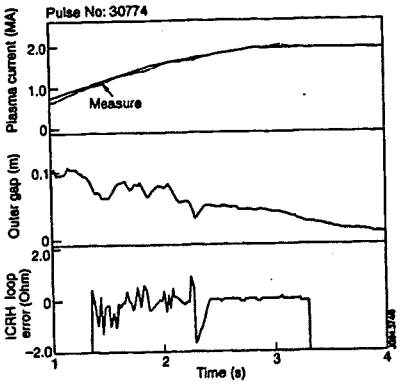

Figure 6. ICRH Coupling Resistance Control

This technique allows a very easy integration of this mode of control in the general decoupling scheme without any further modification.
It is important to note that this feedback is used in a limited range defined by a maximum and minimum distance from the outside wall. The outer gap control is resumed in case of transient tripping of the RF generators.
Figure 6 shows an example of this feedback. The different behaviour during the plasma rise and the flattop phase should be noted.

5.Vertical Stabilisation

The new system is designed to stabilise plasma growth rates of up to $1000s^{-1}$, however the growth rates measured so far do not exceed $160s^{-1}$.
The control algorithm is based on a proportional controller for the current moment derivative feedback and a slower proportional-integral control of the amplifier current.
The proportional gain is time dependent. The value of the gain is decreased by typically 60% after the first second during the plasma pulse. This technique allowed a substantial reduction of the limit cycle present due to the non linear amplifier characteristic.
The plasma breakdown in fact is not successful unless the gain of the fast loop is in a very narrow window (±20% of the nominal value).
Figure 7 block diagram shows the control scheme used. The fast velocity loop is based on a proportional control of the plasma vertical speed. At present the measurement does not yield the vertical speed of the centroid but is based on the derivative of the radial flux. This is due to the high noise

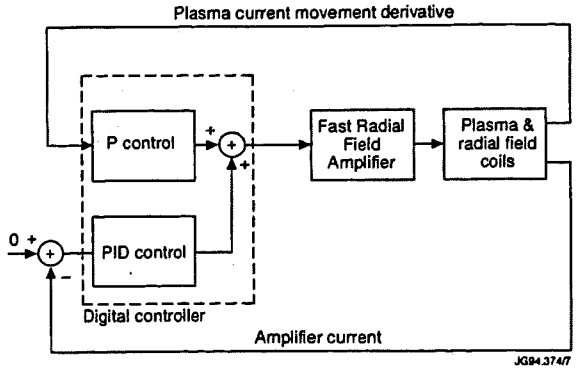

Figure 7. VS block diagram

generated by the divertor power supplies at the 600Hz (and higher harmonics) being amplified by the thin coil casing.

A digital filtering technique for restoring the full current moment measurement has been developed. However these filters are not compatible with the 20kHz sampling rate. The introduction of a third DSP will allow the use of the filters. Operation of the machine was permitted by using of the Mirnov coils located on the top of the vessel only by doubling their contribution in the control signal.

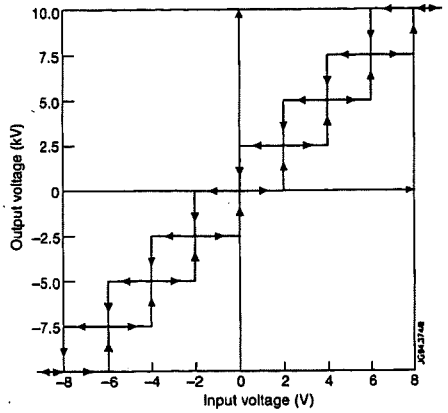

Figure 8. FRFA I/O Characteristic

The amplifier driven for the plasma stabilisation (Fast Radial Field Amplifier) is a ±10kV/±2.5kA GTO DC/DC converter with an input output characteristic given in Figure 8. FRFA shows a maximum input to output delay of 200μs [4].

Figure 9 shows a pulse during which the feedback was suppressed for 20ms. The plasma (1MA) drifted upwards by 10cm and then was recaptured by the stabilisation. A current swing of about 1.5kA and a voltage up to 5kV was needed by the control system.

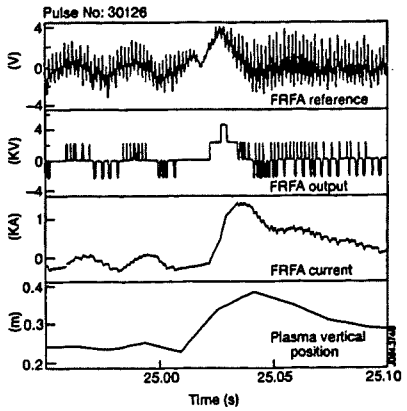

Figure 9. Temporary Switch Off of VS

6. Conclusions

The new PPCC system has been brought in operation and has performed up to the design specifications being capable of handling both the traditional current control of coils and the new concept of gap control using a decoupling controller. The application of the gap control allows a precise positioning of the plasma separatrix at chosen positions. This demonstrates the feasibility of such control systems for ITER.

The Vertical Stabilisation system is also implemented as a digital system. This choice has simplified operation in the view of the unexpected high noise input from the divertor amplifiers. The machine operation is not affected by the non-linear behaviour of the power amplifier.

References

[1] D. O'Brien et al., Local Expansion Method for Fast Plasma Boundary Identification in JET, Nuclear Fusion, Vol. 33, No. 3, 1993

[2] M. Garribba et al., The New Control Scheme for the JET Plasma Position and Current Control Scheme, XV SOFE, Hyannis, Massachusetts, 11-15 October 1993.

[3] E. Bertolini et. al., The JET Magnet Power Supplies and Plasma Control Systems, Fusion Technology, January 1987, Vol 11, No 1

[4] T. Bonicelli et al., Analysis and Specification of the Performances of the New JET Amplifier for the Vertical Stabilisation, XV SOFE, 1993

Irradiation Effects on Magnet Components of the Joint European Torus

A Tesini, E Bertolini, J R Last, G Sordon[1], G P Tartaglia[1].

JET Joint Undertaking, Abingdon, Oxon, OX14 3EA, UK.
[1] JRC, Institute for Advanced Materials, P.O.Box 2,
1755 ZG Petten, The Netherlands.

New coils were installed in 1993 as part of the new pumped divertor for the Joint European Torus to improve the control of the magnetically confined plasma. The coils are insulated by means of the epoxy resin Araldite, which must maintain its property during operation otherwise the whole performance of the machine could be affected. Radiation damage of the coils has been assessed by a series of irradiations of representative components in conditions similar to actual operating conditions, thus obtaining important information for operation.

1. INTRODUCTION

A pumped divertor has been installed in the Joint European Torus (JET). Its scope is to control the shape of the magnetic field at plasma edges and the evacuation of impurities produced during plasma burning phases, which could decrease temperature and fusion reaction rates. This is achieved by magnetic fields produced by coils placed behind the divertor plates, which guide the plasma particles toward areas from where they are pumped away by a cryopump. Coils are electrically insulated using glass tape impregnated with epoxy resin Araldite CY 205 F ($C_{18}O_3H_{20}$). The insulation material must maintain both its mechanical and electrical properties under irradiation, or the performance of the coils could be affected. Under irradiation the covalent bonds of atoms of organic materials are easily broken forming free radicals which recombine in new compounds with alteration of physical, mechanical, chemical properties. Materials loose tensile, shear and impact strength and become brittle. Moreover, radiolysis can occur when protons and freed methylic groups recombine producing mostly hydrogen, methane and ethane. Radiolysis becomes critical if the material is sealed in hermetic enclosures.

2. OBJECTIVE OF THE EXPERIMENT

In order to assess the radiation damage to the magnets insulating material, representative models have been irradiated in conditions close to those found at JET during the active phase. Each model is made of an aluminium box containing two aluminium bars electrically insulated with glass tape impregnated with epoxy resin (about 150 g resin in each component). Parallel irradiation of resin in granular form sealed in quartz vials was also performed (about 400 mg resins per vial).

3. IRRADIATION CAMPAIGN

The irradiation campaign was conducted at the High Flux Reactor (HFR) at Petten [1]. A dedicated rig was built to tailor neutron and gamma spectra by appropriate shielding materials. It was installed in the Pool Side Facility of the HFR for better operational flexibility. Details of the rig are given in [2]. One model (figure 1) and three quartz vials were irradiated in each irradiation. Forced air cooling was used to remove the heat generated. The rig was instrumented for continuous monitoring of

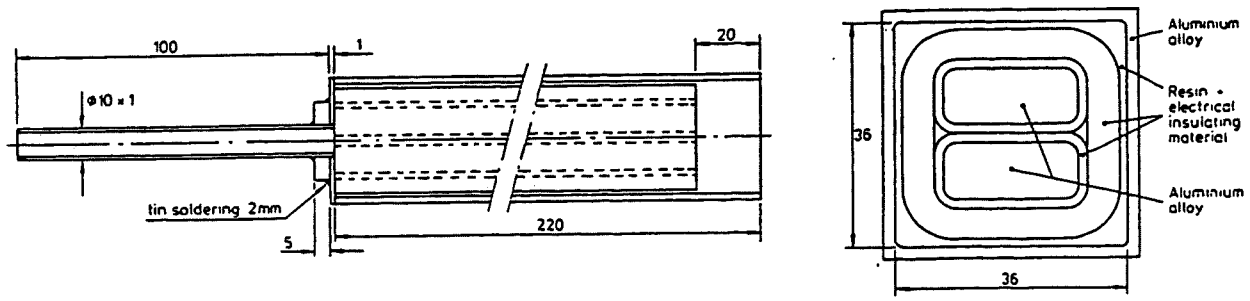

Fig. 1 - Schematic view of the model irradiated

gas released, temperature of the samples and neutron fluence rate. Each component was directly connected to a vacuum pump for evacuation of the internal free space before starting irradiation and to pressure transducers for measurements during irradiation.
Final irradiation conditions achieved were : fast neutron fluence rate (E > 0.1 MeV) of 2.7 10^{15} m^{-2} s^{-1}, corresponding to a dose rate of 6 Gy/s [3]; a gamma rate of 5 Gy/s; temperature in the epoxy resins kept below 80 °C. Four irradiations have been performed : the first one for fine assessment/tuning of boundary conditions (TP272-00), the remaining three up to respective total dose of 10^5, 10^6, 10^7 Gy (TP272-01,02,03).

4. RESULTS AND DISCUSSION

Figure 2 shows the performance of the first irradiation (TP 272-00). Movement of the rig in and out of the irradiation field is shown, together with temperatures measured at different positions along the component. Pressure release in the components was measured continuously during irradiation. The quartz vials were put after irradiation in a sealed chamber, broken and pressure changes measured. Data from both series of measurements were consistent. Figures 3 and 4 show the measured pressure inside the components for the experiments TP272-01, 02, 03 normalized with the free volume available and the amount of resin.
Up to 4 10^5 Gy, the behaviour is quite similar for the three experiments.

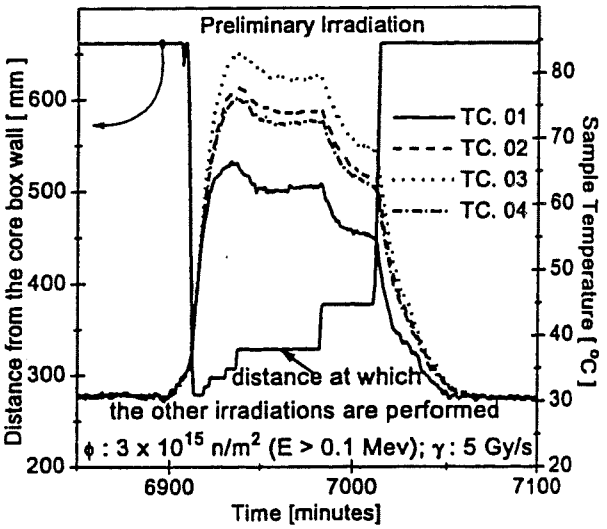

Fig. 2 - Preliminary Irradiation (TP 272-00)

The gas production rate lies in the range 0 - 2 cc/g/MGy, with a slight regular increase with increasing doses. At higher doses the production rate strongly increases with increasing doses, sometimes with abrupt changes, as it is shown in figure 4 (around 2 10^6 Gy).

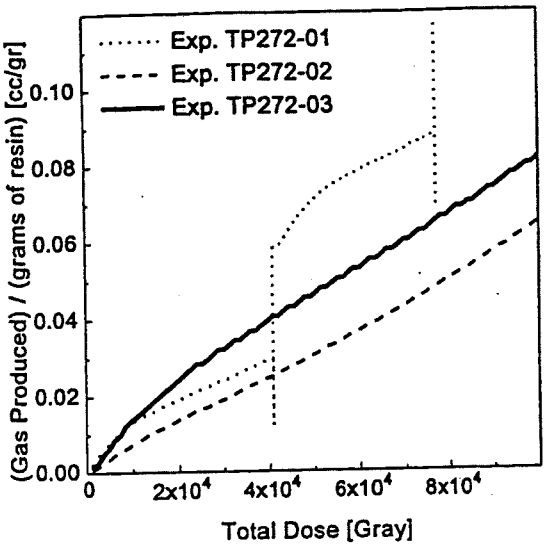

Fig. 3 - Gas released (Exp.TP272 -01, -02, -03)

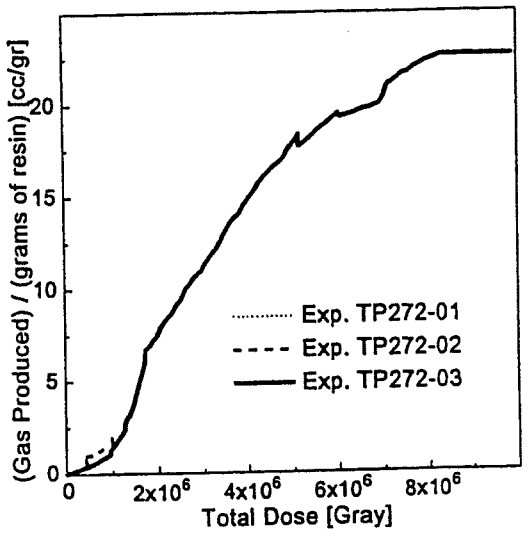

Fig. 4 - Gas released - Exp. TP 272-03

Literature data [3, 4] on epoxy resins irradiated in a pure gamma field, indicates production rate saturation at low doses (10^5 Gy). In the experiment TP 272-03 saturation is visible around 10^7 Gy. Gas release goes up to 10 cc/g/MGy. Pressure developed is such that deformation of the aluminum enclosure at high dose (10^7 Gy) was observed. Moreover, in the first two experiments release of gas after irradiation end was observed (figure 5). This behaviour can be explained by the presence of cavities in the resin, either formed during impregnation and/or formed due to material degradation under irradiation. The gas produced fills the cavities, then it is slowly released. If irradiation time is short, then gas release can continue after irradiation end, while, for long irradiation time, release of gas occurs during irradiation itself. A picture taken by an optical microscope is shown in figure 6. Presence of various cavities is visible. Resin starts to become brittle at doses higher than 10^6 Gy.

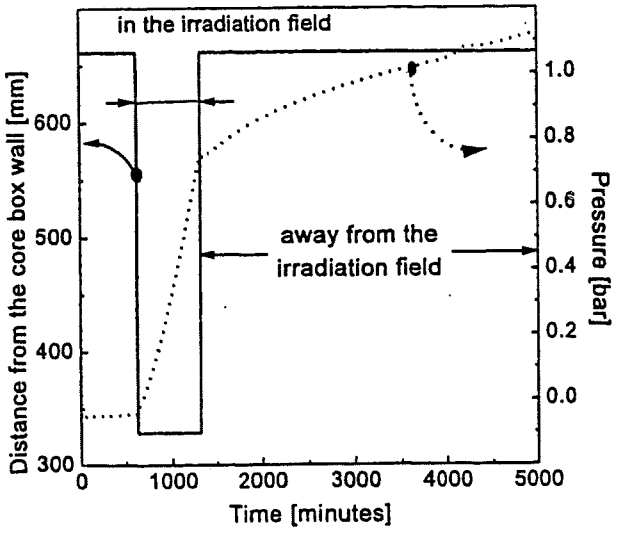

Fig. 5 - Release after irradiation end (TP272-02)

CONCLUSIONS

The mechanical properties of organic insulating materials are severely degraded long before any significant loss of electrical properties. Testing for mechanical behaviour therefore provides a

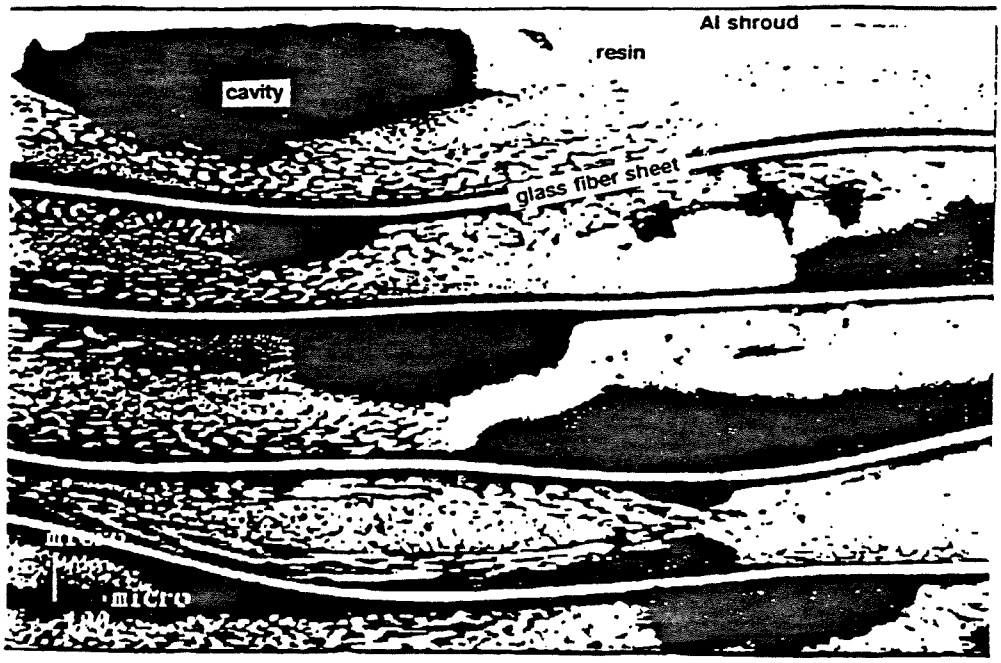

Fig. 6 - Picture of a sample taken by an optical microscope

conservatively safe prediction of loss of insulating properties.
According to IEC 544 norms [5, 6], the radiation index is used to qualify the performance of a particular material. In case of the epoxy resin considered literature data [3, 4] and direct examination of samples show that the relative radiation index could still guarantee residual mechanical properties to ensure the integrity of the material up to 10^7 Gy.
The actual life limiting factor is only the radiolysis phenomenon. Up to doses of 10^5 Gy the small amount of gas produced does not cause problems to the insulating component as a whole. At higher doses, although the mechanical strength of the resin is still ensured, the high gas production (rates of 10 cc/g/MGy) in a sealed containment causes swelling of the enclosure. Precautions (i.e. a gas pumping system) have been taken to evacuate gas from the JET coil cases.

REFERENCES

[1] J. Ahlf, A. Zurita editors, The HFR Characteristics of Installations and the Irradiation Facilities, EUR 15151 EN, 1993
[2] R. Metz, G. Sordon, G.P. Tartaglia, Epoxy Resins Irradiation for JET - EPIRO TP 272, P/F1/93/13, 1993, Petten
[3] M. H. Van de Voorde, Effects of Radiation on Materials and Components, CERN 70-10, 1970, Geneve
[4] J.F. Kircher, R.E. Bowman, editors, Effects of Radiation on Materials and Components, Reinhold Publ. Corp., New York, 1964
[5] Guide for Determining the Effect of Ionizing Radiation on Insulating Materials; Parts I, II, III,IV. Publication IEC 544, International Electrotechnical Commission, Geneve
[6] G.P. Tartaglia, P. Beynel, Radiation Damage to Insulation Materials : Test and Data Evaluation Procedures Following IEC Standard 544, CERN, TIS-RP 180, 1986

The Operation of the JET Beryllium Analysis Laboratory

D C Campling, R A Litchfield, R M Russ.

JET Joint Undertaking, Abingdon, Oxon, OX14 3EA, UK.

1. INTRODUCTION

Since the introduction of beryllium (Be) into the JET machine in 1989 the occupational hygiene screening for Be contamination has been a key feature of JET's Health Physics tasks. Beryllium dust is toxic and if inhaled can result in severe acute and chronic conditions which have been well documented. Techniques to rapidly assess Be contamination have been investigated. A Laser Induced Breakdown Spectroscopy (LIBS) system, in which a laser is used to vapourise Be from a filter paper prior to analysis was found to be inaccurate due to particle size differences between the calibration and JET's samples. A prototype on-line sampler although rapid was found to be insufficiently sensitive. The lack of a practical direct monitoring method for assessing JET Be contamination complicates the procedures required for the safe handling of the material. The requirements of the UK Control of Substances Hazardous to Health Regulations have necessitated the provision of on-site Be analysis facilities to provide the information necessary to protect the work force and demonstrate compliance with these regulations. The technique described here involves the dissolution of filter paper samples bearing Be dust in sulphuric and nitric acids and the analysis of the resulting liquor by atomic absorption spectrometry and is recommended by the UK Health and Safety Executive as suitable for assessing personnel exposure to Be.

2. CAPABILITIES

During shutdown periods this facility is required to process up to 300 samples per day. During the two years of the last long shutdown (1992 - 3) at least 60,000 filter paper surface smears or air sample filter papers were processed annually. The most important of these which constitute about 30% of the total were personal air sample (PAS) papers. These 4.9cm^2 (25mmø) papers are generated by 70% of the workforce of 350 registered Be workers who enter Be controlled areas during shutdown periods. The remainder is largely made up of routine filter paper smears taken whilst surveying Be controlled areas for surface contamination. JET assesses personal Be exposure for every entry into any of the seven major Be controlled areas on the JET site to demonstrate compliance with the UK regulations. In processing this number of samples the JET facility has adopted a two shift working pattern during shutdown periods. Sample turnaround times of < 6 hours are routinely achieved, with urgent samples, results are often available in < 1 hour.

3. SAMPLE PREPARATION

The preparation of samples imposes the greatest delay in obtaining results. Preparation of samples typically takes 1 - 3 hours whilst sample analysis takes just a few minutes.

The paper samples are dissolved in a mixture of 1ml of 98% sulphuric and 5ml of 70% nitric acid and heated from 200 - 400°C. For routine samples (90% of the total) this is carried over approximately two hours in glass tubes in automatic digestors which use a pre-programmed heating cycle. Urgent samples receive individual attention, being heated in beakers on hot plates and manipulated manually with results available within one hour. Cloth, oil and water samples are weighed and ashed in a furnace or boiled to near-dryness prior to the addition of acids. These procedures produce a liquor suitable for analysis by atomic absorption spectrometry (AAS).

4. SAMPLE ANALYSIS

This facility uses two Perkin Elmer 1100B AAS instruments. Briefly, the technique involves the aspiration of the sample into a nitrous-oxide/acetylene flame at 2000°C, this atomises the sample. Light at a very specific wavelength (234.9nm) is directed in a fine beam through the flame. Any Be present in the flame will absorb some of this light, this can be measured and used to quantify the concentration of Be in the sample. Prior to and after analysis of a batch of samples the machine is calibrated with, blank, 1 and 2μg/ml standards. The limit of detection is 0.03μg of Be in the sample.

The machine print-out is used by the analyst to calculate the result in $\mu g/m^3$ of air, μg/ml of fluid or $\mu g/m^2$ for surface contamination. In so doing the accuracy and consistency of the readings of the standard solutions is checked.

5. SAFETY

All procedures used in this facility have been vetted through the JET Safety Assessment system. This has entailed taking safety related precautions which include, restriction on access, Be safety training for all staff and provision of all protective clothing required for handling concentrated acids. All staff working in this laboratory are registered Be workers. The sample preparation procedure produces acidic fumes, these are contained by working in fume cupboards whose containment standards are maintained by ensuring the face velocity airflow is > 1m/sec. The acidic fumes are neutralised by the use of a "scrubbing tower" which uses an alkali spray to neutralise the acid vapour prior to HEPA filtration and discharge to the environment.

Both the laboratory environmental air and the extracted air are sampled for Be, no airborne contamination has ever been seen.

Analytical acidic wastes are handled by a licensed Hazardous Materials Service which disposes of them under the Control of Pollution Act. Other liquid wastes are discharged into JET's monitored, double contained, active waste drainage system.

6. QUALITY ASSURANCE

A well established internal and external QA programme is maintained within this facility. On each day of operation a variable number of samples, contaminated with a known volume of Beryllium Sulphate solution from a calibrated pipette, plus blank samples, which altogether constitute at least 10% of the total number of samples processed, are submitted for analysis. These undergo an identical analytical procedure to all other non-QA samples that the laboratory processes. In addition some samples which give a positive result for Be are submitted to an external laboratory and analysed by a different method (Induction Coupled Plasma Optical Emission Spectroscopy; ICPOES). The results of these two QA programmes show that the JET facility is on average accurate to within ± 5%. The results are summarised in quarterly reports.

Segregation of glassware between that used for PAS and smear samples is maintained in order to avoid cross-contamination of the former because surface smear papers are likely, in some particular instances, to be highly contaminated. For this reason specialised industrial glassware washing machines based on the principles of a domestic machine but capable of cleaning inside small vials and digestor tubes are used to clean all laboratory glassware.

7. RESULTS

Of the PAS samples processed 99% had a Be content corresponding to $< 0.2\mu g/m^3$ of air, which is JET's limit for establishing a Be controlled area and is 10% of the statutory limit. PAS samples exceeding $0.2\mu g/m^3$ are compared with criteria for the selection of appropriate Respiratory Protective Equipment (RPE). A wide range of RPE has been used at JET extending up to full air-fed pressurised suits. Surveillance of PAS results has enabled JET to relax RPE requirements in the torus, following decontamination, to the point where no RPE is worn.

8. COSTS

The running costs of this facility vary with the operational status of the JET machine. During shutdown periods when high numbers of samples have to be processed and a shift roster is manned the annual running costs approach £130k (185kECU). This includes all consumables, glassware, gas supplies, protective clothing, gloves, acids, spares for equipment and some maintenance costs (but excluding the salaries of the five staff). During operational periods with lower sample numbers this figure is ≈ 20% less.

The costs associated with the major items of equipment and plant which includes two AASs, four auto-digestors, three fumecupboards, an acid fume scrubber and air input and extract systems is ≈ £112k (160kECU).

9. SUMMARY

Despite the delay associated with sampling, processing and analysis JET has successfully managed all its potentially hazardous operations with Be. These include pressurised suit operations in the Be lined torus and removal of Be contaminated components up to a vessel octant.

JET's experiences with this facility are relevant to future fusion devices which plan to utilise beryllium.

10. ACKNOWLEDGEMENTS

The authors wish to thank Mr. J. Banham, Mr. K. Cornwall, Mr. A Foster-Jones and Mr. M. Scotcher for their efforts whilst working in the laboratory and Mr. W. Temple of AEA Technology, UK. for consultancy support.

Antennas and Waveguides for the JET Pumped Divertor Microwave Diagnostics

P C S Prior, D V Bartlett, R Prentice, R J Smith, X Tellier.

JET Joint Undertaking, Abingdon, Oxon, OX14 3EA, UK.

1. INTRODUCTION

To facilitate electron density and temperature measurement in JET's new pumped divertor a group of microwave antennas has been incorporated in the divertor target plate connected via waveguides to ex-vessel instruments.

This paper presents the design and engineering detail of the in-vessel/ex-vessel waveguide system and measurements of the system transmission efficiency.

2. DIAGNOSTICS

Six antenna/waveguide channels have been installed to provide three lines of sight as shown in fig 1. These are common to and used simultaneously by three diagnostic systems. These are: 1) an interferometer operating at frequencies of 130 and 200 GHz in 'O'mode which measures the line integral of the electron density[1], 2) an Electron Cyclotron Absorption diagnostic which uses a swept frequency source in the range 120 and 240 GHz (2nd harmonic 'E'mode) to give the spatial profile of the n_eT_e product[2], and 3) a reflectometer operating at eight frequencies between 50 and 100 GHz in 'O'mode providing estimates of peak electron density[3].

3. DESIGN CONSTRAINTS

The waveguides and antennas have been designed to minimise signal loss in the system. The in-vessel environment is hostile in terms of radiation, heat loading, ambient temperature, vacuum, dynamic loading due to plasma disruptions, magnetic fields and eddy currents. In addition the space and remote handling requirements limit the scope further. Ex-vessel the number of bends has been minimised.

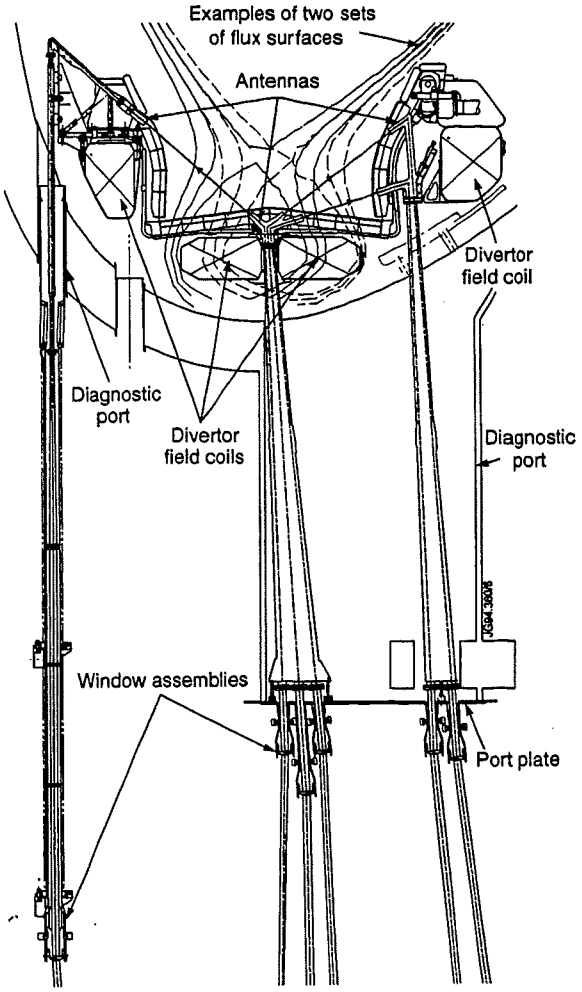

Figure 1. Section through the JET divertor.

3. IN-VESSEL COMPONENTS

3.1. Antennas and mountings

The six antennas are located between the elements of the divertor target plate structure as shown in fig 2. This gap is typically 12mm wide and limits the internal section of the antenna to 7mm in the toroidal direction. Embedded some 8mm below the tile surfaces, the antennas are protected from the particle flux but are subjected to the radiated heat flux. Finite element calculations indicate a maximum temperature of 650°C at the antenna tips.

The antennas have been manufactured in an alumina dispersion strengthened copper, Glidcop®[4]. The single antenna was produced by wire erosion and the multiple antennas by a combination of machining and electrodeposition. The multiple antennas include integral mitre bends.

Each antenna is mounted in a socket and retained by a single clamp screw. This is compatible with the remote handling requirements and allows removal of the antennas for replacement of the adjacent tile assemblies or accommodation of alternative tile configurations. Figure 3 shows the section of the central multiple antenna and its mounting socket.

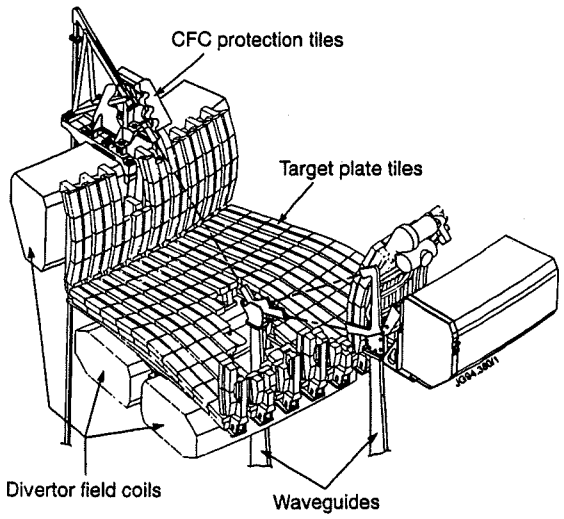

Figure 2. Cutaway view of target plate showing antennas.

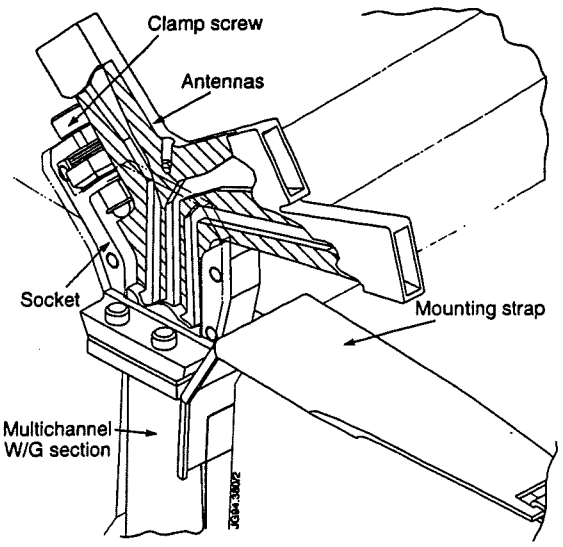

Figure 3. Sectioned multiple antenna and socket.

3.2. Waveguide and tapers.

From the antennas each channel is routed down a diagnostic port. as shown in fig 4: The single wave guide via a small circular port close to the centre of the machine and the others via a large vertical port.

The waveguides below the antennas are manufactured in copper, typically 1.6m long and incorporating electroformed tapers which expand the section from non-standard at the antenna (7×7.5 mm) to WG 16 (X-band, 10x23mm) at the vacuum boundary window.

Each antenna socket is mounted on a structure clamped to a divertor coil. The coils are continuously water cooled and 12mm relative movement occurs between these and the vacuum vessel when it is baked. This movement is accommodated and the required mechanical support provided with by arrangements.

The single waveguide is supported in a tube which is attached to the machine's mechanical structure and not subjected to the thermal expansion of the vessel. A double wall vacuum bellows is used to allow for the vessel movement. Ceramic spacers electrically isolate the waveguide.

The multiple waveguide assemblies are supported against disruption forces by fabricated stainless steel shrouds. These are mounted on a flexible pivot at the coil and located at the port plate

using pins sliding in electrically isolated bushes. Thus as the vessel moves relative to the coils the waveguide can pivot slightly and vertical differential expansion of 8mm can be also be taken up.

4. WINDOWS

Each waveguide channel is provided with a crystal quartz window which forms the vacuum boundary. The window is wedged at an angle of 2.69° to suppress resonance due to internal reflections. All the windows use a gold diffusion bond and are fitted to demountable vacuum flanges.

Clearances in the window assemblies allow the in-vessel waveguide to pivot as previously described. The internal and external waveguides at the window are angled to compensate for refraction and are optically aligned with the vacuum vessel at operational temperature. Fig 5 shows the arrangement.

5. EXTERNAL WAVEGUIDES

Figure 6 shows the routing from the vessel to the JET diagnostics wing. All waveguides are oversized (dimensions >> wavelength) and total waveguide length is ≈100m for each sight line.

Brackets, attached to the vacuum vessel ports, support near-vertical waveguides beneath the JET machine. Each of these incorporates a 5.3m long linear taper increasing the section to WG10 (S-band, 34x72mm) to minimise transmission losses. The tapers consist of bolted aluminium alloy assemblies with epoxy bonded flanges. Movement of the vacuum vessel is accommodated by elastic deformation of the waveguides beneath the machine.

The waveguide section is again reduced to WG16 to accommodate a set of polarising wire grid splitters which are used to separate the 'O'mode and 'E'mode signals. Mylar air seals, set at the Brewster angle, are to be incorporated in the waveguides to maintain the integrity of JET's torus hall ventilation system.

Standard waveguide 10 and 16 sections (aluminium and copper respectively) are used with special compact flanges to allow high density packing. The flanges are attached to the waveguide using a heat setting epoxy adhesive. A jig is used to ensure correct alignment and the flange faces are machined flat and square following bonding.

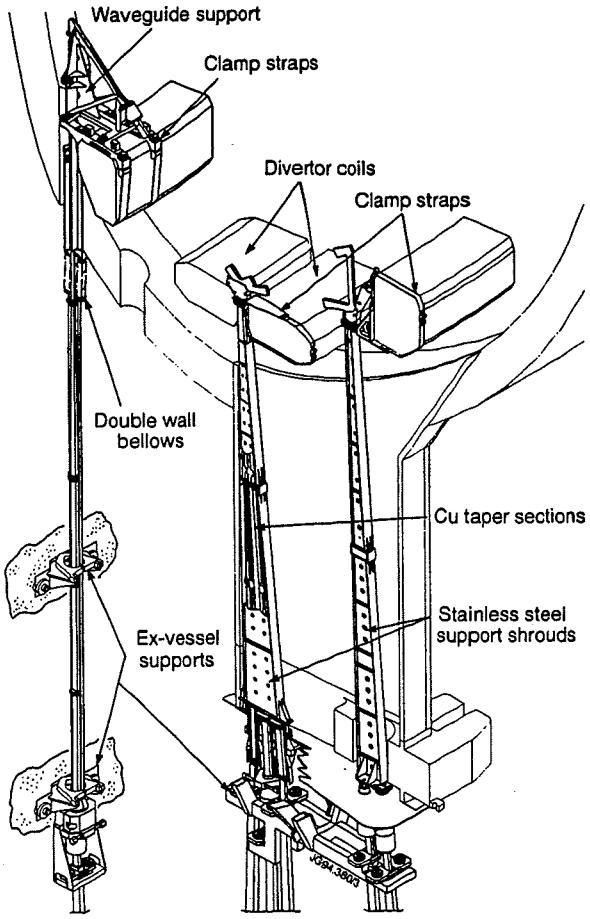

Figure 4. Waveguide routing down diagnostic ports

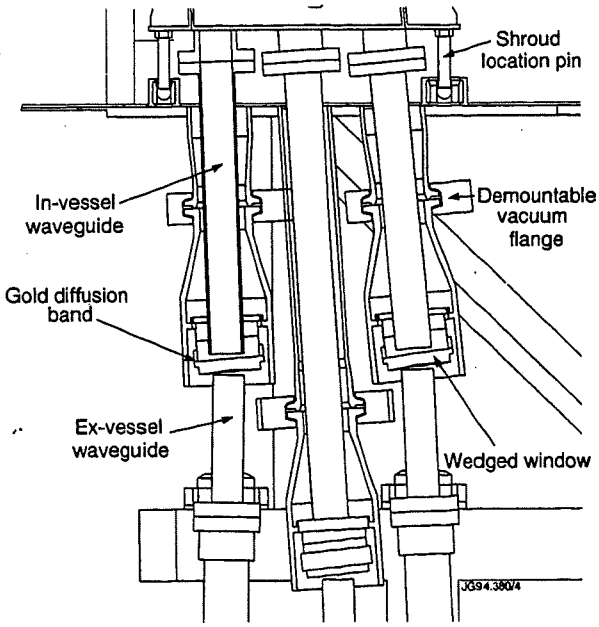

Figure 5. Window arrangement.

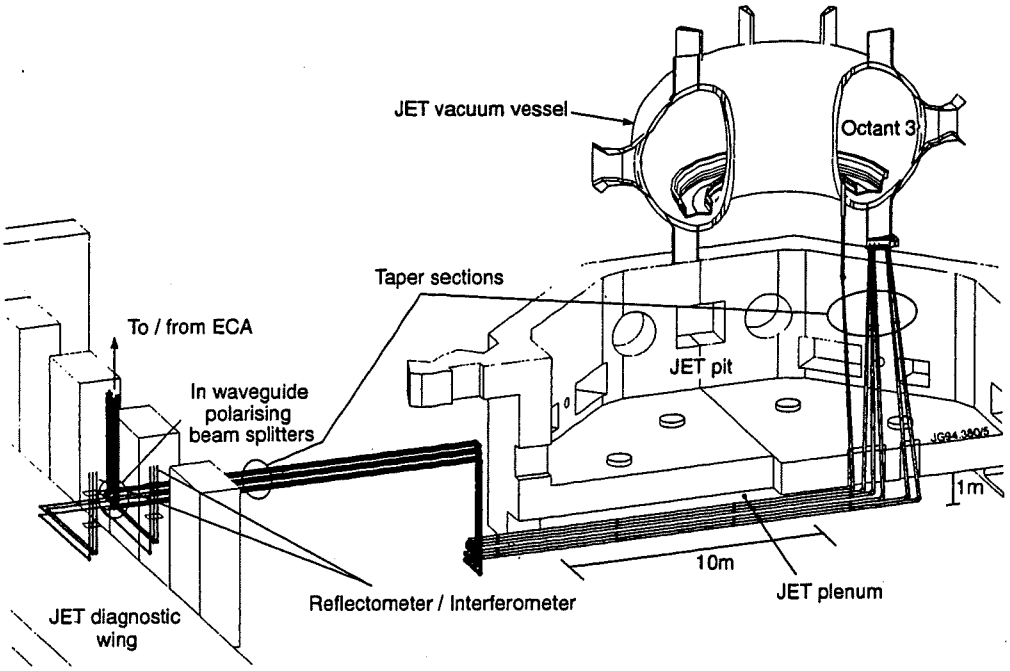

Figure 6. Waveguide routing to diagnostic wing.

All waveguide joints are dowelled to maintain alignment.

The mitre bends and polarising wire grid splitter bodies have been produced in aluminium alloy (WG10) and brass (WG16) using a combination of conventional, wire erosion and spark machining.

A system of supports allows adjustment of the waveguide positions and they have been aligned to within ±1mm using traditional survey techniques.

6. TRANSMISSION PERFORMANCE

Measurements on one of the channels, including transmission between the antennas, give a loss of 45dB at 150 GHz in 'E'mode and 55dB at 110 GHz 'O'mode. These are about a factor of 2 above the calculated losses but still provide a margin of 20dB over the minimum acceptable signal.

REFERENCES

1.R. Prentice et al. - The proceedings of the 10th Topical Conference on High Temperature Plasma Diagnostics (Rochester, New York, USA, May, 1994) - to be published in the Review of Scientific Instruments.

2. R. J. Smith et al. - Proceedings of the 8th International work shop on ECE and ECRH (Gut Ising, Germany, 1992)

3. L. Cupido et al. - New reflectometer diagnostics for JET. to be published in proceedings of 21st EPS Conference on Controlled Fusion and Plasma Physics (Montpellier, France, June, 1994).

4. SCM Metal Products Inc. Ohio, USA.

Engineering a new Compact Soft X-Ray Diagnostic on JET

S Dillon, B Alper, A Edwards, R Gill,
S A B Staunton-Lambert, D Wilson.

JET Joint Undertaking, Abingdon, Oxon, OX14 3EA, UK.

This paper describes the engineering aspects of a new compact in-vessel soft X-ray (SXR) diagnostic system which has been installed onto JET for the pumped divertor phase.

1. Introduction

The main in-vessel components of the diagnostic system occupy two toroidal positions on the JET machine. The first and most important position locates eleven independent camera assemblies (giving six separate views of the plasma) around the inner wall of the vacuum vessel away from access ports. This allows the system to view plasma activity in some detail at a single cross-section of the torus. The second position locates a single camera assembly which can be used to indicate plasma toroidal activity.

Figure 1. General arrangement of the SXR diagnostic system at its main location on the JET machine (octant 2). The central viewing lines of each of the eleven cameras are indicated.

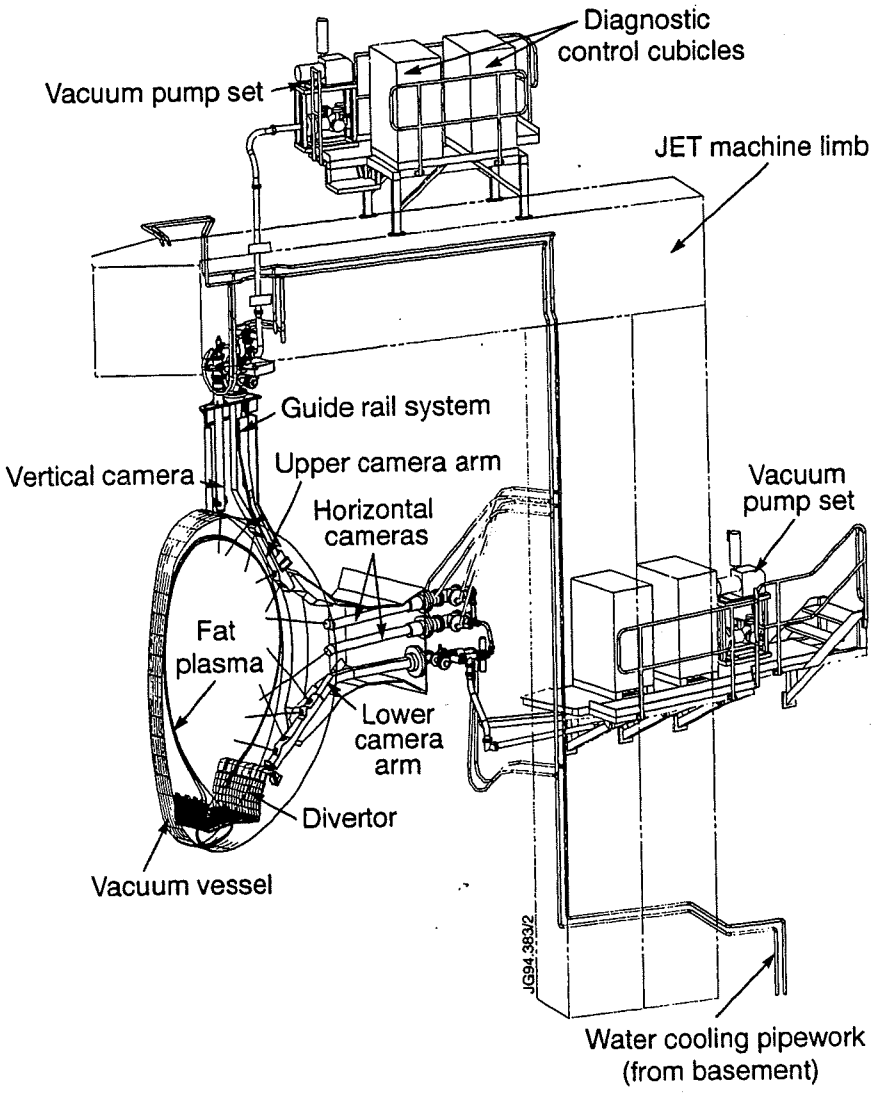

Figure 1 shows the general arrangement of the SXR system at its main position within the JET machine. The cameras are located within five separate sub-assemblies which penetrate the vacuum vessel at octant 2. The sixth camera (not shown) is located at octant 7. The control cubicles which contain the first part of the signal processing package (pre-amplifiers, ADCs, and an optical link), have been located as close as possible to the diagnostic sub-assemblies in order to reduce signal noise pick-up.

The diagnostic assembly within the torus hall also includes separate vacuum pumping systems for providing a quality secondary vacuum within each sub-assembly, and a water supply for cooling the camera heads.

The diagnostic consists of two types of SXR camera sub-assemblies - a single camera system (horizontal and vertical cameras) and a multi-camera system (upper and lower arms). The multi-camera arms contain four individual camera head assemblies which have similar components to the single system and which operate in the same environment.

2. Camera Head Assemblies

Central to the SXR diagnostic is the camera head assembly which monitors plasma activity inside the JET vacuum vessel. Figure 2 shows a camera head assembly as it would be mounted in the upper and lower arms, and Photograph 1 shows an actual assembly prior to being assembled to the cable tray. Figure 3a shows a camera head assembly used in the single camera system. In each case, the SXR detecting component within the camera head is a microchip array of 35 photo diodes which normally operates in the visible spectrum, but has found to operate well in the SXR region. To operate efficiently, the chip is maintained at nominal 20 deg.C - achieved by mounting it on a water-cooled copper block. The detecting elements are also sensitive to neutron and gamma ray activities (more apparent during high performance plasma discharges).

The resulting signal noise from these activities is subtracted using a single version of the detecting element which has been placed in a position screened from the X-rays in the camera head assembly. Other components within the camera head include: two infra-red emitting diodes for camera calibration; two thermometer elements for temperature monitoring; a contoured tungsten aperture which defines the precise viewing angle; and a heat shield for reducing radiation heating effects.

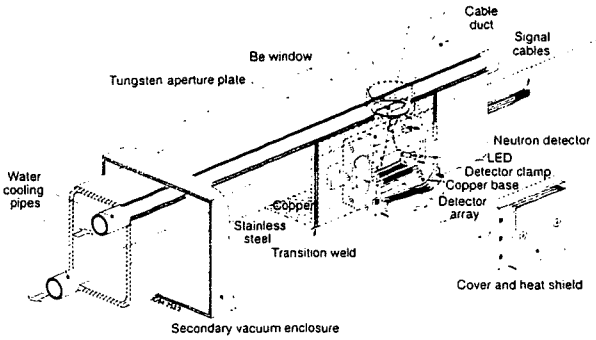

Figure 2. Camera head assembly used in one of the multi-camera arms.

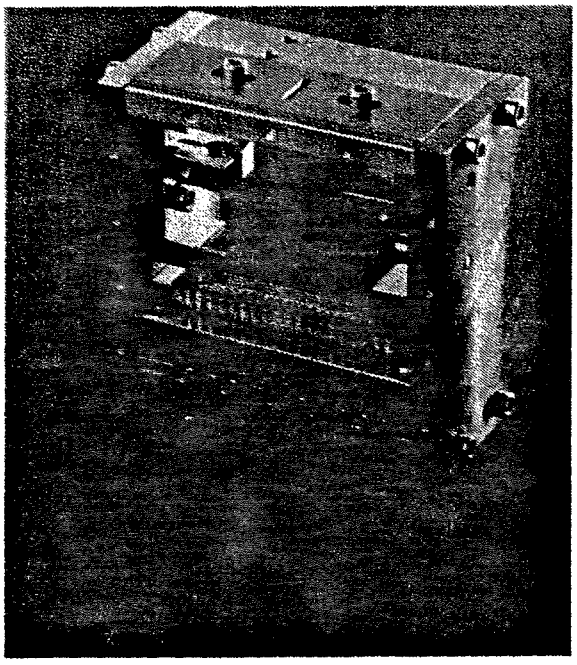

Photograph 1. Camera head assembly for multi-camera arms.

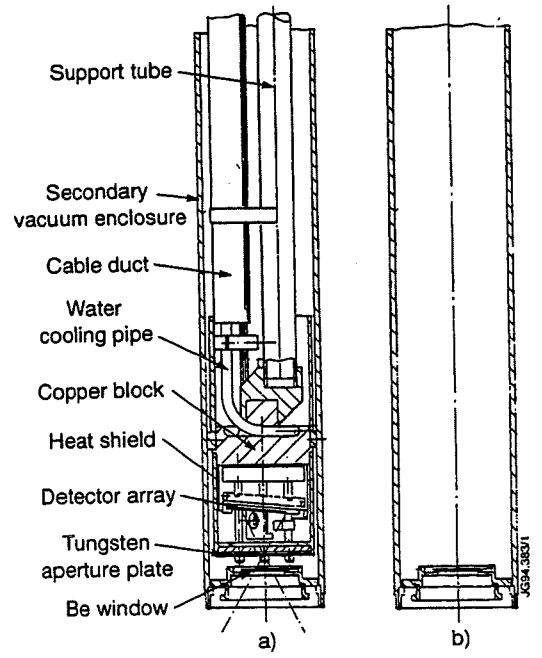

Figure 3. Camera head used in the single camera assembly. 3a shows the complete assembly. 3b shows the camera head retracted from secondary vacuum volume.

The cables used to transmit signals from the assembly are of a special low noise type in order that the signal to noise ratio is maximised. A 250mm thick Be window allows the camera to view the plasma, acting both as a filter to long wavelength radiation which will affect camera sensitivity, and as a boundary between the JET vacuum and the diagnostic secondary vacuum. The secondary vacuum is necessary in order to eliminate thermal conduction from the secondary vacuum enclosure to the camera head assembly, and for X-ray transmission.

3. Camera assembly structure

The body of the camera head is fabricated from OFHC copper and is directly (in the case of the single camera assembly) or indirectly water-cooled to maintain the detecting element strip as close as possible to room temperature. In the case of the multi-camera arms, each of the four camera head assemblies is secured to local copper sections which are welded to a water-cooled cable tray otherwise fabricated from 304L grade stainless steel. Restricting the use of copper to local sections reduces possible forces on the assembly due to eddy currents during plasma disruptions (a cable tray made from copper alone would give rise to a four fold increase in forces). The cable tray assembly within each camera arm is supported inside its secondary vacuum enclosure using a central pivot block and a series of minimum contact bump stops (to reduce conductive heating) which are necessary to locate the camera heads behind the beryllium windows. The beryllium windows are of a race-track design to account for movement due to thermal differential expansion between the secondary vacuum enclosure (which is subjected to radiant heat from the JET environment) and the water-cooled cable tray.

The JET primary vacuum is protected from possible rupture of the beryllium windows (in the event of pressure rise within the diagnostic assemblies) by incorporating a bursting disc between the secondary vacuum volume and the torus hall. The windows are tested to 3 bar abs. prior to assembly whereas the bursting disc will rupture at 1.25 bar abs. Thus, in the unlikely event of pressure rise in the secondary volume, the diagnostic can still be continuously cooled whilst JET is operating - the camera head assembly will be irretrievably lost if it were allowed to exceed 180 deg.C.

4. Installation and removal of the camera assemblies

The lower camera arm is bolted to one of the main horizontal ports of the vacuum vessel and is located in-vessel with a single electrically insulated sliding support - see Photograph 2. This allows for both thermal differential expansion effects and prohibits forces due to current loops between the arm and the vacuum vessel. Installation of the lower arm requires vessel intervention to aid its location in the support assembly. Removal of the arm may be achieved without vessel intervention by applying force to the external flange (removal from the support has yet to be realised). The upper camera arm is welded to one of the main vertical ports and is positioned in-vessel using an electrically insulated guide wheel and rail system - see Photograph 3. This again allows for both thermal differential expansion effects and forces due to current loops, but it also allows the arm to be installed and removed without vessel intervention. With both camera arms, installation and removal requires that the JET vacuum vessel be at room temperature and pressure.

The single camera assemblies are all bolted to the main ports of the JET vacuum vessel. The horizontal cameras require no further support, but the vertical cameras are supported in-vessel to allow for movement of the main vertical port during plasma disruptions. Both the horizontal and vertical camera assemblies can be installed and removed without vessel intervention. In addition, the camera head assembly can be withdrawn from its secondary

vacuum volume without removing the complete assembly from the torus - see Figure 3b. Thus, in principle, the camera head assemblies can be replaced at any time without affecting the torus environment (although the torus would need to be at room temperature to prevent oxidation of the beryllium window and to aid manual handling).

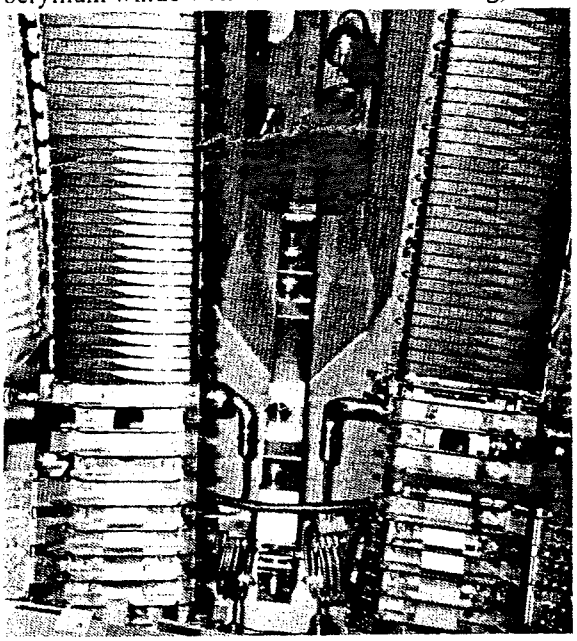

Photograph 2. Lower Camera Arm in position showing in-vessel support

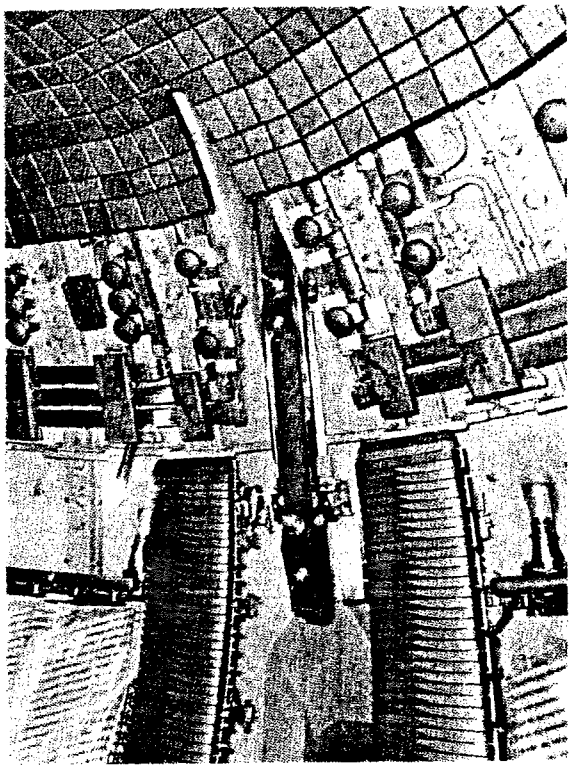

Photograph 3. Upper Camera Arm in position with guide rail assembly

The Engineering of JET Diagnostics

C I Walker, S F Dillon, N P Hammond, C J Hancock,
N Lam, E J McCarron, P C S Prior, J Reid, S Sanders, X Tellier,
A J Tiscornia, G A H Whitfield, C H Wilson, D J Wilson.

JET Joint Undertaking, Abingdon, Oxon, OX14 3EA, UK.

There are some 62 identifiably different diagnostic systems on JET. 22 were installed new at the last, Pumped Divertor, shutdown and a further 22 which were modified, upgraded or repositioned. This paper describes some of the engineering aspects peculiar to the renewed diagnostic systems, reviews their construction and installation and gives an overview of the design of presently installed diagnostic equipment at the Torus. Examples are considered that illustrate the breakdown into a categorisation based on their installation method. This is useful for discussion of many of the associated engineering problems of method and quality control of manufacture, vulnerability, access for installation and maintenance and ultimately system safety and reliability. The function and measured plasma parameter of specific diagnostics is covered in other papers and is not attempted here, neither is a full catalogue of Diagnostics on JET.

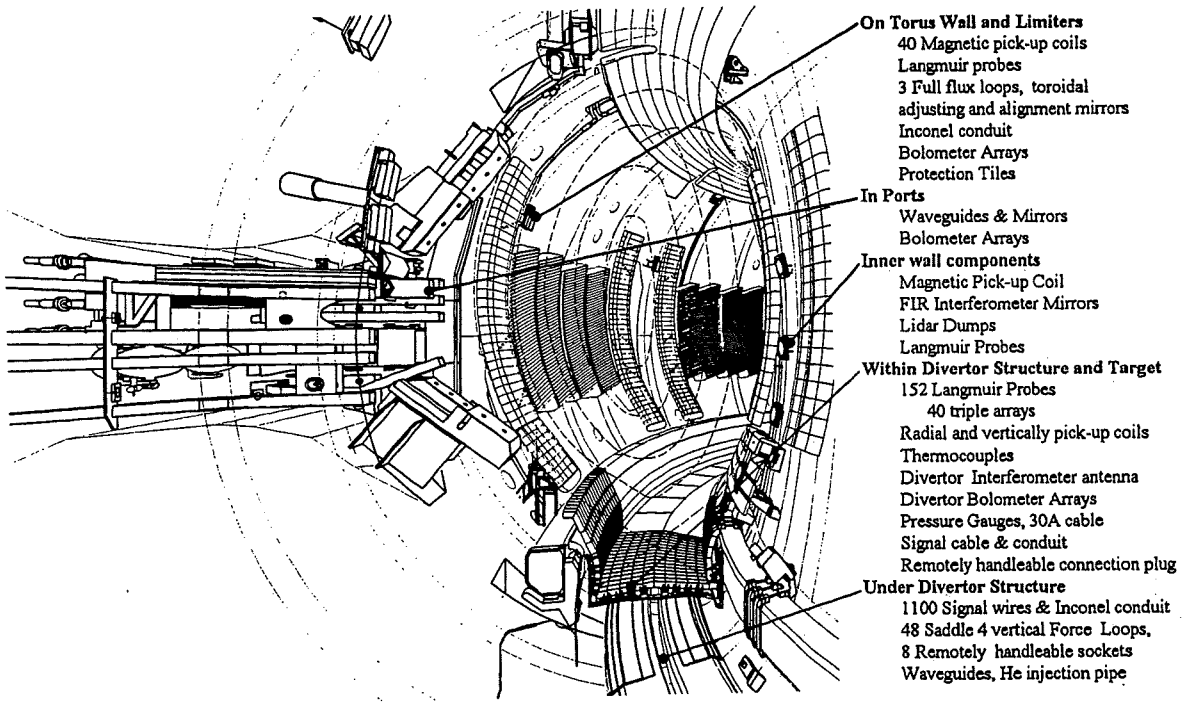

Figure 1. View of the inside of the Torus showing diagnostic equipment installed in-situ.

1. Equipment Installed InVessel in situ

This group of equipment poses the largest intrusion into the In-Vessel shutdown work and is not routinely maintainable. Installation directly in-situ is often chosen as the only option because of the relative economy of space compared with pre-assembled insertion. It also accommodates better dimensional inaccuracies of the in-vessel features. Welded structures are positioned within 20mm of the last closed flux surface of a full sized plasma. Systems are both built up in-situ or preassembled in a modular fashion.

This equipment experiences the most hostile environment and radiation, magnetic interference, temperature, thermal gradients forces from disrupting plasmas & halo currents, Beryllium coating, arc damage, microphony, have to be dealt with. Delicate equipment must be well protected during the installation of other in-vessel components

Mineral insulated cable or Inconel armoured and glass braided wires of acceptably low outgassing, are provided for electrical signals, in twisted pairs or quads to avoid magnetic pick-up. Quick connection techniques limit in-vessel installation time. Substantial, robust Inconel conduits are welded over the cables for protection and screening. Cores of Chromel/Alumel and OFHC are provided. Cables for Bolometer Arrays, in particular, are in second screening conduits, isolated from the Torus wall and particular attention is paid to the avoidance of microphony of these cables by rigid attachment within their conduits. Langmuir probes are fitted within specially modified carbon limiter tiles on the inner wall guard limiter and outer wall poloidal limiter. Pressure gauges mounted within the divertor region both above and below gas baffles require 30 thicker cables rated at 30A experiencing substantial magnetic forces. Glidcop cores are used for high temperature and current applications.

1.1 Pre-assembly in Divertor Target Structure

A major series of diagnostics required to be close to the plasma is fitted directly to the Divertor Target structure allowing installation in a modular fashion with this structure. Pre-assembly here affords greater precision especially of the 40 triple and two sets of 16 single Langmuir Probes tips that are set up ex vessel but finally fitted in-vessel when the divertor tiles are in place, special provision is made to enable remote removal of the tiles. Radial and vertically oriented pick-up coils are mounted with signal cable conduit to the structure. The signals for the divertor target modules are brought out through 40 way plugs and sockets, designed with particular care of material selection for high temperature and remotely handleable in-vessel. All wiring is held in welded Inconel conduits to prevent damage and to simplify the installation of the target modules.

1.2 Inner Wall Components

Here there is limited space, graphite tile protection is inevitably needed and deposition of beryllium must be designed for. Installation in situ is inevitable and attempts are made to install these components as pre-assembled modules.

1.3 Port & Wall Mounted Equipment

Mirror systems are required to access the centre of the plasma, these necessitate rigid, stable mounts with the provision for removal for cleaning .

Microwaveguides, mounted inside Vertical and Horizontal ports, are either built up in-situ or preassembled within a modular structure. Within the divertor target ECA waveguides terminate with remote handling attached antennae to allow Divertor target renewal.

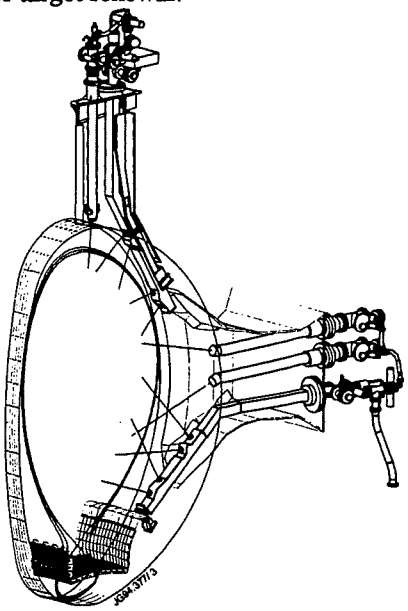

Figure 2. Section of Octant 2 showing Soft X-ray Camera Arrays installed from ex-vessel

2. InVessel Equipment Installed from Ex Vessel

This is an important set of diagnostic equipment because of replaceability, modifications, upgrades, repairs, refurbishments. The design difficulty of these systems is the access lines and the requirement to pre-conform to loosely toleranced parts of the Torus vacuum vessel. The additional complication for installation and removal of these is the potential beryllium or radioactive contamination and absorbed tritium. Local plastic isolators techniques have been developed and

special arrangements have been made for decontamination of Beryllium and active machining.
As well as detectors or collection optics, it is often necessary to bring significant other services such as vacuum and cooling inside the vacuum envelope for protection from the hostile environment. These incur a heavy overhead of Quality Assurance to prevent leaks into the torus. 11 optical periscopes with cooled coherent fibre bundles in interspace vacuum bring primary windows within the Torus, The Divertor LIDAR uses mirrors and protective shutters in Torus with more remote windows to attain better viewing than given by a direct line of sight from a main port flange. Substantial Guideways have been installed in-vessel to receive some of these systems

3. Closing the Vacuum Vessel

Diagnostics use 77 of the 188 apertures through the ports of JET. The attachment method always requires consideration of remote access and is by bolted or clamped metal sealed flange or welding. Reliability of the vacuum boundary is paramount and attracts a high Quality Assurance classification for material and weld integrity.

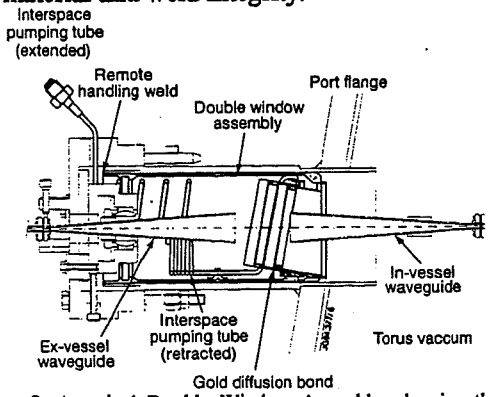

Figure 3. A typical Double Window Assembly, showing the arrangement for microwave transmission

3.1. Windows

Windows for the complete spectrum of e-m radiation comprise the largest set of these components. There are 12 neutron windows of thinned regions (to 2mm) of the Inconel flange plate. X-ray diagnostics make use of 12, 125μm, Beryllium foil windows, vacuum brazed to stainless steel flanges. Pressure stand off has been tested to be better than 3 bar differential, the probable pressure in the interspace given a water leak at temperature and bursting discs ensure further safety.
There are 92 optical and microwave windows on JET. 68 are of a double assembly type with an integral accessible pumped guard interspace provided for added security of the Torus vacuum during Tritium operation. They are designed to be robust and cyclically tested to Torus conditions.
The life requirement to the end of the JET programme is for 42,000 hours at operating temperature (between 40°C and 350°C), 30 venting and 30 thermal full cycles. Sizes vary from 25mm to 197mm diameter. Natural crystal quartz, sapphire and fused silica are used to meet the diverse optical specifications. Diffusion bonding with gold, aluminium and silver-lead alloy is used with geometrical arrangements designed for the material properties and environment of each system. Gold bonded Crystal Quartz windows have been tested to 10,000 hours at 350°C. An active test programme continues now to establish life expectancy and to define the failure modes of the windows used.
Direct views of the plasma are limited, but where they do exist the problem of protection from direct deposition of Beryllium from the Evaporators has to be solved with articulated windows or shutters.

3.2. Electrical Feedthroughs

1372 electrical signals are brought through the vacuum boundary making use of otherwise inaccessible lower ports or small upper circular ports, wired through or plugged at the port. 45 assemblies with different detailed construction are used. The principle of construction with mineral insulated cables vacuum brazed into two bulkheads is used in all. These have proved robust and reliable once installed.

3.3. Mechanical Feedthroughs

Mechanical feedthroughs are required for mirror actuators, shutters and calibration targets etc. At present these all use bellows sealing with an interspace guard vacuum. Linear actuation is the simplest format but the a wobble stick design is used for multi-turn rotary motions. The high speed rotation of the multi-facetted mirrors of the VUV

Spectrometers has been tested to $2x10^6$ revolutions.

3.4. Extensions to the Torus Vacuum

Ex Vessel diagnostic equipment with integral vacuum boundary to the Torus generally pose the problem of including scanning systems within the Torus vacuum and the consequential boundary sealing problems. Configuration of space and provision of support is important in the design. Conventional auxiliary vacuum systems are used which are to be modified in future to more complex gettered systems because of Tritium handling requirements. Where possible these systems incorporate a Torus isolating valve to allow full diagnostic commissioning before opening to the Torus vacuum.

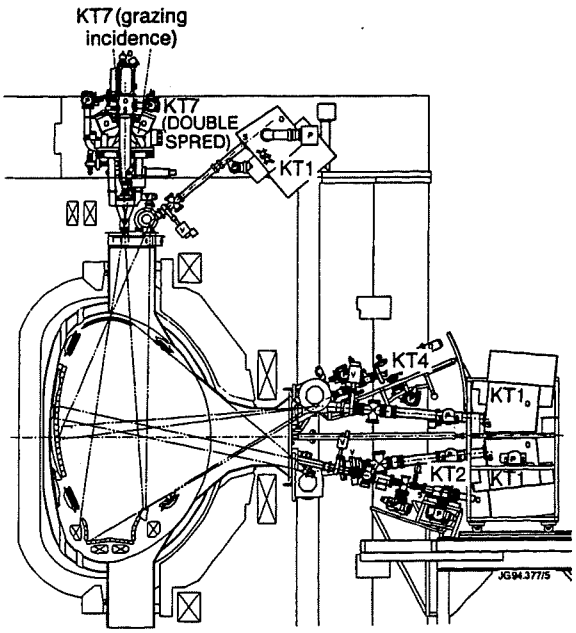

Figure 4. Section through Octant 6 showing how the array of spectrometers has been arranged to scan the whole plasma region with rotating mirrors or oscillating spectrometers

4. Unconnected to Torus Vacuum

Diagnostic equipment in this category comprise the remainder of the diagnostic equipment in the Torus Hall. For detectors within the Torus Hall this normally includes substantial shielding and support structures. The equipment is still kept modular as it is required to be easily removed to gain access to the Torus structure, vacuum ports and windows etc. Enclosed optical beam lines and microwaveguides pose more significant design

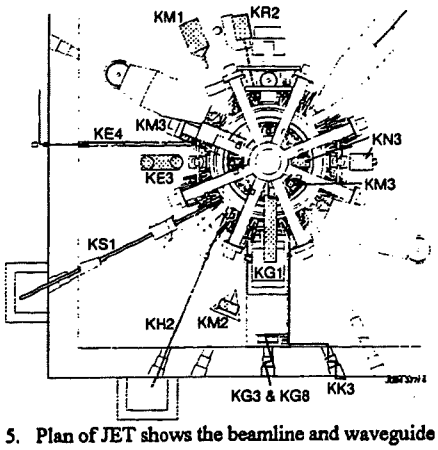

Figure 5. Plan of JET shows the beamline and waveguide bridges tranversing the torus Hall.

problems because of the need for precise alignment back to remote detectors while attached to moving Torus vacuum vessel. The systems are made to be simply removed for access to other systems by construction of remotely handleable bridge structures spanning from the Torus to the Torus Hall wall.

Optical beam lines through the JET biological shield necessitate further shielding outside. Microwave systems however make use of labyrinthed routes through the shield which become grouted into the biological shield with no further possibility of adjustment. Waveguide bends, however, are minimised to preserve signal quality.

Although equipment outside the Torus Hall is not discussed here it is equally important to the proper functioning of the diagnostics. The interfaces with other systems and space conflicts, however, are fewer and several design options are normally presented. The discussion of the interface with CODAS and operational requirements, vital to the project requirements, are better handled elsewhere.

5. Conclusion.

Diagnostics inevitably cause modifications in otherwise regular, simple, or at least symmetric systems of the basic Tokamak and a major part of the engineering of diagnostics is the successful integration of the interfaces with these systems.

We acknowledge the skill and patience of engineers on these parts to accomodate the properly engineered diagnostics and their consequential success.

Detailed Design, Installation and Testing of the New Coil Protection System for JET

V Marchese, E De Marchi, N Dolgetta, J R Last, C Ryle, G Sannazzaro, L Scibile, J van Veen, L Zannelli.

JET Joint Undertaking, Abingdon, Oxon, OX14 3EA, UK.

The recent installed pumped divertor at JET has required an upgrade of the existing coil protection. The new Coil Protection System (CPS) detects electrical faults and protects the coils against mechanical and thermal overstressing due to operation outside safe limits. Protective actions include immediate removal of the voltage from the coils. The paper describes the design, construction, commissioning and early operation of the protection system.

1. INTRODUCTION

The plasma control and protection scheme in use at JET is shown in Fig. 1

The upgrade of the JET magnet system [1] and the general trend towards the extension of the operating region, within machine safe limits, has led to the decision to design and install a new Coil Protection System (CPS) [2]. CPS detailed design started at the beginning of March 1993, and the system became operational in May 1994. The system has required new voltage and current transducers, pick up coils, flux loops, Rogowski coils and temperature sensors for most of the circuits.

Measurements or computed quantities are compared with suitable thresholds. If a threshold is exceeded an alarm is generated and protective actions are taken.

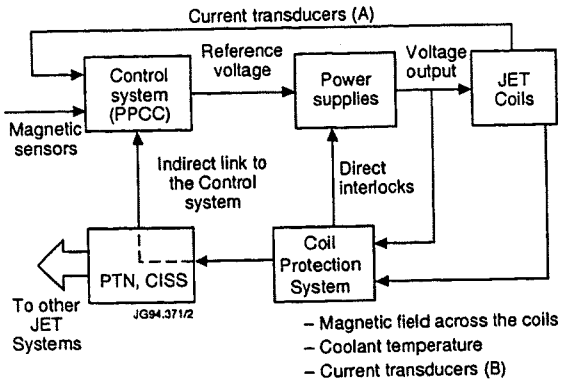

Fig. 1. Control and Protection Scheme

The protection algorithms can be classified into five categories:

C1. Conventional overcurrent and overvoltage protection for all the circuits.
C2. Thermal stresses (e.g.. I2t) in all the coils.
C3. Mechanical stresses on the coils and vacuum vessel.
C4. Circuit equation integration and comparison with the measured currents.
C5. Thermal model for the divertor coils.

2. FAULT DETECTION ALGORITHMS AND PROTECTIVE ACTIONS

The block diagram shown in Fig. 2 summarises the fault detection algorithms implemented in CPS. Details on the five categories of protection are outlined below.

C1. Overvoltage and overcurrent protection has been implemented for both poloidal and toroidal field systems. The poloidal field (PF) system includes up to 10 independent circuits and up to 22 coil elements (or subcoils). The toroidal field (TF) circuit includes up to 2 independent circuits, the first for the odd coils and the second for the even coils [2]. The protection is active all the time. A simple deglitching technique makes this protection more "robust", against unwanted intervention especially in case of plasma disruption.

During the pulse two levels of overvoltage have been defined: 95% and 100% V_{max}, with V_{max} maximum voltage,

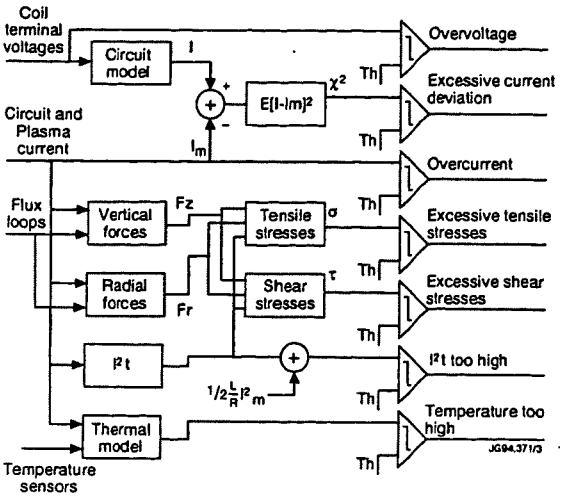

Fig. 2. Fault Detection Algorithms

whilst outside pulses only one level (10% V_{max}) is defined. V_{max} takes into account the maximum voltage of the power supply and the induced voltage during normal transients. A deglitching time of 20ms has been chosen.

Three levels of protection have also been defined for the circuit currents. Two during pulse: 5% and 10% above I_{max}, with I_{max} maximum current allowed in the circuit, and one, 10% of I_{max}, outside pulses. The deglitching time used for the overcurrent protection is 2ms.

The current in the P1 six central pancakes (I_2) in principle can be raised up to 60kA with a current in the toroidal coils of 67kA, whilst the maximum current on the end coils (I_1), made of four pancakes, is 40kA. This is obtained with the poloidal flywheel generator (PFGC) connected to the end coils, and a thyristor converter unit (PFX) connected to the centre coils. A special protection has been implemented to reduce to an acceptable level the ΔI in the end coils in case of full inversion of PFX when I_1 and I_2 are close to the limits. The protection is activated when the "average current" in P1 coil, defined as $0.4I_1 + 0.6I_2$, exceeds 45kA and the current in the end coils exceeds 42kA. The above protection has been tested and operates successfully.

C2. The limits on the I^2t are a function of the initial temperature of the coolant and, for a given cooling rate of the coils, affects the pulse repetition rate.

C3. The protection system makes real time computations of the forces using flux loops and ampere-turn measurements or analytic coefficients.

The tensile and shear stress (σ and τ in Fig. 2) of each coil is computed as a linear combination of vertical force F_z, radial force F_r and temperature (computed from the energy dissipated). The radial and vertical forces on each coil are given by equations of the form:

$$F_r = NI \cdot B_z, \quad F_z = NI \cdot B_r \qquad (1)$$

where NI is the measured ampere-turns of the coil and B_z and B_r the measured field crossing the coil. The total vertical force transmitted to the vacuum vessel by the divertor coils is the sum of the forces acting on the four coils. Fig. 3 shows a comparison of the vacuum vessel vertical force experienced during a pulse with currents of 16.5kA and 15.5kA in divertor coils 2 and 3, plus 10% sweeping, measured with this method and with strain-gauges mounted on the vessel restraint legs at the main vertical ports.

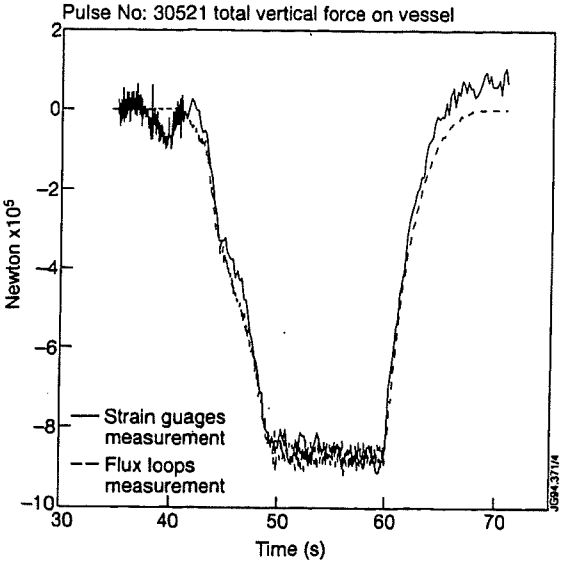

Fig. 3. Vessel Vertical Force (No. 30521)

The vertical field at the divertor coils is not measured but is estimated as a linear combination of the ampere-turns of all coils and the plasma current.

C4. This protection, based on circuit equation integration in real time, has been implemented for the toroidal field circuit and soon will also be implemented for the poloidal circuit. The inputs to the circuit models are the coil terminal voltages. In either case the computed currents are compared with the measured currents. A large difference would indicate a possible fault and would terminate the pulse.

The two models are integrated only during pulses. The poloidal and toroidal field models are decoupled and therefore they can be integrated separately.

The PF circuit equations, when the iron core is saturated, are given by:

$$L_\theta \frac{dI_\theta}{dt} + R_\theta I_\theta = V_\theta - g^T \frac{dI_p}{dt} \quad (2)$$

where: V_θ is the vector of the input voltages, I_θ is the vector of the computed PF currents, L_θ is the circuit inductance matrix R_θ is the circuit resistance matrix and g is the vector of the mutual inductances with the plasma. The system inductance matrix is computed multiplying the single turn inductance matrix by the matrix of the number of turns with the proper sign. The unsaturated state of the iron has been modelled too.

C5. A simple model will be used to estimate the temperature of the epoxy insulation and copper windings of the divertor coil. The inputs to the model are the vessel temperature, coil case temperature, coil currents, coolant flow and coolant inlet and outlet temperatures.

During operation the temperature of the vessel is maintained at about 300°C. In spite of being protected by radiation heat shields over most of their surface, the coils are heated by the surrounding environment as well as by energy dissipation during pulses. This means that as long as the vessel is hot, the divertor coil cooling has to be maintained.

The object of the protection system is to keep the epoxy glass insulation in the main body of the coil below a safe temperature (60°C). This is achieved by limiting the differential temperature of the coolant within 20°C *(to avoid thermal stresses between turns)* and the maximum I^2t on the basis of the initial temperature of the coolant before the pulse.

Two fail-safe commands [2] are sent individually to the PF and TF power supplies (see Fig. 1): a Voltage Off and a Circuit Breaker Open command. These direct interlocks are backed-up by the actions performed via the Pulse Termination Network (PTN) and the Central Interlock and Safety System (CISS).

3. IMPLEMENTATION

CPS is a multiprocessor and multitasking system based on VME (Fig. 4). Data is continually collected from the Analogue and Digital I/O boards by the DSP Master Board, via the VME Bus. These values are used to provide continual protection of the coils.

While JET is not pulsing it is possible to suspend the protection for a short period of time and to load from the Level 1 software on the host computer a new set of operating parameters.

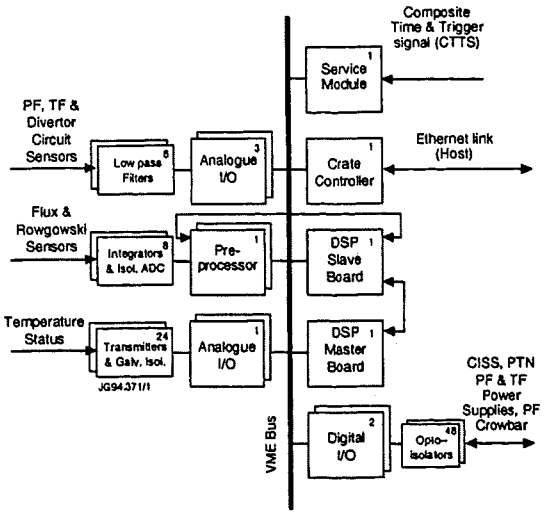

Fig. 4. CPS Hardware Configuration

As a pulse is started messages are received from the host computer via the Crate Controller, preparing the CPS software for the next pulse. The information in these messages instructs CPS what data channels to collect during the next pulse and also indicates the state of other parts of the plant. From this point on CPS monitors the progress of the pulse using the status information from the Service module together with values from some of the digital inputs.

While JET is actually pulsing, further data is collected from the Pre-processor card, by the DSP Slave board. This board provides drift and offset compensation of the integrated signals received from the Pre-processor. This data is then combined with the data already being collected by the DSP Master board, to provide the large number of inputs upon which the full range of protective algorithms are run. If a fault is detected, appropriate actions are taken directly using the digital outputs to issue commands to the remainder of the plant, while at the same time messages are sent to the host indicating the source of the fault and the actions taken.

During the pulse, samples of the collected and calculated signals are simultaneously stored in a Shared Memory block on the DSP Master board. After each pulse these stored values are collected by the GAP programme on the host, via the Crate Controller, and archived.

The code for the DSPs was mostly written in C using the facilities of the SPOX operating system both to share the CPU power between the various protection algorithms and to control the communication channels between the various boards involved.

4. OPERATING EXPERIENCE

During the first six weeks of operation, the protection system monitored the running of 815 pulses, and failed only once. Even this failure did not compromise the safety of the machine since fail safe design criteria has been adopted extensively. The majority of CPS actions took place near or after the end of the pulse without hindering the actual experiment, while several potentially damaging maloperations have been terminated. During these pulses CPS took action on 106 occasions as shown in Table 1.

Table 1. Faults detected by CPS

No.	Type of faults
7	Test pulses: produced deliberately to test the CPS system
26	I^2t trips: due to operation of the machine approaching safety limits
17	Temperature trips: due to noise on thermocouples during disruptions
8	Voltage Out of Pulse trips: due mainly to residual voltage on coils after pulses
19	Overvoltage or P1 ΔV trips: usually due to disruptions or failures of other machine components (e.g. S4A Switch, etc).
24	Overcurrent trips: mainly due to initial limits being set too low or unexpectedly high currents during disruptions
5	Central Timing System Errors

The number of trips per week is decreasing as parameters are adjusted and operational experience gained.

5. CONCLUSION

Early experience indicates that CPS will be useful and reliable. Because of its flexibility, protections not included in the original design have already been implemented and others (eg. TF Coil Torque Calculation) are planned.

6. ACKNOWLEDGEMENT

The authors would like to thank Magnet & Power Supply and the Control & Data Acquisition Divisions for their assistance.

7. REFERENCES

[1] J.R. Last et al, The JET Divertor Magnetic Configuration and Coil Design, 16th SOFT Conference, London, 1990.

[2] V. Marchese et al, A new Coil Protection System for the Divertor Configuration at JET, 15th SOFE Conference, Hyannis, USA, 1993.

Alignment Systems for Pumped Divertor Installation at JET

B Macklin, R Brade[1], G Celentano, J J Cordier[2],
G Israel, J Tait, E van Lente.

JET Joint Undertaking, Abingdon, Oxon, OX14 3EA, UK.
[1] GEC Alsthom, Leicester, UK.
[2] Assigned Associate Staff from Tore Supra, CEA, Cadarache, France.

The installation of the JET Pumped Divertor, designed to study impurity control, has recently been completed. The main components are four magnetic coils, forty eight divertor plate assemblies, one toroidal cryopump, eight ICRH antennae, sixteen inner wall guard limiters and twelve poloidal limiters. Due to the high thermal loads, accurate positioning of plasma facing components to the magnetic centre of the machine was a major requirement. Typically alignment within ± 2 mm was required, with steps between tiles on a component being controlled to ± 0.25 mm. In some cases a set of components was required to be concentric, while also lying within a narrow band defined by the position of some other components. A typical example of this was the positioning of the poloidal limiters, which perform the dual function of limiting the plasma and also protecting the antennae. Clearly, a measuring system accurate to better than ± 0.5 mm was required.

1. INTRODUCTION

In previous shutdowns at JET component surveys and alignment checks depended on some combination of conventional metrology equipment and jigs usually based on a precise survey ring. JET decided to continue with this philosophy for the Pumped Divertor installation. A sophisticated survey ring system was designed and built. This was used successfully for the installation of the lower vessel components e.g. divertor coils and divertor modules. During preparations for the installation of the outer wall components it became apparent that to achieve the required accuracy at a height of over two metres above the survey rings would result in an extremely cumbersome system, requiring a long and elaborate set-up procedure for each new working position. In addition, this philosophy required the presence of the survey rings in vessel over an extended period (in excess of five months). This would not have been compatible with many of the tasks planned for execution in parallel with the main inner and outer wall tasks and therefore would have seriously compromised the flexibility of the overall planning. As a result other techniques were investigated, resulting in the purchase of a three dimensional non-contact measuring system. As it is JET's philosophy to minimise risk to shutdown program by using only proven methods it was decided to continue with the development of the mechanical system in parallel. This paper describes the development necessary before this system could be used inside the JET vacuum vessel. The transition from jig-based to optical system is discussed along with techniques being developed for future use at JET.

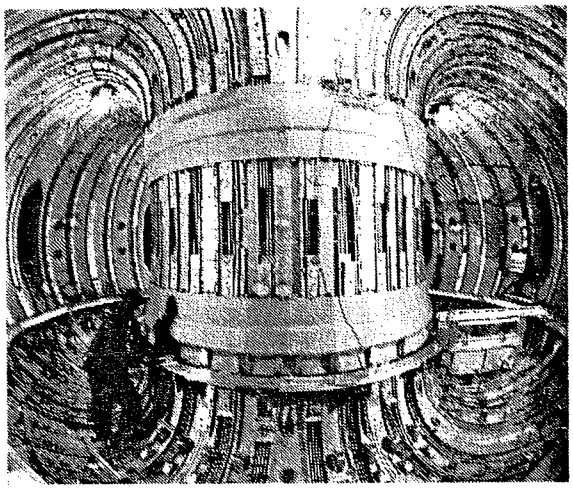

Figure 1. Survey Ring System in use In-vessel

2. MECHANICAL SYSTEMS

A setting system based on a pair of very accurately machined survey rings together with a system of dedicated precision jigs was used to position the divertor coil support bosses[1]. The inner ring (4200 mm diameter) fitted with two targets 90° apart, was accurately positioned toroidally and radially in-vessel by optically aligning the targets with the centre of the mechanical structure of the JET machine. This datum is also used for ex-vessel components. Through investigation of the plasma/wall erosion surveys, the mechanical centre of JET had previously been shown to be coincident with the magnetic centre to within ± 2 mm. Then the outer ring (8500 mm diameter),

which consisted of sixteen beams, was assembled using a jig from the inner ring. A radial arm location tool was then suspended from the inner and outer rings to facilitate the positioning of components on the vessel floor (fig. 1). Later in the shutdown, the survey ring system was used for the positioning of the divertor plate assemblies[1].

3. OPTICAL SYSTEMS

In December 1992 JET began to investigate the possibility of using optical systems, of which there were a number on the market. A number of these were quickly ruled out on the basis of their inaccuracy or other limitations such as focal length of the instruments being incompatible with the internal dimensions of the vacuum vessel. The ability to operate accurately in the expected residual magnetic field at JET was also an important consideration. JET evaluated the use of Leica's ECDS3 [2] system in a similar application at Tore Supra [3]. This system consists of two electronic theodolites, with dual axis liquid compensators, linked to a personal computer and a software package called ECDS3 (Electronic Coordinate Determination System).

JET carried out a series of trials which confirmed the systems performance and accuracy. Finally, following assurances from Leica that the residual magnetic field in the JET vacuum vessel would not affect the operation or the accuracy of the system, JET ordered the ECDS3 system and began to plan the use and development of the system in detail.

4 COMPUTER AIDED THEODOLITE

Generally referred to at JET as the CAT (Computer Aided Theodolite) system, ECDS3 operates by measuring the horizontal and vertical angles to a network of targets and a calibrated scale bar and solving the resulting simultaneous equations using a mathematical technique known as 'bundling' At JET, 184 targets were welded to the inner and outer walls of the vessel. These targets, called control points, define the volume in which all subsequent surveys will be carried out. When all these targets and the scale bars have been sighted by at least two theodolites in a multiple set-up process known at JET as a 'Global Survey', the ECDS3 'bundling' process is used to calculate the co-ordinates of all the targets relative to theodolite No. 1. These co-ordinates can be mapped unto the Torus master system, whose origin is the centre of the Torus, using a co-ordinate transformation with known datums. Datum positions were determined relative to the Torus using the same technique as used for setting the survey ring (fig. 2).

JET's major requirement was for a three-dimensional setting system suitable for locating the jigs used to position the mounting pads for the various components on the vacuum vessel wall. In some cases the system would also be used for direct positioning of the actual components. Use of the CAT system for setting involves sighting onto at least three targets whose positions are known in

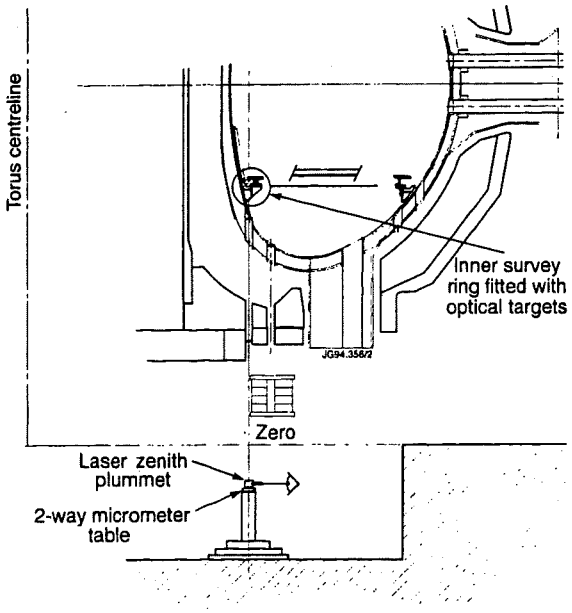

Figure 2. Inner Survey Ring Alignment from Pit

the Torus master system. As the ECDS3 software can then calculate the positions of the theodolites relative to the centre of the Torus, it is only necessary to place the theodolites so that good sighting can be achieved. The theodolites are then used to determine the co-ordinates of the component datum points via targets fitted to the components. These co-ordinates are then converted from the default Cartesian (X,Y,Z) to a cylindrical (R,θ,Z) co-ordinate system for setting adjustments. This conversion simplifies the setting process as the cylindrical system is the 'natural' coordinate system of the torus .

5. ACCURACY

The accuracy of the CAT System depends largely on geometry, redundancy of the sightings taken and the operator's understanding of how these two factors effect the data. Using JET's CAD system, CATIA, the optimum theodolite & target

positions were determined considering the unique multiple set-up techniques which would be required due to the shape of the vacuum vessel. It was necessary to ensure that all targets were visible from at least two theodolites positons, even at the end of the shutdown when all components would be installed. In parallel with this design and development, JET personnel received training from Leica in the use of the system. In addition a full size mock-up of the JET vacuum vessel was built to allow the multiple set-up technique to be developed and its accuracy assessed. During this four month period an improved multiple set-up technique was developed, which shortened survey time by 50%. A dedicated procedure for carrying out a CAT global survey of the vacuum vessel was prepared. This procedure was followed closely and with continued practice allowed survey time to be cut further. In parallel JET's spare octant was used for extensive setting trials for the major inner and outer wall components using the actual jigs and actual or prototype components. These trials also provided the opportunity to develop the measuring and adjusting technique for each component as well as providing an opportunity for installation personnel to become familiar with the CAT system.

6. DEVELOPMENT FOR IN-VESSEL USE

As well as developing a method for using the CAT system in-vessel, it was necessary also to package the system suitably. Wall-mounted vibration-free theodolite supports which could be used in any of sixteen toroidal positions at four heights with a variable radius were developed (fig. 3). Special removable spherical targets were also developed. The targets consisted of a boss welded to the vessel wall, a uniquely identified screw-in target, a unique identity label, designed to be visible through the theodolite, and a protective cover. The colour laptop computer was built into a special aluminium case along with the necessary interface modules. This allowed safe and convenient storage of all the hardware, reducing the number of electrical connections to be made and so reducing the setup time and the risk of damage. In addition, the computer was fitted with an integral modem which allowed fast downloading of data at the end of every shift to a dedicated computer ex-vessel. Data was not only duplicated by this process, but easy access to it was immediately available to selected personnel to allow report writing to proceed. Transfer of data on floppy disc was complicated by the risk of beryllium and tritium contamination.

7. SURVEY TECHNIQUE

To satisfy the requirements identified in the CATIA model, the majority of targets were positioned reasonably accurately with regard to height, otherwise following the geometric features of the vacuum vessel wall. To minimise the possibility of errors two global surveys of six set-ups were carried out on opposite shifts. Each target was sighted by two theodolites, 20% being viewed by four theodolites, 5% being viewed by six theodolites throughout the survey. This redundancy of sightings increases the accuracy. Each survey took two surveyors approximately 1.5 shifts (12 hours). Results of the surveys were compared and checked in detail and found to agree, in general, to better than 0.2mm. From these surveys the Torus nominal master system was established. This system was then checked for correlation with the fixed inner wall reference balls, used in previous shutdowns, and to the inner survey ring used for the first phase of the shutdown. The co-ordinates determined by the different systems agreed to within ± 0.9 mm. Additional checks on the scale accuracy of the CAT system were carried out by surveying accurately machined details of the survey ring confirming a measuring accuracy of better than 0.05mm/metre.

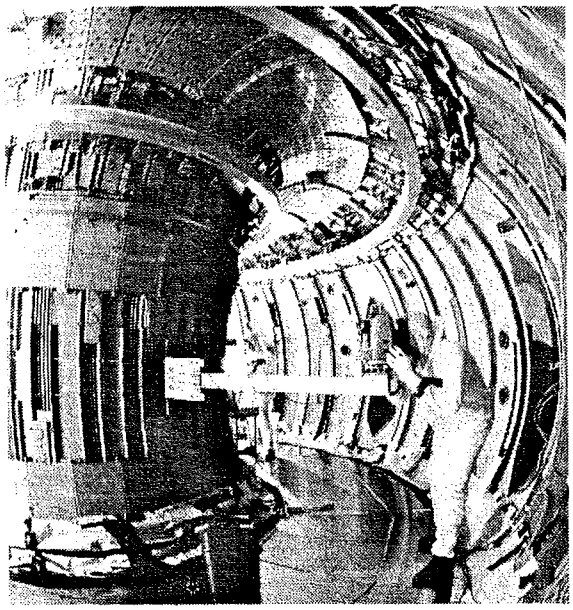

Figure 3. CAT System in use In-vessel

8. COMPONENTS INSTALLED WITH AID OF THE CAT

Major components installed with the aid of the CAT system included RF antennae, inner wall guard

limiters and poloidal limiters. For the limiters the vacuum vessel wall was surveyed directly with the CAT so that mounting pads could be machined to approximately the correct dimensions to take account of local variations in the vacuum vessel wall. Generally the CAT system was used to position jigs which ensured pads were welded to the wall at the required height and radial and toroidal position. Use of a jig was the quickest way of ensuring that up to ten pads were correctly positioned relative to each other. When the actual component was mounted on the pads the CAT was used for final positioning in an iterative process of suveying and adjusting. For most components the major requirement was for correct radial positioning. Height and toroidal position, though important, were usually secondary. During setting, components were frequently resurveyed from different theodolite setups and by different teams of surveyors so that accuracy was continually monitored, confirming that components were measured to better than ±0.3mm. Apart from the major components, for which the CAT system was primarily intended, it was also used to carry out 'as-built' surveys of divertor coils 2, 3 and 4. The CAT was also used for positioning or providing 'as-installed' survey data for many of the major diagnostics. As many of these were situated in inaccessible places e.g. main vertical ports, it would not have been possible to determine their position accurately using conventional methods.

8. FUTURE DEVELOPMENT

During future JET shutdowns, in-vessel work will be hampered by high (300Sv/hr) radioactivity levels. Contamination of the vessel by beryllium and tritium will necessitate the use of full pressurised suits. This will mean that the measurement systems used in the future must be pressurised suit compatible and eventually fully remote-handleable, while maintaining present levels of accuracy and flexibility. To this end JET is currently investigating ongoing changes in measurement technology in an attempt to determine the most suitable systems for use in the next planned shutdown and the subsequent remote-handling shutdown.

Towards the end of this shutdown the opportunity was taken to survey the in-vessel CAT targets using Convergent Photogrammetry so that JET could assess its potential for use in the next shutdown. Comparison with the CAT global survey data showed good agreement [4]. In conjunction with these investigations, on-going developments of systems currently in use at JET are being made. A modified CAT system is being developed which will allow operators to use the CAT system when wearing full pressure suits. This system utilises a miniature video camera fitted to the theodolite together with a monitor which means the operator does not need to sight directly through the instrument. Connection to an ex-vessel monitor will mean that in-vessel work can be supervised by an experienced CAT user with a resulting reduction in both the time and expense incurred in training new surveyors.

10. CONCLUSION

During the last shutdown at JET a major conceptual change in in-vessel measurement technology was made. Numerous checks were made to ensure the compatibility and concentricity of the new optical system with the old jig-based mechanical system. The advantages of the CAT system in terms of time, accuracy and flexibility were clearly seen. The CAT system will continue to be used at JET in conjunction with convergent photogrammetry with reduced use of jigs. The possibility of links with other non-contact systems is now the subject of research at JET.

11. ACKNOWLEDGEMENTS

The author wishes to acknowledge the skill and dedication of the GEC Inspection team, the assistance of JET's Drawing Office staff for their assistance with CAT-CAD interfaces and the staff of Leica(UK) for their technical support throughout the development.

REFERENCES

1. The Installation of the JET MkI Divertor Features and Achievements. G. Celentano at al., 18th Symposium on Fusion Technology, Karlsruhe 1994.

2. Leica AG, Photogrammetry and Metrology, CH-5035, Unterentfelden, Switzerland.

3. Effect of Misalignment and braze flaws on the Tore Supra Inner First Wall Behaviour. JJ Cordier et al., 17th Symposium on Fusion Technology, Rome 1992

4. CAT vs Photogrammetry: Details of Transformation Method and Analysis Results. E van Lente, JET internal report.

The JET Glow Discharge Cleaning System

P Andrew, G Bosia, R Claesen, L Grobusch[1], J Harling, J How, H S Jensen, H McBryan, J McCarthy[2], R Monk, J Orchard, R J Pearce, G Saibene, J Winter[1].

JET Joint Undertaking, Abingdon, Oxon, OX14 3EA, UK.
[1] Institut für Plasmaphysik, Association Euratom-KFA, Forschungszentrum Jülich GmbH, D-52425, Jülich, Germany
[2] University of Adelaide, Adelaide, SA 5001, Australia.

The JET tokamak has been fitted with a new glow discharge cleaning system. Four electrodes of a novel design, offer the following advantages over their predecessors: they do not need water cooling and they do not take up significant port space. Results are presented for the initial use of these electrodes including current density distribution and impurity removal rate.

1. INTRODUCTION

Recently the JET experiment was upgraded to include a divertor; 4 internal copper coils and a set of target tiles cover the lower part of the machine. The resulting reduction in the number of useful ports created a need for a more compact GDC electrode. The original JET electrodes [1] used the largest size of vertical port on the torus.

An electrode concept developed at KFA-Jülich [2] not only met the above criterion for economy of space, but also did not require water cooling. The absence of cooling water (and therefore potential water leaks), is especially desirable in the case of JET where routine operation with tritium is foreseen.

An effort was also made to streamline the electrical components on the exterior of the vessel. Coupling the DC and RF power needed for GDC was done at the power supply some 80m from the torus, instead of near the port.

2. THE GDC HARDWARE

Each of the GDC electrodes is powered by an independent power supply (Fig. 1). The coaxial feedthrough at the port was designed to have the same characteristic impedance as the coaxial cable thus eliminating the need for an RF matching network in the vicinity of the torus. The DC supplies feature an arc protection system which shuts off the power supply upon detecting a sustained drop in the output voltage.

All the power supplies are computer controlled. The impedance matching network, however, was manually tuned since the RF frequency and the length of cable were not expected to change. In practice, however, the conditions for ideal RF transmission changed with the glow pressure and DC glow current. It was never-the-less possible to choose a setting of impedances which limited the reflected RF power to less than 20% of the forward power for all conditions.

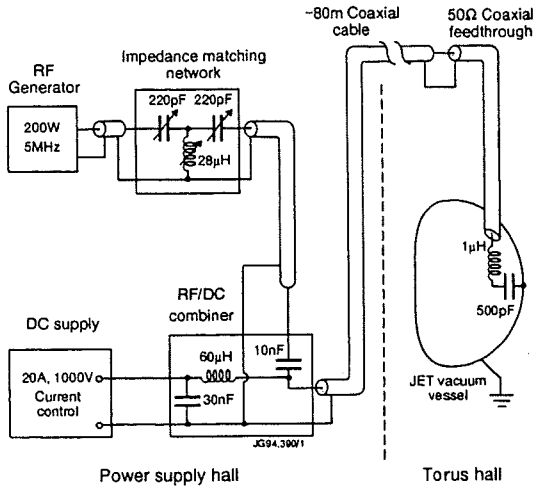

Figure 1. Electrical circuit for each electrode

The electrodes themselves are made of two inconel plates, insulated by a 2 x (0.45mm) thick plasma-sprayed layer of alumina, forming an ~1000pF capacitor. One plate is mounted to the inner wall of the torus, and the other is attached to a spiral coil with about 1μH inductance, forming a LC circuit with about 5MHz resonance frequency (Fig. 2).

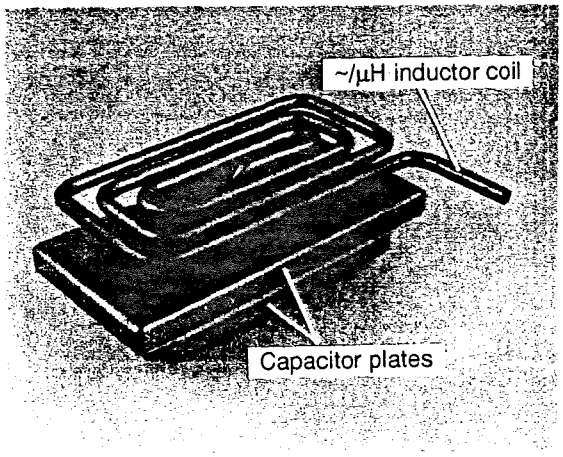

Figure 2. A GDC electrode.

The 4 electrodes are spaced 90° apart toroidally near the top of the vessel. The

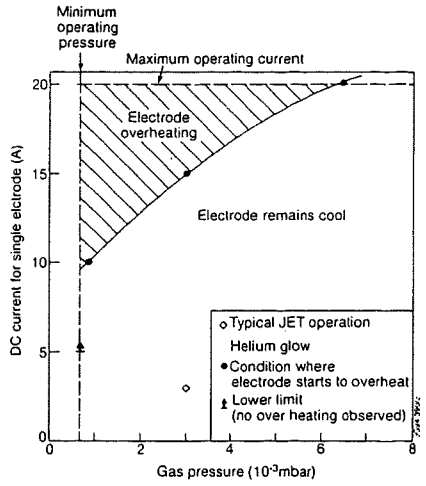

Figure 3. The electrode operating space, as measured in a 1.5 m^3 test vessel.

outer capacitor plate (which forms the anode together with the coil) has an area of 110mm x 220mm. The installed electrodes are within 100mm of the vessel wall, and are surrounded on all sides by protective carbon tiles which extend ≥150mm from the vessel wall.

The electrode (anode) is heated by electron bombardment. Although most of the GDC voltage drop 200-300V is between the glow plasma and the wall (cathode), a small (typically 10-20V) anode drop exists [3]. Heat is removed by conduction to the walls through the electrode itself and the surrounding gas. This places a boundary on the possible operating pressures and DC currents (Fig. 3), but has not hampered operation in JET.

3. PERFORMANCE

During the initial operation of the glow discharge, transitions to arcs were frequent. This is a result of relatively dirty surfaces; the JET vacuum vessel had recently been the site of nearly two years of in-vessel work. At low pressures, individual glows would spread out about the electrodes over a larger surface and coalesce. Under these conditions an arc would often simultaneously trip a second or even all 4 of the electrodes (Fig. 4). This problem was eliminated by reducing the power supply sensitivity to arcs from 1 msec to 10 msec.

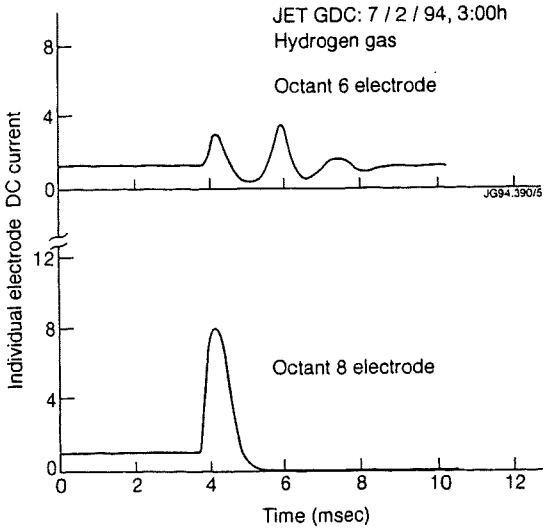

Figure 4. Effect of arcing on adjacent electrodes. The octant 8 electrode is tripped by a drop in voltage at the power supply output.

The current density was measured at a variety of positions for a range of pressures and currents for both D_2 and He glow discharges [4]. Fig. 5 shows the current density distribution for a typical operating pressure and current.

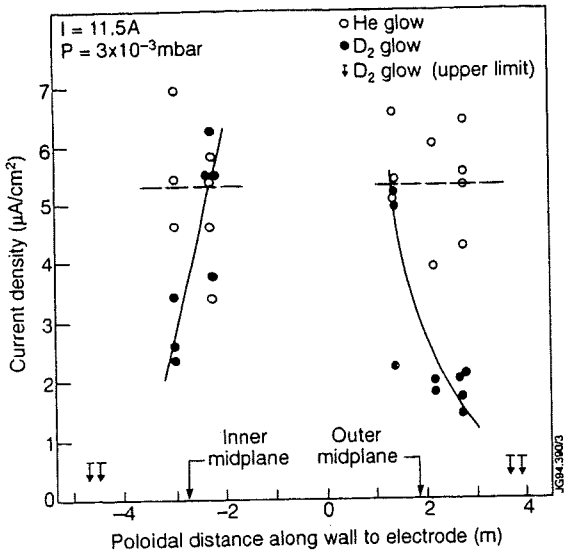

Figure 5. The current distribution as measured by the Langmuir probes in the JET vessel. The upper limits for D_2 are based on relative current densities on the bottom of the machine assuming the He current density is uniform.

The current density for the He glow is relatively uniform. The total current over the total projected vessel surface area, $11.5A/200m^2 = 5.75\ \mu A/cm^2$ is consistent with the measured He current density. The ion flux for the D_2 glow, however, appears to become much less intense over the lower half of the torus (i.e. far from the electrode). Since the total current is the same for the two cases, one may infer the current density must be higher close to the electrode for the D_2 glow.

For conventional glow discharges (so-called "normal" glows between plane electrodes) j/P^2 is the constant of the system, where j = current density and P = gas pressure, and it is found to be more than 10 times greater for hydrogen [5] than helium. Although the JET glow discharge is different because of its hollow cathode geometry, the above character of j/P^2 is consistent with the basic trends:

1. The glow spread over a larger area (hence current density decreased) as pressure was decreased at a constant total current.

2. The deuterium glow had a higher current density but was limited to a smaller area.

The impurity removal rate was measured as a function of the glow current using a quadrupole mass spectrometer (Fig. 6). The absolute value of the signal merely reflects the conditions of the wall at that date; care was taken to make sure that the wall condition had not changed significantly over the course of making measurements at different currents.

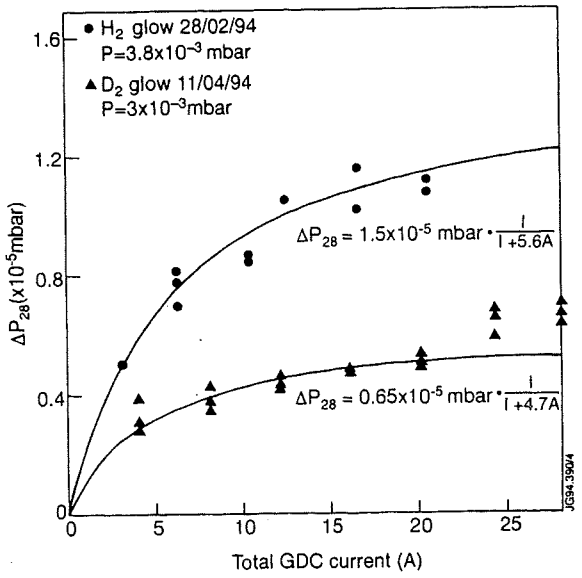

Figure 6. The impurity removal rate during GDC measured as the mass 28 partial pressure in the JET vessel.

As the current is increased the number of impurities released from the walls increases, but the probability of reionization also increases. As a result the removal rate saturates. However, a step increase in the removal rate was observed beyond 20A total

current, and was accompanied by a step increase in voltage [4]. This may be due to the glow extending onto a relatively dirty surface when the current is increased at constant pressure, as we did not often operate at such a high current.

The saturation of the cleaning rate has been treated extensively by Waelbroeck [6], but a simplified version is shown below to emphasize the role of the various parameters: I = current, A = surface area, and S_p = pumping speed. The rate of removal, R, of a particular impurity is given by $R = S_p P_{im}$ where P_{im} is the impurity partial pressure. The rate of release of wall impurities, $\emptyset_o$, will be proportional to the ion flux to the walls. Since the current at the cathode of a glow discharge is predominantly ion current [5], $\emptyset_o = \sigma$ jn A where n is the surface concentration of impurities and σ is the cross-section for the impurity release reaction. Assuming the rate of ionization of released impurity molecules, $\emptyset_i$, is proportional to the rate of ionization of working gas molecules, then $\emptyset_i = k\ I\ P_{im}$ where the proportionality constant k is in principle a function of the total gas pressure only. Since $R = \emptyset_o - \emptyset_i$, the rate of impurity removal is given by

$$R = S_p P_{im} = S_p \left(\frac{\sigma n}{k}\right) \frac{I}{I + S_p/k}$$

A curve of this form is fitted to the data in Fig. 6.

The curves shown give $k \sim 1.2 m^3 s^{-1}/A$ given that the JET pumping speed during GDC is about 6.3 m^3/s. This is comparable to the results of Waelbroeck et al. [6] for removal of H_2O from a stainless steel tank : $k \sim 0.9\ m^3 s^{-1}/A$, at a similar total gas pressure.

Although the JET cleaning rate starts to saturate at a current well below the maximum available current, 80A, larger currents may prove useful if GDC can be performed in conjunction with the recently installed in-vessel cryopump.

4. CONCLUSIONS

Four compact GDC electrodes, which do not require water cooling, have been successfully used on the JET tokamak. During initial cleaning, arcing frequently tripped the electrode power supplies. At low pressures, when glows from individual electrodes coalesced, more than one power supply could be tripped by an arc. By setting the arc trip level to 10 msec, this problem was eliminated.

The measured current density for He GDC at I = (4 electrodes) x (3A each), P = 3 x 10^{-3} mbar, was found to be consistent with the total current over the total projected vessel surface area (~ $200m^2$). D_2 glows, however, only seemed to cover ~ $25m^2$ per electrode.

The CO removal rate for H_2 and D_2 glows did not increase appreciably with current beyond ~ 10A total. The full 80A that the system may deliver, however, may be useful if the pumping speed of impurities during glow is increased by using the vessel cryopump.

ACKNOWLEDGEMENTS

We are indebted to Dr. J.P. Coad and Dr. H. Lingertat for providing us with excellent CCD camera views of the inside of JET during glow discharges.

REFERENCES

[1] K.J. Dietz, Proc. 9th Int. Vacuum Congress, ASEVA (1983) 706.

[2] patent no. DE 4227296 C1

[3] F. Llewellyn-Jones, The Glow Discharge, Methuen and Co., London (1966).

[4] G. Saibene, A. Rossi, R.D. Monk, J. Orchard, P. Andrew, R. Barnsley, D. Cushing, P.J. Coad, S. Davies, K. Erents, H.Y. Guo, K. Lawson, J. Lingertat, G. Matthews, G. Sips, M. Stamp and A. Tanga, J. Nucl. Mater. (in print).

[5] A. Von Engel, Ionized Gases, Second Edition, Oxford University Press, London (1965).

[6] F. Waelbroeck, J. Winter, P. Wienhold, J. Vac. Sci. Technol. A2 (1984) 1521.

Remote Handling Experiments with the MASCOT IV Servomanipulator at JET and Prospects of Enhancements

D Hamilton, S Colombi[1], L Galbiati, B Haist[2],
S Mills, T Raimondi

JET Joint Undertaking, Abingdon, Oxon, OX14 3EA, UK.
[1] EPFL Lausanne, Switzerland.
[2] KfK Karlsruhe, Germany.

Ongoing remote handling trials are being performed at JET, using the MASCOT IV servomanipulator, in order to establish the feasibility of proposed remote handling tasks. This promotes the development of appropriate tools and methods, the determination of time scales, and suggests modifications to be incorporated into the final design of the related JET components.

1. INTRODUCTION

Remote handling at JET is structured around the MASCOT IV servomanipulator, a two armed master-slave device. The master unit is located in a control room, and the slave unit is positioned, using the TARM and BOOM transporters, around the JET vacuum vessel.

Camera's are mounted on: the MASCOT slave unit, the transporters, and around the torus hall to allow viewing of the environment.

Models of the robots and environment are monitored on a Silicon Graphics workstation running KISMET.

After tritium experiments have been performed in the vessel, man access to the torus hall will be severely limited, and critical maintenance will be performed using the remote handling equipment.

1.1. Aims

The trials described in this paper are based predominantly on the servomanipulator handling tasks. The task descriptions, preparations and trial outcomes are outlined.

1.2. Abbreviations

MASCOT: Master-Slave servomanipulator.
TARM: Articulated ex-vessel transporter.
BOOM: Articulated in-vessel transporter
KISMET: Kinematic Simulation and Monitoring system.
MKII: JET Mark 2 divertor.

1.3. Overview.

As remote handling tasks are identified, trials are performed with the servomanipulator. This helps to establish the areas of difficulty, and provides feedback regarding design modifications which may simplify the task, and the types of tools that need to be developed.

Initially, these trials are usually carried out at the bench test area, with MASCOT mounted on a support stand in front of a bench. If necessary, the trials are extended to involve the transporters.

2. VACUUM VESSEL PORT DOOR MOCK-UP

An exact duplicate of a vacuum vessel port door was used for these trials, the purpose of which was to discover the difficulties involved in the task and to stimulate the development of the methods and tools to resolve them (1).

The servomanipulator was mounted onto the TARM transporter, and the environment and robots were modelled on KISMET.

The 1.5m diameter port door has a silver coated Cefilac seal that deforms when the 48 bolts are tightened, creating a vacuum tight fit.

The trials attempt to perform the task of undoing the bolts, opening the door, changing the seal, cleaning and inspecting the mating surfaces, closing the door and tightening the bolts.

Three people were involved: a MASCOT operator, a TARM operator, and a supervisor.

then bolted into position. Each wide carrier has a diagnostic connector plug which must be screwed into the socket before the narrow carrier is inserted.

The clearances between neighbouring tiles will nominally be 3mm and 10mm. Diagnostics (most critically langmuir probes) fill the bigger gap, reducing this clearance down to 3mm also.

Contact with the sharp tile edges and the diagnostic probes must be avoided at all cost as damage would likely ensue. The most critical operation is the insertion of the narrow carrier between two wide carriers.

Rigid lifting frames are being designed to be bolted to the tile carriers so they may be handled without damaging the tiles. The frames will be left attached to the two wide carriers during the insertion of the narrow carriers, and the narrow carrier frame will be guided by these so that contact between carriers is impossible.

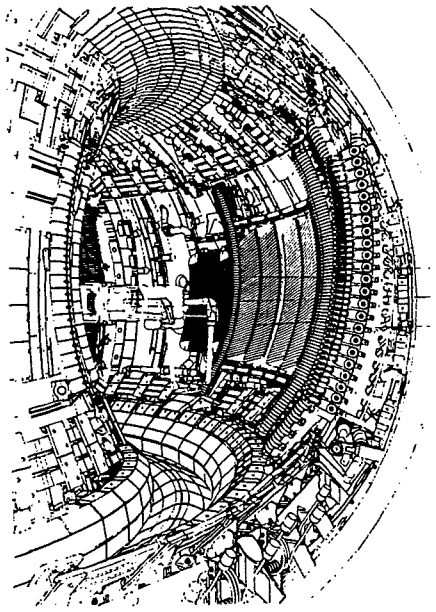

Figure 2. In-vessel handling of MKIIb divertor.

3.2. Winch for MASCOT

The heaviest tile carrier, with attached diagnostics will weigh in the region of 35kg. This is close to the maximum lifting limit of the combined MASCOT arms. In order to retain high sensitivity, to avoid overloading the arms, and to provide extra safety, a winch has been designed to be attached to the front of MASCOT, and will be used to assist the lifting of the tile carriers by taking most of the load.

The lifting point of the winch is at the end of a 0.4m long arm which can be rotated about a horizontal axis. The arm can thus be adjusted to bring it back to horizontal when MASCOT is at an angle.

The winch is actuated by a backdriveable gearbox and current controlled D.C motor, and will operate like a force controlled tensator. The hook can be gripped by MASCOT (operating the safety latch) and attached to the tile carrier lifting frames.

With the winch taking 90% of the weight, the MASCOT arms can manipulate the tile carriers with high sensitivity.

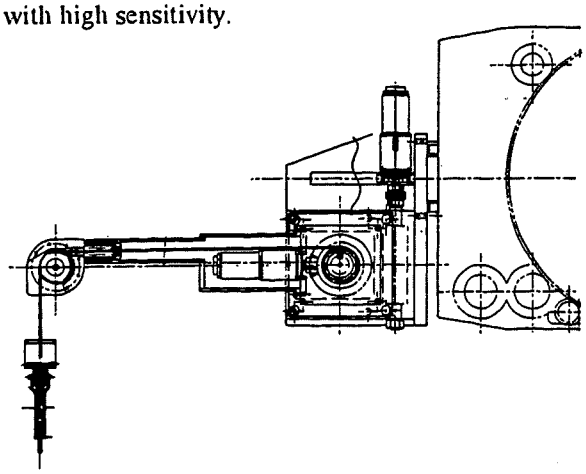

Figure 3. Drawing of the MASCOT IV winch.

3.3. Special tools

A number of proprietary tools have been adapted for this remote handling task. An electric screwdriver, a dial indicating torque wrench, and a power drill, have all been fitted with gripping features.

The screwdriver is powered via an electrical connector at the wrist, and is used to attach the lifting handles to the carriers and to operate the diagnostic connector. To minimise the number of journeys to the toolbox, a stowage position has been created on the MASCOT forearms for this tool.

A torque of 35Nm is to be used to tighten the carrier bolts and an estimated 70Nm will be needed to undo them. A dial indicating wrench will be operated by the servomanipulator, with the applied torque visible through the Cyclops camera.

An electric drill, powered from the tool connector will be used to drill out seized bolts.

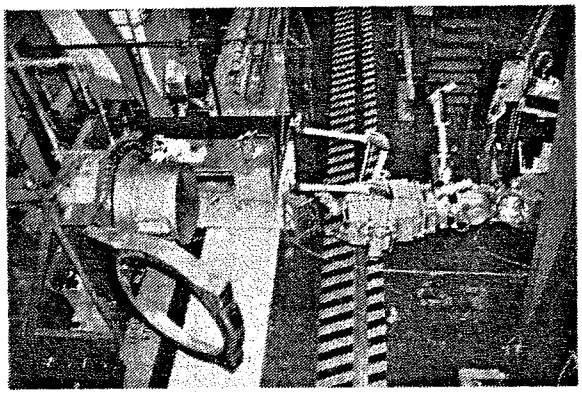

Figure 1. Vacuum vessel port mock-up.

2.1. Preparation

Some tools had to be adapted for remote handling usage. An electric impact wrench for torque-ing the bolts was given suitable handles, and the switching modified to allow remote operation via a long cable. Similarly, a ball ended hexagon key suitable for the seal captive screw was adapted for MASCOT gripping. Some pads with scotch brite and soft cloth's were introduced for the cleaning process.

A number of useful transporter positions were identified:- In front of the port, at the bolts, and at the toolbox. Teach and repeat files moving between these points were prepared for TARM with the assistance of KISMET. With the TARM positioned at the bolts, its A6 axis of rotation was colinear with the central axis of the port. The servomanipulator could then be rotated, giving identical access, as far as the master operator was concerned, to all 48 bolts.

2.2. Discussion

Over a period of two days, the complete task was performed, and the area behind the vessel was successfully tested for vacuum tightness.

KISMET proved to be a fundamental tool for navigating the TARM transporter. Its superiority over fixed camera's is due to its ability to present a clear overview from any desired viewpoint. However, the Cyclops camera, located on the MASCOT chest between the arms, is the primary viewing tool for MASCOT operation.

The impact wrench performed well, but it was finally agreed that the vibrations caused by such a tool was not consistent with the delicate diagnostics mounted on the door.

The handling of the door was performed with combined TARM and MASCOT movements. A need for an explicit handle on the door was highlighted when scratches were made to the seal surfaces through inappropriate gripping.

Inspection of the seal surfaces can be performed with the MASCOT cameras. Two equivalent approaches can be used:- the Cyclops camera on maximum zoom and a torch in the hand, or, use a camera in the hand. Varying the light reflection angle helps the detection of the smaller scratches.

Scratches were successfully removed by the servomanipulator, using the scotch brite pads. A smooth repetitive movement over a small arc is more important than high force sensitivity.

A timed operation sequence for the whole task was produced, together with a programme of necessary improvements to be made to the tool kit.

3. MKIIb DIVERTOR HANDLING

In 1996, a short program of tritium experiments will be performed which will activate the vessel. It is then planned to replace the MKIIb divertor tile carriers with MKIIc tile carriers remotely before continuing with the experiments. Although the MKIIb tile carriers are being installed manually, it is intended to install a section of them remotely in preparation for the fully remote task.

The remote handling group at JET have been closely involved during the design of the MKIIb tiles and carriers, proposing modifications to allow the attachments of lifting frames, relocating the dowel pins, and negotiating clearances for the manipulation of the tile carriers in and out of place.

In parallel, the handling tools and methods for this task are beginning to be developed.

3.1. Tile carrier lifting frames

There are 6 types of carriers: wide inner, narrow inner, wide base, narrow base, wide outer, and narrow outer. The tiles on the narrow carriers rest on the wide carriers, so the wide carriers on either side must be installed before the narrow carrier.

The tile carriers have dowel pins which locate them with respect to the support structure, and are

4. TRIALS ON PROPOSED STANDARD COMPONENTS FOR ITER

On the assumption that the remote handling system for ITER will be based on the 'man-in-the-loop' philosophy that was adopted in JET, some bench test trials were performed with MASCOT on standard connectors (2).

The two handed operations required are not necessarily more difficult to perform than single handed operations, the basis used for selecting the more specialised, more expensive, and ultimately less reliable, quick connectors at JET.

4.1. Electrical connections

The single handed quick connectors standardised for JET are rather complex and delicate, and have proved less than totally reliable. The connectors are not robust enough and are prone to accidental deformation due to mishandling and impacts during installation. This experience, together with some trials with different standard industrial connectors, has led to a list of conclusions, some of which are given here:-

- Connectors must be simple, rugged, and robust, taking into consideration the dimensions and weight of the cables.
- To avoid accidental disconnection, lever type fasteners are proposed.
- A rectangular, rather than cylindrical shape, is favoured to give a clear indication of the orientation of the plug before connection, and easier grip for the manipulator.

4.2. Flanged connections.

The performance of bolted flanges has been very reliable over 13 years of operation at JET. The vacuum vessel port mock-up demonstrated the successful remote handling of these flanges.

"V" clamp flanges used at JET have had 4 or 5 segments with a single fastening bolt. One problem that has been noted is that in some cases the compression along the seal appears to be uneven and in places close to the minimum limit. The high friction between clamp and flange causes the clamping force opposite the bolt to be much lower than at the bolt.

Bolted flanges are preferred if space allows. If "V" clamps must be used, it is suggested that clamps with two bolts rather than one be considered.

5. MASCOT ENHANCEMENTS

The force-feedback Master-Slave manipulator adopted in JET for remote maintenance uses a.c. induction motors, with which, because of their low friction, the required force sensitivity can be achieved. In view of the need to manipulate heavier loads, both in JET and ITER, the replacement of the a.c. motors with more efficient brushless d.c. motors is now being studied. The aim is to increase the load capacity, at the same time attaining lower thermal losses and better dynamic response.

The big drawback of brushless motors are the parasitic torques which impair force sensitivity. A method of digital compensation has been worked out at the Ecole Polytechnique of Lausanne under a JET Art.14 contract (3). These torque values are acquired directly on the manipulator using its own control system in velocity or position mode at high gain. A single degree of freedom, tested with a PC based control, gave 1.5 times load capacity and approximately one third of the inertia reflected with respect to the present MASCOT, with comparable friction.

Efficient and compact gearboxes are now being developed which should bring the load capacity to more than 50kg from the present 20kg, once the MASCOT arms have been mechanically strengthened.

REFERENCES

1. D. Hamilton, "Vacuum Vessel Port Mock-up" JET RH Group TN/014.

2. T. Raimondi., "Considerations on the standardization for ITER of connections suitable for remote handling in the light of experience at JET", Workshop on standard components for ITER, ITER, San Diego, May 1993.

3. S. Colombi and T. Raimondi, "Improvement of brushless DC motor actuators", 23rd ISIR, Barcelona 1992.

Key Features of the New In-Vessel Inspection System at JET

T Businaro, G Dalle Carbonare[1], J F Junger, T Raimondi.

JET Joint Undertaking, Abingdon, Oxon, OX14 3EA, UK.
[1] ITER, 801-1, Mukouyama, Naka, Japan.

The JET In-Vessel Inspection System (IVIS) has been modified to improve its performances and better cope with the inspection of newly installed in-vessel components, resulting in clearer pictures and wider range of view. The inspection time has also been reduced whilst a complete pictorial documentation of the vessel status is provided. All main IVIS components have been neutron radiation tested with neutron energy above 0.1 Mev, and the results showed that the TV camera will not withstand D-T phase neutron fluence and its remote installation is required. A proposal of a high resolution viewing probe for next step machines is presented.

1. INTRODUCTION

During the 1992-93 JET machine shut-down, the In-Vessel Inspection System has undergone major modifications involving the viewing probes and the lighting units. These modifications were needed to obtain clearer pictures of the newly installed in-vessel components, to overcome the shading effect of the saddle coils and the poloidal limiters (fig. 1a), to facilitate the system maintenance and the remote installation of the probes necessary after the negative results of the neutron radiation tests of the TV camera (see par. 5).

The new viewing probe was designed to obviate the need for the glass cylinder, the cause of optical aberrations and glares, using a vacuum tight flat sapphire window as the vacuum barrier and window for the TV cameras. The new optical arrangement, which requires the prism and its mechanisms in vacuum, increased the range of view of the probe including the direct view underneath it, without the optical limitations of the previous system. To demonstrate the feasibility of this design, a study of a new viewing probe, based on the JET concept, was contracted to ENEA's Research Centre of Frascati (Rome). Tests of a prototype of the new probe were extensively carried out at JET using a special rig simulating the vessel's working conditions (vacuum and temperature). At the same time, in view of the D-T phase, a neutron radiation test campaign of the main critical components was started at JRC Petten, The Netherlands.

Whilst the tests of the new viewing probe were successful (the prism movements were tested beyond 20,000 cycles), the neutron radiation ones showed the TV camera could not permanently be installed in the machine during the D-T phase and its remote installation would be required.

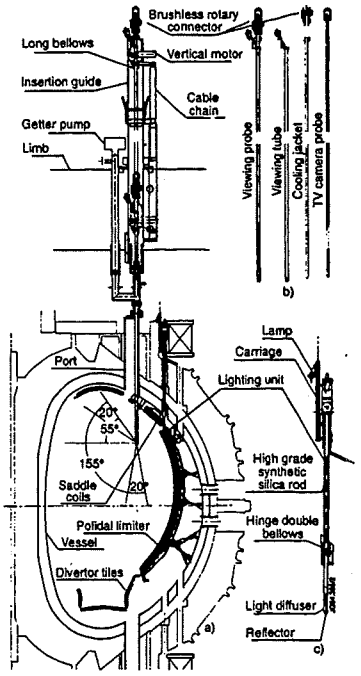

Fig. 1

Therefore one of the main objective of the new design was to address the maintenance problems so that a viewing probe where all its main components were easily replaceable in remote handling operations could be manufactured. This was achieved by making all its main components independent and easily disconnectable one from the other.

In addition the vessel illumination was increased by installing eight rather than four lighting units, with a longer stroke. Finally new features have been added to the control system to improve the analysis of the pictures and the inspection time.

2. DESCRIPTION OF THE NEW PROBES

Each of the viewing probes is made up of four independent coaxial devices (fig. 1b), installed one inside the other: viewing tube, cooling jacket, brushless rotary connector and TV camera probe.
The viewing tube, provides the optical window to look inside the vessel whilst maintaining the vacuum seal. The cooling jacket is inserted inside the viewing tube and shields the TV camera probe from the heat radiating from the vessel at up to 350°C. The TV camera probe is inserted inside the cooling jacket and contains the TV capsule, its lenses and the focus and iris motorised mechanisms. The brushless rotary connector is fixed on top of the cooling jacket and allows the TV camera to rotate in synchronism with the prism rotation. The entire viewing probe is inserted into the existing insertion guide described in detail in [1]. The water pipes connected to the cooling jacket, the air pipe and electric cables connected to the TV camera probe and the vertical motor, need to comply with approx. 3 m vertical movement. This is achieved by using a cable chain, fixed on one side to the vertical carriage and on the other to a distribution box attached to the insertion guide.

The viewing tube is (fig. 2) connected to the long bellows of the insertion guide by remote handling vacuum tight V-band flange coupling. The two movements of the prism are independently operated by two identical motorised vacuum tight "wobbling" feedthrough mechanisms. The rotations of these two are transferred to the bottom end of the viewing tube by long shafts. There, one of the two shafts is terminated by a pinion engaging the rotation movement gear of the prism. The second shaft is terminated by a screw engaging a floating nut, which operates the tilt movement of the prism through a ball bearing without affecting the pan scanning. In order to reduce the friction of the moving parts (which for mechanisms operating in vacuum and at temperature can lead to seizure) special materials, ceramic ball bearings where possible, loose fit and special surface treatment (high speed implantation of Molybdenum disulphide) are used. During the inspection considerable differential thermal expansion effects are expected, due to the presence of the cooled jacket inside the viewing tube. To overcome these effects the long shafts are allowed to expand using hexagonal junctions. Highly polished surfaces of the main part of the viewing tube are required to reflect the heat irradiated from the vessel wall.

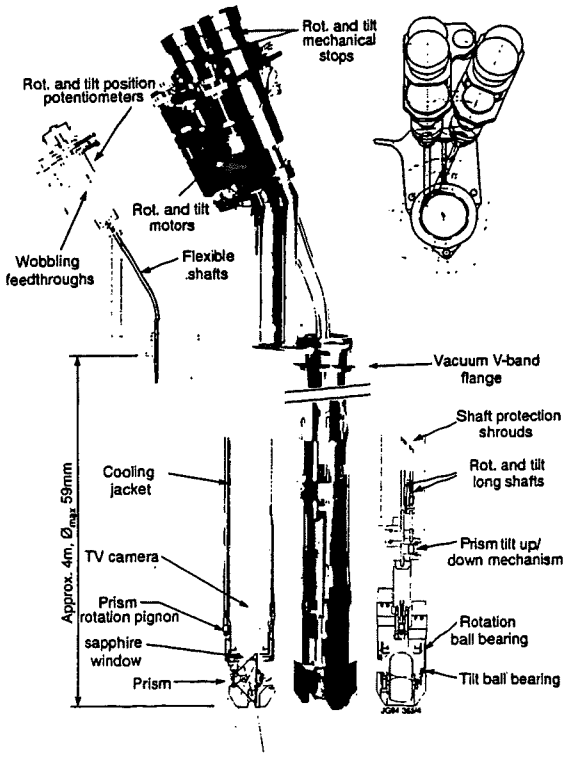

Fig. 2

The cooling jacket, described in [2], is laid down by gravity inside the viewing tube, supported by the titanium frame of the sapphire window. The contact between the cooling jacket and the sapphire window is made by a knife shaped conical collar (fig. 3c), in order to reduce the contact surface and the thermal stress on the window. A mechanical stop prevents the cooling jacket from rotating, but leaves it free to move vertically to comply with thermal expansion effects.

The TV Camera probe design (fig. 3a) is based on a commercial gamma radiation resistant camera (REES mod. 93R) using 25 mm focal lenses. This probe, approx. 4 m long, is terminated by a ball bearing and laid down by gravity into the cooling jacket supported by its conical collar. At the top is engaged in a brushless rotary connector by two pins, which make it rotate inside the cooling jacket, but at the same time allow the probe to comply with the thermal expansion of the viewing tube. The iris and focus D.C. motors are installed at the top of the probe to avoid the magnetic field of the machine and their movements

are transmitted to the lenses through long shafts and position potentiometers.

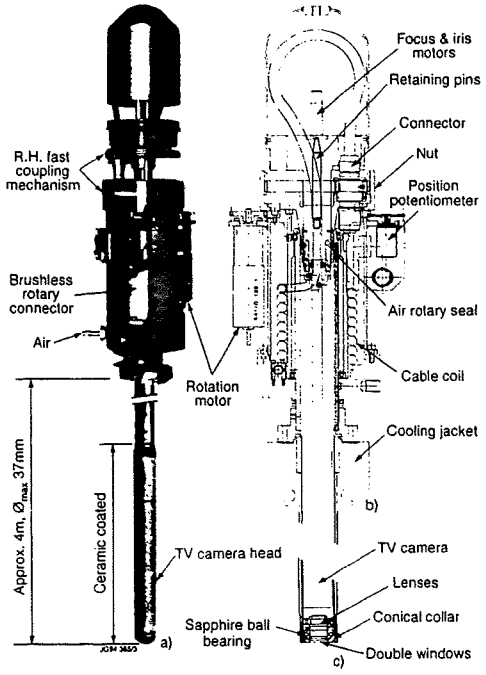

Fig. 3

Ceramic coating and sapphire balls have been used where necessary to electrically insulate the probe from the machine earth (>1.5KV)

In the new design a brushless rotary device (fig. 3b) is used to connect the TV probe to the cable chain. Inside, the electric cable is shaped to form a few turns coil. A geared motor winds and unwinds the coil, resulting in a rotation of > 360°. The device also includes a rotary seal for the air, which is needed to cool down the synthetic silica windows in front of the camera [2]. At the top of the rotary connector, a large nut locks the TV camera probe in less than a full turn, whilst actuating the electrical and air connections. This fast coupling mechanism has been designed to facilitate remote handling operations.

3. THE NEW LIGHTING UNITS

Although the general design layout of these units and their working principle remain the same as described in [2] , the detailed design differs significantly from the previous system (fig. 1.c). The hinge single bellows of the previous design have been replaced with double bellows to meet the safety requirements of the D-T operation phase. Metal reflectors have been added to the light diffusor which, together with higher grade synthetic silica 25 mm rod (Spectrosil B), resulted in doubling the light intensity diffused by each single unit. Finally the rod support mechanism has been modified using a special spring , which has simplified the design of the light guide and increased its efficiency while significantly reducing its manufacturing cost.

4. FEATURES OF THE NEW CONTROL SYSTEM

The whole software of the control system has been rewritten to enhance reliability, documentation and maintainability. In addition to the features of the previous system described in [3], the control system provides the synchronisation of the rotation movements of the prism and the TV camera probe. An automatic scanning mode has also been added allowing the full survey of the entire vessel reducing the inspection time. The pictorial documentation produced with this new control mode is a mosaic of 180 slightly overlapping pictures, as partially shown in fig. 4. These pictures are displayed on the screen in a proper compressed form to allow the entire mosaic to be shown. At the end of the inspection an easy to use programme allows retrieval of the documentation stored.

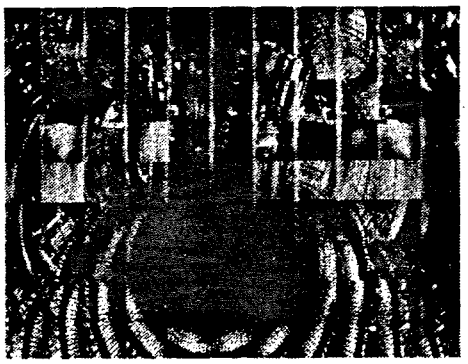

Fig. 4

5. NEUTRON RADIATION TESTS

TV camera, sapphire windows, lamps, D.C. motors and rubber hoses, strategic components of IVIS, have been tested for neutron radiation resistance at JRC Petten. These components have been irradiated in a special shielding container in order to achieve a

neutron spectrum as close as possible to the one produced at JET during the D-T phase (i.e. 75% neutron energy >0.1Mev , of which 50% >1Mev, and γ–dose << neutron dose). the main result of these tests, reported in detail in [4], is that the neutron radiation damages to the TV camera are higher than expected (the camera failed after neutron fluence of approx. 10^{18} m^{-2}) so that the cameras cannot be left on the machine during D-T operations, but should be remotely installed and removed each time an inspection is required.

6. CONCLUSIONS

The new IVIS system has been used several times since the start of the new machine operation after the divertor installation. The results of the inspection campaigns have been considered satisfactory. The picture quality has improved significantly (600 TV lines in all prism tilt positions) mainly due to the new viewing tube performances and the improved illumination of the vessel. The viewing of the divertor tiles underneath the probes is also very good (fig. 5).

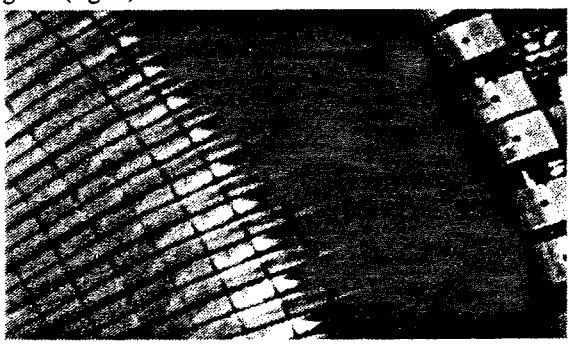

Fig. 5

The tilt and rotation mechanisms of the prism have performed as expected after several hours of continuous functioning inside the vessel under its present vacuum and temperature operation conditions ($<10^{-8}$ mBar and 250°C).

The low neutron radiation resistance of the TV camera is a major limitation for fusion experiments, especially for next step machines (e.g. ITER). The use of coherent optical fibres to position the TV cameras in partially shielded areas could be considered. To further improve the resolution and limit the number of fibres, an optical fibre linear array viewing system maybe considered for future applications (fig. 6). This probe should provide a quick acquisition (few minutes) of a whole vessel picture with 180,000,000 pixels. Imaging techniques are used to reconstruct the picture. The illumination is provided by a powerful pulsed laser and light guides embedded in the probe itself which concentrate the light in the viewing plane only.

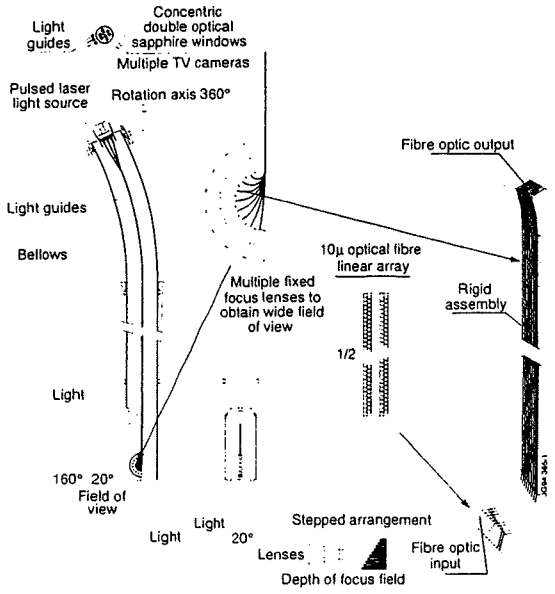

Fig. 6

ACKNOWLEDGEMENTS.

Important contributions are acknowledged from Ing. A. Pizzuto and Sig. A. Moriani of the ENEA's Energy Research Centre of Frascati (Rome) for the mechanical design and the tests of the new system.

REFERENCES

1. T Raimondi, R. Cusack, L Galbiati, "The JET In-Vessel Inspection System", 14th SOFT , Avignon, France, 8-12th September 1986.
2. T Businaro, R. Cusack, L Galbiati,T. Raimondi, "The JET High Temperature In-Vessel Inspection System", 15th SOFT, Utrecht, The Nederlands, 19-23rd September 1988.
3. T Businaro , J.F. Junger, "The JET In-Vessel Inspection Man-Machine Interface", 16th SOFT, London, United Kingdom, 3-7th September 1990
4. G Sardon, G.P. Tartaglia, T Businaro, "Neutron Radiation Testing of JET In-Vessel Inspection System Components", 18th SOFT, Karlsruhe, Germany, 22-26th August 1994

The Installation of the JET MkI Divertor – Features and Achievements

G Celentano, B Macklin, M Pick, S M Scott, R Shaw, J Tait.

JET Joint Undertaking, Abingdon, Oxon, OX14 3EA, UK.

ABSTRACT

The installation of the MkI divertor involved the removal of 25 tonnes and installing nearly 80 tonnes of equipment into the JET vacuum vessel. The work was carried out over a twenty-two and a half month shutdown period requiring over 50,000 man hours of in-vessel effort. JET's requirements were successfully achieved in terms of component installation, dimensional accuracy and timescale.

The work was organised into three stages:

Stage One dealt with the stripout of all components and the removal from the vessel wall of many welded bosses. Two external toroidal coils were also replaced. This work was carried out in a Beryllium and Tritium contaminated environment with a high radiation level. An extensive cleaning and decontamination exercise completed the stage.

Stage Two involved the fabrication of the four divertor coils at the end of which another full vessel cleaning was carried out.

Stage Three was the installation of the pumped divertor and the associated wall and roof components.

This paper reviews the overall concept of the shutdown and looks at the organisations, training and logistical support required. Certain key features will be described. These include the cleaning and decontamination of the vessel, without this full pressurised suits would have been needed for phases two and three, thus extending the programme to an unacceptable length. Material handling in the vessel which ranged from temporarily supporting the 24 tonne weight of the four coils from the roof of the vessel to an in-vessel crane and mobile personnel carriers. Finally, the installation and correct alignment of the target plates on which the success of the shutdown largely depended.

1. INTRODUCTION

The main design features and installation principle of the JET pumped divertor have already been described in previous papers [1] [2]. This included the reconfiguration of the inner wall protection [3], the exchange of the defective toroidal coils by removing an octant [4] and the installation of the saddle coils [3].

The in-vessel work closely followed the prepared planning schedules.
The original shutdown timescale was lengthened (by about 3.5 months) due to additional activities not envisaged at the early stage. These included: the second removal of octant 4 to exchange a second toroidal coil, thermal shields around the divertor coils, gas shield in the divertor area to improve gas circulation, a second cleaning - decontamination process of the vessel after the fabrication of the coils, shine-through protection tiles from neutral beam and several diagnostic probes and devices to improve control of the plasma parameters.

2. GENERAL ORGANISATION

In spite of the complexity of the procedures and the working condition (Beryllium, Tritium, Radiation and limited space), the factors that have contributed to the technical and time achievements of the in-vessel shutdown are mainly the following:

i) Extreme care of the work preparation through trial assemblies carried out on specially built mock-ups to achieve an effective training of personnel.

ii) The two decontamination/cleaning operations of the in-vessel wall allowed a greater number of staff to work in-vessel with greater efficiency, without respiratory protection.

iii) The new survey system ECDS (Electronic Coordinate Determination System), used in-vessel, enabling alignment of most of the components with accuracy and flexibility and in a much shorter time than using expensive and difficult jigs and fixtures.
iv) Purpose built floors and handling equipment made it possible to perform difficult lifting and loading of components into the vessel with high accuracy and safety for the personnel involved.
v) The management and planning effort implemented through daily and weekly meetings to co-ordinate the different teams working a two or three shift pattern.

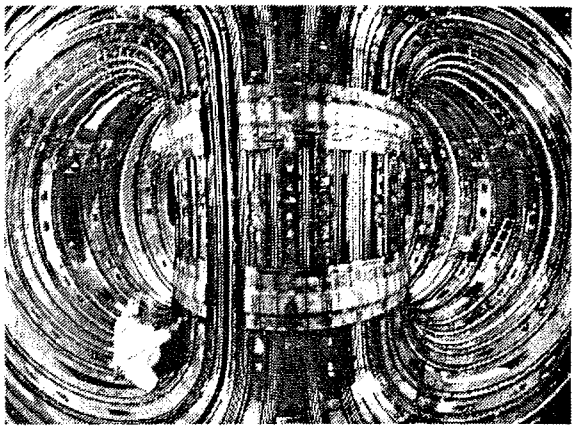

Figure 1. The vessel stripped prior to cleaning

3. DECONTAMINATION - CLEANING

Cleaning and Decontamination activities during the Shutdown were important for two reasons. They were required to reduce the respiratory protection requirements for people working in the vessel and maintain clean conditions suitable for later plasma operations.

The first objective was achieved by using a wet grit blasting technique to remove the beryllium coating on the inside of the vacuum vessel [5]. This proved to be very successful and enabled 88% of the shutdown to be performed without any respiratory protection being worn.

The second objective was achieved by:
a) Implementing a regular night shift of specialist cleaners who used wet wiping and vacuum techniques.
b) Thorough control of all invessel processes, equipment, clothing and procedures.
c) Use of a CO_2 pellet blasting cleaning technique after construction of the divertor coils [6].
d) Thorough cleaning of all equipment and components before use invessel.

CO_2 pellet blasting proved to be a very successful technique. This method uses CO_2 which is cooled, converted into snow and then compressed into pellets. The pellets are then entrained in a stream of dry compressed air and blasted at the vessel works. A combination of intense thermal shock, mechanical momentum and rapid volume expansion detaches contamination from the vessel wall. The CO_2 pellets sublime immediately and so generate no secondary waste. The debris removed is collected by a high velocity extract system which was mounted concentrically with the blasting nozzle.

The effectiveness of maintaining clean conditions was difficult to monitor. The results would only be known once pump down and commissioning were completed. In fact pump down and commissioning after nearly a two year shutdown went very well and the amount and type of impurities detected are comparable with that found after a typical short shutdown. The amount of effort applied to cleaning and decontamination during the shutdown has proved to be a substantial benefit.

4. HANDLING AND EQUIPMENT

Each stage required different handling facilities in the Vessel. The Remote Handling Boom [7] was used to strip out the major components at the start of the shutdown.

To facilitate the handling of the coils in Stage Two sixteen arched beams were attached to load bearing bosses welded to the roof of the vessel. The six month coil build programme was analysed in detail in the form of fifty sequence drawings. Every lift and movement were identified and agreed

with the two main coil contractors. This defined the ten lifting points on each arched beam. As the beams also supported suspended stored components, the major lifts were independently checked to ensure that none of the beams exceeded one of the four approved loading conditions. The analysis also checked the design of the load bearing floor. This had to be rigid enough to support the precision coil build tables while allowing sections to be removed for casings and windings to pass through for storage below. Low headroom self lifting beams were developed for handling the coil rings. The final lift had all four coils suspended from the arched beams, a total load of twenty-four tonnes.

For Stage 3 the arched beams were removed and after fitting of the roof components a 1.4 tonne capacity manual crane was suspended from the roof bosses. The crane could travel both radially and toroidally. Access to the roof was achieved by two mobile personnel platforms suspended from the crane rails. With the coils installed the load bearing floor could no longer be used. A bridge floor was therefore installed and used in conjunction with the crane while all the wall components and divertor modules were installed.

For Stages 1 and 3 the boom accessed the vessel via the Pumping Chamber at Octant 5. Generally during Stage 3 the load was transferred to the crane once inside the vessel.

The large size of the new RF A2 Antennae (installed during Phase Three) necessitated access through a specially modified port at Octant 3. For this operation the TARM (Telescopic Articulated Remote Mast) [8], being used for the first time, transferred the Antennae to the in-vessel crane. The crane then utilised a counter balanced beam to mount the Antennae on the wall.

Material access for Stage 3 also used Octant 3, typically for sections of the curved coil conductor bars up to 6.6m long.

To satisfy the clean condition requirements the majority of the lifting and floor structures were made from aluminium alloy, occasionally stainless steel, and, for highly stressed components, nickel plated carbon steel. Proprietary lifting equipment suitable for clean conditions were found to be too bulky and expensive.

5. SETTING OF THE MkI DIVERTOR

Prior to coil build a series of temporary supports and radial datum staffs were set on the floor of the vessel using the master survey ring [9]. After supporting the coils during impregnation the supports were adjusted to bring the top face of the coils to the correct level. Based on survey information the support links were machined and fitted. With part of the weight taken on the arched beams the coils were jacked into correct toroidal position and concentric to the machine centre.

To guarantee the correct functioning of the divertor surface facing the plasma, the rails supporting the target plate modules had to be set for level to ± 0.3mm.

While the coils were positioned to ± 0.5 mm, the top surface of the two central coils (coils 2 and 3) carrying the 640 rail supporting pads varied by 4 mm. The solution adopted was to individually machine each of the rails before welding the rails to the pads.

Extensive surveys on the support pads were then carried out. Due to a certain flexibility in the coil cases the pads were clamped down simulating the module fixing loads. In addition to the global measurements of radius, height and azimuth, the toroidal and radial inclination of each pad had to be determined. This necessitated taking a total of 4300 separate measurements using a series of purpose built jigs, optical instruments and the ECDS [9]. The conversion of this data to machining input was reliably carried out using a combination of computer programmes and CATIA 3-d models.

To minimise the positional variation of the 448 rail segments during installation a purpose built jig was first used, in conjunction with the master survey ring, to locate the rails on coils 2 and 3. The positional accuracy of each interface on each rail was surveyed prior to welding. Finally, after installation of the target plate modules, a global survey was carried out to confirm the alignment of the plasma facing surface.

The extensive development and training programme, which preceded the in-vessel work, enabled the task to be completed on schedule and control the target plate steps to approximately 60% of the allowable size.

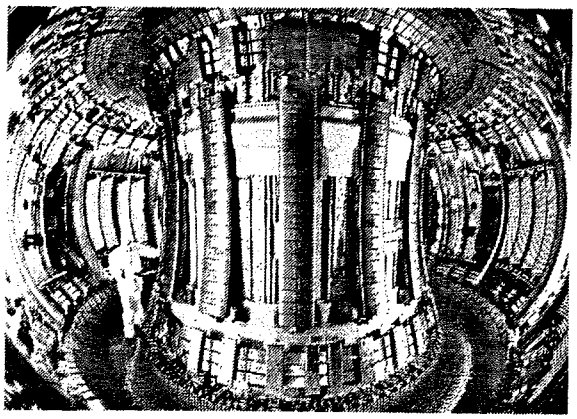

Figure 2. Final Inspection

6. RESULTS AND ACKNOWLEDGEMENTS

No installation faults were found during re-commissioning which included vacuum bakeout and filling of the cooling systems. A two year shutdown with almost 50,000 working hours inside the vessel required at least twice the number of hours for work preparation and logistics.

The authors would like to thank the staff of First Wall Division for their collaboration during the shutdown. Equally valuable support was given by the Drawing Office - Health Physics - Waste Management - Machine Assembly - Technical Service - Quality Assurance and Main Assembly contractor (GEC-A), etc.

7. REFERENCES

[1] JET P(90) 56 Vol I, Vol II 16th Symposium on Fusion Technology, London, 3-7th September 1990. Several authors.

[2] The Installation of the JET Pumped Divertor Systems inside the Vacuum Vessel, G. Celentano et al. 17th Symposium on Fusion Technology, Rome, September 1992.

[3] Integrated Engineering Design of New In-Vessel Components, M. Pick. 15th Symposium on Fusion Technology, Utrecht 1988, pp 771-775.

[4] Octant Removal at JET for a Toroidal Field Coil Exchange, G. Celentano et al. 16th Symposium on Fusion Technology, London, September 1990, pp 1604-1608.

[5] Decontamination of the JET vacuum vessel from Beryllium and Tritium. S.M. Scott et al. 17th Symposium on Fusion Technology, Rome, September 1992.

[6] Decontamination of the JET vacuum vessel using the CO_2 pellet blasting (cold jet) technique. S.M. Scott et al. 1994 International Symposium on Decontamination & Decommissioning, Knoxville, April 1994.

[7] Design and Operations of the JET Articulated Boom, L. Jones et al. Proc. 11th Symposium of Fusion Engineering, Austin 1985

[8] The Design and Construction of the TARM-A Crane-mounted Remotely-Controlled Transporter for JET. L. Jones et al. 16th Symposium of Fusion Technology, London 1990

[9] Alignment Systems for Pumped Divertor Installation at JET. B. Macklin et al. 18th Symposium of Fusion Technology, Karlsruhe 1994.

A Real Time Plasma Boundary Determination and Display System using Transputers

J Ellis, E van der Goot, D P O'Brien.

JET Joint Undertaking, Abingdon, Oxon, OX14 3EA, UK.

A transputer based system has been developed to perform real time determination of the plasma boundary. The system calculates the plasma boundary in less than 2ms, using digitised data from a set of the magnetic pickup coils and saddle loops. The result of this analysis is passed on simultaneously to a display station and to a second transputer system for further analysis. The display station provides, on-line, an animated display of the plasma boundary cross-section during the pulse. Although this display only shows the results at a suitable rate for animation, all incoming data is stored. This makes it possible to replay all the data after the pulse for more detailed analysis (Fig. 1).

1. PLASMA BOUNDARY DETERMINATION

The plasma boundary determination is based on a local expansion technique that was originally introduced at JET in order to have a fast and accurate determination of the plasma boundary in the X-point region (Ref. 1) and was subsequently used to demonstrate the feasibility of a real-time system using transputers (Ref. 2,3).

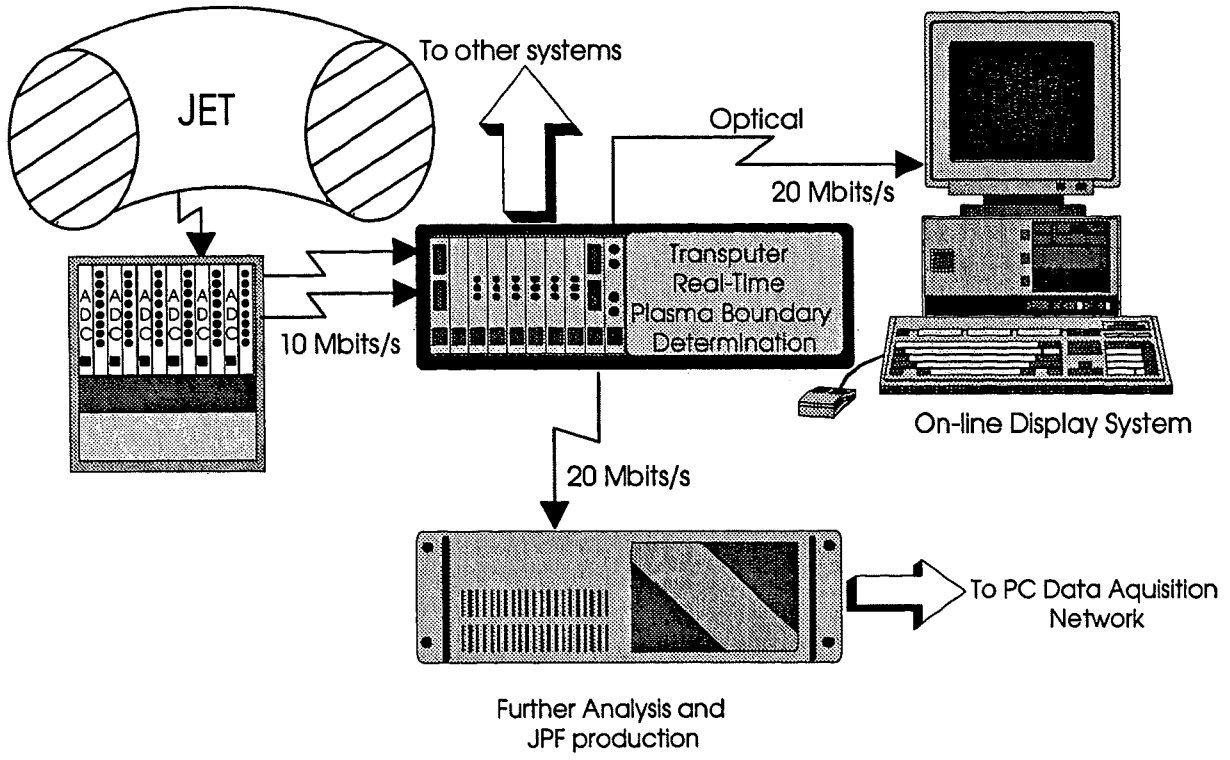

Figure 1. System Overview.

The method makes use of five 6th order expansions of the flux function which are symmetric in major radius and constrained by the vacuum field equations so that the flux function is parameterized by 65 coefficients, 13 for each of the 5 local expansions. By fitting to the local field and flux measurements the expansions can give an accurate determination of the plasma boundary, especially where it is near the vacuum vessel. The method has been extended to determine the whole plasma boundary and can be used for arbitrary plasma configurations. The five expansions used to describe the poloidal flux are centred at the upper and lower parts of the RF antennae, the upper and lower X-point areas and the inner wall of the vessel.

Following the installation of the pumped divertor at JET, the number of signals in the input data has increased to about 160. Of these only 140 are relevant for the calculation and between 60 and 80 signals are finally selected for the calculation process

The calculation proceeds roughly as follows:

1. select the appropriate signals from the available input data
2. for the five regions, multiply the data vector with a geometry dependent matrix
3. use the resulting coefficients to calculate the flux function in the five regions
4. calculate the lower and upper x-point position (if any)
5. using 3 and 4, determine the flux at the boundary

The hardware of the real time plasma boundary system consists of a stand-alone network of twelve transputers (Fig. 2). The software for this system is written in occam and is based on a well tested single processor version of the analysis code (Ref. 2, 3). The software takes full advantage of the inherent algorithmic parallelism in the method of solution and furthermore uses pipelining to increase the rate at which results are produced.

The processing pipeline consists of four stages with the calculation of the flux function and the X-point position taking place in parallel. In addition, parallelism is almost fully exploited in each of the stages, relying on the independence of the different

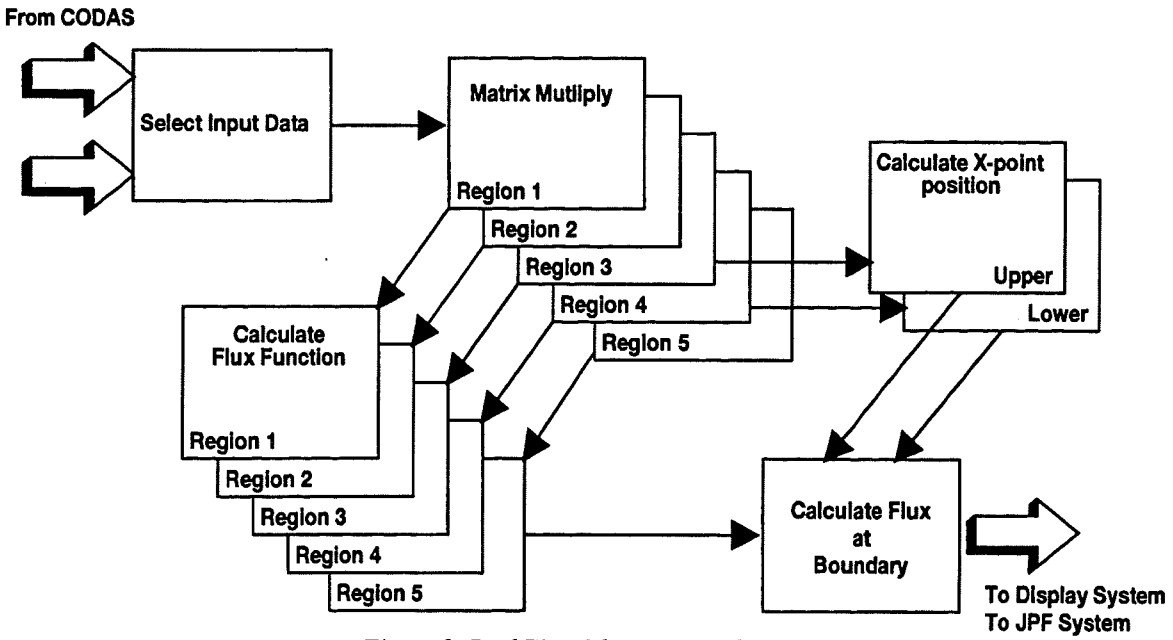

Figure 2. Real Time Plasma Boundary System.

regions. Due to the limited number of communication links on the transputer some of the processors run small despatch processes concurrently with the main calculation processes to distribute the data across the network. The distribution of the calculation processes over the available processors has been established using timing tests to obtain a balanced network and at the same time trying to optimise the mapping of the logical data flow to the available links. As can be seen from Figure 2, the flux function calculations for regions 2 and 3 and regions 4 and 5 are combined on two processors. These processors currently dictate the maximum processing speed of the real time system. The next bottleneck would be created by the calculation of the X-point location, which is the slowest single process in the system.

2. DISPLAY SYSTEM

The display system consists of a PC and a small transputer network consisting of three transputer modules (Fig. 3). The connection between transputers in the PC and the real time system is provided by a fibre-optic transputer link. The transputers in the display station provide the communication and on-line storage facilities.

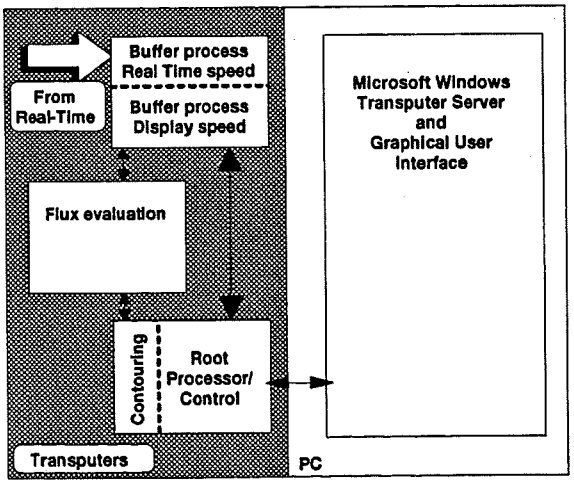

Figure 3. Display System Overview

For the purpose of on-line storage, one of the transputers has 16 megabytes of local memory. The final calculation of the co-ordinates of the plasma boundary cross-section is also performed by one of these transputers. This leaves the PC free to run the display software and provide the user interface (Fig. 4).

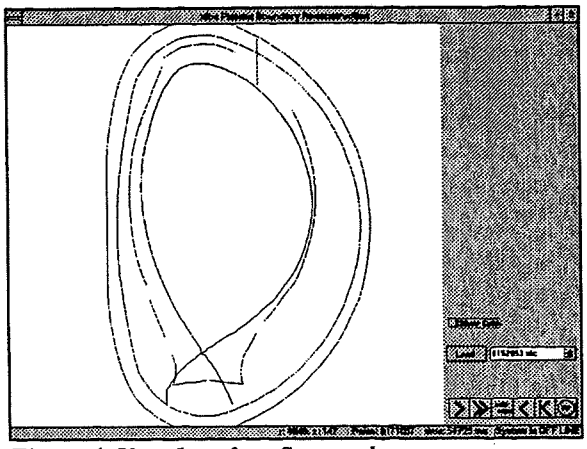

Figure 4. User Interface Screen shot

The PC software consists of a Microsoft Windows C++ program to provide the services normally provided by the transputer server (iserver/afserver) and to provide the user interface. Playback facilities for single step, fast forward and reverse play are provided. The user interface is disabled automatically when a pulse begins, and enabled again after the data has been saved on the PC's hard disk for future reference.

3. ANALYSIS SYSTEM

The transputer based analysis system produces data to be archived in the JPF (Jet Pulse File), based on the coefficients provided by the real-time system. This analysis system consists of an industrial PC with some transputer modules. The PC is only used to provide an environment for the transputer modules, and to provide system services such as disk storage. The software for the analysis system is written in FORTRAN rather than in occam, to make it easier to maintain the software. The PC is connected to the JET PC diagnostic data acquisition network to allow the produced data to be included in the JPF. The analysis takes the parameterized flux and boundary data and calculates global plasma parameters such as poloidal beta, internal inductance and stored energy (Ref. 4).

4. FIRST RESULTS

The system is now operational in the JET Control Room and working on-line. During the pulse it provides a good display of the plasma boundary and clearly shows the formation and the location of the X-point. If desired, the system can zoom in on a smaller region of the vessel to observe the plasma boundary in a particular location more closely (Fig. 5).

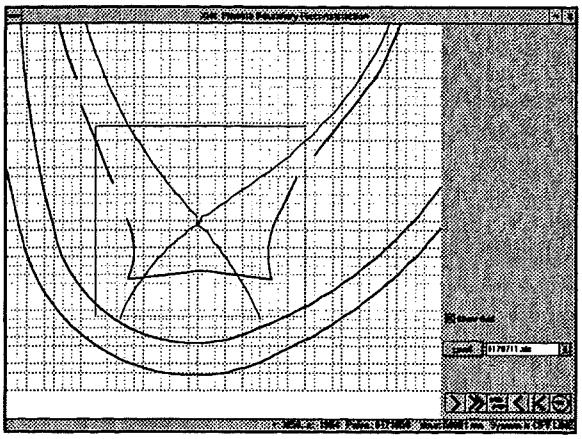

Figure 5. Zoom in on a smaller region.

The display can be enhanced by a grid (5*5 cm) to give more visual feedback. Immediately after the pulse, the system can be used to analyse the temporal behaviour of the plasma boundary in greater detail, and can be used as an aid in understanding the results from the plasma control system. Again, the system can zoom in on a particular location if desired. Further valuable feedback is provided via a cross-hair cursor. The real-world co-ordinates of this cursor are updated and displayed continuously at the bottom of the screen. Another feature is the display of a line, indicating the maximum possible position of the reciprocating probe. Using the zoom facility and the cross-hair cursor it is very easy to find the distance of the plasma boundary with respect to the probe. The spatial resolution of the reconstruction is in the order of 2 cm. although this varies along the boundary.

5. CONCLUSIONS

A real-time plasma boundary determination system based on transputers has been developed. This system, combined with a display system and a further analysis system will provide valuable feedback for the operation of JET with respect to plasma position and shape. The system will also provide data for other diagnostic systems, for control on a real-time basis, and as part of the JPF for post pulse analysis.

6. REFERENCES

1. D.P. O'Brien, J.J. Ellis, J. Lingertat, 'Local Expansion Method for Fast Plasma Boundary Identification at JET', Nuclear Fusion 33 (1993) 467.
2. van der Goot E., Edwards A.W., Ellis J.J., O'Brien D.P., 'Real Time Diagnostic Data Acquisition and Plasma Control using Transputers', Conf. Proc. SOFT '90 Vol 2. p. 1244
3. van der Goot E., Ellis J.J., O'Brien D.P., 'Real Time Plasma Boundary Determination for Display and Control using Transputers', Conf. Proc. SOFT '92 Vol 2. p. 1091
4. Christiansen, J.P., 'Integrated Analysis of Data from JET', J. Comput. Phys. 73 (1987) 85

ICRH Antennae System for the JET Pumped Divertor

P Crawley, G Agarici[1], T Brown, C Gormezano, G Jessop, A Kaye, H Panissie, R Walton.

JET Joint Undertaking, Abingdon, Oxon, OX14 3EA, UK.
[1] CEN Cadarache, F-13108 St Paul lez Durance, France.

SUMMARY

Eight A2 ICRH antenna designed to couple with the JET plasma have been produced and installed. Novel features and methods have been employed to minimise disruption loading and achieve good positional accuracy.

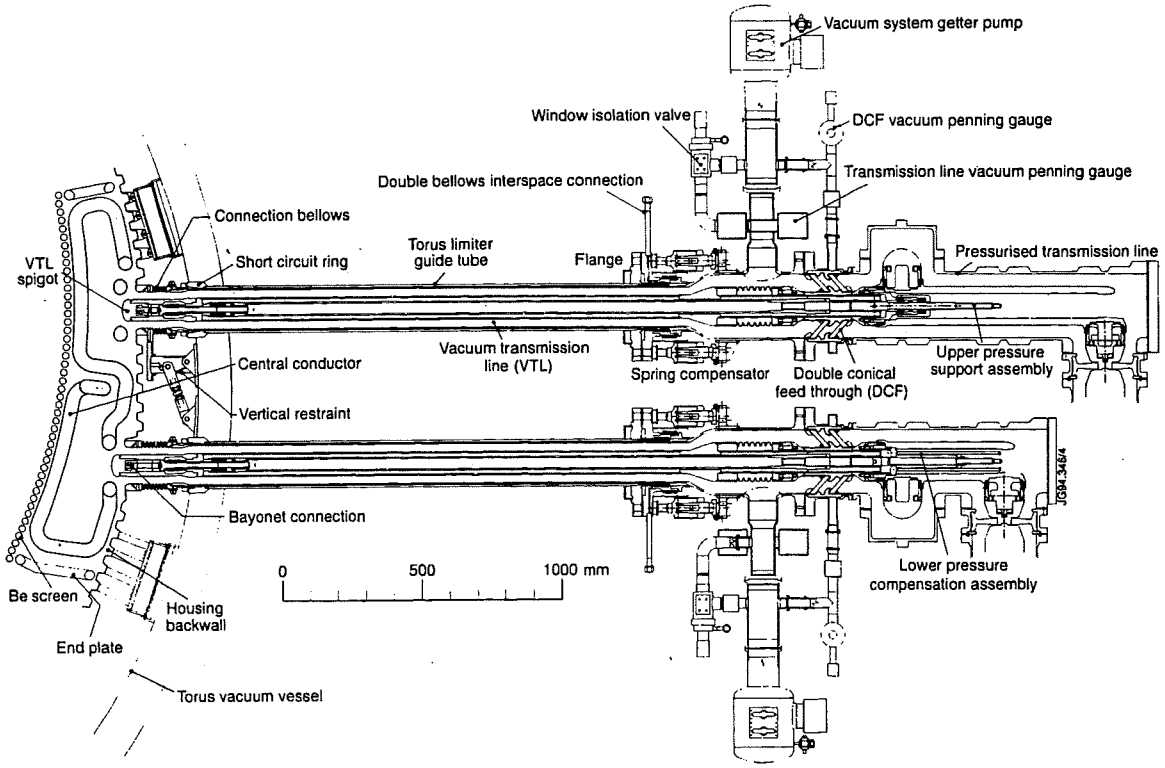

Figure 1. The A2 Antenna and Vacuum Transmission Line System

1. THE A2 ANTENNA.

The JET pumped divertor has required the production of eight new ICRH antenna [1,2,3] in order to achieve adequate coupling to the divertor plasma configuration (Figure1).

In order to better define the spectrum for Fast Wave Current Drive the antennae are arranged in two groups of four in opposed sectors in order (Figure 2).

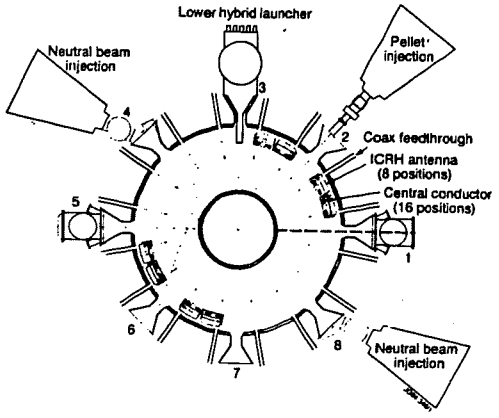

Figure 2. Toroidal antenna positions.

Each antenna contains two current straps separated toroidally by a central septum and has an open beryllium screen cooled by radiation (figure 3).

Disruption loads are reduced by using a thin wall, nickel plated, corrugated Inconel construction for the housing and resistors consisting of five microns of nickel and a similar thickness of molybdenum/manganese on a BeO substrate connected in series with the screen elements. The antenna has a distributed attachment to the torus that accommodates thermal expansion and vessel tolerances. Originally these mountings were electrically isolated. However following prototype RF testing it was found that flux leakage caused sufficient voltage (1 to 2KV) for arcing to occur across the insulating breaks. Plates plasma sprayed with alumina now provide a capacitively coupled short circuit for RF currents while still providing an insulating break for the low voltage disruption currents. DC breaks have been installed in the main transmission lines. DC currents flowing in the antenna short circuit to the vessel wall through the two VTL connection bellows.

Table 1 The A2 Antenna

Size:	0.9m x 0.6m x 0.45m
Number of Antenna:	8
Conductor straps:	16 total
Radial Screen accuracy:	-1mm to +3mm
Antenna Material:	Nick plated Inconel 600
Screen Material:	Beryllium
Operating Temperature:	500°C
Maximum Pule length:	20 seconds
Design Voltage:	42 KV
Cooling:	Radiation only
Maximum Duty Cycle:	60:1

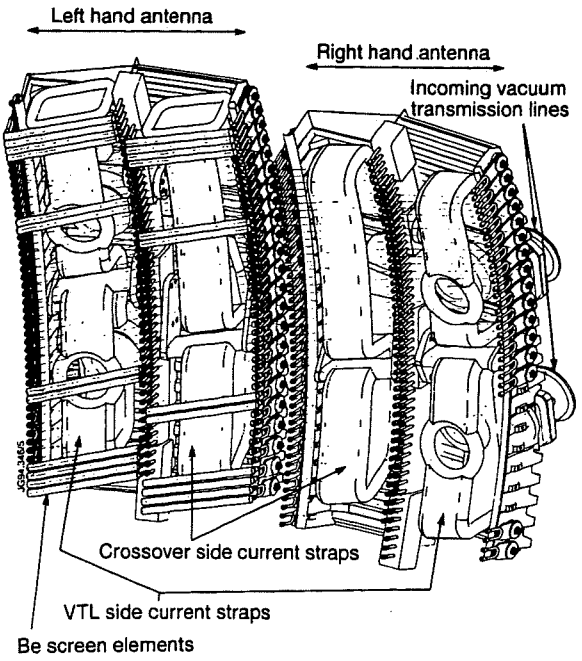

Figure 3. Left and Right hand antenna showing current straps.

2. VACUUM AND TRANSMISSION LINE SYSTEMS.

Radioactive, beryllium and tritium contaminated vacuum transmission lines (VTL's) have been modified to remove the conical support ceramic (a previous weak point at high voltage). A new antenna to VTL connection incorporates a silver plated current carrying bellows that accommodates thermal expansion and establishes a short circuit between the outer conductor and the vessel wall (Figure 4).

The RF window interspace vacuum is maintained by SAES St 707 Zr-V-Fe getter pumps operating at room temperature. The VTL vacuum is maintained by the 100 l/s conductance into the torus. The VTL vacuum is monitored and interlocked to prevent operation in the event of pressure greater than 10^{-4} mbar. The window pressure is monitored and interlocked to prevent operation at pressures greater than 10^{-6} mbar.

5. CONDITIONING.

Baking, multipactor and high voltage conditioning is now complete. Initially large pressure rises were recorded in the vacuum transmission lines at the ramp up and ramp down periods of each RF pulse. The size of the pressure rise was found to be strongly dependent on the presence of a magnetic field from the closest coil P4 (figure 6).

This effect is believed to be caused by the magnetic field changing the effective free path length and thus raising the voltage at which the multipactor resonance occurs. This difficulty was overcome by extensive baking to 150°C of the cold VTL regions that are external to the JET vacuum vessel baking system.

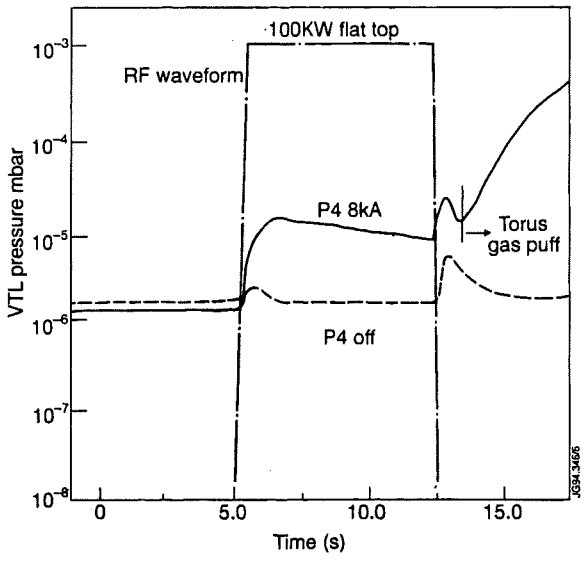

Figure 6. Influence of magnetic field from P4 coil on VTL pressure rise during conditioning.

6. OPERATION.

RF operations have started. Unexpectedly low coupling resistance has been found on the inner straps of the array; the reasons for this are currently being investigated. Plasma matches have been achieved in a variety of combinations of frequency and phase at coupled powers up to 11 MW.

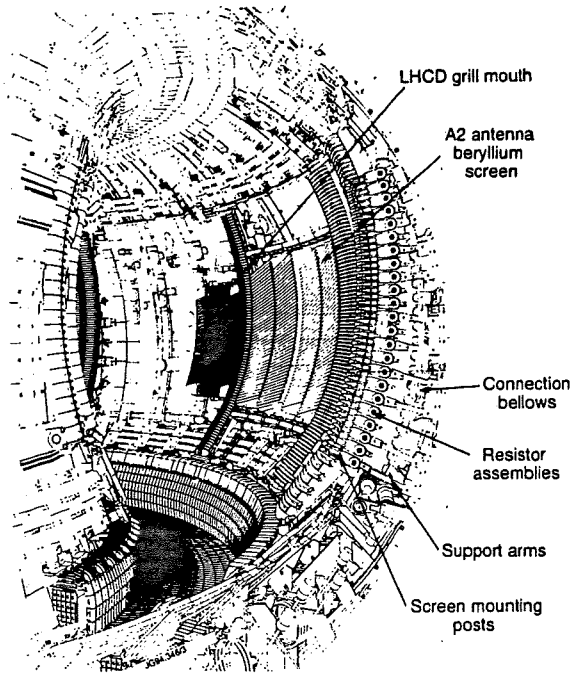

Figure 7. The JET ICRH antenna installation

REFERENCES.

[1] R.Lobel et al, ICRF Antenna for the JET Pumped Divertor Configuration. Fusion Tech 1990.

[2] A.Kaye et al. Present and Future JET ICRF Antennae. Fusion Engineering and Design July 1992.

[3] JET Joint Undertaking, Progress Report 1993.

[4] T.Brown et al. High Power RF Testing of The JET "A2" FWCD Antennae. SOFE 1993.

[5] P.Becher and M.Ferber. Mechanical Reliability of Current Alumina and Beryllia Ceramics used in Microwave Windows for Gyrotrons. ORNL/TM-8555. February 1983.

[6] B.Macklin et al. Alignment Systems For The Pumped Divertor Installation at JET. This conference

[7] L.Jones et al. The Design and Construction of the TARM - A Crane Mounted Remotely-Controlled Transporter for JET. SOFT 1990.

Low Level Tritium Assessment in JET Solid Waste Materials

P Pacenti[1], G Atkins, F Campi[1], G Newbert, S Terrani[1].

JET Joint Undertaking, Abingdon, Oxon, OX14 3EA, UK.
[1] Dipartimento Ingegneria Nucleare CESNEF, Politecnico di Milano, Milano, Italy.

Introduction

An important aspect of fusion technology research is the assessment and development of low level tritium measurement methods for waste management. In the UK, demonstration of radioactive content less than 0.4Bq/g enables waste disposal options other than consignment to radioactive waste repositories. It is desirable to develop a measurement technique for tritium at very low specific activity. The principal source of tritium contamination at JET is the inside of the toroidal vacuum vessel. Tritium is strongly bound to particles of co-deposited carbon and beryllium which are present on surfaces. These particles transfer to other materials during in-vessel maintenance and cleaning operations which can result in them becoming radioactive waste. During storage of the waste tritium outgasses from the dust contaminating surfaces in the oxidised form which can be removed for analysis.

The total extraction of tritium from materials such as carbon and beryllium is normally achieved by high temperature combustion over a period of several hours in an excess of oxygen or air. A method has been developed which enables extraction of tritiated water from waste samples by heating in a stream of humid nitrogen or air. The resultant tritiated water is condensed, collected and analysed by liquid scintillation counting to determine specific activity of the sample. The technique is reproducible, relatively rapid and involves less extreme procedural conditions than are employed in other established methods.
An evaluation of tritium extraction efficiency for the specific forms of contamination found in JET waste was carried out.

Experimental Objectives

- By comparison with an established measurement method, derive operating parameters which give an extraction efficiency equating to a limit of detection less than 0.4Bq/g.
- Minimise processing time and maximise sample size to ensure representation of the parent material.
- Evaluate the reproducibility of the technique.

Schematic diagram of the apparatus

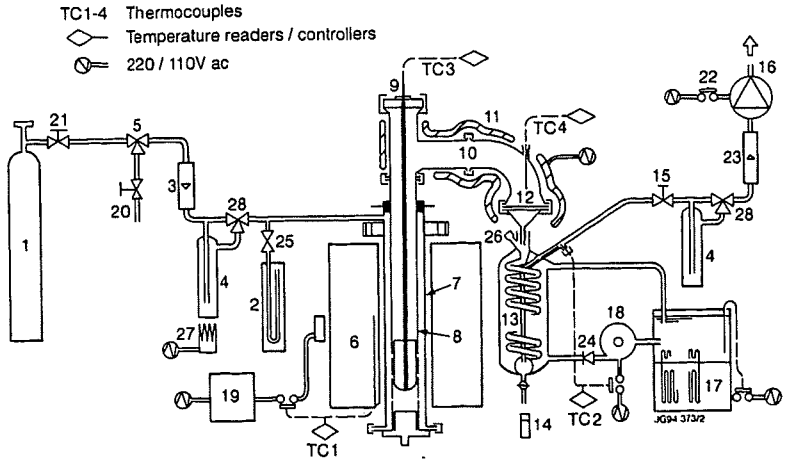

1. Nitrogen cylinder with pressure regulator
2. Differential manometer
3. Air flow meter (flux meter)
4. Distilled water bubblers
5. 3 way valve
6. Electric furnace with insulator
7. Outer flanged stainless steel cylinder
8. Inner flanged and drilled AlAl 310-S cylinder
9. Sample carrier
10. Pyrex glass tubing
11. Heating band 110V ac with neoprene insulation
12. Filter holder
13. Condenser vessel
14. Standard 20cm^3 scintillation vial
15. Regulating needle valve
16. Membrane pump - for extraction from apparatus
17. Refrigeration unit
18. Ethylene glycol recirculation pump
19. AC-AC transformer
20. Clean pressurised air supply
21. Pressure regulator valve
22. Membrane pump switch
23. Air flow meter (fluxmeter)
24. Non-return valve
25. Differential manometer valve
26. Distilled water inlet
27. Bubbler heater
28. 3 way valve

Description of Apparatus and Operation

The apparatus consists essentially of a vertical tube furnace into which a sample (maximum 20 grams) packed inside one of two sample carriers is inserted from the top. A small depression is maintained within the apparatus to avoid the hazard of external contamination during sample introduction.

Sample introduction system
(showing gas flow path)

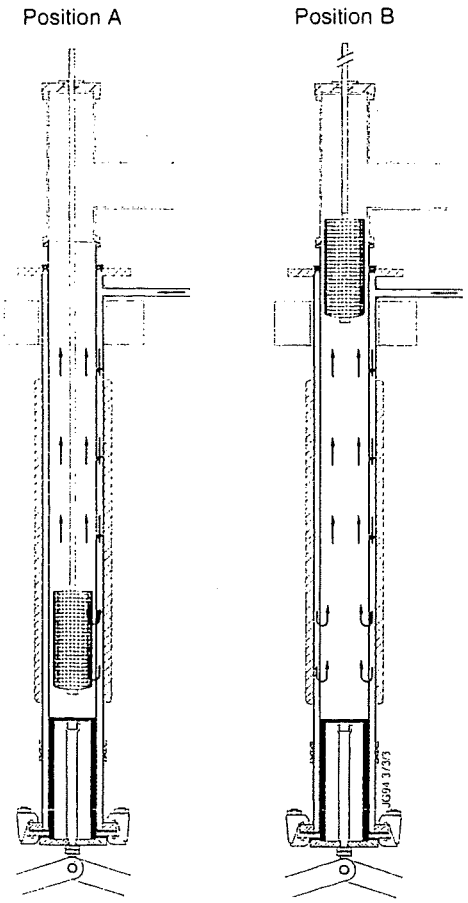

Nitrogen passes through a water bubbler at 30°C becoming saturated before being heated to several hundred degrees in the outer of two concentric tubes within the furnace. The heated gas passes through a matrix of holes in the base of the inner tube and then around and through the material being processed. Tritium is stripped from the sample and incorporated into the flowing gases which are then passed through heated glass tubes and through a heated (120°C), replaceable filter assembly before entering a condenser. The condenser consists of a vessel containing circulating, cooled ethylene glycol with an internal, vertical glass coil terminating in a collection reservoir through which the expelled gases flow. The temperature of the gases is rapidly lowered causing condensation of tritiated water on the inside of the coil. After a predefined time the condensate is flushed down the coil to the collection reservoir and then drained through a tap into a sample vial. Analysis for tritium content is carried out by liquid scintillation counting. Knowledge of extraction efficiency for worst case materials (i.e. carbon at JET) and application of a conservative conversion factor allow the concentration of tritium in the original sample tobe derived. Pre-operative checks were carried out to ensure reproducible conditions for the processing of each sample. The glass fibre filter was renewed prior to extraction to ensure a reproducible build up of resistance to gas flow from one extraction to the next. Tritiated samples representing JET waste were prepared by wiping ex. JET Torus graphite tiles with a combustible substrate.

During sample introduction and prior to attaining a predefined temperature only nitrogen is used to prevent combustion from occurring. For materials from which tritium can be easily liberated the process can either be continued with nitrogen only. Alternatively, the nitrogen can be replaced by air flowing at such a rate as to avoid sudden, uncontrolled flaring.

Tritium Extractor
(note condenser vessel on right of the picture and sample introduction point at top/centre)

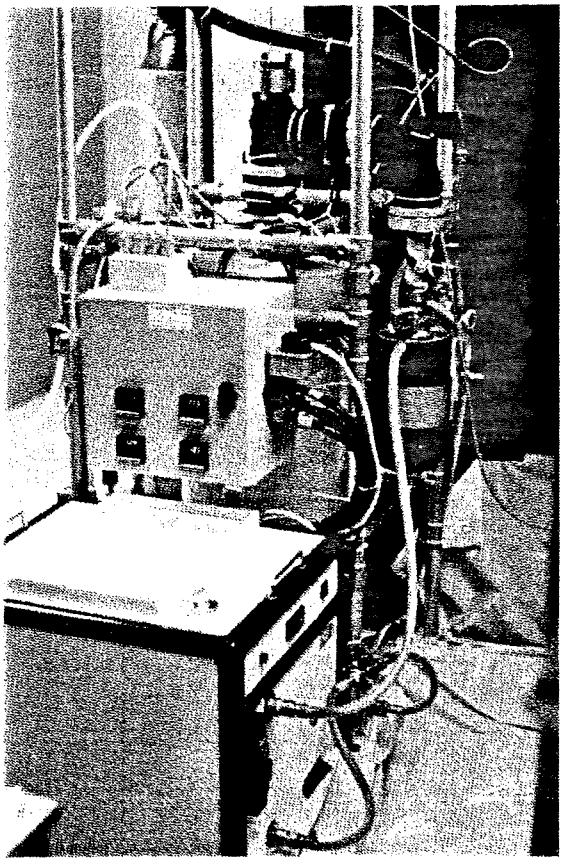

The use of controlled combustion destroys most of the non-metallic waste materials at 400°C and will liberate a significant amount of the tritium retained by the graphite found in JET waste. Important aspects such as determination of background count rates and liquid scintillation counting efficiency evaluation were taken into account. Many of the samples produced from combustion carried out at 400°C were coloured yellow. When mixed with a proprietary liquid scintillant (Optiphase Hisafe II) the resultant solutions darkened with time changing from pale yellow, following preparation, to deep brown after approximately 2 days. In order to establish the effect on counting efficiency a calibration curve was produced to enable measurements to be corrected to account for this colouration. Using the same materials as the contaminated samples a further coloured solution of low radioactive content was produced by combustion in the tritium extraction apparatus. Aliquots of this solution were used to produce samples of varying colour intensity. To each sample a small, known quantity of a high activity solution (approximately 3.3MBq/litre) was added. The calculated efficiency was plotted against the spectral quench parameter from the liquid scintillation counter. Counting continued for 2 days to observe the effect of progressive darkening in the samples. The data obtained from this experiment was used to correct measurements of all samples produced where colour quenching occurred.

Results

Non-graphite bearing materials contaminated with tritiated water:

- high extraction efficiency can be achieved at low temperature (200°C) using only humidified nitrogen.

Controlled combustion of tritiated graphite supported on a combustible substrate:

- at 400°C the extraction period and air flow rate were optimised achieving an extraction efficiency of 23.2%.
- reproducible results were obtained with a first standard deviation of 19% of the mean tritium concentration.

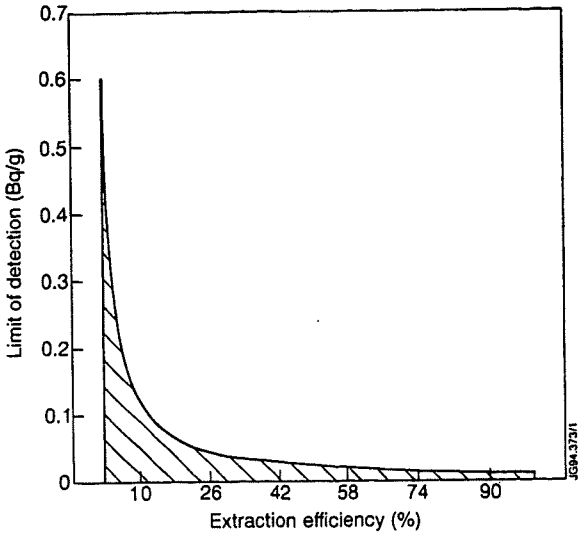

Conclusion

The reproducibility of the method was demonstrated during trials using contaminated waste material samples at low temperature (200°C), using only nitrogen and demonstrated at a higher temperature (400°C) using the controlled combustion technique. An extraction efficiency of 23.2% gives a limit of detection of 0.05Bq/g. The graph (above) shows that, even after accounting for the deviation of the obtained results, the limit of detection would still be significantly below 0.4Bq/g. The large sample size and reduced processing time, compared with other established extraction techniques, provide increased confidence of true representation of the parent material and reduced costs. The high sensitivity of this simple, rapid and reasonably accurate technique, coupled with representative sampling procedures, may provide a means of confidently reclassifying potentially radioactive waste as non-radioactive. Further work will establish linearity between known levels versus extracted tritium level for progressively lower concentrations. Tritium memory effect will also be examined to establish cleaning procedures to avoid the occurrence of false positive extractions.

Design of the MkII Divertor with Large Carbon-Fibre Composite (CFC) Tiles

H Altmann, E B Deksnis, J Fanthome, C Froger,
C Lowry, R Mohanti[1], M Nilsen[2], A Peacock, M A Pick,
D Spencer, R B Tivey[3], G Vlases.

JET Joint Undertaking, Abingdon, Oxon, OX14 3EA, UK.
[1] AEA Technology, Culham, UK.
[2] General Atomics, San Diego, USA.
[3] ITER, Garching, Germany.

1. INTRODUCTION

The MkII Divertor will be installed inside the JET torus over a six month period, starting before mid-1995. It will replace the MkI Divertor which has been in operation since February 1994.

The design of this new divertor has two main purposes. Firstly it aims to maximise the power handling capability of the plasma-facing surface which intercepts the magnetic field lines at very shallow angles with large, accurately aligned, CFC tiles. The alignment is controlled by pulling each tile down on to support pads at all four corners. These support pads are shared with the adjacent tiles, thereby ensuring accurate edge alignment and shadowing, particularly in the important toroidal direction.

The second main purpose of the design is to create a flexible system for studying different divertor geometries and concepts. This is achieved by constructing a water-cooled support structure in the shape of a U-channel above the divertor coils. This structure becomes a permanent fixture inside the torus. Carriers for supporting the plasma-facing CFC tiles are attached to the support structure. These carriers and tiles are cooled only through radiation and contact conduction to the support structure. Their exchange with a differently shaped set is therefore relatively straightforward. Figure 1 shows a poloidal cross-section through the design to be installed in mid-1995.

Impurity control is aided by the provision of a pumping gap with access to the in-vessel cryo-pump. Water-cooled louvres shield the cryo-pump from radiation loads.

De-contamination of the vessel interior, as carried out before the last shutdown, is no longer possible, owing to the large number of concealed areas and closed diagnostic conduits. Consequently all installation work for the MkII Divertor has to be carried out by personnel working in full protection suits supplied by air through flexible hoses. This prevents intricate assembly work taking place inside the vessel and the MkII design needs to take these limitations into consideration.

2. SUPPORT STRUCTURE

This is formed from three concentric rings consisting of a base plate plus inner and outer rings. The joints between these rings is made at the corners through flexible hinges which avoid bending stresses during disruptive and non-uniform loading of the structure. They also play a role during assembly of the structure inside the torus by allowing some flexibility between the assembled components.

The choice of 24 modules was dictated by the size of the largest single module that could fit through a torus horizontal port (17mm nominal clearance with the present design).

Figure 2 shows a CAD view of one of the 24 modules which is assembled from the three ring sections, corner hinges and water-cooled louvres. The joints between the modules are assembled with fishplates either side, located by dowels and bolts. Water-cooling of the structure is introduced through Ø8mm gun-drilled holes. Each module has a single cooling path with the water passing between the side rings and baseplate through the louvre pipes.

Support of the structure on to the divertor coils takes place at each of 32 main coil clamps. The original purpose of these clamps was to hold the divertor coils in position inside the torus and any load on to them passes into the wall of the torus. A T-slot locator is fitted between the baseplate and clamps to permit radial movement between them during high temperature baking but

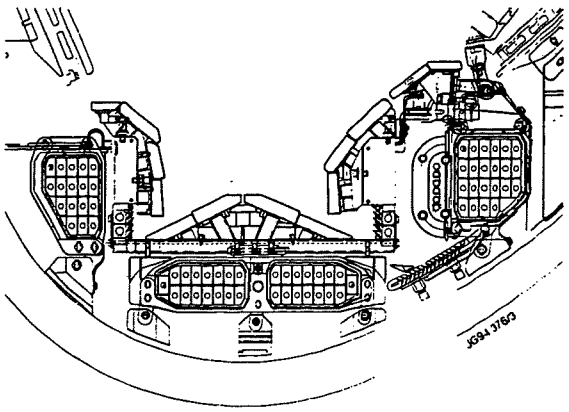

Figure 1. Poloidal section

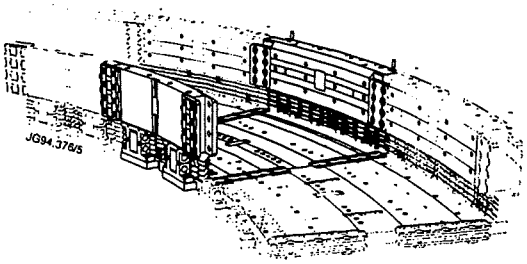

Figure 2. CAD perspective of module

restraint against forces in the vertical and toroidal directions.

The support structure has been designed to resist a variety of forces that are predicted to arise from plasma disruptions and halo currents (ref. 1). Figure 3 summarises the loading cases that have been studied using ABAQUS and NASTRAN computer codes.to arise from plasma The structure is manufactured almost entirely from Inconel 600 because of its high resistivity, stability and strength at elevated temperatures. Although the structure is cooled almost to room temperature during operation, vacuum conditioning takes place up to 350°C so elevated temperature material stability is animportant parameter. The structure also forms an electrically conducting ring inside the torus magnetic field and a high material resistivity is necessary to minimise induced electrical currents.

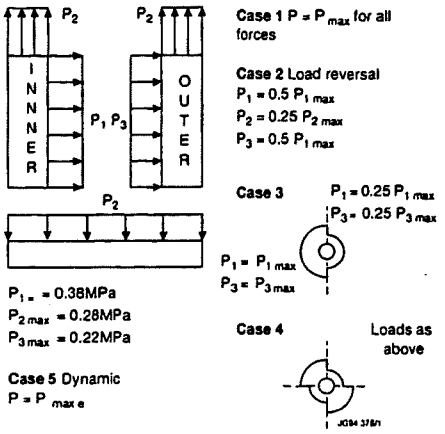

Figure 3. Downward, Upward, Mode 1, Mode 2.

Final assembly of the components to form the support structure will take place inside the torus. The manufacturing process has been chosen to ensure that all the modules fit together accurately and that the final set of locating dowels and bolts will locate correctly in the closing module. The manufacturers will assemble the complete structure on a vertical axis turntable inside the factory before machining the dowel and bolt holes in the fishplates. After bolting the structure together, the inside surfaces of the U-channel will be machined by turning to create the highly accurate mounting surfaces for the tile carriers. The slots for locating the carrier alignment dowels will be marked with the complete structure on the turntable and then have the final machining done after dismantling the modules. This procedure will lead to a final tolerance of ± 0.2mm between adjacent carriers.

3. TILE CARRIERS

The aim behind the carrier design is to create lightweight, rigid structures for locating the tiles accurately while providing support for diagnostics and their electrical connections. To this end, the carrier design has evolved into an assembly of tile support pads and mounting bosses, joined together with ribs. Each module is fitted with six different carrier designs, i.e. one pair each for the inner ring, outer ring and base. Each pair consists of one wide and one narrow carrier. Installation on to the support structure requires that the carriers alternate between

wide and narrow versions around the torus. Figure 4 shows a CAD representation of the outer ring carriers where the wide carrier has the tile corner support pads built in. These pads provide the location for the tiles from the adjacent narrow carriers, ensuring that pads are shared to minimize the tolerance in tile-to-tile step heights. Location of the tiles on to the carriers takes place through a spring-loaded bar through the body of tile to pull it down on to the pads. Support pads at the ends of this bar give it a dumbbell appearance and apply the tile loads in line with the corner supports. This avoids a bending moment across the tile. Early trials at pulling down the tiles with a single central fixing point led to the initiation of longitudinal cracks along the tile centre line. Each tile position on the carriers is defined by three dowels that fit into matching slots in the rear tile face, i.e. one toroidal and two poloidal/rotational location dowels. The slots allow tile movement under thermal expansion. The pull down force of the tiles on to the carriers is set nominally at 1KN, determined by the need to deflect the tile until all four corner pads touch simultaneously, taking into account the build-up of tolerances.

Attachment of each carrier on to the support structure is achieved with spring loaded bolt assemblies. The spring loading is required to allow thermal expansion of the carriers with respect to the structure, the fixed references being dowel locations in the structure. For the base plate, one toroidal and two poloidal/rotational dowels are used. For the side rings, a single toroidal dowel is required with the vertical face and top edge of the rings providing the radial and poloidal references.

Manufacture of the carriers is suitable either through investment casting or welded assembly. The final dimensional tolerances are achieved through NC machining of the dowel holes, bolting locations and tile support pads with respect to the interface on to the support structure.

A wide range of diagnostics will be fitted to the MkII Divertor, many of which will be attached to the tile carriers. These include thermocouples, bolometers and Langmuir probes. Later stages of the MkII Divertor require the present set of carriers to be replaced by ones designed to create a different divertor profile. This exchange is planned for late 1996, after the next limited tritium experiment but before the torus has time to recover from the tritium loading and neutron radiation. Consequently any carrier exchange has to be carried out by remote manipulation and without personnel intervention into the torus. Lifting points and clearances have been taken into account for these purposes.

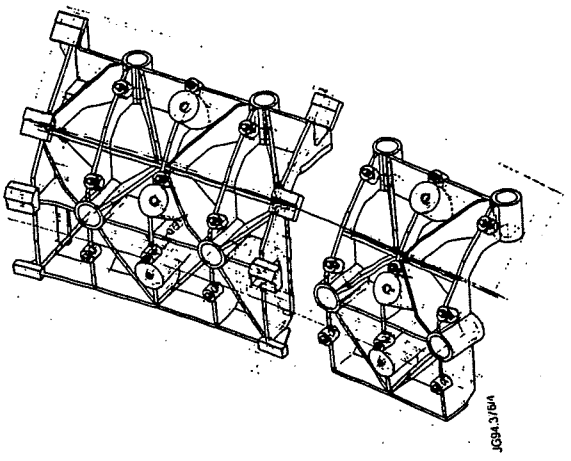

Figure 4. Outer ring carrier

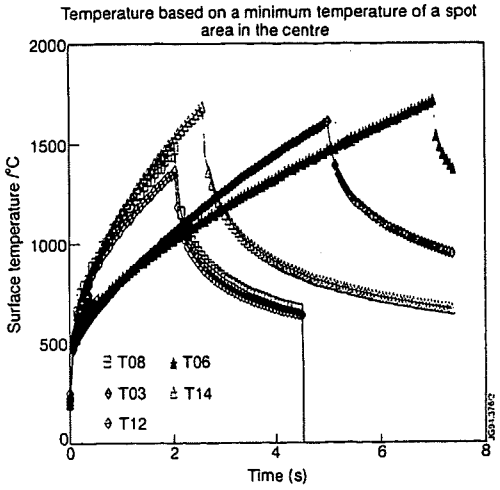

Figure 5. Thermal performance of tile material

4. TILES

4.1 Material properties

The three criteria for selection of the tile material were thermal conductivity, expansion coefficient and mechanical integrity.

The most important requirement was the thermal conductivity perpendicular to the tile plasma-facing surface. This should be as high as possible to maximise the time for the tile surface to reach any specified temperature.

The field lines impinge on the tiles at angles between 1° and 8°. This should be kept as low as possible to minimise the surface heat flux. Thermal gradients through the tile and toroidal expansion coefficient cause the tile to bow, thereby increasing the flux angle. Consequently the lowest toroidal thermal expansion coefficient is required.

For mechanical integrity, the tiles must be able to withstand both the thermal stresses and the mechanical loads imposed by the combination of magnetic fields and halo currents passing through the tiles during disruptions.

4.2 Thermal performance

Eight different materials from four different European suppliers were tested to rank them in terms of thermal conductivity and bowing under a neutral beam heat flux. Figure 5 shows the surface temperature as a function of time for five of these materials with a heat flux of $10MW/m^2$.

The best materials, when bowing was taken into account, were the 2D materials. These were oriented with the fibre plane direction running in the toroidal and away from the beam directions. One of these materials cracked along the lamination during testing with a surface temperature of 2400°C (much higher than the maximum expected at JET of 1800°C). To retain the best thermal solution, a method was developed for holding together 2D materials with metal tie rods.

Figure 6 shows a tile with the holes for the metal tie-rods and the tie-rods of Ø4mm Inconel 718 threaded into conical nuts. Prototypes had thicker rods spaced at twice the pitch of the existing and were tightened up to 6kN but it was later found necessary to tighten only to 1.5kN.

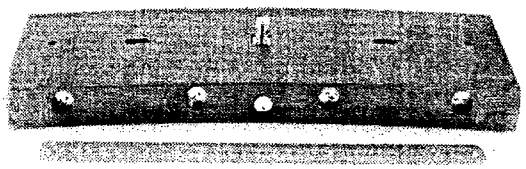

Figure 6. MkII tile

4.3 Thermal testing of prototype tile

Once the basic components of the tile had been determined, a prototype tile was tested. The tile was taken through ~ 200 pulses, 2 seconds long, at $15MW/m^2$, cycling between 600°C and 2000°C surface temperature. The bulk surface temperature did not exceed 600°C. No cracking of the material was observed.

4.4 Surface profile

The main criterion for the design of the tiles is that no edges are exposed either poloidally or toroidally. The thermal performance is defined to a large extent by the toroidal angle of the tile, α. To minimize α, tiles as long as possible are used and gaps are kept to a minimum. A schematic of the design of the tiles is shown in Figure 7. The adjacent gaps are different which means the tiles are stepped to gain the maximum performance. The centre line height difference between tiles is ~0.6 and the height difference at the end of the tiles is ~ 2mm.

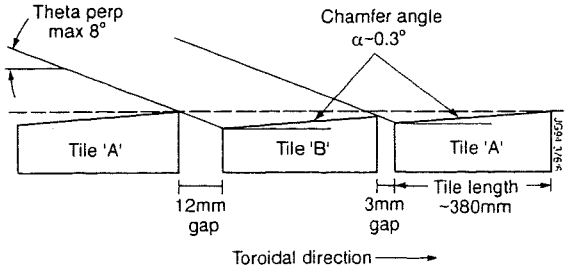

Figure 7. Schematic tile design

Transforming this into toroidal co-ordinates means that α changes across the tile but, for manufacturing reasons, α was held constant across each tile face to give a conical surface profile for a 1-2% reduction in power handling capability at the lowest field line angles.

4.5 Tile manufacture

Prototypes have been produced both for neutral beam testing and for determining the build-up of tolerances. Machining of the front and rear faces will be done by a conical cutter with the tiles supported in vacuum chucks at the same orientation that exists on the divertor.

REFERENCES

1. P. Noll, P. Barabaschi, G. Sannazzaro, C. Sborchia, "Electromagnetic forces during JET Divertor operation, unpublished.

Ten Year Operational Experience of the JET Flywheel-Generators

M Huart, P G Doyle, E Beedham[1].

JET Joint Undertaking, Abingdon, Oxon, OX14 3EA, UK.
[1] ex GEC Alsthom Large Machines Ltd., Rugby, Warwickshire, CV21 1BD, UK.

ABSTRACT

The JET Pulsed Power Supply Scheme relies on a combination of flywheel-generator-converters and mains driven transformer-thyristor rectifiers. The availability of a 400KV network with considerable pulse capability (575MW, 475MVAR) has allowed the FGCs to be dedicated, one to the poloidal magnetising coils and the other to the toroidal field coils. Both flywheel-generators have been operating on the JET coils since entering service in June 1983 and have each totalled approximately 25,000 pulses to date. The paper will review the experience from ten years of operation as well as results of the comprehensive mechanical and electrical survey of one generator and driving motor performed in 1992.

1. MECHANICAL DESIGN OF THE FLYWHEEL-GENERATOR

The mechanical design of the generator is derived from typical low speed, large diameter hydro-generators as driven by low-head high-volume water turbines. It uses a heavier and axially longer than normal rim to achieve the necessary stored energy in the rotor, which acts as an integrated flywheel. However, the duty required has similarities to heavily cycled pumped-storage hydro-generators from which most of the data on mechanical fatigue is derived.

A design life of 100,000 cycles at the full energy rating was specified.

Extensive analysis, complemented by laboratory tests, was made during the design stage to assess the integrity of the rotor under fatigue conditions as well as of the stator end windings under short circuit conditions [1], [2].

These analyses concluded that the probability of failure of the pole attachments or the rotor rim as a whole is below the typical figure of 10^{-5} normally adopted for machinery of this type. Fig. 1 shows a cross section of the generator and driving motor.

2. COMMISSIONING OF THE FLYWHEEL-GENERATOR

During the commissioning of the flywheel-generators in 1982/83, three problems were identified [3] and successfully resolved, namely:

2.1 Unbalanced magnetic pull in driving motor

The motor shaft is cantilevered to the end of the generator shaft as can be seen in Fig. 1. An asymmetry in the motor air gap (nominally 5mm), such as caused by a rotor displacement resulting from the clearance in the generator top and bottom bearings, produces an imbalance in the magnetic field within the air gap, thus producing a net radial force (UMP). This enhances the initial displacement. The problem was solved by adding equalising connections in the two stator windings, so as to maintain the same flux in two opposite groups of poles.

2.2 Thrust bearing temperature

Using computer codes, during the design stage, the predicted thrust pad temperature was expected to be 65°C for an

oil bath temperature of 50°C. Measurements obtained during the bearing runs indicated a temperature of approx. 80°C for bath temperature of 50°C at a constant generator speed of 150rpm. Investigations concluded that the mixing that occurs between the hot oil ejected from the oil film, and the cold oil drawn from the oil bath, was not as good as expected. The problem was solved by injection of cold oil at the leading edge (low pressure) of each of the twelve thrust pads.

2.3 Balancing of the rotor of the generator

The flexibility of the spider hub and arm arrangement and the large mass of the rotor rim is responsible for a critical speed estimated to be in the range 260-300rpm. Traditional methods of fitting balance weights on the spider arms produced low vibration in the speed range 112-180rpm. However, vibrations increased rapidly above 180rpm. The problem was solved by designing new balance weights to be fitted in the dedicated keyways on the bore of the rotor rim, since the major cause of mechanical imbalance is the rim itself. In this way, low vibrations were achieved up to the nominal speed of 225rpm.

3. OPERATION OF THE FLYWHEEL GENERATORS OVER TEN YEARS

3.1 Low friction pads and balancing of the generator rotor

The 650 tonne rotor rim is supported by twelve support blocks each fitted to a spider arm. In view of the radial expansion of the rotor rim (2.5mm at nominal speed) due to the hoop stress, the support blocks are fitted with teflon coated low friction pads to ensure that the expansion of the rim is concentric to the shaft.

During the first half of 1985 the vibrations of the TFGC progressively increased. "Shaft Displacement Signature" taken during balancing runs indicated a change in the phase angle. During the 1985 shutdown, the rotor rim was lifted and the low friction pads were inspected. It was discovered that one of the rim tapered keys had been driven into hard contact with one low friction pad and had worn off the teflon coating. The increased friction was responsible for the non-concentric expansion of the rim and the increase in vibration. The low friction pads were replaced during the 1985 shutdown and subsequently in 1989 and 1992. No subsequent abnormal wear of the pads was discovered.

3.2 Restarting the flywheel-generator after a shutdown

It was observed after the 1984 and 1985 shutdowns that the flywheel-generators experience large vibration above 180rpm when starting after several months shutdown. Rebalancing proved to be a long and tedious procedure. It was concluded that the rotor out-of-balance was resulting from the non-concentric expansion of the rotor rim due to uneven friction among the twelve low friction pads.

The procedure now adopted since 1985 consists of: a) increasing progressively the idling speed from 112rpm to 150rpm, b) speed cycling from 150 rpm to 112rpm repeatedly until vibrations stabilise, c) increasing the speed cycling from a maximum speed of 180rpm and then 200-225rpm. The complete procedure takes two to three weeks. During the speed cycling phase, regular balancing runs are performed to check the "Shaft Displacement Signatures". Following this procedure, no rebalancing of the rotor was necessary since 1985. Fig. 3 shows typical "Shaft Displacement Signatures" following the 1990, 1991, 1992/93 shutdowns.

3.3 Statistics of faults

A centralised and systematic system of recording operation faults in the Tokamak Magnet Power Supplies was introduced in February 1985. The statistics of faults for 1985/86 have already been reported in [4.]. In Fig. 2, the statistics for 1994 (twenty weeks of operation) are compared with those of 1985/86 (fifteen weeks of operation). It is concluded that the number of faults has been reduced and the majority of faults fall among three systems: Control system (PLC, electronic modules), excitation (DC circuit breaker) and liquid rheostat (hydraulic ram). It is intended to replace the offending hardware during the 1995 shutdown.

4. ELECTRICAL AND MECHANICAL SURVEY OF THE TOROIDAL FLYWHEEL-GENERATOR

A comprehensive mechanical and electrical survey of the Toroidal Flywheel-Generator was carried out during the 1992/93 shutdown. The survey programme was agreed with the manufacturer prior to the start of the shutdown. The Toroidal generator was selected because of its larger operational speed range (higher delivered energy). As a result of this extensive mechanical survey, no signs of cracks or movement were detected in the critical parts of the generator (rotor and stator), the pony motor (rotor and stator), or the top and bottom bearing housings.

The electrical survey did not reveal any abnormalities. When necessary the bracing of the generator stator end-winding was retightened. The electrical survey included: Check of slot wedges for sign of looseness, check bracing of end windings, visual inspection of end windings for both generator and pony motor, DLA (Dielectric Loss Analysis) test on both generator and pony motor stator windings and the TVA (Tennessee Valley Authority) test on individual generator stator bars and measurement of insulation resistance to ground for the generator field winding. The DLA test [5] forms part of the generator preventative maintenance programme and the results of the integrated discharge energy versus applied voltage for the toroidal generator and pony motor over ten years is shown in Fig. 4.

5. CONCLUSION

The JET flywheel-generator-diode converter systems have proved to be reliable over a period of ten years, once the initial period of commissioning had been completed and a proper programme of maintenance had been established. The faults in ancillary equipment have gradually been reduced as the maintenance programme has been refined. Over the same period, maintenance outages have been reduced from once per week to once per month.

A comprehensive electrical and mechanical survey of one of the flywheel-generators after ten years of operation did not reveal any weakness in the design and construction of the flywheel-generator. It proves that dedicated large diameter low speed flywheel-generators with output diode converters are a viable alternative for the supply of large pulsed DC magnets.

The large diameter allows many AC stator windings (six are used in JET FG) to be connected in parallel to a common AC bus to deliver the high AC current without the need for step-down transformers and associated switchgear. The short core length reduces the risk of chafing/movement of the stator bars due to the repeated heating and cooling inherent with the heavy pulsed loading.

The generator has its first critical speed above the nominal speed range. Hence a wide speed range (such as 2:1) allows the recovery of a large fraction of the stored energy (~75%). The critical speed corresponds to a radial deflection of the rotor structure supporting the rim. It must be ensured that this structure is made stiff enough.

REFERENCES

[1] M. Huart, E. Beedham "Large Flywheel Generator Diode Converter for the JET Tokamak", Proceedings of 11th Symposium on Fusion Technology, Oxford, 15-19 September 1980.

[2] M. Huart "Design, Fabrication and Erection of Flywheel-Generator-Converters for the JET Tokamak", Proceedings of 9th Symposium on Engineering Problems of Fusion Research, Chicago, 26-29 October 1981.

[3] M. Huart "Commissioning of the JET Flywheel-Generator-Converter Systems", Proceedings of 13th Symposium on Fusion Technology, Varese, 24-28 September 1984.

[4] M. Huart et al. "Operation of the JET Magnet Power Supplies. Reliability and Improvements", Proceedings of 14th Symposium on Fusion Technology, Avignon, 8-12 September 1986.

[5] J.S. Simons "Diagnostic Testing of High Voltage Machine Insulation", IEE Proceedings, Vol. 127, Pt. B, No. 3, May 1980.

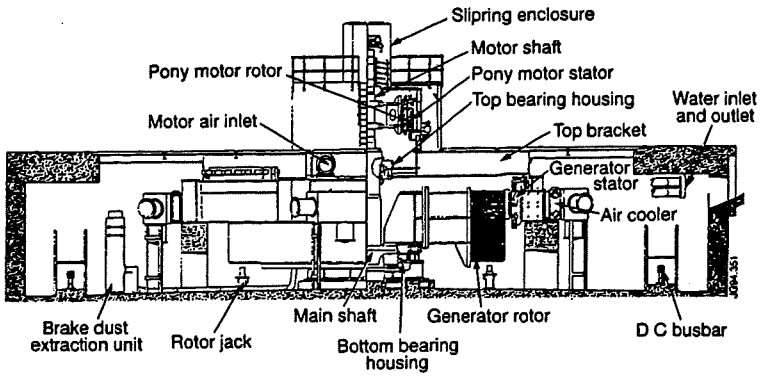

Fig 1: Cross section of the motor-generator.

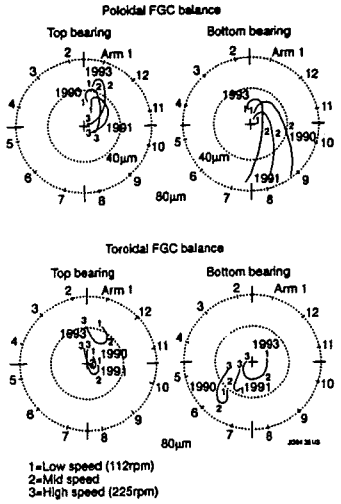

Fig 2: Characteristic of shaft movement in top / bottom bearings (Shaft Displacement Signature).

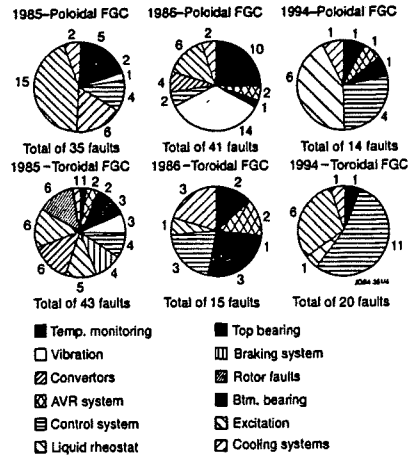

Fig 3: Fault Distribution (1985, 1986, 1994) over 15-20 week period.

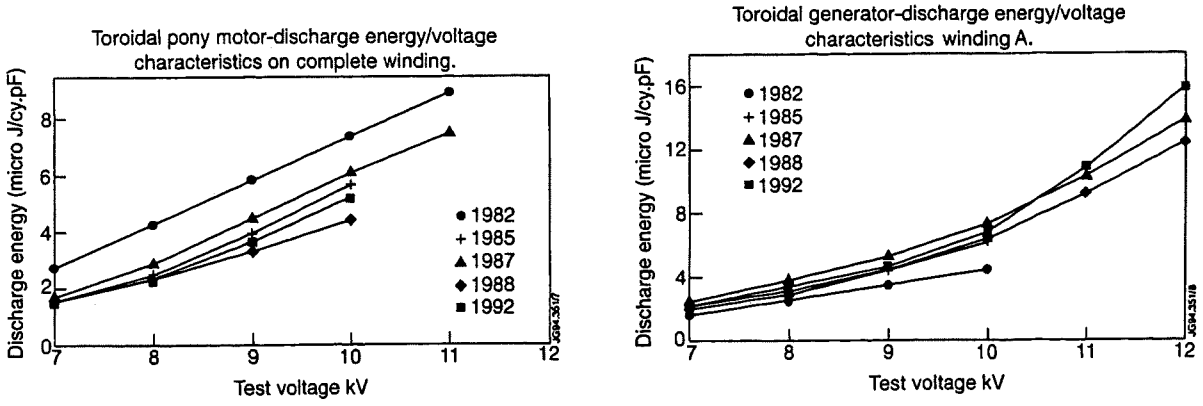

Fig 4: Discharge energy / voltage characteristic (DLA tests).

LHCD Operations in JET and Developments for Fusion Applications

P Froissard, G Agarici[1], Y Baranov, M Brandon, M Brusati, J A Dobbing, A Ekedahl, P Finburg, B Fischer, C Gormezano, P Haydon, A Kaye, M Lennholm, T McCarthy, R Page, P Paling, G Platt, D Pledge, J Plancoulaine, F Rimini, P Schild, F X Söldner.

JET Joint Undertaking, Abingdon, Oxon, OX14 3EA, UK.
[1] CEN Cadarache, 13108 St Paul lez Durance Cedex, France.

Abstract: The full Lower Hybrid Current Drive (LHCD) launcher in JET has been completed and installed. Up to 6 MW has been coupled to the plasma and 2 MA full current drive was achieved with 4 MW of LH power. Coupling is improved by using active feedback control on the launcher and plasma position. A new launcher design concept, called Hyperguide, has been developed and tested successfully in JET to replace eventually conventional launchers using multijunctions for next step machines like ITER.

1. INTRODUCTION

The Lower Hybrid Current Drive (LHCD) system on JET consists of 24 klystrons with a total power of 12 MW for 20 seconds at 3.7 GHz. 3 different $N_{//}$ spectra can be launched simultaneously with the main peak ranging from 1.4 to 2.3 [1].
Three systems for controlling the coupling in real time have been implemented: the launcher position and the plasma position, which can both be controlled under feedback with the reflected coefficient as input signal, and a gas feed to modify the plasma edge density at the grill mouth.
In order to improve the conditioning speed of the launcher made of 48 multijunctions and the grill made of 384 reduced waveguides, an automatic grill conditioning technique and a cryopump installed on top of the launcher vessel have been used.
A new design concept for the launcher, called Hyperguide, has been developed on JET to simplify the design and improve the power handling capabilities of LHCD launcher for present and next step machines like ITER.

2. LHCD OPERATIONS IN JET

Operations on a variety of plasmas both in limiter and divertor configurations with central density ranging from 1 to 4 $10^{19}m^{-3}$ have been performed. Above 6 MW of power have been coupled to an X-point plasma and a maximum of 55 MJ of energy was injected with combined ICRH heating.

2.1 Current Drive Experiments

Up to 2 MA was driven with 4 MW of LH power resulting in a current drive efficiency $\eta=0.21$ 10^{20} $AW^{-1}m^{-2}$ (figure 1). Transformer recharging was also achieved in 1 MA discharges through loop voltage reversal with 4 MW of LH power.

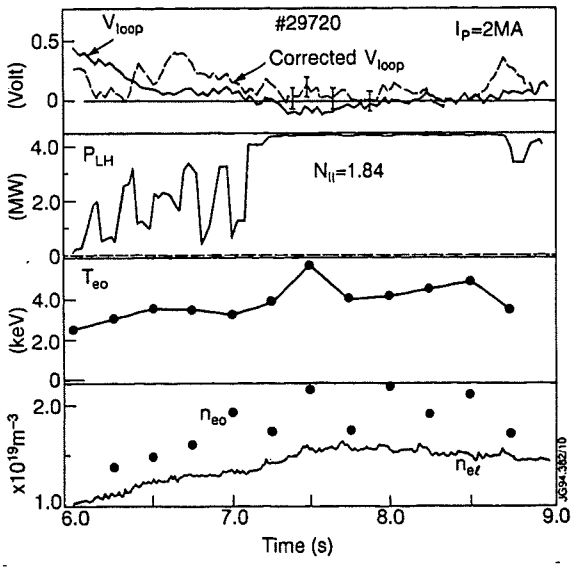

Figure 1: 2 MA Full CD shot

2.2 Coupling

Figure 2 shows the variation of the reflection coefficient with the distance between the separatrix and the limiter. Good coupling is achieved with the plasma up to 6 cm away from the limiter.

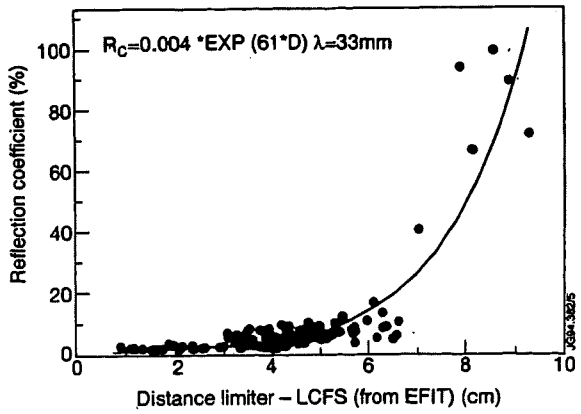

Figure 2: Reflection coefficient with distance separatrix-limiter

The effect of the plasma and launcher position on the coupling is indicated in figure 3 where the plasma is moving away from the limiter when LH is applied. Once the launcher reaches its preset position the coupling degrades. Improved coupling has been since achieved with active feedback control.

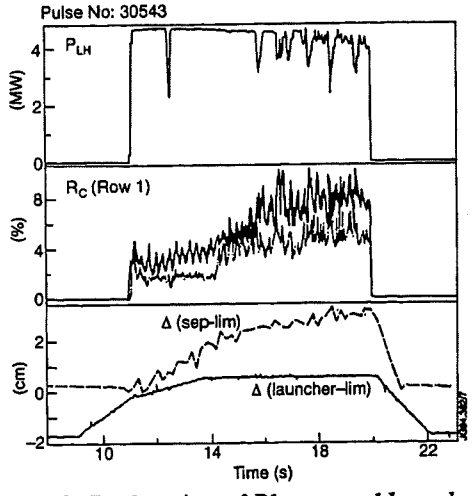

Figure 3: Rc function of Plasma and launcher position

Coupling on H-mode plasma is more difficult for LH as the density gradient is much steeper than in L-modes. However successful coupling on ELM'y H-modes has been achieved as shown in figure 4. Reduced reflection can be attributed to the strong density increase during the H-mode phase.

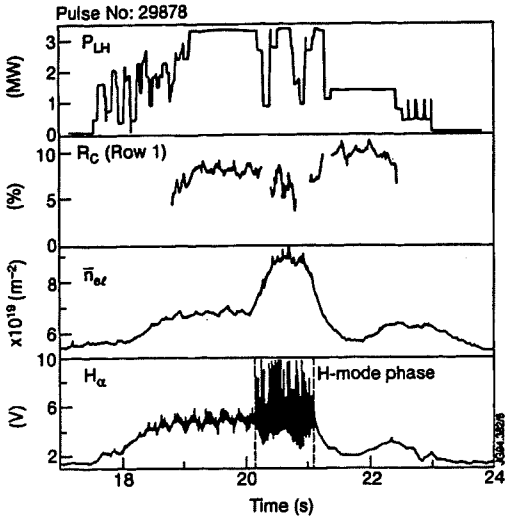

Figure 4: LH Coupling on H-mode plasma

2.3 Launcher conditioning and power optimisation

In order to increase the conditioning speed of the launcher, an automatic grill conditioning system has been developed. The klystrons are being pulsed in vacuum for 3 seconds with a 1:30 repetition rate. Depending on the number of trips on each generator, such as arcs, RF trips (VSWR, unbalanced reflection at the launcher, window arc prevention trips...), the power is incremented or decremented by 5 kW for the following pulse. Using this system, all klystrons were pulsed up to 200-300 kW in vacuum and no arcs were observed at the windows.

After one day of conditioning, the temperature at the grill mouth can increase by 100-200°C. The evolution in power transmission capability is indicated in figure 5 where the temperature increase rate of the load multijunctions, proportional to the average input power in the multijunction, is plotted versus the operation time. The gas released during conditioning is pumped by a 80000 l/s cryopump installed on top of the launcher vessel, keeping the pressure inside the launcher below 10^{-7} mbar.

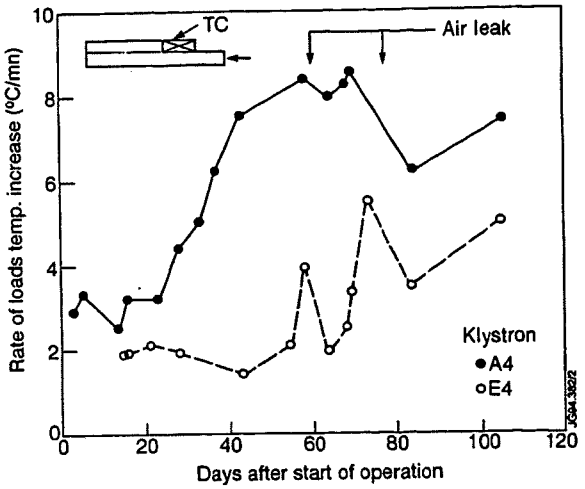

Figure 5: Temperature increase rate during grill conditioning

The pressure increase in the launcher as a function of the multijunctions temperature increase (measured at the 2 wg section) is indicated in figure 6 for cases with and without the cryopump.

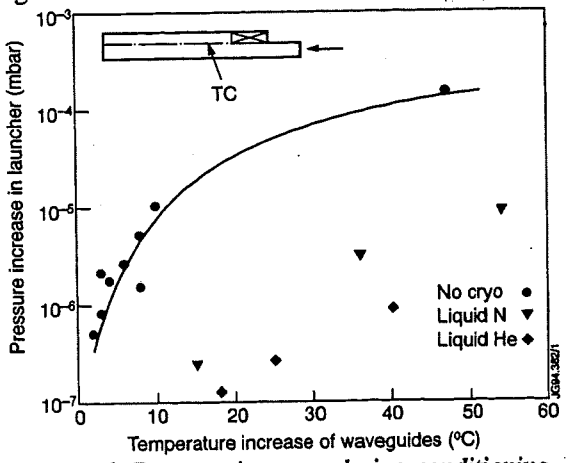

Figure 6: Pressure increase during conditioning

A power optimisation software has also been successfully used to increase the launched power during plasma pulses and determine the maximum operating power possible for a given set of plasma conditions.

3. HYPERGUIDE CONCEPT

For next step machines like ITER, a conventional launcher made of multijunctions is clearly impractical as it would require thousands of waveguides facing the plasma. The gas accumulation inside the launcher would limit the power handling capabilities of the antenna. A new design concept called Hyperguide [2], which is much lighter, simpler and cheaper to manufacture, has been developed in JET to overcome these difficulties.

The Hyperguide is an overmoded waveguide providing nearly total power transmission between an emitter plate, fed by standard waveguides operating at the fundamental $TE_{0,1}$ mode or mode converters operating at $TE_{0,m}$, and a receiver providing the slow wave launching structure facing the plasma. The main propagating mode in the Hyperguide is $TE_{0,N}$ where $N=m*n$ with n the number of waveguide rows emitting a $TE_{0,m}$.

3.1 Low Power Testbed

A low power testbed has been developed to simulate the behaviour of a full scale Hyperguide for JET (figure 7).

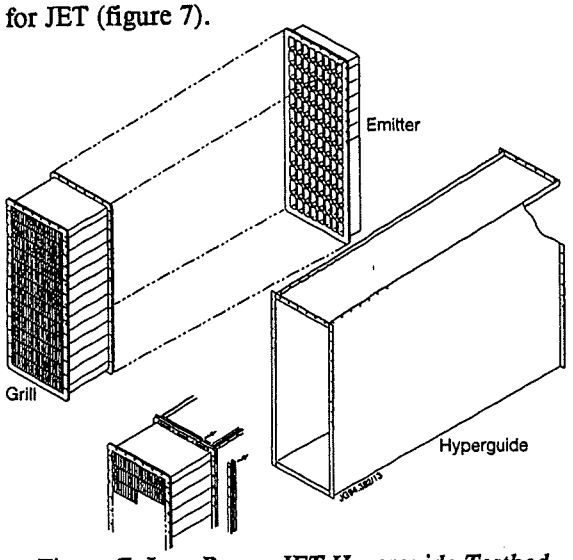

Figure 7: Low Power JET Hyperguide Testbed

It is made of 4 parts: the generators, providing up to 100 CW at 3.7 GHz, and splitting network, the emitter plate, made of 8x12 WR284 standard waveguides, a 1.5 m long tapered Hyperguide and finally the grill mouth, made of 24x12 reduced waveguides coupled to a RF load array, providing a return loss better than 30 dB in each waveguide. Various scenarii with homogeneous and inhomogeneous power and phase distribution at

the emitter plate have been studied. For each case, the results have been compared with numerical predictions for a straight Hyperguide from a code called HYPER based on mode matching at the Hyperguide interfaces.
In the ideal case where homogeneous power and phase distribution is used at the emitter plate, the measured forward phase inside the reduced waveguides of the grill indicate that 180^0 phasing between rows is preserved. The measured power distribution in the grill mouth indicate that a transmission coefficient Qt (Qt=Total TE0,1 power in grill / Incident Power from emitter) better than 0.9 is achieved, which is in agreement with the numerical prediction.
Figure 8 shows the measured and predicted power distribution at the grill when the first 4 rows of the emitter are switched off. Good agreement is obtained even when strong inhomogeneous power is used to feed the Hyperguide. In this case the experimental Qt=0.6.

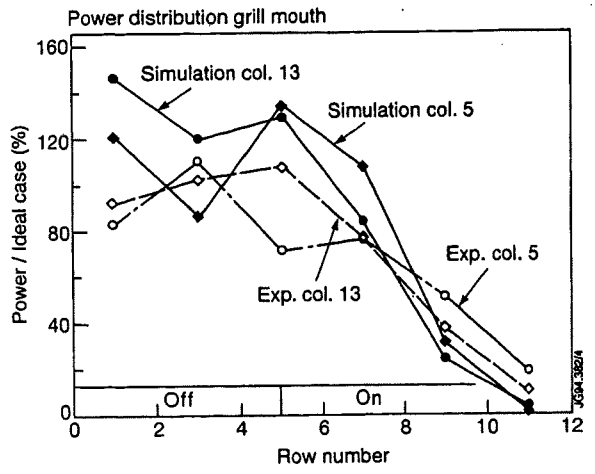

Figure 8: Power distribution when 4 rows are off

3.2 Future developments

The Hyperguide testbed results indicate that the Hyperguide concept is a viable solution for the design of a new launcher on JET and future applications on ITER.
A LHCD system using 2 launchers of 8 Hyperguides operating in $TE_{0,6}$ mode to launch around 50 MW at 5 GHz in ITER [3] has been proposed (figure 9).

The Hyperguides are fed by $TE_{0,3}$ mode converters and the grill mouth is made of alternate active-passive waveguides to provide space for cooling channels [4]. In this case the estimated Qt in each Hyperguide for zero reflection from the plasma is 0.9 and the power distribution inhomogeneity in the grill Qd=(Pmax-Pmin)/Pmean=1.24.

4. CONCLUSION

First operations with the full LHCD system on JET have demonstrated that LH is an efficient tool for current drive and profile control on large size Tokamaks. A new launcher concept called Hyperguide has been developed and tested successfully in JET. It is proposed to use this concept as part of an ITER LHCD Launcher.

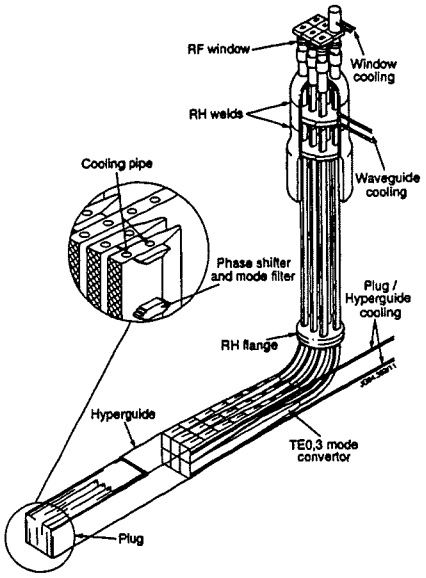

Figure 9: LHCD Launcher design for ITER

5. REFERENCES

1. F.X. Söldner et al., Proc. IAEA Meeting on RF Launchers, Naka, Japan, 10-12/11/93.
2. M.Pain et al., Fusion Engineering and Design, 22(1993) 251-256.
3. Final Report on the ITER TASK IVA-LH, 13/07/94, to be published as JET/CEA report.
4. P.Bibet, D.Litaudon, D. Moreau, Proc. IAEA Meeting on RF Launchers, Naka, Japan, 10-12/11/93.

Further Developments in the Brazing of Beryllium to CuCrZr

C M Ibbott, H D Falter, P Meurer[1], E Thompson,
M J Watson, G Critchlow[2], D Ciric.

JET Joint Undertaking, Abingdon, Oxon, OX14 3EA, UK.
[1] Siemens AG-KWU, Friedrich Ebert Str, PO Box 100100,
W-5060 Bergisch Gladbach 1, Germany.
[2] Loughborough Consultants Ltd., Institute of Surface Science & Technology,
University of Loughbrough, UK.

ABSTRACT

We report on further studies and results relating to the development of induction brazing of beryllium to CuCrZr. This technology is of interest for water-cooled plasma facing components capable of continuous operation at power densities in the range 5-15MWm^{-2}. As a continuation of previous work [1] in this area we have been able to demonstrate the successful transfer of the technology and in addition have carried out further detailed studies of the braze technique, mechanical strength and failure modes of the brazed joint.

Significant extensions to previous work include a direct comparison between the measured shear strength of various brazed joints to that of the beryllium as obtained under identical test conditions and also high heat flux tests of differing geometries of Be brazed on to hypervapotrons.

The results of extensive finite element computations which have been carried out in support of differing aspects of the experimental programme will also be presented.

1. INTRODUCTION

For future fusion devices Beryllium (Be) is considered the prime candidate first wall material, especially in high heat flux regions such as the pumped divertor target plates. The manufacture of the target plates is foreseen as Be bonded to CuCrZr high heat flux components using brazing as a possible bonding method. Reference [1] detailed the development of an induction heating technique and the comparison between three candidate brazes. From that work, Incusil 'ABA' (containing 1.25% titanium) brazed at 720°C for 60 seconds stood out as a good choice of braze for further study. This paper also reported that 2mm thick tiles withstood high power loads $\leq$ 17MW/m^2 and high cycle life (1000 cycles) at 13.5 MW/m^2 with relatively good reliability.

During the transfer of the technology to a second company the following detailed studies have been carried out.

- assessment of the shear strength of the parent materials,
- an investigation into the shear strength of the Incusil 'ABA' braze material as a function of the temperature,
- surface analysis of fracture planes,
- high power density trials on 2mm thick Be tiles.

2. TECHNOLOGY TRANSFER

The apparatus used in reference [1] was transferred to a second company. Using the same 4kHz generator and induction coil, the company was asked to braze two samples with overall dimensions 100×30×6mm of CuCrZr using 3mm thick Be. The braze material was Incusil 'ABA', braze temperature 720°c and dwell time 60 sec. Identical vacuum conditions and heating rates were attained. From these samples sufficient material was available to obtain three micro graphs and 12 shear test specimens. Shear tests were carried out at room temperature, 250, 350 and 400°C. Figure 1 shows the results of these shear tests.

Comparison of the results from each company, revealed that although the cross-section of the braze, the braze cycles and the vacuum conditions etc. were identical, the magnitude of the shear strengths differed by as much as 30% (lower in the case of the second company). A detailed investigation of the experimental techniques revealed that the shear tests carried out during the first studies [1] (which gave higher peak strengths but considerable variations) were performed with the force being applied through the CuCrZr and not through the brazed joint. When tested in an identical manner both companies obtained the same result.

We conclude that this technology is both transferable and respectable and can be considered as an industrial process. In the event of future studies

being carried out for alternative (e.g. silver free) braze materials, considerable care should be exercised to ensure that meaningful results are obtained from the shear testing of small samples.

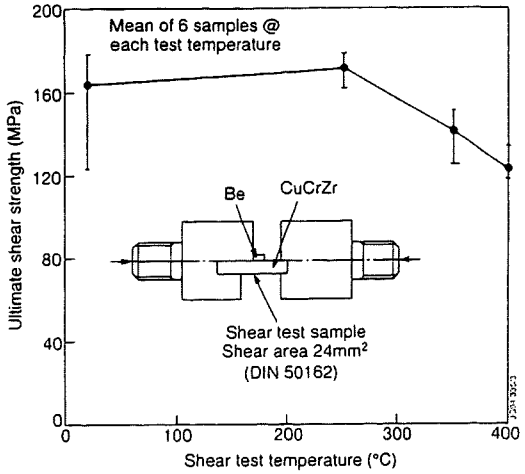

Figure 1. 720°C braze cycle shear strengths

3. BRAZE AT HIGH TEMPERATURE

In an attempt to improve the braze wet ability, Incusil 'ABA' was brazed at 750°C and 800°C with a dwell time of 60 sec. Figure 2 shows the comparison of shear strengths. Higher braze temperature reduces the shear strengths.

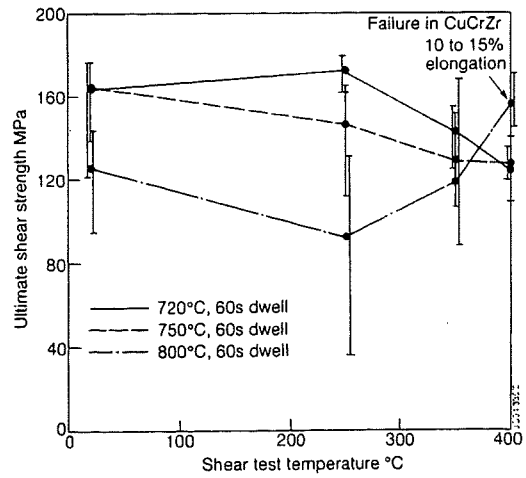

Figure 2. Comparison of shear strength with various braze cycles

Joint ductility (shown in Fig 3) increases with increased temperature. Note the increased ductility of the higher braze and test temperatures.

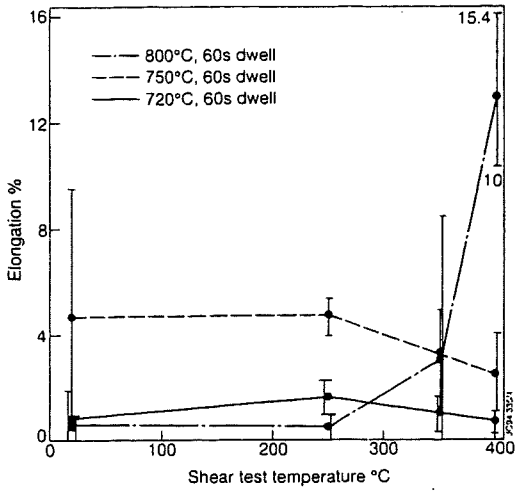

Figure 3. Comparison of ductility with braze temperature

It is interesting to note that after a high temperature braze cycle the 400°C temperature shear tests failed in the CuCrZr, indicating that the joint strength is greater than the yield of the CuCrZr..

The micro graphs at each braze temperature shown in Fig 4 reveal a distinct change in the morphology of the joint with braze temperature. It would appear that at higher braze temperatures the titanium goes into solution providing a possible explanation for the reduction in strength being the loss of rigidity in the joint.

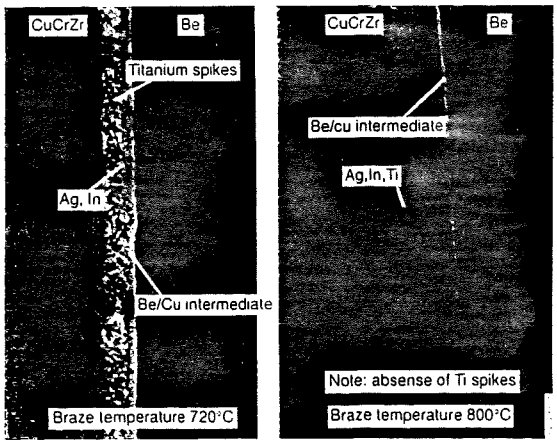

Figure 4. Change in joint morphology with braze temperature

4. SHEAR STRENGTH OF PARENT MATERIALS

Having a braze material with shear strength in excess of either of the parent materials is of little practical value. Clearly however, a compromise must be found when joining a brittle material such as Be to a more ductile one such as CuCrZr.

Be S200FH, CuCrZr parent materials and brazed samples were all shear tested at room temperature, 250, 300 and 400°C. The results (Fig 5) indicate that at room temperature the brazed joint is stronger than the Be. This may well result from the wide difference in ductility between Be and CuCrZr. At 400°C however, the brazed joint fails at the yield stress of the Be. This suggests that the shear strength of the braze, over the temperature range tested, does not limit the integrity of the joint.

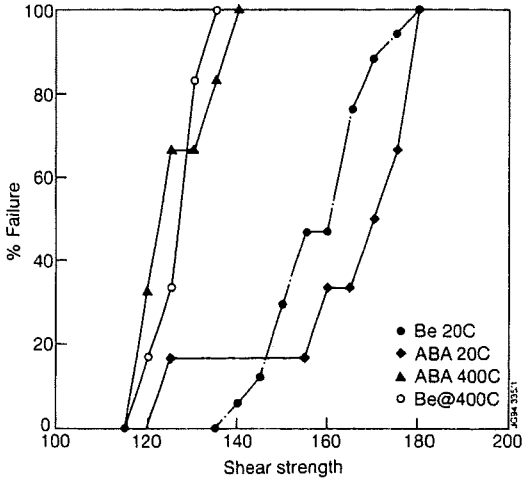

Figure 5. Percentage failure versus shear strength of Be and 'ABA' braze joint at 20 and 400°C

5. SURFACE ANALYSIS OF FRACTURE PLANES

Visually there appeared to be distinct differences in the failure of the braze samples for different braze temperatures.

Several fractured shear samples were selected from each braze temperature and shear test temperature. The surfaces of these samples were analysed using Auger Electron Spectroscopy (AES) at two points on the sample a) at the crack initiation and b) the centre of the sample. Figure 6 shows a typical optical image of the fracture surface for a low ductility failure. The AES shows the presence of Cu, Ag, In and Ti at the onset of failure and only Be (Be being typically 10-17%) and Cu at the centre of the sample. From equilibrium diagrams Ref [2], the latter suggests the presence of disordered bcc β phase and ordered bcc β' phase.

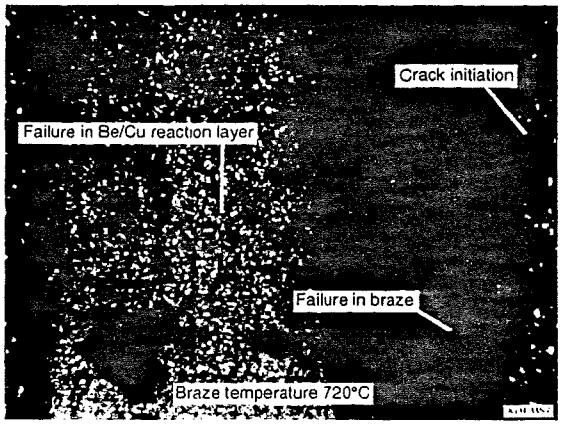

Figure 6. Typical fracture surface for 720°C braze temperature

Figure 7 shows typical sample for the 750°C braze temperature. Note cracking of the CuCrZr at the onset of failure. AES results are similar to those presented above.

The 800°C braze temperature samples demonstrated highest ductility at high shear test temperatures. The AES results for these samples shows failure in the CuCrZr interface.

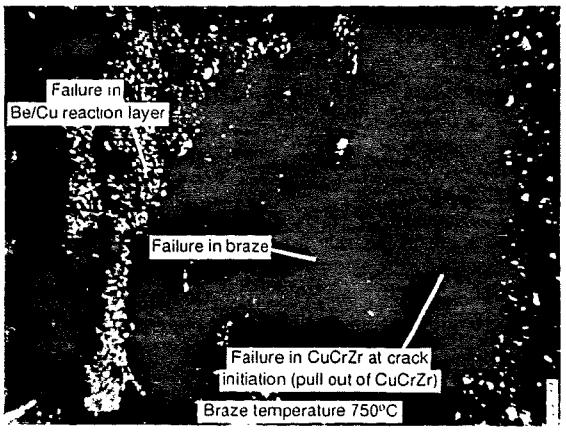

Figure 7. Typical fracture surface for 750°C braze temperature

6. POWER DENSITY TRIALS

Previous power handling trials [1] demonstrated that 6×6mm castellated 2mm thick Be tiles failed at power densities in the range 12.5 to 17MW/m^2. These failures were always located at the edge of the tile where finite element analysis shows the stresses are highest.

2D linear elastic finite element (FE) models considering both the braze cooldown and applied power stresses have been analysed. These have shown that chamfering the edges of the Be tiles and providing a 'hinge' in the target plate along the edge (Fig 8) can reduce the magnitude of the stress field in the area adjacent to the stress singularity located at the edge. An elastic/plastic FE analysis of this system has been performed. Figure 8 shows the stress history of one element in the Be at the joint interface after two heating and cooling cycles at each power density.

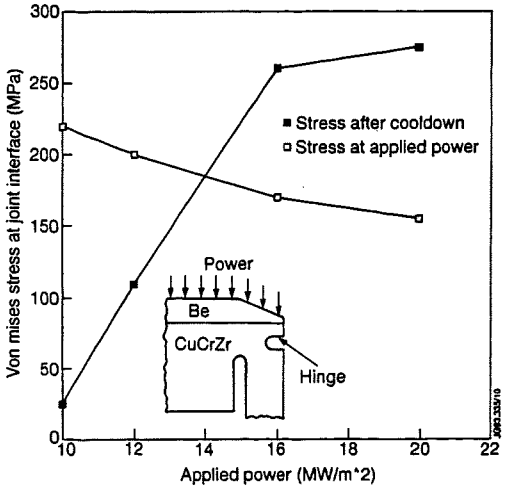

Figure 8 Theoretical peak stress in joint for applied load and after cooldown

This analysis indicates that for an uncastellated tile plastic deformation occurs on the top face and at high powered densities (> 16MW/m^2) a non shake down situation occurs. Because of this plastic deformation after cooldown, the compressive strain at the interface is increased until failure takes place. A target plate with this geometry has been tested in the JET NB Test Bed.

The target plate underwent 100 cycles of 1 sec pulses, at 14.5MW/m^2, 33 cycles at 16MW/m^2 and 24 cycles at 17.5 to 18.5MW/m^2. Two further cycles of 17 and 18.5MW/m^2 caused five tiles to fail. All failures occurred during cooldown when the braze temperature reached approximately 100°C. Examination of the fracture surfaces revealed that failure occurred at the Be/braze interface and also that there was plastic set in the target plate.

At 18.5MW/m^2 the braze temperature is 400°C and the surface temperature of the Be is 700°C. The recommended maximum operating temperature of this braze is 450°C at which the shear strength is approximately half that at room temperature. This work clearly shows that for 2mm Be clad target plates there is a definite operating limit of 17 to 19MW/m^2.

7. CONCLUSIONS

- There now exists a repeatable production method for brazing Be to CuCrZr.
- The braze strength is equal to or better than the strength of the Be and CuCrZr.
- Power density trials and finite element analysis both show that the maximum power handling capabilities have been reached using this braze.

REFERENCES

1. H. Altmann et al.
   An analysis of induction brazed beryllium on copper alloy substrates. Pro. 15th JEEE/NPSS Symposium on Fusion Engineering Oct. 11-15 1993; Hyannis, MA, USA

2. Constitution of Binary Alloys, Hansen, second edition, McGraw-Hill.